State University of New York Report

Large Eddy Simulation and Direct Numerical Simulation of High Speed Turbulent Reacting Flows

by

V. Adumitroaie, S.H. Frankel,
C.K. Madnia and P. Givi

Department of Mechanical and Aerospace Engineering
State University of New York at Buffalo
Buffalo, New York 14260-4400

Semi-Annual Report Submitted to
NASA Langley Research Center

Progress Report on Activities Supported Under Grant NAG 1-1122

for the Period

February 1, 1993 - October 31, 1993

Contents

Large Eddy Simulation and Direct Numerical Simulation of High Speed Turbulent Reacting Flows

V. Adumitroaie*, S.H. Frankel†, C.K. Madnia and P. Givi
Department of Mechanical and Aerospace Engineering
State University of New York at Buffalo
Buffalo, New York 14260-4400

Abstract

The objective of this research is to make use of *Large Eddy Simulation* (LES) and *Direct Numerical Simulation* (DNS) for the computational analyses of high speed reacting flows. Our efforts in the first phase of this research conducted within the past three years have been directed in several issues pertaining to intricate physics of turbulent reacting flows. In our previous 5 semi-annual reports submitted to NASA LaRC, as well as several technical papers in archival journals, the results of our investigations have been fully described. In this progress report which is different in format as compared to our previous documents, we focus only on the issue of LES. The reason for doing so is that LES is the primary issue of interest to our Technical Monitor and that our other findings were needed to support the activities conducted under this prime issue. The outcomes of our related investigations, nevertheless, are included in the appendices accompanying this report. The relevance of the materials in these appendices are, therefore, discussed only briefly within the body of the report.

Here, results are presented of *a priori* and *a posteriori* analyses for validity assessments of assumed Probability Density Function (PDF) methods as potential subgrid scale (SGS) closures for LES of turbulent reacting flows. Simple non-premixed reacting systems involving an isothermal reaction of the type $A + B \rightarrow Products$ under both chemical equilibrium and non-equilibrium conditions are considered. *A priori* analyses are conducted of a homogeneous box flow, and a spatially developing planar mixing layer to investigate the performance of the *Pearson Family* of PDF's as SGS models.

*One of the two Primary Graduate Research Assistants supported partially under this Grant.

†Former Graduate RA supported partially by this Grant. Present Affiliation: Assistant Professor of Mechanical Engineering, Purdue University, West Lafayette, India 47109-1077.

A posteriori analyses are conducted of the mixing layer using a hybrid one-equation Smagorinsky/PDF SGS closure. The Smagorinsky closure augmented by the solution of the subgrid turbulent kinetic energy (TKE) equation is employed to account for hydrodynamic fluctuations, and the PDF is employed for modeling the effects of scalar fluctuations. The implementation of the model requires the knowledge of the local values of the first two SGS moments. These are provided by additional modeled transport equations. In both *a priori* and *a posteriori* analyses, the predicted results are appraised by comparison with subgrid averaged results generated by DNS. Based on these results, the paths to be followed in future investigations are identified.

This research is sponsored by the NASA Langley Research Center under Grant NAG-1-1122. Dr. J. Philip Drummond, Theoretical Flow Physics Branch (TFPB), Mail Stop 156, Tel: 804-864-2298 is the Technical Monitor of this Grant

1 Introduction

In the last three decades computer simulation has gained a substantial impetus as one of the most promising tools in scientific research, already having a major effect on the human understanding and discovery of complex physical phenomena. Factually, in areas where experiments are very difficult, if not impossible, to be performed (*e.g.* plasma physics, astrophysics, cosmology, *etc.*), numerical simulation have become the only method of verifying theories. Turbulence, as one of the unsolved problems with significant range of applications, has been the subject of broad numerical investigations - the rate significantly increased with the advent of the supercomputer technology since early 80's. In general, presently there are three methodologies by which turbulent flows are treated by computer simulations: Direct Numerical Simulations (DNS), Large Eddy Simulations (LES) and Reynolds Averaged Navier-Stokes simulations (RANS). Each of these portray its advantages and its (often severe) limitations. In a recent review,[1] DNS and LES have been grouped together as "model-free simulations", since both approaches are aimed to provide a detailed description of the large structures of the flow evolution. Although DNS involves computation in the entire bandwidth associated with the turbulent field, it remains confined to relatively

low Reynolds numbers - to say the least - for the proximate future. Nevertheless, DNS has become indispensable in turbulence research in assessing and calibrating models and also in exploring new concepts.[2,3]

LES is considered somewhere between DNS and RANS computation.[1-16] Over the past thirty years, since the early work of Smagorinsky[17] there has been relatively little effort, compared to that in RANS calculations, to make full use of LES for engineering applications. The most prominent model has been the Smagorinsky based eddy viscosity closure which relates the unknown subgrid scale (SGS) Reynolds stresses to the local large scale rate of strain. This viscosity is aimed to provide the role of mimicking the dissipative behavior of the unresolved small scales. With sound SGS models, LES is expected to be used extensively in the study of high Reynolds numbers turbulence and flow prediction in complex situations. The nonlinear trait of scales interaction makes the task of developing correct SGS models very challenging even in the case of non-reacting turbulent flows. The difficulty is augmented with the increase in the number of degrees of freedom (*e.g.* variable density flows, and currents with finite electrical conductivity) and with coupling between different phenomena (such as fluid dynamics and chemistry in combusting flows).[18] Dealing with this complexity necessitates serious efforts by the scientific community, consequently at this time the grand ensemble of turbulence theories tends to exhibit a somewhat familiar disorderly appearance.

The extensions to one-equation models, typically based on the SGS turbulent kinetic energy,[19,20] have shown some improvements[21,22] over Smagorinsky based closures. This is particularly the case in simulating transitional flows where the assumption of a balance between the production and the dissipation of turbulent kinetic energy may not always be valid. Thus, the higher degree of freedom provided by one-equation closures allow more flexibility for the subgrid scale eddies to adjust to local flow conditions.

A survey of combustion literature reveals relatively little work in LES of chemically reacting

turbulent flows.[1,23] It appears that Schumann[24] was one of the first to conduct LES of a reacting flow. However, the assumption made in this work to simply neglect the contribution of SGS scalar fluctuations to the filtered reaction rate is debatable. The importance of such fluctuations is well recognized in RANS of reacting flows in both combustion[25–27] and chemical engineering[28–31] problems. Therefore, it is natural to expect that these fluctuations will also have a significant influence in LES.

Modeling of scalar fluctuations in RANS has been the subject of intense investigations since the pioneering work of Toor.[32] One approach which has proven particularly useful is based on the Probability Density Function (PDF) or joint PDF of scalar quantities.[33–36,1,37,23] This approach offers the advantage that all the statistical information pertaining to the scalar field is embedded within the PDF. Therefore, once the PDF is known the effects of scalar fluctuations are easily determined. Because of their capabilities, PDF methods have been widely used in RANS for a variety of reacting systems (see Refs.[23,38] for recent reviews). A systematic approach for determining the PDF is by means of solving the transport equation governing its evolution.[39,40] In this equation the effects of chemical reactions appear in a closed form. However, modeling is needed to account for transport of the PDF in the domain of the random variables. This transport describes the role of molecular action on the evolution of PDF. In addition, there is an extra dimensionality associated with the composition domain which must be treated. These two problems have constituted a stumbling block in utilizing PDF methods in practical applications, and developments of turbulence closures and numerical schemes which can effectively deal with these predicaments have been the subject of numerous investigations within the past two decades.

An alternative approach in PDF modeling is based on *assumed* methods. In these methods the PDF is not determined by solving a transport equation. Rather, its shape is assumed *a priori* usually in terms of the low order moments of the random variable(s). Obviously, this

method is *ad hoc* but it offers more flexibility than the first approach. Presently, the use of assumed methods in RANS is justified in cases where there is a strong evidence that the PDF assumes a particular distribution.

Among these two approaches obviously the first one is preferable if an appropriate closure is available to account for the effects of molecular action. In its application in RANS, traditionally the family of models based on the coalescence/dispersion (C/D) closures,[41–43] or least mean square methods[44] have been employed. These closures are plausible from a computational standpoint and can be effectively simulated via Monte Carlo numerical methods.[45] However, there are several drawbacks associated with these closures that restrict their use for accurate and reliable predictions.[46–48] Some of these drawbacks are overcome in the newly developed *Amplitude Mapping* Closure (AMC).[49,50,23] This has been established in a number of recent validation assessments of the AMC by means of comparison of its predicted results with those of DNS,[51–54] and experimental[55] data.

Despite its demonstrated properties, there are some deficiencies associated with the AMC which require further investigations. These are discussed in detail in Ref.;[56] the most serious of these are: (1) the "single-point" nature of the closure, (2) the difficulties associated with its numerical implementation, and (3) its inability to account for the migration of scalar bounds as mixing proceeds. The first problem is shared with C/D models and indicates the deficiency of the approach in accounting for the variation of turbulent length (time) scales. The other problems are exclusive to AMC and can cause difficulties in its applications.

Considering the current state of affairs in PDF modeling, it can be cautiously concluded that assumed PDF methods are somewhat more "feasible" than the transport equation approach for simulating practical problems. This is not to advocate the superiority of assumed methods. Rather, it is to encourage further research on the first approach before it can be implemented routinely. In this regard, in several recent studies[56,54] we have conducted

detailed investigations pertaining to both these approaches. The general conclusion drawn from these studies is that in cases where the AMC has proven useful, other approaches based on assumed probability distributions are also effective. In the cases considered in Ref.,[56] it is shown that in simple flows where the AMC can be employed, the class of PDF's based on *Johnson Edgeworth Translation* (JET)[57,58] can also be used. In fact, for the simple problem of binary mixing in isotropic turbulence - a standard test case - the solution generated by AMC[51,59] can be viewed as a member of the JET family. Furthermore, due to established similarities of JET with the simpler distributions belonging to the *Pearson Family* (PF) of PDF's,[60] it can be argued that the PF can also be considered as a viable alternative.

In turbulent combustion there has been widespread use of PF assumed PDF's (*e.g.* Refs.;[61–66] for recent reviews see Refs.[18,1,67]). In most applications to date, this family has been used in the form of the Beta density of the first kind (Pearson Type I and Type II distributions). This is due to the flexibility of this density in portraying bimodal distributions. The capabilities of this density for the purpose of RANS have been studied in Refs.[52,56,54] According to these studies there are some similarities between the PF and the AMC, as well as some distinct differences. As indicated before, both these methods are utilized in the context of a single-point closure. Therefore, in both cases the magnitudes of the moments up to second order must be provided externally. Also, both methods suffer from an inability to account for the shrinking bounds of the scalar domain as mixing proceeds. This is manifested by the failure of both closures in producing a correct evolution for the conditional statistics of the scalar; namely, the conditional expected dissipation and the conditional expected diffusion. This behavior could be troublesome and may produce significant errors especially in predicting the rate of reactant conversion in non-equilibrium flames. In their application for modeling of reacting homogeneous flows, both closures are satisfactory for equilibrium flames regardless of the equivalence ratio.[52,54] However, the use of AMC is very difficult, if not impossible, for modeling of non-homogeneous flows regardless of the chemistry model. In such systems the

mapping transfer function must be evaluated numerically and in the non-equilibrium case the multivariate form of the PDF must be considered. These require further investigations before they can be implemented routinely.[51] In these cases the application of the PF is much more straightforward but obviously cannot be justified rigorously for all applications. The corresponding multivariate form of the Beta density is the *Dirichlet* distribution,[68–71] and its mathematical implementation is straightforward.

Here, we report the results of our investigations pertaining the use of the Pearson family of PDF's in LES of turbulent reacting flows. This investigation is based on *a priori* and *a posteriori* analyses of simple homogeneous and shear flows under reacting, non-premixed conditions. Both equilibrium and non-equilibrium chemical reactions are considered. *A priori* analyses are performed of equilibrium flames in both flow configurations. *A posteriori* analyses are performed only for the shear flow with non-equilibrium chemistry. In all cases, the LES generated results are appraised by comparison with data provided via DNS.

2 Flow Configurations

Two flow configurations are considered: (1) two- and three-dimensional homogeneous box flows, and (2) a two-dimensional spatially developing planar mixing layer. In both configurations, a constant rate, non heat releasing chemical reaction of the type $A + B \rightarrow P$ is considered.

The procedure in homogeneous DNS is similar to that of previous simulations of this type (see for example Ref.[1]). The computational package is based on a modification of the computer code developed in Refs.[72–74] The code makes use of the spectral collocation algorithm with Fourier expansion functions[75–77] to approximate the spatial derivatives at N grid points in

each direction. It is now widely recognized that the collocation method is less expensive than other spectral variants (*e.g.* Galerkin and Tau methods) in evaluating nonlinear terms. The aliasing errors inherent in collocation simulations can be effectively reduced by de-populating the large wave number interval (this can be accomplished by an isotropic truncation). To describe the temporal evolution, a time-splitting method is adopted in order to account properly for acoustic effects. The advancing in time is achieved using a third-order Runge Kutta scheme with a variable step determined from the Courant-Friedrich-Levy (CFL) stability condition. The hydrodynamic field is assumed isotropic and is initialized in a manner similar to that in Refs.[73,78] In this setup, the energy contained in spherical shells is obtained applying an imposed energy spectrum function $E(k) = k^4 \exp(-2k^2/k_0^2)$ (where k_0^{-1} represents the integral scale of the flow) to the randomly distributed Fourier components of the scalar fields. The compressible energy content can be varied by means of a proper parameter related to the energy ratio between the two velocity modes (solenoidal and irrotational) resulting from the Helmholtz decomposition. No forcing mechanism at the low wave numbers is applied; therefore, the turbulent field decays in time. Several other parameters are necessary to control the compressibility level in the turbulent field. These are the intensities of density and temperature fluctuations in addition to the root-mean-square (RMS) of the Mach number $M_t = M_\infty \left\langle \frac{u_i u_i}{T} \right\rangle^{1/2}$. The reacting scalar fields, assumed dynamically passive, are configured with smoothed square waves (error functions) in anti-phase, with the two species at the stoichiometric conditions. This is identical to the conditions considered in previous simulations of this type.[79,48,80]

The mixing layer configuration consists of two co-flowing streams traveling at different velocities and merging at the trailing edge of a partition plate.[81–88] Two reactants, A and B, are introduced into the high- and the low-speed streams, respectively. To expedite the formation of large scale vortices, low amplitude perturbations are imposed at the inflow plane of the layer. The flow field which develops in this setting is dominated by large scale coherent

structures. The numerical procedure is based on a hybrid finite-difference/pseudospectral scheme. A third order upwinding method is used in the streamwise direction and a spectral collocation method employing Fourier expansions is used for cross stream discretization[1] Time discretization is done by the Adams-Bashforth technique. The computational domain is bounded by $0 < x < 32\delta, -8\delta < y < 8\delta$, where δ is the vorticity thickness at the inflow. The highest resolution consists of 512 finite difference nodes and 256 collocation nodes. With this resolution, reliable DNS with a Reynolds number $Re = 1000$ and a Damköhler number $Da = 10$ (based on the velocity difference and the vorticity thickness at the inlet) are possible.

In both flows, all the species (A, B, P) are assumed thermodynamically identical and the fluid is assumed to be calorically perfect. The value of the molecular Schmidt number is set equal to unity in all simulations. It is also assumed that there is no trace of one of these species at the feed of the other one, *i.e.* complete initial segregation. With unity normalized mass fractions of the two species at their respective streams, a mixture fraction denoted by $\mathcal{J}$ can be defined:[18]

$$\mathcal{J}(x_i, t) = \frac{Y_A(x_i, t) - Y_B(x_i, t) + 1}{2}, \quad \mathcal{J} \in [0, 1]. \tag{1}$$

where Y_i denotes the mass fraction of species i. With total initial segregation the magnitude of the mixture fraction is unity in the stream containing A, and zero in the stream containing B. In non-reacting flows, the transport of this mixture fraction portrays the mixing process. In reacting flows, the variable $\mathcal{J}$ denotes a conserved "Shvab-Zeldovich" scalar variable.[18] In the limit of an infinitely fast chemical reaction all the statistics of the two reactants are

[1]Within the past year, Geoffrey Shieh has modified this code by employing a sixth order compact parameter finite difference scheme for discretization in the streamwise direction. We have obtained many exciting results pertaining to both DNS and LES. However, these results are not at a stage that can be included in this report.

directly related to those of the Shvab-Zeldovich variable:[32,89,18,47]

The assessment of the models is facilitated by direct comparison with DNS data. The resolution in DNS is dictated by the magnitudes of the physical parameters, with sufficient testing on the independency of the results to the number of grid points. All the subgrid statistics are constructed directly from the filtered DNS data bank. In *a priori* analyses the statistical properties of subgrid data are considered. In *a posteriori* analyses, the results predicted by LES on coarse grids are compared with those of filtered DNS. These analyses, correspond effectively to simulations with a homogeneous box filter in which the values of the filtered means are constant within the box. The ratio between the coarse grid and the fine grid is, therefore, a measure of the filter width. That is, it determines the scale at which the subgrid fluctuations are not accounted for deterministically. Consequently, the statistical behavior of the variable within the subgrid is dependent on the magnitude of the sample size there. If this size is too small, statistical analyses are meaningless. If it is too large, the essential features of large scale transport are masked. In *a priori* analysis of the box flow, a coarse grid consisting of 16^3 grid points are considered. In the shear flow, LES is performed on the domain with 64 finite difference grid points and 32 Fourier collocation points.

3 Problem Formulation. I: DNS Framework

Under the assumptions of ideal gas and negligible body forces the set of nondimensional governing equations (continuity, momentum and pressure) in Cartesian tensor notation, which relate the thermodynamical variables ρ (mass density), u_i (velocity components), p (pressure), T (temperature) are given by:

$$\frac{\partial \rho}{\partial t} + \frac{\partial \rho u_j}{\partial x_j} = 0, \tag{2}$$

$$\frac{\partial \rho u_i}{\partial t} + \frac{\partial (\rho u_i u_j)}{\partial x_j} = -\frac{\partial p}{\partial x_i} + \frac{1}{Re}\frac{\partial \sigma_{ji}}{\partial x_j}, \tag{3}$$

$$\frac{\partial p}{\partial t} + u_j \frac{\partial p}{\partial x_j} + \gamma p \frac{\partial u_j}{\partial x_j} = \frac{1}{M_\infty^2 Pr Re}\frac{\partial}{\partial x_j}\left(k^* \frac{\partial T}{\partial x_j}\right) + \frac{\gamma - 1}{Re}\Phi, \tag{4}$$

In these equations, the indices i and j are integer values adopting values $1, \ldots, \zeta$, where $\zeta = 2$ in two-dimensional (2D) and $\zeta = 3$ in 3D simulations. The viscous stress tensor σ_{ij} and the viscous dissipation Φ are defined, in order, as:

$$\sigma_{ij} = \mu^* \left(\frac{\partial u_i}{\partial x_j} + \frac{\partial u_j}{\partial x_i}\right) - \frac{2}{3}\mu^* \frac{\partial u_k}{\partial x_k}\delta_{ij}, \tag{5}$$

$$\Phi = \mu^* \left(\frac{\partial u_i}{\partial x_j} + \frac{\partial u_j}{\partial x_i}\right)\frac{\partial u_i}{\partial x_j} - \frac{2}{3}\mu^* \left(\frac{\partial u_k}{\partial x_k}\right)^2, \tag{6}$$

For a binary chemical reaction of the type $A + B \rightarrow Products$ the above system is supplemented by the equations of conservation of species:

$$\frac{\partial \rho Y_\alpha}{\partial t} + \frac{\partial (\rho Y_\alpha u_j)}{\partial x_j} = \frac{1}{ScRe}\frac{\partial}{\partial x_j}\left(\Gamma^* \frac{\partial Y_\alpha}{\partial x_j}\right) + \dot{\omega}_\alpha, \quad \alpha = A, B \tag{7}$$

Here Y_α denotes the mass fraction of species α, Γ is the binary Fickian diffusion coefficient and $\dot{\omega}_\alpha = -Da\rho Y_A Y_B$ indicates the chemical source term. The Damköhler number $Da = \rho_0 L_0 k_f / U_0$, where k_f is the rate constant of reaction and gives a measure of the speed

of reaction. In the present formulation, for simplicity, the diffusion coefficients are considered constant and the Soret-Dufour and pressure gradient diffusion effects are neglected. Moreover, it is assumed that the Lewis number is unity and the chemical rate is independent of temperature. The system is closed with the equation of state for perfect gases:

$$\gamma M_\infty^2 p = \rho T. \tag{8}$$

The equations are scaled by reference values which appear in the expressions of the dynamical parameters: the characteristic Reynolds number $Re = \rho_0 U_0 L_0/\mu_0$, the Prandtl number $Pr = c_p\mu_0/k_0$, the Schmidt number $Sc = \mu_0/\Gamma_0$ and the reference Mach number.

4 Problem Formulation. II: LES Framework

In most cases of practical interest the motion on the order of the dissipation scale cannot be evaluated explicitly since the available computational resolution fails to meet the severe mesh requirements. In the homogeneous flow simulation, to insure a resolved flow simulation one has to consider a number of points in the range of $N^3 \approx 0.1 Re_\lambda^{9/2}$, while Re_λ is the Reynolds number based on the Taylor microscale and RMS of velocity fluctuations[2]). This implies that a 96^3 DNS can accommodate at most a modest $Re_\lambda \approx 35$. In order to overcome this limitation the governing equations have to be "altered" in such a way that the activity at the level of the unresolved scales is mimicked by a proper model, and only the large-scale fluctuations are explicitly computed. The rationale for this idea remains the fact that the primary momentum transport and turbulent diffusion is sustained by large-scale energy-containing eddies. Certainly a smoothing ("low pass" filter) operator achieves this goal, decomposing a given field into a resolved component and a residual component (also called

sub-grid field).

It is customary to define for a flow variable $f(\mathbf{x},t)$ the resolvable-scale component $\overline{f}$ through a convolution of f with a filter function[90] $G(\mathbf{x},t,\Delta_f)$:

$$\overline{f}(\mathbf{x},t) = \int_D G(\mathbf{x}-\mathbf{x}',t,\Delta_f) f(\mathbf{x}',t) d^{\zeta}\mathbf{x}' \tag{9}$$

where $\mathbf{x} = (x_i, i = 1,\ldots,\zeta)$, and Δ_f is the filter width representing the smallest scale of the resolved field (it is desirable that Δ_f corresponds to a wavenumber in the inertial range) and D is the domain of interest. Several types of filters are employed in previous attempts in LES: The Gaussian filter, the sharp-cutoff filter and the box filter.[90] The convolution with these filters is equivalent with a moving volume average and generates moderate subgrid fluctuations; therefore the modeling of the subgrid correlations is less critical than in the case of a fixed average. However, additional terms have to be modeled and an ill-posed Fredholm integral equation has to be solved in the necessary process of de-filtering.

For the ease of implementation we employ the fixed average approach (used in a different manner in Ref.[20] by defining the "filter" function as:

$$G(\mathbf{x},t,\Delta_f) = \begin{cases} \frac{1}{\Delta_f^{\zeta}}, & \text{if } \frac{n-1}{1-\frac{1}{n_{SG}}}\Delta_f \le x_i \le \frac{n-\frac{1}{n_{SG}}}{1-\frac{1}{n_{SG}}}\Delta_f; \\ 0, & \text{otherwise} \end{cases} \tag{10}$$

with $n = 1, N_{SG}$ represents the index of coarse grid points in each direction and n_{SG} is the number of points per subgrid cell (box) side. Evidently the "filtered" variable is now defined only at discrete points. In the study of compressible turbulent flows it is convenient to prescribe a Favre filtered variable:

$$\tilde{f} = \frac{\overline{\rho f}}{\overline{\rho}}, \tag{11}$$

along with the corresponding decomposition of the instantaneous field

$$f = \tilde{f} + f'', \tag{12}$$

which defines the SGS fluctuations f''. The direct application of the filtering operator to the conservation of mass equation yields:

$$\frac{\partial \overline{\rho}}{\partial t} + \frac{\partial \overline{\rho}\tilde{u}_j}{\partial x_j} = 0, \tag{13}$$

where the commutativity of linear operators is exerted with the caveat that the density and the pressure can be meaningfully related only to a non-weighted filtered quantity. Similarly, the Navier-Stokes equations become

$$\frac{\partial \overline{\rho}\tilde{u}_i}{\partial t} + \frac{\partial(\overline{\rho}\tilde{u}_i\tilde{u}_j)}{\partial x_j} = -\frac{\partial \overline{p}}{\partial x_i} + \frac{1}{Re}\frac{\partial \overline{\sigma}_{ji}}{\partial x_j} + \frac{\partial(-\overline{\rho}\widetilde{u_j''u_i''})}{\partial x_j}, \quad i,j = 1,\ldots\zeta; \tag{14}$$

with $\gamma M_\infty^2 \overline{p} = \overline{\rho}\tilde{T}$. The evaluation of the nonlinear term $\rho u_i u_j$ gives:

$$\overline{\rho u_i u_j} = \overline{\rho}(\widetilde{\tilde{u}_i\tilde{u}_j} + \widetilde{u_i''\tilde{u}_j} + \widetilde{\tilde{u}_i u_j''} + \widetilde{u_i''u_j''}). \tag{15}$$

With this relation the stress tensor is composed of a so-called "cross stress" $C_{ij} = -\overline{\rho}(\widetilde{u_i''\tilde{u}_j} + \widetilde{\tilde{u}_i u_j''})$ and the SGS Reynolds stress $\tau_{ij} = -\overline{\rho}\widetilde{u_i''u_j''}$. From this definition, it is apparent that in the present filtering procedure the cross stress is zero. Here, we employ the linear gradient

class of isotropic models, which relate the SGS Reynolds stress to the large-eddy rate of strain $S_{ij} = (\partial\widetilde{u_i}/\partial x_j + \partial\widetilde{u_j}/\partial x_i)$:

$$\tau_{ij} = -\overline{\rho}(\widetilde{u_i''u_j''} - \frac{1}{3}\widetilde{u_k''u_k''}\delta_{ij}) + (-\frac{1}{3}\widetilde{u_k''u_k''}\delta_{ij}) = \overline{\rho}\nu_t(2S_{ij} - \frac{2}{3}S_{kk}\delta_{ij}) - \frac{2}{3}\overline{\rho}\Xi\delta_{ij} \qquad (16)$$

where the SGS Reynolds stress is separated into anisotropic and isotropic parts. The model developed by Speziale and co-workers is a compressible generalization of the Smagorinsky model which postulates that the eddy viscosity $\nu_t = C_R\Delta_f^2 \mathrm{II}_S^{1/2}$, *i.e.* ν_t is related to the second invariant of the large scale strain tensor $\mathrm{II}_S = S_{kl}S_{kl}$. Although the isotropic part is relatively small compared to the thermodynamic pressure we prefer not to neglect it and use instead a model elaborated by Yoshizawa giving $\Xi = C_I\Delta_f^2\mathrm{II}_S$. C_R and C_I are empirical constants to be determined. An alternative procedure is analogous to the "one-equation closure" in RANS. With this closure, the viscosity is expressed as $\nu_t = C_\nu\Delta_f\sqrt{\tilde{k}}$ in terms of the SGS kinetic energy $\tilde{k} = \frac{1}{2}\widetilde{u_i''u_i''}$. In this case $\Xi = \tilde{k}$ and $C_I = 1.0$. The term $\overline{\sigma}_{ij}(u_i, u_j)$ is treated like $\sigma_{ij}(\tilde{u}_i, \tilde{u}_j)$. The filtered pressure equation becomes:

$$\begin{aligned}\frac{\partial\overline{p}}{\partial t} + \tilde{u}_j\frac{\partial\overline{p}}{\partial x_j} + \gamma\overline{p}\frac{\partial\tilde{u}_j}{\partial x_j} \;=\; & \frac{1}{M_\infty^2 PrRe}\frac{\partial}{\partial x_j}\left(k^*\frac{\partial T}{\partial x_j}\right) + \frac{1}{\gamma M_\infty^2}\frac{\partial(-\overline{\rho}\widetilde{u_j''T''})}{\partial x_j} + \\ & \frac{\gamma-1}{Re}\overline{\Phi} - (\gamma-1)\overline{p}\frac{\partial\overline{u_j''}}{\partial x_j} - (\gamma-1)\overline{p'\frac{\partial u_j''}{\partial x_j}}\end{aligned} \qquad (17)$$

The SGS velocity-temperature correlation $\Lambda_j = -\overline{\rho}\widetilde{u_j''T''}$ is modeled based on the gradient transport approximation:

$$\Lambda_j = \overline{\rho}\frac{\nu_t}{Pr_t}\frac{\partial\tilde{T}}{\partial x_j} \qquad (18)$$

With this, the turbulent Prandtl number Pr_t is taken as an empirical constant, implying the assumption that the transport of momentum and scalar quantities is characterized by a single length scale. Also, since the term $\overline{u_j''}$ can be interpreted as a SGS mass flux, we can write:

$$\overline{u_j''} = -\frac{\overline{\rho' u_j''}}{\overline{\rho}} = \frac{\nu_t}{\overline{\rho}} \frac{\partial \overline{\rho}}{\partial x_j}. \tag{19}$$

In the Smagorinsky model the eddy viscosity, ν_T, is related to the large scale strain rate. A suggestion made in Ref.[91] and discussed in Ref.[92] is to model the eddy viscosity in terms of the trace of the resolved vorticity field. Here, since the SGS moments up to second order are required for the species field, an extension is made to utilize a one-equation hydrodynamics closure. The conjecture utilized for the molecular stress is also applied to the molecular heat flux and dissipation. A modeling of the pressure dilatation term would require an additional transport equation of a subgrid quantity, for example the SGS density variance.[93] Therefore, we neglect this term for simplicity. This is justified only when consistent decay occurs, that is after the adjustment between the thermal energy and TKE modes from the initial conditions is achieved. To complete the hydrodynamic system, an equation for the SGS turbulent kinetic energy is required:

$$\begin{aligned} \frac{\partial \overline{\rho}\widetilde{k}}{\partial t} + \frac{\partial (\overline{\rho}\widetilde{k}\widetilde{u}_j)}{\partial x_j} &= \frac{\partial}{\partial x_j}\left[-(\overline{\rho}\widetilde{u_j''k} + \overline{p'u_j''} - \frac{1}{Re}\overline{u_i''\sigma_{ji}''})\right] - \overline{\rho}\widetilde{u_i''u_j''}\frac{\partial \widetilde{u}_i}{\partial x_j} + \\ &\quad \overline{p'\frac{\partial u_j''}{\partial x_j}} - \frac{1}{Re}\overline{\sigma_{ji}''\frac{\partial u_i''}{\partial x_j}} - \overline{u_i''}\frac{\partial \overline{p}}{\partial x_i} + \frac{1}{Re}\overline{u_i''}\frac{\partial \widetilde{\sigma}_{ji}}{\partial x_j}. \end{aligned} \tag{20}$$

The classical closure used for the SGS transport term $T_j = -(\overline{\rho}\widetilde{u_j''k} + \overline{p'u_j''} - \frac{1}{Re}\overline{u_i''\sigma_{ji}''})$ reads:

$$T_j = \left(\frac{\overline{\rho}\nu_t}{\varsigma_k} + \frac{1}{Re}\right)\frac{\partial \widetilde{k}}{\partial x_j}, \tag{21}$$

where ς_k is an empirical constant. The SGS TKE dissipation, $\widetilde{\epsilon} = \frac{1}{\overline{\rho}Re}\overline{\sigma''_{ji}\frac{\partial u''_i}{\partial x_j}}$ contains a solenoidal part and a dilatational part, the latter being associated with the SGS viscous losses. A possible closure for the SGS dissipation including the compressible effects is:

$$\widetilde{\epsilon} = C_\epsilon[1 + c_d(M_t^{SGS})^2)]\frac{\widetilde{k}^{3/2}}{\Delta_f}. \tag{22}$$

Here C_ϵ is the SGS dissipation constant, $c_d = 1.0$ and M_t^{SGS} denotes the RMS of the SGS turbulent Mach number. The Favre filtering applied to the conservation of species equations demonstrates the coupling effects of all the aerothermochemical processes in the density-weighted variables. With this, we have:

$$\frac{\partial \overline{\rho}\widetilde{Y}_\alpha}{\partial t} + \frac{\partial(\overline{\rho}\widetilde{Y}_\alpha\widetilde{u}_j)}{\partial x_j} = \frac{1}{ScRe}\frac{\partial}{\partial x_j}\left(\Gamma^*\frac{\partial Y_\alpha}{\partial x_j}\right) + \frac{\partial(-\overline{\rho}\widetilde{u''_j Y''_\alpha})}{\partial x_j} + \overline{\dot{\omega}_\alpha}, \quad \alpha = A, B. \tag{23}$$

The Favre flux of species fluctuations $\Psi_{j\alpha}$ represents the interactions between the two principal phenomena: the turbulence and the chemical reaction. Based on the previous assumptions regarding the scalar fields, we have

$$\Psi_{j\alpha} = -\overline{\rho}\widetilde{u''_j Y''_\alpha} = \overline{\rho}\frac{\nu_t}{Sc_t}\frac{\partial \widetilde{Y}_\alpha}{\partial x_j} \tag{24}$$

where Sc_t denotes the turbulent Schmidt number, also an empirical constant. The chemical source term establishes the rate of reactants consumption. This contains both large scale interactions and chemical SGS activity:

$$\overline{\dot{\omega}_\alpha} = -\overline{\rho} Da(\tilde{Y}_A \tilde{Y}_B + \widetilde{Y_A'' Y_B''}). \tag{25}$$

The SGS covariance $\widetilde{Y_A'' Y_B''}$ is of the same order of magnitude as the mean reaction term $\tilde{Y}_A \tilde{Y}_B$, consequently introduces an additional transport equation:

$$\frac{\partial \overline{\rho} \widetilde{Y_A'' Y_B''}}{\partial t} + \frac{\partial (\overline{\rho} \widetilde{Y_A'' Y_B''} \tilde{u}_j)}{\partial x_j} = \frac{1}{ScRe} \frac{\partial}{\partial x_j} \left(\overline{\Gamma^* \frac{\partial Y_A'' Y_B''}{\partial x_j}} \right) + \frac{\partial (-\overline{\rho} u_j'' \widetilde{Y_A'' Y_B''})}{\partial x_j} -$$
$$(\overline{\rho} u_j'' \widetilde{Y_A''} \frac{\partial \widetilde{Y}_B}{\partial x_j} + \overline{\rho} u_j'' \widetilde{Y_B''} \frac{\partial \widetilde{Y}_A}{\partial x_j}) - \frac{2}{ScRe} \overline{\Gamma^* \frac{\partial Y_A''}{\partial x_j} \frac{\partial Y_B''}{\partial x_j}} + \overline{\dot{\omega}_A Y_B''} + \overline{\dot{\omega}_B Y_A''} +$$
$$\frac{1}{ScRe} \left[\frac{\partial}{\partial x_j} \left(\overline{\Gamma^* Y_B''} \frac{\partial \tilde{Y}_A}{\partial x_j} \right) - \overline{\Gamma^* \frac{\partial Y_B''}{\partial x_j}} \frac{\partial \tilde{Y}_A}{\partial x_j} + \frac{\partial}{\partial x_j} \left(\overline{\Gamma^* Y_A''} \frac{\partial \tilde{Y}_B}{\partial x_j} \right) - \overline{\Gamma^* \frac{\partial Y_A''}{\partial x_j} \frac{\partial \tilde{Y}_B}{\partial x_j}} \right] \tag{26}$$

In the above equation, the last term on RHS is relatively small for flows with large Peclet numbers or if $\overline{Y_\alpha''}$ is negligible. The gradient of the SGS correlation flux is transformed in a diffusion term expresses as:

$$-\overline{\rho} u_j'' \widetilde{Y_A''} Y_B'' = \overline{\rho} \frac{\nu_t}{Sc_t} \frac{\partial \widetilde{Y_A'' Y_B''}}{\partial x_j}. \tag{27}$$

The simplest model for the SGS covariance dissipation $\tilde{\epsilon}_{AB} = \frac{2}{\overline{\rho} ScRe} \overline{\Gamma^* \frac{\partial Y_A''}{\partial x_j} \frac{\partial Y_B''}{\partial x_j}}$ in terms of $\widetilde{Y_A'' Y_B''}$ and the time scale of the turbulence τ (the Smagorinsky model states that $\tau = 1/\sqrt{\Pi_S}$, whereas the one-equation model prescribes $\tau = \Delta_f / \sqrt{\tilde{k}}$) is given by

$$\tilde{\epsilon}_{AB} = C_\phi \frac{\widetilde{Y_A'' Y_B''}}{\tau}. \tag{28}$$

The remaining unclosed terms from this respectable set of equations are also among the most

difficult to model. Obviously, triple correlations like $\overline{\dot{\omega}_A Y_B''}$ convey information from the high order subgrid statistics to the large scale field. These terms could be directly determined from the SGS joint PDF (if known) as the expectation of an arbitrary function M of the random variable $\psi = (Y_A, Y_B)$:

$$\widetilde{M}(\psi) = \int M(\psi)\widetilde{P_{AB}}(\psi)d\psi. \tag{29}$$

Here $\widetilde{P_{AB}}$ is the SGS Favre PDF obtained from the joint SGS PDF of density and species $P_{AB}(\psi, \rho)$

$$\widetilde{P_{AB}}(\psi) = \frac{1}{\overline{\rho}} \int \rho P_{AB}(\psi, \rho)d\rho. \tag{30}$$

Since the PDF of a random variable embodies the entire stochastic information pertaining to that variable, it is very tempting to consider a multivariate PDF of all the dynamical variables for a complete description. A general transport equation can be derived in order to depict the evolution time. Unfortunately, the complexity of the full PDF method makes it very cumbersome for practical purposes.[36] Restricting this approach only for the treatment of the chemical species still poses serious closure problems.[47,23] A less rigorous technique, but extremely facile, is to assume *apriori* the shape of the joint PDF which will represent the statistical behavior of the reactants within the subgrid.

As indicated before, from the family of many different densities, the Pearson system of frequency curves and its multivariate generalizations have been found to display certain advantages, *e.g.* flexibility, over other possible candidates. In fact, the Beta density of the first kind yields a reasonable prediction for the probabilistic behavior of the conserved scalar variable in equilibrium flows (see the references cite in the Introduction). In general the Dirichlet distribution of the n species, maintaining the Favre convention, is given by:[70,69,94,68]

$$\tilde{P}(\psi_1, \psi_2, \cdots, \psi_n) = \frac{\Gamma(\eta_1 + \eta_2 + \cdots + \eta_{n+1})}{\Gamma(\eta_1)\Gamma(\eta_2)\cdots\Gamma(\eta_{n+1})} \psi_1^{\eta_1 - 1} \psi_2^{\eta_2 - 1} \cdots \psi_n^{\eta_n - 1} (1 - \psi_1 - \psi_2 - \cdots - \psi_n)^{\eta_{n+1} - 1} \tag{31}$$

with the constraints $\psi_j > 0$, $j = 1, n$; $\sum_{j=1}^{n} \psi_j \leq 1$; $\eta_k > 0$, $k = 1, n+1$. The $n+1$ parameters η_k can be evaluated if the values of an equal number of moments are supplied, therefore knowledge of at least one second order moment is necessary, a recognizable feature of single-point closures. It is straightforward to show that the product moments about the origin of order $r = \sum_{j=1}^{n} r_j$ are

$$\tilde{\mu}'_{r_1 r_2 \cdots r_n} = \int_{S_n} \psi_1^{r_1} \psi_2^{r_2} \cdots \psi_n^{r_n} \tilde{P}(\psi_1, \psi_2, \cdots, \psi_n) d\psi_1 d\psi_2 \cdots d\psi_n = \frac{\Gamma(\eta_1 + \eta_2 + \cdots + \eta_{n+1})\Gamma(\eta_1 + r_1)\Gamma(\eta_2 + r_2)\cdots\Gamma(\eta_n + r_n)}{\Gamma(\eta_1)\Gamma(\eta_2)\cdots\Gamma(\eta_n)\Gamma(\eta_1 + \eta_2 + \cdots + \eta_{n+1} + r_1 + r_2 + \cdots + r_n)}, \tag{32}$$

where S_n is the support of $\tilde{P}(\psi)$ in the composition space. With this PDF, the mean of the mass fraction of species i is given by:

$$\tilde{\psi}_i = \frac{\eta_i}{\sum_{k=1}^{n+1} \eta_k}. \tag{33}$$

Furthermore, the $r_i + r_j$th order correlation (product moment about the mean) between species ψ_i and ψ_j can be calculated as

$$\tilde{\mu}_{r_i r_j} = \sum_{l=1}^{r_i}\sum_{k=1}^{r_j}(-1)^{l+k}\binom{r_i}{l}\binom{r_j}{k}(\widetilde{\psi_i})^l(\widetilde{\psi_j})^k \frac{\eta_i(\eta_i+1)\cdots(\eta_i+r_i-l-1)\eta_j(\eta_j+1)\cdots(\eta_j+r_j-k-1)}{(\sum_{m=1}^{n+1}\eta_m+1)\cdots(\sum_{m=1}^{n+1}\eta_m+r_i-l+r_j-k-1)} \tag{34}$$

The variance of species i and the covariance of species i and j are, in order:

$$\widetilde{\psi_i''^2} = \frac{\eta_i(\sum_{k=1}^{n+1}\eta_k-\eta_i)}{(\sum_{k=1}^{n+1}\eta_k)^2(\sum_{k=1}^{n+1}\eta_k+1)};\ \widetilde{\psi_i''\psi_j''} = \frac{\eta_i\eta_j}{(\sum_{k=1}^{n+1}\eta_k)^2(\sum_{k=1}^{n+1}\eta_k+1)} \tag{35}$$

In the particular case of our study $n = 2$, hence three parameters must be determined from known SGS moments. Our detailed investigations, some of which reported in Refs.[95,96] indicate that there is no optimum choice between the moments up to the second order in the above setting, but two equally valid combinations[2]. These are provided by the subgrid averaged scalars $\tilde{Y}_A$, $\tilde{Y}_B$ along with either the SGS scalar energy $E_\phi = \widetilde{Y_A''^2} + \widetilde{Y_B''^2}$ or the SGS covariance $\widetilde{Y_A''Y_B''}$. In general we have:

$$\eta_1 = \tilde{Y}_A\lambda;\ \eta_2 = \tilde{Y}_B\lambda;\ \eta_3 = (1-\tilde{Y}_A-\tilde{Y}_B)\lambda;\ \lambda = \eta_1+\eta_2+\eta_3. \tag{36}$$

Also the unclosed terms in SGS covariance transport equation (which appear in the same form in the SGS scalar energy transport equation) are closed by means of the assumed PDF method in terms of known quantities as:

$$\overline{\omega_A Y_\alpha''} = \tilde{Y}_A\tilde{Y}_B(1-2\tilde{Y}_\alpha)\frac{\lambda}{(\lambda+1)(\lambda+2)}. \tag{37}$$

[2]This issue is being seriously investigated by George Sabini in a detailed study in which all the results generated by various assumed PDF's are being compared with laboratory data.

The parameter λ has the form:

$$\lambda = \frac{\tilde{Y}_A(1-\tilde{Y}_A)+\tilde{Y}_B(1-\tilde{Y}_B)}{\widetilde{Y_A''^2}+\widetilde{Y_B''^2}} - 1 \tag{38}$$

when the scalar energy is used, and is given by

$$\lambda = -(\frac{\tilde{Y}_A\tilde{Y}_B}{\widetilde{Y_A''Y_B''}} + 1) \tag{39}$$

5 Results. I. Homogeneous Box Flow

5.1 DNS and *a priori* LES Analyses

One objective of our direct simulations is to provide an extended data base for the purpose of SGS model validation. Although from *a priori* analyses one may extract a rather "pessimistic" conclusion about the performance of the models, it is the preferred manner to determine the best estimates for the unknown parameters appearing in the closures. In addition, the ultimate test for a LES formulation is the comparison between a parallel evolutions DNS-LES. The most disturbing drawback of the single-point closures is the flow dependence, which can be alleviated to some extent by testing and fine-tuning under various conditions. The majority of the high-compressible turbulent flows include noticeable zones where the character of the flow shifts toward the quasi-incompressible regime. Hence it is required to endow the models with some flexibility. Finally, the assumptions made with respect to the magnitudes of neglected terms can be assessed by examining the balance of the equations.

The present simulations, based on 256^2 (in 2D) and 96^3 (in 3D) collocation grids, are conducted to attain marginal levels of compressibility, that is either a weakly compressible

turbulence or towards a relatively high dilatational flow. As remarked before the initial conditions play a primary role in placing the simulation in the desired realm.[3] The results of recent investigations at ICASE, NASA LaRC reveal that for $0 < M_t < 0.3$ and initially ρ_{RMS}, $T_{RMS} \ll M_t$ a quasi-incompressible turbulence statistics prevail, whereas for values of order $\mathcal{O}(M_t)$ the compressible TKE reaches the order of magnitude of the incompressible TKE. The set of initial parameters establishing the low compressible regime was $M_t = 0.2$, $\rho_{RMS} = 0.01$, $T_{RMS} = 0.01$, $\chi = 0.01$, where $\chi = \mathcal{E}^{\mathcal{C}}/(\mathcal{E}^{\mathcal{C}} + \mathcal{E}^{\mathcal{I}})$. To produce stronger compressibility effects, computations are performed with the initial conditions $M_t = 0.6$, $\rho_{RMS} = 0.1$, $T_{RMS} = 0.1$, $\chi = 0.2$. The box Reynolds number is taken in the range $100 - 250$ (the lower value corresponds to the high compressible case).

The above mentioned effects can be evidenced qualitatively through visualization of relevant quantities and reflected quantitatively in the time history of various ensemble averages. An illustrative contour plot of the thermodynamic pressure, presented in Fig. 1 allows the identification of small compression waves (shocklets) within the high compressible turbulent field. For extensive phenomenological descriptions we refer the reader to our previous works.[80] From the balance of the TKE equation (Fig. 2) for the 3D compressible case (with initial $Re_\lambda = 12$) it can be pointed out that the pressure dilatation term creates strong interference in the early phases of the energetic decay (all terms are obtained by Favre ensemble average). Moreover, the dilatational dissipation represents a considerable part of the total dissipation (about the same percent of compressible energy injected into the flow). These contributions have to be taken into account by means of external models.

The evolution of the reacting scalars is a reflection of the development of the flow. Figure 3 presents the contour plot of species A in a 2D compressible simulation with $Da = 10$. The figure shows that the initially segregated structure has been contorted by turbulence and the species are depleted by chemical reaction. The influence of the source term on the decay

of the second order moments can be appraised by Fig. 4 where we present the balance of the transport equations for the reactants covariance and the variance of species A. It can be noticed that the contribution of the reaction term is significant, affecting the rate of decay set up by the scalar dissipation. Figure 4(c) justifies the neglect of the last term in Eq. (26) based on small values of $\overline{Y_\alpha''}$.

In order to evaluate the performance of the Dirichlet joint PDF an *a priori* analysis is conducted on the data obtained from high compressible 3D non-equilibrium chemistry case with $Da = 5$. A striking feature displayed in the statistics of the reacting scalars is that the density corrupts the time history of all the moments except the second order ones which exhibit essentially the same profiles under both ensemble and Favre ensemble averaging procedures (Figs. 5(a)-(d)). For practical purposes, a reacting flow is completely determined if the scalar's moments up to the second order are known, hence the particular case of binary systems necessitates five quantities. Although the Dirichlet density is not able to accommodate five parameters, it is preferred for its flexibility and tractability. Obviously, an optimum choice has to be made based on the best approximation of the scalar covariance and of third order moments needed to be closed in the transport equations of the lower order moments. The examination of the Figs. 6(b) and 7(b) gives more credit to the means-scalar energy parameterization, but a careful reconsideration of the fact that the source term in the species conservation equation is under the direct influence of the scalar covariance evolution, shifts the option towards the means-covariance triad. Figure 6(a) enforces whereas Fig. 7(a) weakens this choice.

More insight can be acquired exploring the evolving shape of the scalar joint PDF (based on the fine grid statistics) as resulting from DNS. Figures 8, 9 and 10 portray this evolution in the composition space. At initial times when the scalars A and B are still isolated (to be rigorous, there are overlapping regions due to the initial conditions-error functions) the PDF

is roughly composed of two impulse functions at the higher bound. Later, the PDF breaks into a wave-like surface, which travels to the lower bound. Towards the completion of the reaction the PDF is converted to an unique impulse shape situated at $\psi = 0$. An examination (Fig. 11) of the subgrid joint PDF's exposes skewed shapes and similar trends as described before (the resolution is insufficient to obtain smooth surfaces). From a purely "geometric" standpoint, the PDF can be depicted as a family of Beta functions (in vertical planes) having as support a hyperbola in the horizontal plane (Fig. 12) which is the contour representation of Fig. 9. Unfortunately, the Dirichlet density does not possess these geometrical features as portrayed in Fig. 13 (this case corresponds to the parameterization with the scalar energy E_ϕ - the one based on covariance produces a similar shape). This mismatch is evidently translated into statistical disagreements. In an effort to overcome this deficiencies we propose a PDF (Fig. 14) which holds sufficient degrees of freedom and also behaves similarly to the joint PDF of reacting scalars:

$$\tilde{P}(\psi_1, \psi_2) = \frac{1}{C_N}(\psi_1^{\eta_1 - 1} + \psi_2^{\eta_2 - 1})(\psi_1 + \psi_2)^{\eta_3 - 1}(1 - \psi_1 - \psi_2 - \frac{\psi_1 \psi_2}{\eta_5})^{\eta_4 - 1} \qquad (40)$$

where C_N is the normalization constant. For the case considered here, this PDF is very accurate. However, there are two severe drawbacks which does not allow its use for general applications. First, the extension of this PDF for multiple scalars is not trivial. Second, it is not possible to relate the parameters of this PDF to the moments (or cross moments) of the random variable. While the first problem can be potentially overcome with availability of DNS data, the second problem is the compelling reason for abandoning this PDF for LES.

The data generated from DNS is now employed to validate the subgrid models and to determine the unknown model constant. In both 2D and 3D, a coarse grid is superimposed on the fine grid (*e.g.* $256^2 -> 32^2$ and $96^3 -> 16^3$) and all the relevant quantities are determined: averages, fluctuations and correlations (stresses and fluxes). The second order information

which is not available in LES is compared against the proposed closures. The inspection and statistical analysis of the scatter plots of the exact quantities vs. the predicted values provide qualitative and quantitative assessments. The correlation coefficient between the exact SGS stress and its closure is defined as:

$$C_{EM} = \frac{< (E - < E >)(M - < M >) >}{< (E - < E >)^2 >^{1/2} < (M - < M >)^2 >^{1/2}} \tag{41}$$

where the brackets denote the ensemble average. This correlation coefficient provides a proper mean of diagnosing the reliability of the closures. Examining the time histories of the correlation coefficients extracted for each SGS variable from 2D and 3D simulations, it can be concluded that the Smagorinsky closure and the one-equation model attain similar degrees of reliability even in compressible regimes. This point is illustrated in Fig. 15(a)-(d) for the xy SGS stresses, SGS species and covariance fluxes in x-direction and scalar dissipation. The degrees of correlation are relatively poor except for dissipation closures. A large variety of algorithms can be employed in the calculation of the model constants at various levels. We made determinations only at the scalar level using three techniques: mean matching, RMS matching and linear regression. The matching method involves the computation at each time step the ratios between the ensemble averages and between the RMS values, respectively:

$$C_A = \frac{< E >}{< M >}; \; C_{RMS} = \frac{< (E - < E >)^2 >^{1/2}}{< (M - < M >)^2 >^{1/2}}. \tag{42}$$

The linear regression method is applied to the scatter data obtained from time steps within a large eddy turnover time. The mean matching method produces variations of the ratio over several order of magnitudes. This reflects the deficiency of the models (Fig. 16). A smoother evolution is obtained through RMS matching (Fig. 17). The decisive estimation is provided by the linear regression based on a larger sample of data (Fig. 18) which displays

indeed relatively strong dispersion from a linear variation. Through this final procedure we fixed the values of the constants as follows: For the Smagorinsky model

$$C_R = 0.16;\ C_I = 0.008;\ C_\phi = 5.9; \tag{43}$$

and for the one-equation model

$$C_\nu = 0.034;\ C_\epsilon = 0.78;\ C_\phi = 2.1. \tag{44}$$

From the scatter of the species flux a turbulent Schmidt number was estimated at $Sc_t = 0.77$. Also, this value was assigned to the turbulent Prandtl number.

5.2 LES: *A posteriori* Analysis

The effective performance of the SGS models have to be proved by conducting actual LES with the same dynamical parameters as the peer DNS. In order to start the LES from an equivalent initial state the DNS fields are filtered and introduced into the coarse grid. The comparison between parallel simulations is achieved at each time step by filtering the DNS output.

The first test of the LES framework presented here is related to the fact that the assumed PDF has a considerable influence over the reacting scalar evolution. We used the results of 3D DNS of a binary mixing ($Da = 0$) field in a weakly compressible turbulence as the prime test for LES. In this case the transport of the SGS covariance decoupled from the other equations. The obliteration of the source terms in the chemical equations also removes the weight of the assumed PDF. In Fig. 19 the mixing structures are presented by means

of contour plots of the species field. These results are presented at one half turnover time. There is an overall agreement between the two pictures, the large scale structures being predicted fairly accurately. However, the small scale structures appear to be different in some areas. Comparisons can be made in a global sense considering various moments of the LES scalars based on ensemble average. The resulting correlation (connected to the concept of unmixedness), the variance, the kurtosis and one of the cross third moment show satisfactory concordance with the DNS results (Fig. 20). A more stringent test stemming from the contrast at the subgrid level divulge inadequate evolutions of the second order SGS moments. Figures 21 and 22 depict the time evolution of the SGS variables at different locations (starting with different initial values). Although the SGS mean species evolve in group, there are visible discrepancies in the predictions of the covariance and turbulent kinetic energy, as a consequence of the inferior quality of the models.

The non-equilibrium chemistry case was investigated for a relatively high rate of reaction $Da = 5$. In the present situation, a correct appreciation of the output from LES must be weighted with respect to the degree of success exhibited by the PDF closure. Namely, after examining Figs. 23 and 24, the results could be considered "satisfactory." The predicted ensemble averages of the product and of the scalar A tend to give to the $k - \Delta$ model an advantage over the Smagorinsky closure. Further examination of the higher order moments enforces this opinion.

6 Results. II. Spatially Developing Planar Shear Flow

In employing assumed PDF methods in an actual LES, the filtered mean values and SGS moments of the scalar variable must be provided without resorting to DNS. Here, LES results obtained by the full Smagorinsky/PDF closure are presented to examine the overall

performance of the hybrid model. This examination is conducted for the mixing layer since it provides a more stringent test for model assessments. The formulation presented above is in a closed form with the specification of model constants appearing in the LES transport equations. Based on our investigations, it was clear that the magnitudes of these constants are *different* from those in the homogeneous flow simulations. Therefore, a nominal parametric study was done to re-estimate the values of these constants for the mixing layer simulations. From this study, the magnitudes of some of these constants were found also different from those typically used in RANS.[97] The results presented in the next section are based on $C_\phi = 0.15, Sc_t = \varsigma_k = 1.0, C_\nu = 0.01$, and $C_\epsilon = 0.5$. No attempt was made to determine the optimized values of these constants.

In Fig. 25, cross-stream profiles of the instantaneous streamwise velocity component are shown at several downstream locations. This figure shows that the large scale velocity field is predicted well in LES as the results compare reasonably well with those of filtered DNS. The comparison of the subgrid scale TKE as predicted by the model, with the TKE obtained from the filtered DNS are shown in Figs. 26-27. These figures also indicate a relatively good agreement between the LES predictions and the DNS filtered results. The exception is at far distances from the inlet, where it is shown that the TKE equation severely underpredicts the subgrid turbulence level. This trend has also been observed in the simulations of Ref.[22] and may be due to deficiencies in modeling of the Reynolds stresses in terms of the strain tensor alone. Inclusion of other terms such as the rotation tensor and/or products of the strain rate and rotation tensors may be necessary to improve the predictions of TKE.[93,98]

Figure 28 portrays the LES and DNS contours of the filtered mass fraction of species A in the non-reacting case. The agreement is generally good and the two results are relatively close. The difference is due to the effects of the gradient diffusion closure which results in smearing of the small scale features within the large scale coherent structures. The lack of agreement

becomes more pronounced for the covariance. This is shown in Fig. 29 where contour plots of the SGS species covariance are presented. Despite this difference, it is useful to examine the model's performance in the reacting shear flow LES. In Fig. 30, contour plots of the filtered product species mass fraction obtained from LES and DNS are presented. Figure 31 shows an instantaneous product thickness distribution obtained from the filtered DNS and LES data, including also some LES results without the PDF model. These figures suggest that LES captures the large scale feature in accord with DNS. The figures also suggest that the inclusion of SGS fluctuations gives results which are closer to DNS data than those predicted by the mean chemistry model. However, the PDF method still needs to be improved further in order to exhibit a better predictive capability.

The primary reasons for the discrepancies above are attributed to errors associated with: (1) the estimation of the covariance, and (2) the shape of the PDF. We feel that with the simplified reaction mechanism considered in this flow , the first factor is more important. This is indicated in Fig. 32, where contour plots of SGS covariance are presented. Again, while the LES and filtered DNS results show similar trends, the agreement is not very good (see Fig. 33 for a quantitative comparison of the covariance thickness). These two figures, along with Fig. 29 highlight the modeling deficiencies associated with the covariance transport equation for LES applications. Therefore, while this equation has been met with some success in RANS, its use here does not provide acceptable predictions. The same is true for the SGS kinetic energy as shown in Figs. 26-27. In this regard, it must be noted that these problems do not vanish in PDF approaches based on a transport equation for the single-point PDF (AMC, C/D, LMSE, *etc*). That is, the first two SGS moments must be determined by a reliable subgrid closure. The problem may be somewhat alleviated by considering the transport equations for SGS correlations.[99] This is very challenging and computationally demanding. Some saving in computations can be made by approximating the transport terms in the scalar flux equation in a way analogous to what is done in algebraic Reynolds stress closures

(see Refs.[100–102,93]). The performance of these more elaborate models are presently being assessed for the modeling of SGS covariance and TKE.

7 Some Remarks

During the past century, dating back to the early pioneering contributions in statistics and biometrics,[60,58,57,103] the construction of "appropriate" PDF shapes has been a subject of broad interest within the statistics and (old) biometrics research communities. The outgrowth of these contributions has been useful to investigators in other branches of physical science. In fact, in classical turbulence research, statistical methods[104] of one form or another had been the primary means of dealing with turbulence and its "random" causes and effects.[105–107] In statistical modeling of turbulent reacting flows, the use of PDF methods has proven particularly useful. This is especially true if the PDF (or joint PDF) of scalar quantities is considered. The preferred method is to obtain the PDF by means of its transport equation. This method is a subject of ongoing research[23] and there are still a number of questions in regard to its suitability for practical applications. LES can be viewed as an example of such an application, since it is viewed as more of a potential engineering tool than a robust scientific tool. With this view, assumed PDF methods are advocated as the present method of choice, at least in the context of the simple flows considered here.

In this work, an attempt has been made to borrow knowledge from the statistics literature in order to "presume" an appropriate PDF which performs reasonably well in LES. In simple flows of research interest such as a homogeneous box flow or a parallel shear flow this is a viable approach in light of the richness of literature on their behavior (see Ref.[86] for a recent review). Consistent with the current state of affairs in RANS, these PDF's are all considered in the context of a single point. This implies that all the moments up to the

second order (either Reynolds moments or SGS moments) have to be provided externally. Based on our earlier investigations along these lines,[52,54,56] the use of the Pearson family of PDF's appears to be most practical. This suggests a Beta density of the first kind for equilibrium (and frozen) chemistry, and the Dirichlet density for non-equilibrium chemistry. In the specific cases considered, the use of the Beta density provides a reasonable model for SGS probability description of a conserved scalar variable. However, its actual use in LES requires the knowledge of the filtered mean and the SGS variance. This is currently troublesome in that conventional turbulence closures do not seem to work well for predicting second order SGS moments. The same problem exists in LES of non-equilibrium flows and manifests itself in the inability to accurately predict SGS scalar covariance (and/or SGS scalar energy). Moreover, it is not clear which of the sets of low order moments are to be used to parameterize the multivariate PDF. This drawback is, however, deemed less troublesome in that the Dirichlet density can be replaced with other members of the joint Beta family which are constructed with a higher degree of freedom. Again, the statistics and biometrics literature can be helpful for this purpose, and this issue is currently under investigation.

At this point, it is useful to make some remarks in regard to some situations where assumed PDF methods are not very successful. These correspond to cases where an obvious choice for the PDF can not be made. For example, in highly non-equilibrium flames with complex multi-step multi-scalar chemistry with strong temperature dependent reactions rates. In LES of such flows, the application of the PDF transport equation may also be difficult. However, other less computational intensive closures may prove useful. For example, the "laminar diffusion flamelet model",[108,64,109,110,18] or the "conditional moment method"[111-113] may provide some alternatives. An appraisal study of the performance of these models in RANS of turbulent mixing layers has been reported in Ref.[114] The first model is applicable to cases where chemical reactions occur in a narrow region near the flame surface. For sufficiently fast chemistry, but with finite values of the Damkōhler number, the flame is

located somewhere within the (unresolved) subgrid. The actual LES with this model requires the construction of a flamelet library within the subgrid by which the reacting scalar values can be approximated. The approximation requires the knowledge of the filtered mean values of the mixture fraction (*e.g.* the Shvab-Zeldovich variable), and its SGS rate of dissipation. Therefore, modeled transport equations are needed to approximate these quantities. How effectively the dissipation field can be modeled and how accurate the whole procedure would be, needs to be determined. The second approach can be considered somewhere between the PDF approach and traditional moment methods. In its implementation for LES, the averages of the reacting scalar field are defined "conditionally" on the values of the mixture fraction. The argument in support of this closure is that such conditional statistics portray less scatter than their unconditional counterparts. Therefore, their treatment may be easier. However, an extra dimensionality (associated with the domain of the mixture fraction) is involved. Also, the actual application of the model requires the input of the SGS conditional expected dissipation. This could be very difficult since the behavior of this dissipation is less understood.[53] Furthermore, as discussed in Ref.,[114] the use of the model can be recommended only for determining the first order moments in flames near equilibrium. This is acceptable if the mean compositional structure in near-equilibrium flames is desired. Otherwise, the usage of the method is complicated in RANS and even more complex in LES.

8 Further Information

As indicated in the abstract of this report, here we have *only* discussed the results of our efforts pertaining to LES of turbulent reacting flows. Also, as indicated in the abstract, the scope of the research conducted under this grant is much more broad - perhaps much more than that can be described in a single report. No attempt is, therefore, made

here to describe all our contributions. However, for those who are interested we refer to Refs.[115,80,52,116,117,56,118,88,96] Copies of some of these papers are provided in Appendix I through Appendix VII.

Mr. Craig J. Steinberger is the other Graduate Research Assistant supported partially by this Grant. For a summary of his contributions, please see the appendices.

References

[1] Givi, P., Model Free Simulations of Turbulent Reactive Flows, *Prog. Energy Combust. Sci.*, **15**:1–107 (1989).

[2] Reynolds, W. C., The Potential and Limitations of Direct and Large Eddy Simulations, In Lumley,[119] pp. 313–343.

[3] Hussaini, M. Y., Speziale, C. G., and Zang, T. A., The Potential and Limitations of Direct and Large Eddy Simulations, In Lumley,[119] pp. 354–368.

[4] Givi, P., Spectral and Random Vortex Methods in Turbulent Reacting Flows, in Libby, P. A. and Williams, F. A., editors, *Turbulent Reacting Flows*, Academic Press, London, UK, 1993, in press.

[5] Ferziger, J. H., Higher Level Simulations of Turbulent Flows, Stanford University Report TF-16, Department of Mechanical Engineering, Stanford University, Stanford, CA, 1981.

[6] Ferziger, J. H., Higher-Level Simulations of Turbulent Flows, in Essers, J. H., editor, *Computational Methods for Turbulent, Transonic and Viscous Flows*, pp. 93–182, Hemisphere Publishing Co., 1983.

[7] Rogallo, R. S. and Moin, P., Numerical Simulation of Turbulent Flow, *Ann. Rev. Fluid Mech.*, **16**:99–137 (1984).

[8] Ferziger, J. H., Large Eddy Simulations: Its Role in Turbulence Research, in Dwoyer, D. L., Hussaini, M. Y., and Voigt, R. G., editors, *Theoretical Approaches in Turbulence*, pp. 51–72, Springer-Verlag, New York, NY, 1987.

[9] Love, M. D., An Introduction to the Large Eddy Simulation Technique, *J. Inst. Nuc. Eng.*, **20**(2):35–42 (1979).

[10] Ferziger, J. H. and Leslie, D. C., Large Eddy Simulation: A Predictive Approach to Turbulent Flow Computation, AIAA Paper 79-1471, 1979.

[11] Voke, P. R. and Collins, M. W., Large Eddy Simulation: Petrospect and Prospect, *PhysicoChemical Hydrodynamics*, **4**(2):119–161 (1983).

[12] Schumann, U. and Friedrich, R., editors, *Direct and Large Eddy Simulations of Turbulence*, Proc. EUROMECH Coll. No. 199, Vieweg-Verlag, Braunschweig, 1986.

[13] Schumman, U. and Friedrich, R., On Direct and Large Eddy Simulation of Turbulence, in Comte-Bellot, G. and Mathieu, J., editors, *Advances in Turbulence*, pp. 88–104, Springer-Verlag, 1987.

[14] Jou, W.-H. and Riley, J. J., Progress in Direct Numerical Simulations of Turbulent Reacting Flows, *AIAA J.*, **27**(11):1543–1556 (1989).

[15] Moin, P., Towards Large Eddy and Direct Numerical Simulations of Complex Turbulent Flows, *Computer Methods in Applied Mechanics and Engineering*, **87**:329–334 (1991).

[16] Galperin, B. and Orszag, S. A., editors, *Large Eddy Simulations of Complex Engineering and Geophysical Flows*, Cambridge University Press, Cambridge, U.K., 1993, in press.

[17] Smagorinsky, J., General Circulation Experiments With the Primitive Equations. I. The Basic Experiment, *Monthly Weather Review*, **91**(3):99–164 (1963).

[18] Williams, F. A., *Combustion Theory*, The Benjamin/Cummings Publishing Company, Menlo Park, CA, 2nd edition, 1985.

[19] Lilly, D. K., The Representation of Small-Scale Turbulence in Numerical Simulation Experiments, in *Proceedings of IBM Scientific Computing Symposium Environmental Sciences*, pp. 195–210, IBM Form No. 320-1951, 1967.

[20] Schumman, U., Subgrid Scale Model for Finite Difference Simulations of Turbulent Flows in Plane Channels and Annuli, *J. Comp. Phys.*, **18**:376–404 (1975).

[21] Horuiti, K., Large Eddy Simulation of Turbulent Channel Flow by One-Equation Modeling, *J. Phys. Soc. Japan*, **54**(8):2855–2865 (1985).

[22] Claus, R. W., Huang, P. G., and MacInnes, J. M., Mesh Refinement in a Two-Dimensional Large Eddy Simulation of a Forced Shear Layer, NASA TM 102129, 1989.

[23] Pope, S. B., Computations of Turbulent Combustion: Progress and Challenges, in *Proceedings of 23rd Symp. (Int.) on Combustion*, pp. 591–612, The Combustion Institute, Pittsburgh, PA, 1990.

[24] Schumann, U., Large Eddy Simulation of Turbulent Diffusion with Chemical Reactions in the Convective Boundary Layer, *Atmospheric Environment*, **23**(8):1713–1726 (1989).

[25] Libby, P. A. and Williams, F. A., editors, *Turbulent Reacting Flows*, *Topics in Applied Physics*, Vol. 44, Springer-Verlag, Heidelberg, 1980.

[26] Kollmann, W., *Prediction Methods for Turbulent Flows*, Hemisphere Publishing Co., New York, NY, 1980.

[27] Jones, W. P. and Whitelaw, J. H., Calculation Methods for Reacting Turbulent Flows: A Review, *Combust. Flame*, **48**:1–26 (1982).

[28] Brodkey, R. S., editor, *Turbulence in Mixing Operation*, Academic Press, New York, NY, 1975.

[29] Toor, H. L., The Non-Premixed Reaction: $A + B \rightarrow Products$, in Brodkey, R. S., editor, *Turbulence in Mixing Operations*, pp. 123–166, Academic Press, New York, NY, 1975.

[30] Hill, J. C., Homogeneous Turbulent Mixing with Chemical Reaction, *Ann. Rev. Fluid Mech.*, **8**:135–161 (1976).

[31] Brodkey, R. S., Fundamental of Turbulent Motion, *Chem. Eng. Comm.*, **8**:1–23 (1981).

[32] Toor, H. L., Mass Transfer in Dilute Turbulent and Nonturbulent Systems with Rapid Irreversible Reactions and Equal Diffusivities, *AIChE J.*, **8**:70–78 (1962).

[33] Dopazo, C., Non-Isothermal Turbulent Reactive Flows: Stochastic Approaches, Ph.D. Thesis, Department of Mechanical Engineering, State University of New York at Stony Brook, Stony Brook, NY, 1973.

[34] Pope, S. B., The Statistical Theory of Turbulent Flames, *Phil. Trans. Royal Soc. London*, **291**(1384):529–568 (1979).

[35] O'Brien, E. E., The Probability Density Function (PDF) Approach to Reacting Turbulent Flows, in Libby, P. A. and Williams, F. A., editors, *Turbulent Reacting Flows*, chapter 5, pp. 185–218, Springer-Verlag, Heidelberg, 1980.

[36] Pope, S. B., PDF Methods for Turbulent Reacting Flows, *Prog. Energy Combust. Sci.*, **11**:119–192 (1985).

[37] Kollmann, W., The pdf Approach to Turbulent Flow, *Theoret. Comput. Fluid Dynamics*, **1**:249–285 (1990).

[38] Libby, P. A. and Williams, F. A., editors, *Turbulent Reacting Flows*, Academic Press, London, UK, 1993, in press.

[39] Lundgren, T. S., Distribution Functions in the Statistical Theory of Turbulence, *Phys. Fluids*, **10**(5):969–975 (1967).

[40] Lundgren, T. S., Model Equation for Nonhomogeneous Turbulence, *Phys. Fluids*, **12**(3):485–497 (1969).

[41] Curl, R. L., Dispersed Phase Mixing: I. Theory and Effects in Simple Reactors, *AIChE J.*, **9**(2):175–181 (1963).

[42] Janicka, J., Kolbe, W., and Kollmann, W., Closure of the Transport Equation for the Probability Density Function of Turbulent Scalar Field, *J. Nonequil. Thermodyn.*, **4**:47–66 (1979).

[43] Norris, A. T. and Pope, S. B., Turbulent Mixing Model Based on Ordered Pairing, *Combust. Flame*, **83**:27 (1991).

[44] Dopazo, C. and O'Brien, E. E., Statistical Treatment of Non-Isothermal Chemical Reactions in Turbulence, *Combust. Sci. and Tech.*, **13**:99–112 (1976).

[45] Pope, S. B., A Monte Carlo Method for the PDF Equations of Turbulent Reactive Flow, *Combust. Sci. and Tech.*, **25**:159–174 (1981).

[46] Pope, S. B., An Improved Turbulent Mixing Model, *Combust. Sci. and Tech.*, **28**:131–145 (1982).

[47] Kosaly, G. and Givi, P., Modeling of Turbulent Molecular Mixing, *Combust. Flame*, **70**:101–118 (1987).

[48] McMurtry, P. A. and Givi, P., Direct Numerical Simulations of Mixing and Reaction in a Nonpremixed Homogeneous Turbulent Flow, *Combust. Flame*, **77**:171–185 (1989).

[49] Kraichnan, R. H., Closures for Probability Distributions, *Bull. Amer. Phys. Soc.*, **34**:2298 (1989).

[50] Chen, H., Chen, S., and Kraichnan, R. H., Probability Distribution of a Stochastically Advected Scalar Field, *Phys. Rev. Lett.*, **63**(24):2657–2660 (1989).

[51] Pope, S. B., Mapping Closures for Turbulent Mixing and Reaction, *Theoret. Comput. Fluid Dynamics*, **2**:255–270 (1991).

[52] Madnia, C. K., Frankel, S. H., and Givi, P., Reactant Conversion in Homogeneous Turbulence: Mathematical Modeling, Computational Validations and Practical Applications, *Theoret. Comput. Fluid Dynamics*, **4**:79–93 (1992).

[53] Jiang, T.-L., Gao, F., and Givi, P., Binary and Trinary Scalar Mixing by Fickian Diffusion-Some Mapping Closure Results, *Phys. Fluids A*, **4**(5):1028–1035 (1992).

[54] Frankel, S. H., Madnia, C. K., and Givi, P., Comparative Assessment of Closures for Turbulent Reacting Flows, *AIChE J.*, **39**(5):899–903 (1993).

[55] Frankel, S. H., Jiang, T.-L., and Givi, P., Modeling of Isotropic Reacting Turbulence by a Hybrid Mapping-EDQNM Closure, *AIChE J.*, **38**(4):535–543 (1992).

[56] Miller, R. S., Frankel, S. H., Madnia, C. K., and Givi, P., Johnson-Edgeworth Translation for Probability Modeling of Binary Mixing in Turbulent Flows, *Combust. Sci. and Tech.*, **91**(1-3):21–52 (1993).

[57] Johnson, N. L., Systems of Frequency Curves Generated by Methods of Translation, *Biometrika*, **36**:149–176 (1949a).

[58] Edgeworth, F. Y., On the Representation of Statistical Frequency by a Series, *Journal of the Royal Statistical Society, Series A.*, **70**:102–106 (1907).

[59] Gao, F., An Analytical Solution for the Scalar Probability Density Function in Homogeneous Turbulence, *Phys. Fluids A*, **3**(4):511–513 (1991).

[60] Pearson, K., Contributions to the Mathematical Theory of Evolution: II. Skew Variations in Homogeneous Material, *Philos. Trans. of the Royal Soc. of London, Series A.*, **186**:343–414 (1895).

[61] Rhodes, P. R., A Probability Distribution Function for Turbulent Flows, in Murthy, S. N. B., editor, *Turbulent Mixing in Non-Reactive and Reactive Mixing*, pp. 235–241, Plenum Press, New York, NY, 1975.

[62] Jones, W. P. and Priddin, C. H., Predictions of the Flowfield and Local Gas Composition in Gas Turbine Combustors, in *17th Symp. (Int.) on Combustion*, pp. 399–409, The Combustion Institute, Pittsburgh, PA, 1978.

[63] Lockwood, F. C. and Moneib, H. A., Fluctuating Temperature Measurement in a Heated Round Free Jet, *Combust. Sci. and Tech.*, **22**:63–81 (1980).

[64] Peters, N., Laminar Diffusion Flamelet Models In Non-Premixed Turbulent Combustion, *Prog. Energy Combust. Sci.*, **10**:319–339 (1984).

[65] Janicka, J. and Peters, N., Prediction of Turbulent Jet Diffusion Flame Lift-Off Using a PDF Transport Equation, in *Proceedings of 19th Symp. (Int.) on Combustion*, pp. 367–374, The Combustion Institute, Pittsburgh, PA, 1982.

[66] Frankel, S. H., Drummond, J. P., and Hassan, H. A., A Hybrid Reynolds Averaged/PDF Closure Model For Supersonic Turbulent Combustion, AIAA paper 90-1573, 1990.

[67] Priddin, C. H., Turbulent Combustion Modeling-A Review, in Johansson, A. V. and Alfredsson, P. H., editors, *Advances in Turbulence 3*, pp. 279–299, Springer-Verlag, Berlin, 1991.

[68] Johnson, M. E., *Multivariate Statistical Simulation*, John Wiley and Sons, New York, NY., 1987.

[69] Johnson, N. L. and Kotz, S., *Distributions in Statistics: Continious Multivariate Distributions*, John Wiley and Sons, New York, NY, 1972.

[70] Wilks, S. S., *Mathematical Statistics*, Wiley, New York, NY, 2nd edition, 1962.

[71] Narumi, S., On the General Form of Bivariate Frequency Distributions Which are Mathematically Possible When Regression and Variation are Subjected to Limiting Conditions, I, *Biometrika*, **15**:77–88 (1923).

[72] Erlebacher, G., Hussaini, M. Y., Speziale, C. G., and Zang, T. A., Toward the Large Eddy Simulation of Compressible Turbulent Flows, ICASE Report 87-20, NASA Langley Research Center, Hampton, VA, 1987, Also available as *NASA CR 178273.*

[73] Erlebacher, G., Hussaini, M. Y., Speziale, C. G., and Zang, T. A., Toward the Large Eddy Simulation of Compressible Turbulent Flows, ICASE Report 90-76, NASA Langley Research Center, Hampton, VA, 1990, Also available as *NASA CR 187460.*

[74] Erlebacher, G., Hussaini, M. Y., Speziale, C. G., and Zang, T. A., Toward the Large Eddy Simulation of Compressible Turbulent Flows, *J. Fluid Mech.*, **238**:155–185 (1992).

[75] Hussaini, M. Y. and Zang, T. A., Spectral Methods in Fluid Dynamics, *Ann. Rev. Fluid Mech.*, **19**:339–367 (1987).

[76] Canuto, C., Hussaini, M. Y., Quarteroni, A., and Zang, T. A., *Spectral Methods in Fluid Dynamics*, Springer-Verlag, New York, NY, 1987.

[77] Givi, P. and Madnia, C. K., Spectral Methods in Combustion, in Chung, T., editor, *Numerical Modeling in Combustion*, pp. 409–452, Hemisphere Publishing Co., New York, NY, 1993.

[78] Passot, T. and Pouquet, A., Numerical Simulation of Compressible Homogeneous Flows in the Turbulent Regime, *J. Fluid Mech.*, **181**:441–466 (1987).

[79] Givi, P. and McMurtry, P. A., Non-Premixed Reaction in Homogeneous Turbulence: Direct Numerical Simulations, *AIChE J.*, **34**(6):1039–1042 (1988).

[80] Madnia, C. K. and Givi, P., On DNS and LES of Homogeneous Reacting Turbulence, in Galperin, B. and Orszag, S. A., editors, *Large Eddy Simulations of Complex Engineering and Geophysical Flows*, Cambridge University Press, Cambridge, U.K., 1993, in press.

[81] Drummond, J. P., Two-Dimensional Numerical Simulation of a Supersonic, Chemically Reacting Mixing Layer, NASA TM 4055, 1988.

[82] Mukunda, H. S., Sekar, B., Carpenter, M. H., Drummond, J. P., and Kumar, A., Direct Simulation of High-Speed Mixing Layers, NASA TP 3186, 1992.

[83] Givi, P. and Jou, W.-H., Mixing and Chemical Reaction in a Spatially Developing Mixing Layer, *J. Nonequil. Thermodyn.*, **13**(4):355–372 (1988).

[84] Givi, P. and Jou, W.-H., Direct Numerical Simulations of a Two-Dimensional Reacting, Spatially Developing Mixing Layer by a Spectral Element Method, in *Proceedings of 22nd Symp. (Int.) on Combustion*, pp. 635–643, The Combustion Institute, Pittsburgh, PA, 1988.

[85] Lowery, P. S., Reynolds, W. C., and Mansour, N. N., Passive Scalar Entrainment and Mixing in a Forced, Spatially-Developing Mixing Layer, AIAA Paper 87-0132, 1987.

[86] Givi, P. and Riley, J. J., Some Current Issues in the Analysis of Reacting Shear Layers: Computational Challenges, in Hussaini, M. Y., Kumar, A., and Voigt, R. G., editors, *Major Research Topics in Combustion*, pp. 588–650, Springer-Verlag, 1992.

[87] McMurtry, P. A. and Givi, P., Spectral Simulations of Reacting Turbulent Flows, in Oran, E. S. and Boris, J. P., editors, *Numerical Approaches to Combustion Modeling*, *Progress in Astronautics and Aeronautics*, Vol. 135, chapter 9, pp. 257–303, AIAA Publishing Co., Washington, D.C., 1991.

[88] Drummond, J. P. and Givi, P., Suppression and Enhancement of Mixing in High-Speed Reacting Flow Fields, in Buckmaster, J. D., Jackson, T. L., and Kumar, A., editors, *Combustion in High-Speed Flows*, 1993, in press.

[89] Bilger, R. W., Perturbation Analysis of Turbulent Nonpremixed Combustion, *Combust. Sci. and Tech.*, **22**:251–261 (1980).

[90] Aldama, A. A., *Filtering Techniques for Turbulent Flow Simulations, Lecture Notes in Engineering*, Vol. 49, Springer-Verlag, New York, NY, 1990.

[91] Kwak, D., Reynolds, W. C., and Ferziger, J. H., Three Dimensional Time Dependent Computation of Turbulent Flows, Stanford University Report TF-5, Department of Mechanical Engineering, Stanford University, Stanford, CA, 1975.

[92] Mansour, N. N., Ferziger, J. H., and Reynolds, W. C., Large Eddy Simulations of a Turbulent Mixing Layer, Report TF-11, Department of Mechanical Engineering, Stanford University, Stanford, CA, 1978.

[93] Taulbee, D. B., An Improved Algebraic Reynolds Stress Model and Corresponding Nonlinear Stress Model, *Phys. Fluids A*, 4(11):2555–2561 (1992).

[94] Mardia, K. V., *Families of Bivariate Distributions*, Hefner Publishing Company, Darien, Conn., 1970.

[95] Frankel, S. H., Probabilistic and Deterministic Description of Turbulent Flows with Nonpremixed Reactants, Ph.D. Thesis, Department of Mechanical and Aerospace Engineering, State University of New York at Buffalo, Buffalo, NY, 1993.

[96] Frankel, S. H., Adumitroaie, V., Madnia, C. K., and Givi, P., Large Eddy Simulations of Turbulent Reacting Flows by Assumed PDF Methods, in Ragab, S. A. and Piomelli, U., editors, *Engineering Applications of Large Eddy Simulations, FED-Vol. 162*, pp. 81–101, ASME, 1993.

[97] Launder, B. E. and Spalding, D. B., *Lectures in Mathematical Modeling of Turbulence*, Academic Press, 1972.

[98] Lund, T. S. and Novikov, E. A., Parameterization of Subgrid-Scale Stress by the Velocity Gradient Tensor, Ctr manuscript, Center for Turbulence Research Annual Brief, Stanford, CA, 1991.

[99] Taulbee, D. B., Engineering Turbulence Models, in George, W. K. and Arndt, R., editors, *Advances in Turbulence*, pp. 75–125, Hemisphere Publishing Corp., New York, N.Y., 1989.

[100] Gibson, M. M. and Launder, B. E., On the Calculation of Horizontal, Turbulent, Free Shear Flows Under Gravitational Influence, *ASME Journal of Heat Transfer*, **98C**:81–87 (1976).

[101] Rodi, W., Turbulence Models for Environmental Problems, In Kollmann,[26] pp. 260–349.

[102] Schmidt, H. and Schumann, U., Coherent Structure of the Convective Boundary Layer Derived from Large-Eddy Simulations, *J. Fluid Mech.*, **200**:511–562 (1989).

[103] Johnson, N. L., Bivariate Distributions Based on Simple Translation Systems, *Biometrika*, **36**:297–304 (1949b).

[104] Taylor, G. I., Statistical Theory of Turbulence, *Proc. Roy. Soc. (A).*, **151**:421–478 (1935).

[105] Panchev, S., *Random Functions and Turbulence*, Pergamon Press, Oxford, U.K., 1970.

[106] Lumley, J. L., *Stochastic Tools in Turbulence*, Academic Press, New York, NY, 1970.

[107] Lesieur, M., *Turbulence in Fluids*, Kluwer Academic Publishers, Boston, MA, 1990, Second Revised Edition.

[108] Williams, F. A., Recent Advances in Theoretical Description of Turbulent Diffusion Flames, in Brodkey, R. S., editor, *Turbulence in Mixing Operations*, pp. 189–209, Academic Press, New York, NY, 1975.

[109] Peters, N., Laminar Flamelet Concepts in Turbulent Combustion, in *Proceedings of 21st Symp. (Int.) on Combustion*, pp. 1231–1250, The Combustion Institute, Pittsburgh, PA, 1986.

[110] Peters, N. and Williams, F. A., Liftoff Characteristics of Turbulent Jet Diffusion Flames, *AIAA J.*, **21**:423–429 (1983).

[111] Bilger, R. W., Conditional Moment Closure for Turbulent Reacting Flow, *Phys. Fluids A.*, **5**(2):436–444 (1993).

[112] Smith, N. S., Bilger, R. W., and Chen, J.-Y., Modeling of Non-premixed Hydrogen Jet Flames Using a Conditional Moment Closure Method, in *Proceedings of 24th Symp. (Int.) on Combustion*, pp. 271–278, The Combustion Institute, Pittsburgh, PA, 1992.

[113] Klimenko, A. Y., Multicomponent Diffusion of Various Mixtures in Turbulent Flow, *Fluid Dynamics*, **25**:327–334 (1990).

[114] Miller, R. S., Madnia, C. K., and Givi, P., Structure of a Turbulent Reacting Mixing Layer, *Combust. Sci. and Tech.*, (1993), in press.

[115] Givi, P., Madnia, C. K., Steinberger, C. J., Carpenter, M. H., and Drummond, J. P., Effects of Compressibility and Heat Release in a High Speed Reacting Mixing Layer, *Combust. Sci. and Tech.*, **78**:33–68 (1991).

[116] Frankel, S. H., Madnia, C. K., and Givi, P., Modeling of the Reactant Conversion Rate in a Turbulent Shear Flow, *Chem. Eng. Comm.*, **113**:197–209 (1992).

[117] Steinberger, C. J., Model Free Simulations of a High Speed Reacting Mixing Layer, AIAA Paper 92-0257, 1992.

[118] Steinberger, C. J., Vidoni, T. J., and Givi, P., The Compositional Structure and the Effects of Exothermicity in a Nonpremixed Planar Jet Flame, *Combust. Flame*, (1993), in press.

[119] Lumley, J. L., editor, *Whither Turbulence? Turbulence at the Crossroads, Lecture Notes in Physics*, Vol. 357, Springer-Verlag, 1990.

Figure Captions

Figure 1: Pressure contours for the high compressible case.

Figure 2: Balance of turbulent kinetic energy transport equation.

Figure 3: Mass fraction contours of reacting scalar A, $Da = 10$.

Figure 4: Balance of transport equations for: (a) Reactants covariance, (b) reactant A variance, (c) time evolution of the mean magnitudes of the scalars and the scalar Favre fluctuations.

Figure 5: Temporal variations of the scalar statistics under ensemble and Favre ensemble averaging: (a) Mean, (b) covariance, (c) variance, (d) third order joint moment.

Figure 6: Temporal variations of the (a) second and (b) the third order Favre cross moments, using the means-scalar energy parameterization.

Figure 7: Temporal variations of the (a) second and (b) the third order Favre cross moments, using a means-covariance parameterization.

Figure 8: Snapshot in the composition space of the scalar joint PDF after 1/10 turnover time.

Figure 9: Snapshot in the composition space of the scalar joint PDF after 1/2 turnover time.

Figure 10: Snapshot in the composition space of the scalar joint PDF after one turnover time.

Figure 11: Snapshot in the composition space of the scalar subgrid joint PDF after one turnover time.

Figure 12: Contour representation in the composition space of the scalar joint PDF after 1/2 turnover time.

Figure 13: Dirichlet distribution with the means-scalar energy parameterization after 1/2 turnover time.

Figure 14: Proposed joint PDF after 1/2 turnover time.

Figure 15: Temporal evolution of the correlation coefficients (between exact value and closure) for SGS quantities: (a) xy stress, (b) species x-flux, (c) covariance flux, (d) scalar dissipation.

Figure 16: Temporal evolution of the mean ratio (exact/closure) for SGS quantities: (a) xy stress, (b) species x-flux, (c) covariance flux, (d) scalar dissipation.

Figure 17: Temporal evolution of the RMS ratio (exact /closure) for SGS quantities: (a) xy-stress, (b) species x-flux, (c) covariance flux, (d) scalar dissipation.

Figure 18: Scatter plots of the exact versus $k - \Delta$ closure for SGS quantities: (a) xy-stress, (b) species x-flux, (c) dissipation, (d) scalar dissipation.

Figure 19: Mixing structures in a binary reacting field after one turnover time: (a) DNS, (b) LES.

Figure 20: Temporal variation in the global statistics of the SGS scalars: (a) covariance, (b) variance, (c) kurtosis, (d) third order cross moment, $Da = 0$.

Figure 21: Temporal variation of the SGS variables (location 1): (a) mean of scalar A, (b) mean of scalar B, (c) covariance, (d) turbulent kinetic energy, $Da = 0$.

Figure 22: Temporal variation of the SGS variables (location 2): (a) mean of scalar A, (b) mean of scalar B, (c) covariance, (d) turbulent kinetic energy, $Da = 0$.

Figure 23: Temporal variation in the global statistics of the SGS scalars: (a) mean product, (b) mean scalar A, (c) super-skewness, (d) fifth order cross moment, $Da = 5$.

Figure 24: Temporal variation in the global statistics of the SGS scalars: (a) covariance, (b) variance, (c) kurtosis, (d) third order cross moment, $Da = 5$.

Figure 25. Cross-stream variations of the of streamwise filtered velocity at several streamwise locations of the mixing layer. (a) $x = 5\delta$, (b) $x = 20\delta$, (c) $x = 25\delta$.

Figure 26. Plot of subgrid scale turbulent kinetic energy contours. (a) LES, (b) DNS.

Figure 27. Cross-stream variations of the of subgrid kinetic energy at several streamwise locations of the mixing layer. (a) $x = 5\delta$, (b) $x = 20\delta$, (c) $x = 25\delta$.

Figure 28. Plot of subgrid averaged species A mass fraction contours for non-reacting mixing layer. (a) LES, (b) DNS.

Figure 29. Plot of subgrid scale covariance contours for the non-reacting mixing layer. (a) LES, (b) DNS.

Figure 30. Plot of product species mass fraction contours in the reacting mixing layer with $Da = 10$ (a) LES, (b) DNS.

Figure 31. Streamwise variation of the instantaneous product mass fractions thickness for the reacting mixing layer with $Da = 10$.

Figure 32. Plots of subgrid scale covariance contours for the reacting mixing layer with $Da = 10$. (a) LES, (b) DNS.

Figure 33. Streamwise variation of the instantaneous covariance thickness for the reacting mixing layer with $Da = 10$

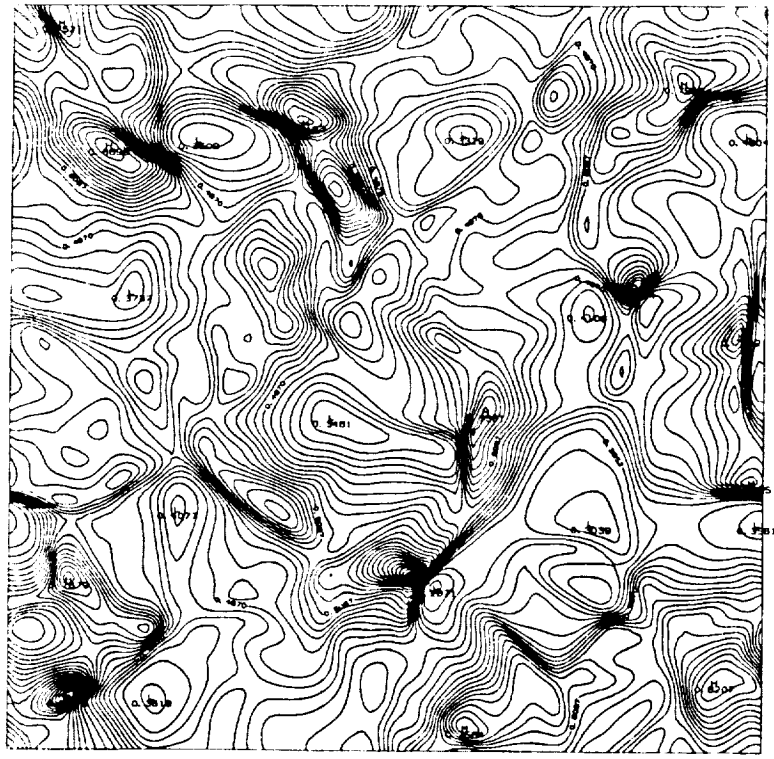

Figure 1

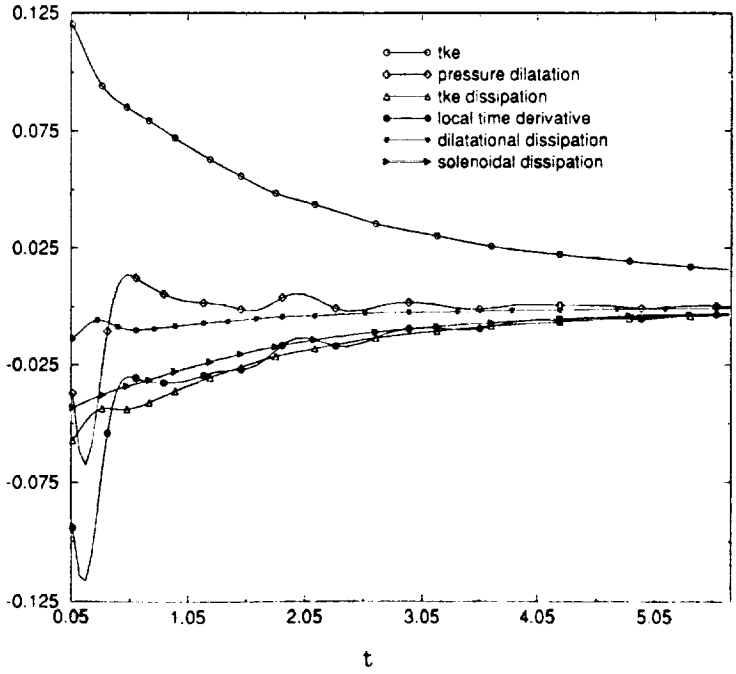

Figure 2

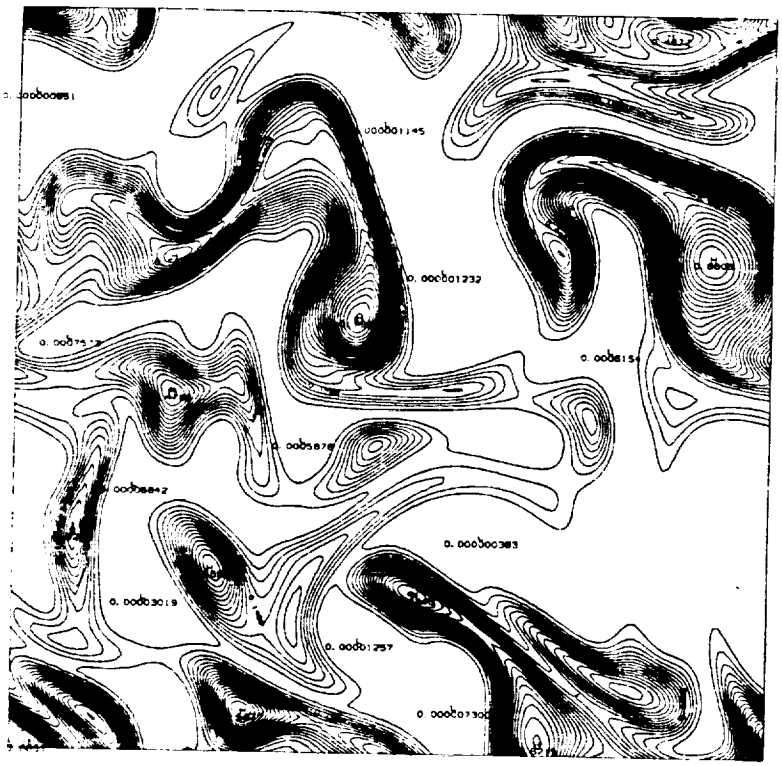

Figure 3

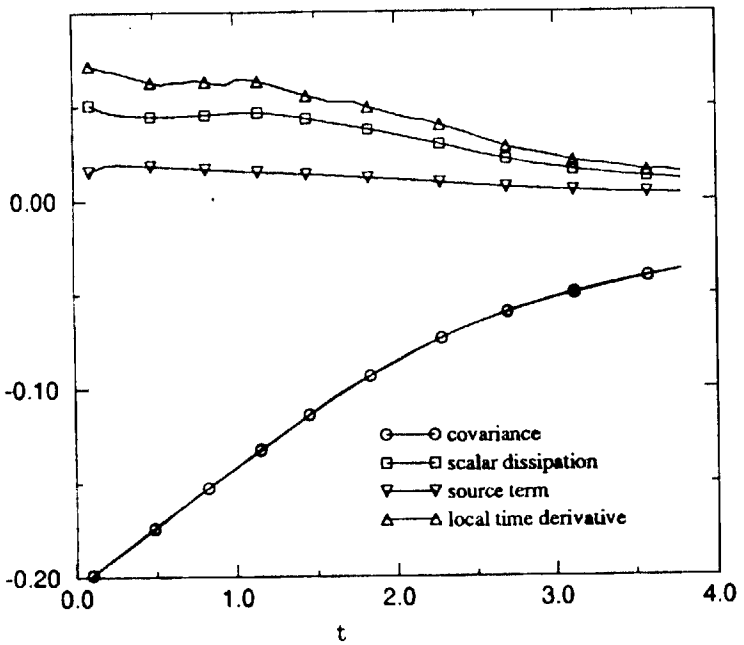
0.00
-0.10
-0.20
0.0
1.0
2.0
3.0
4.0
t
covariance
scalar dissipation
source term
local time derivative

(a)

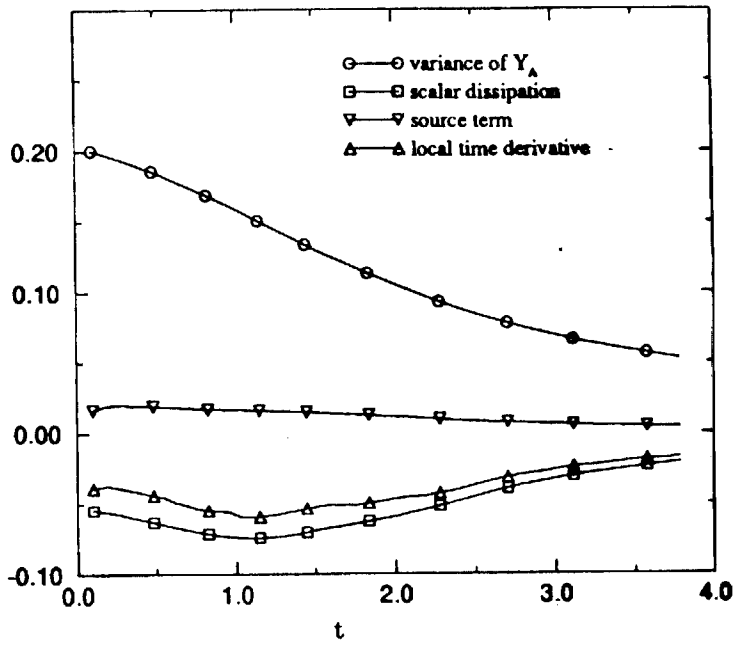
0.20
0.10
0.00
-0.10
0.0
1.0
2.0
3.0
4.0
t
variance of Y_A
scalar dissipation
source term
local time derivative

(b)

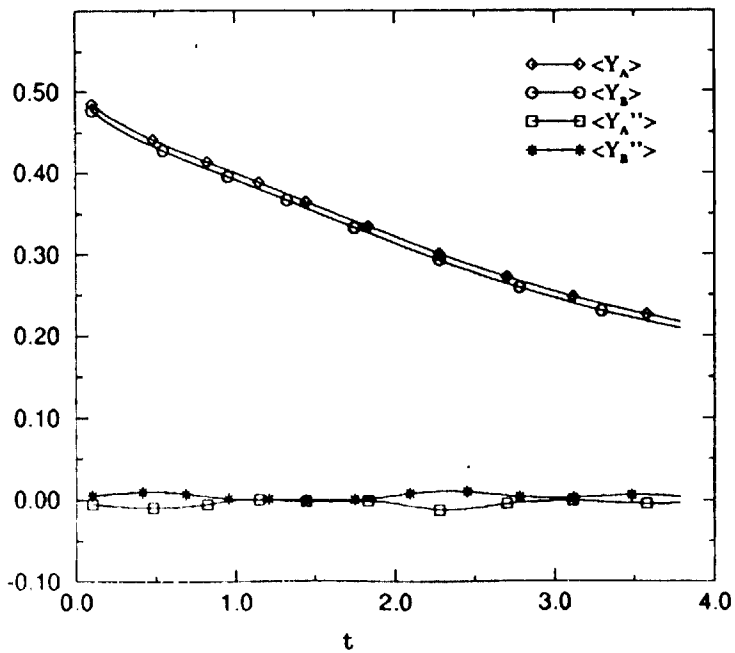
0.50
0.40
0.30
0.20
0.10
0.00
-0.10
0.0
1.0
2.0
3.0
4.0
t
$\langle Y_A \rangle$
$\langle Y_B \rangle$
$\langle Y_A'' \rangle$
$\langle Y_B'' \rangle$

(c)

Figure 4

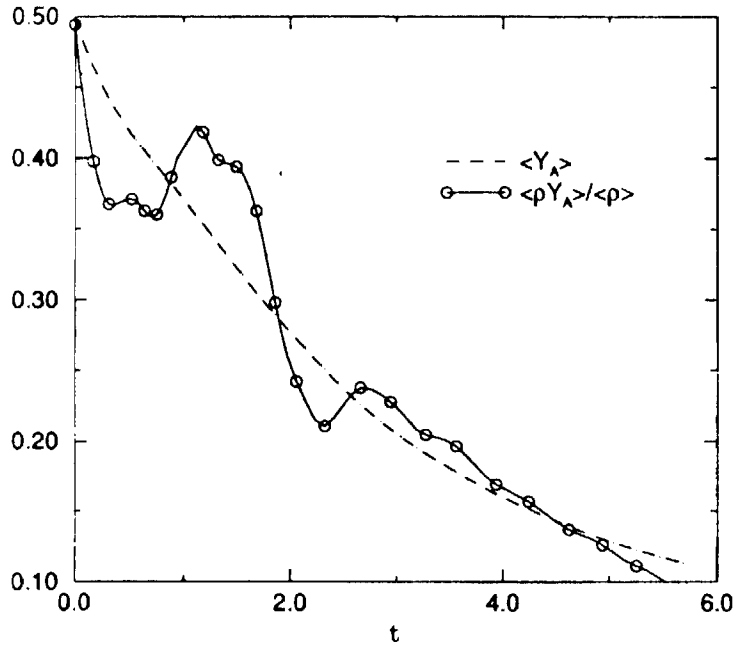

(a)

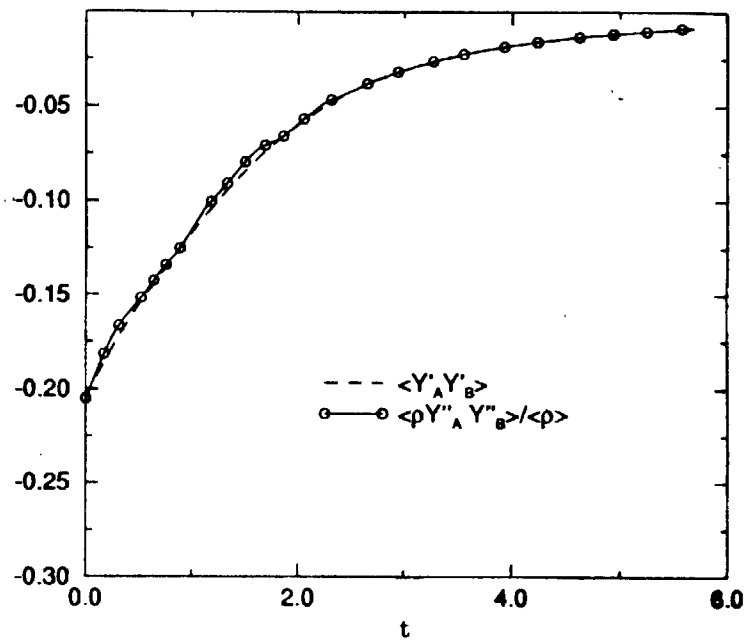

(b)

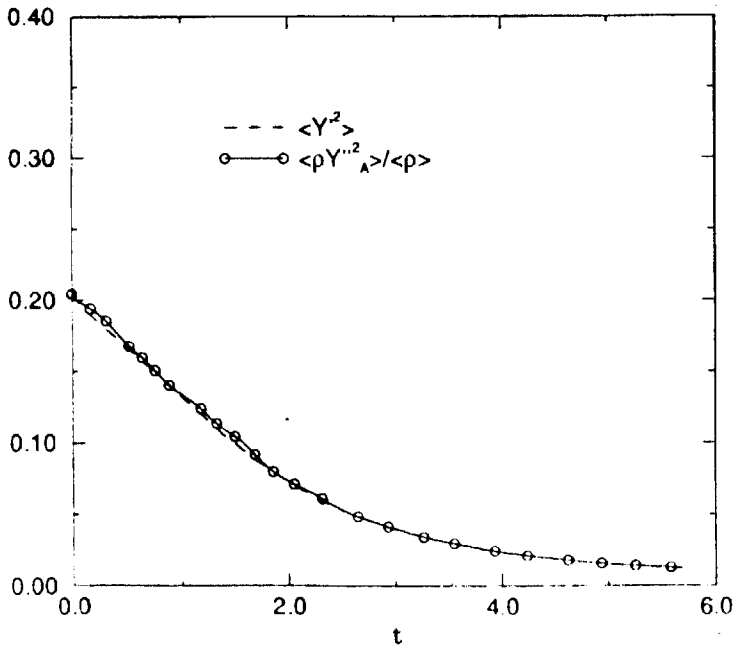

(c)

Figure 5

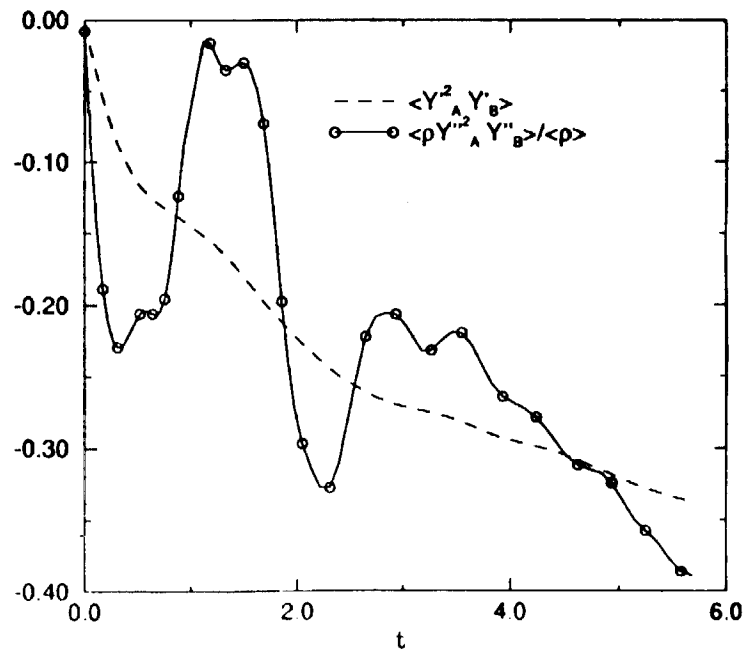

(d)

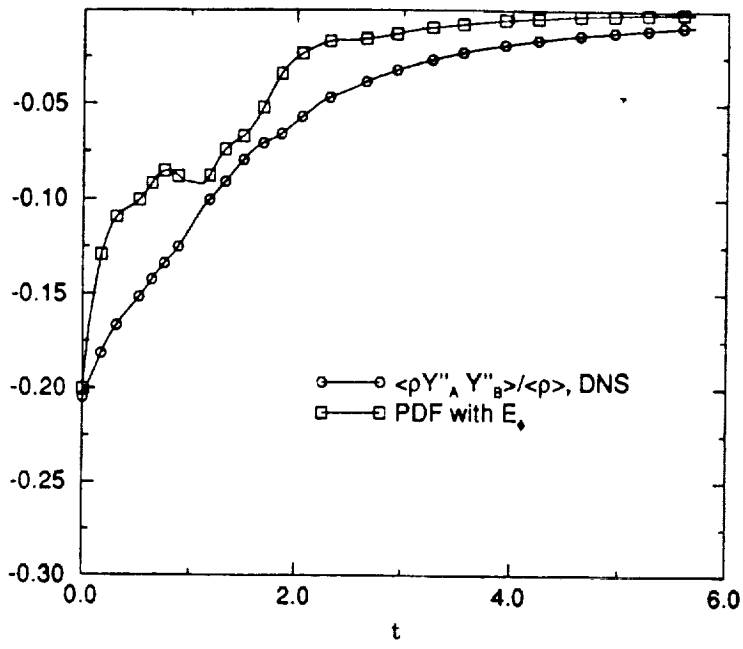
-0.05
-0.10
-0.15
-0.20
-0.25
-0.30
0.0
2.0
4.0
6.0
t
<ρY"A Y"B>/<ρ>, DNS
PDF with Eφ

(a)

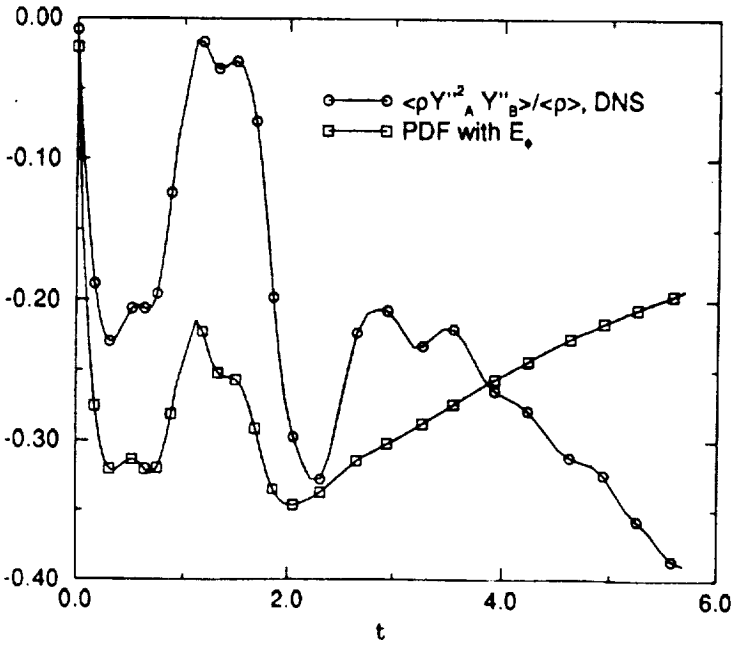
0.00
-0.10
-0.20
-0.30
-0.40
0.0
2.0
4.0
6.0
t
<ρY"2A Y"B>/<ρ>, DNS
PDF with Eφ

(b)

Figure 6

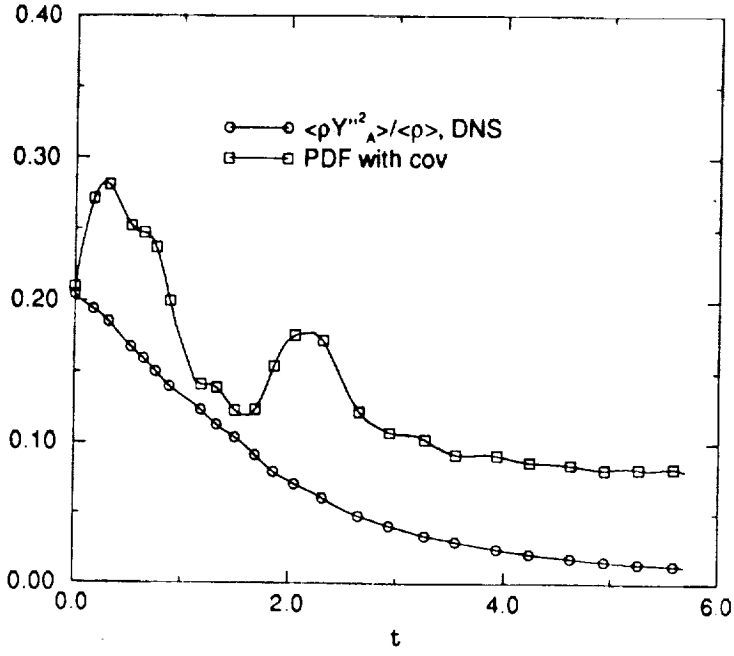
0.40
0.30
0.20
0.10
0.00
0.0
2.0
4.0
6.0
t
<ρY''²A>/<ρ>, DNS
PDF with cov

(a)

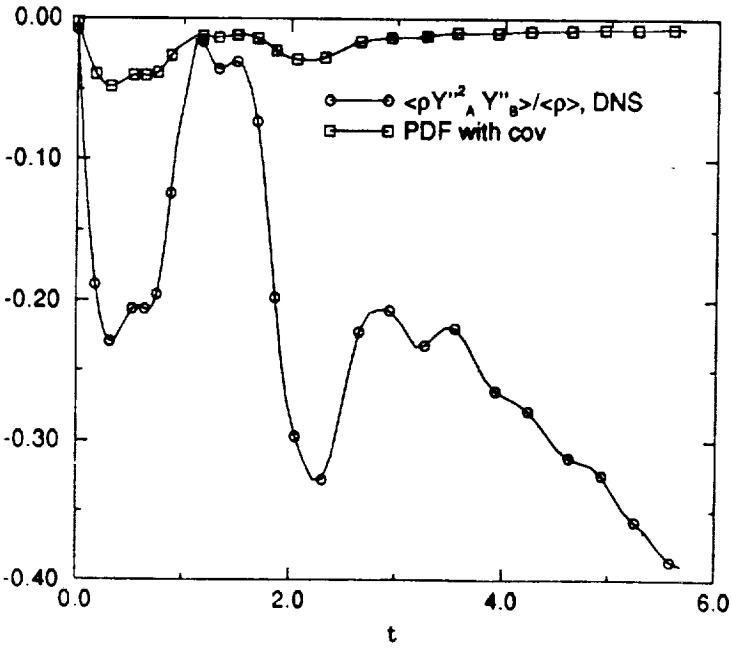
0.00
-0.10
-0.20
-0.30
-0.40
0.0
2.0
4.0
6.0
t
<ρY''²A Y''B>/<ρ>, DNS
PDF with cov

(b)

Figure 7

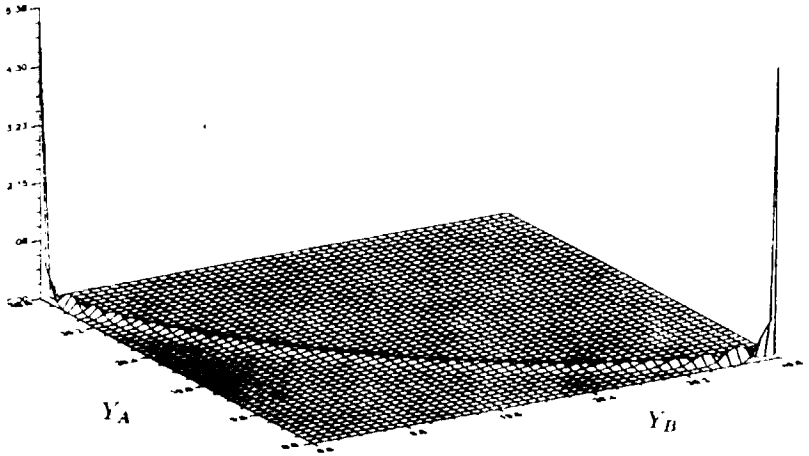

Figure 8

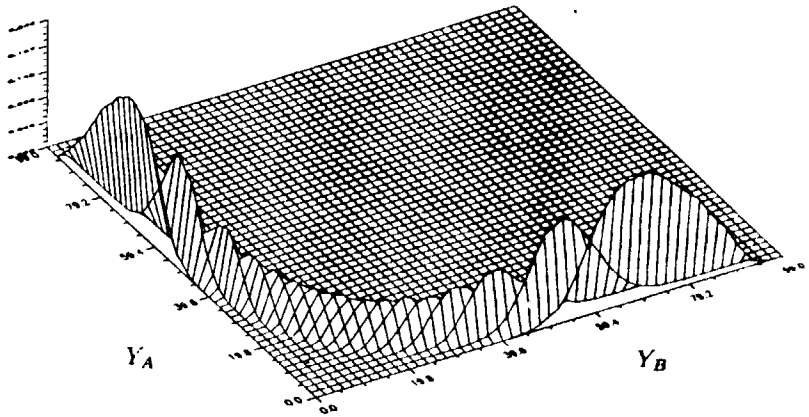

Figure 9

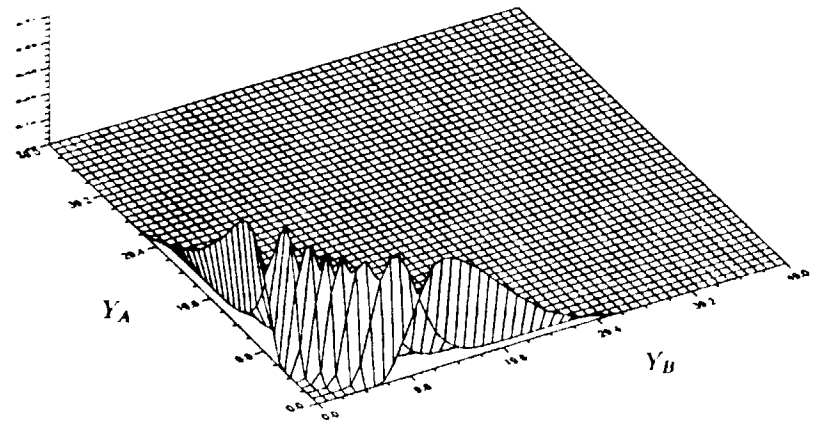

Figure 10

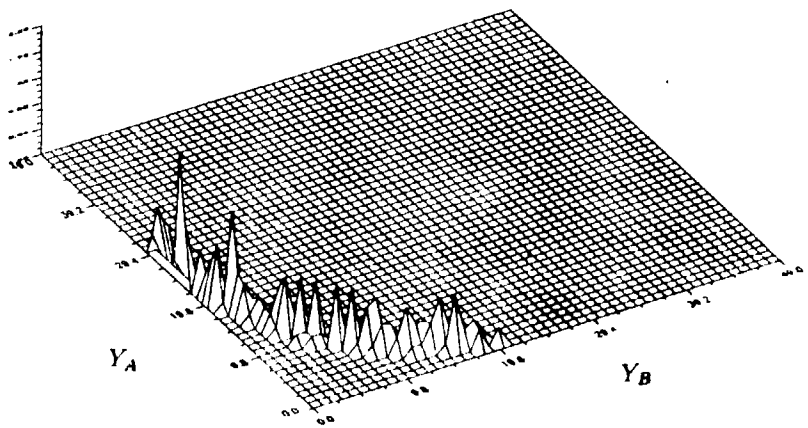

Figure 11

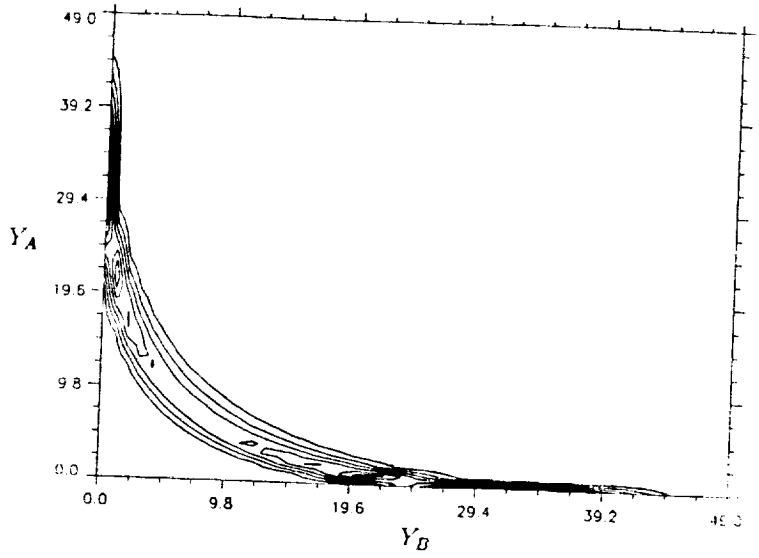

Figure 12

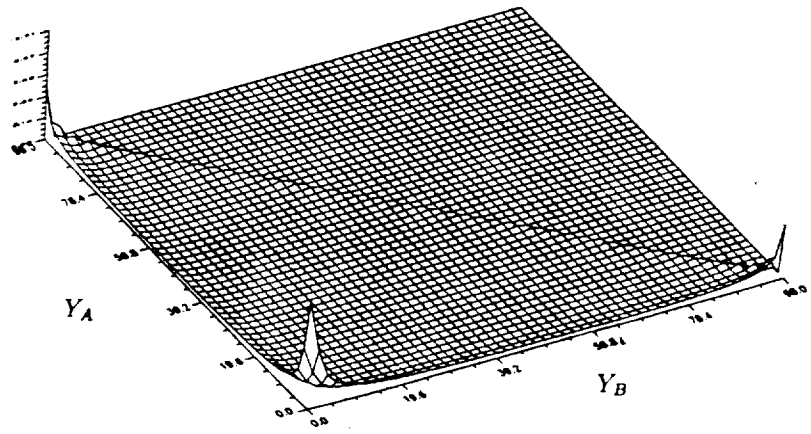

Figure 13

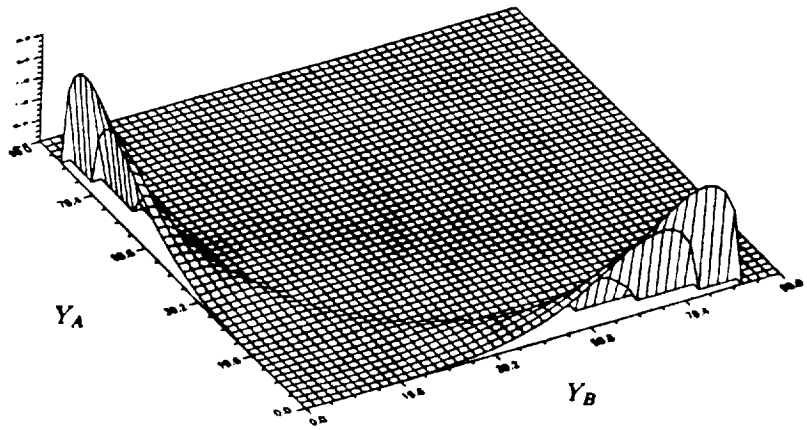

Figure 14

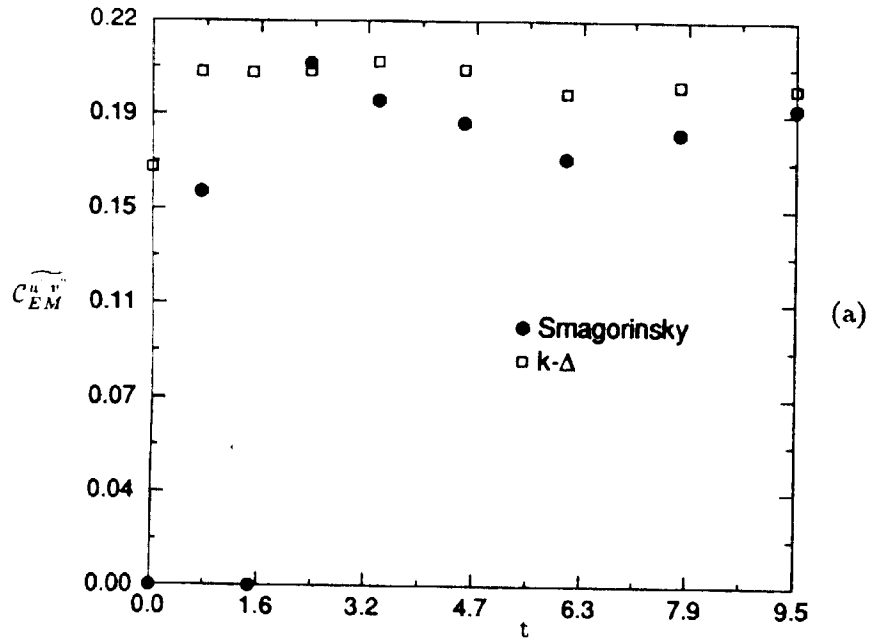

(a)

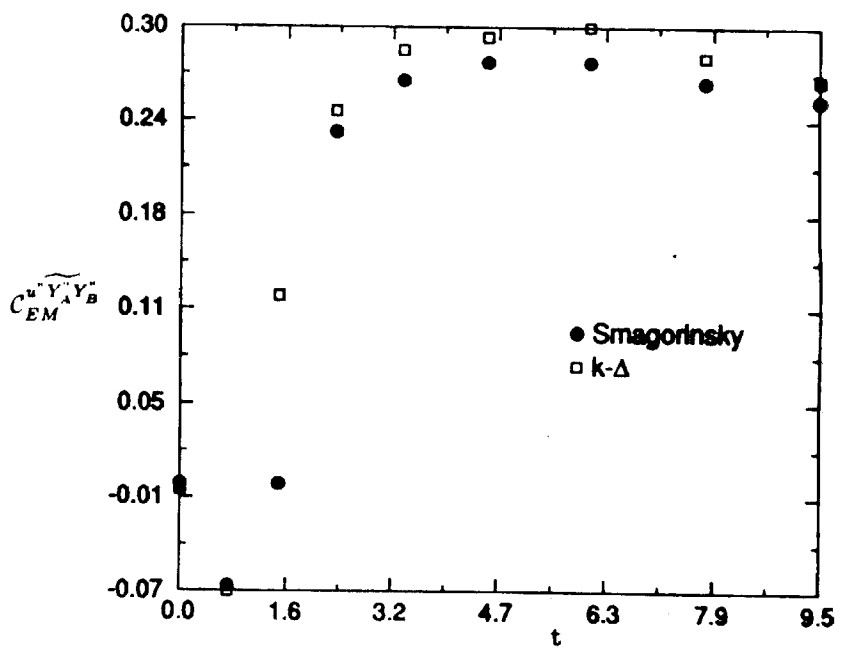

(b)

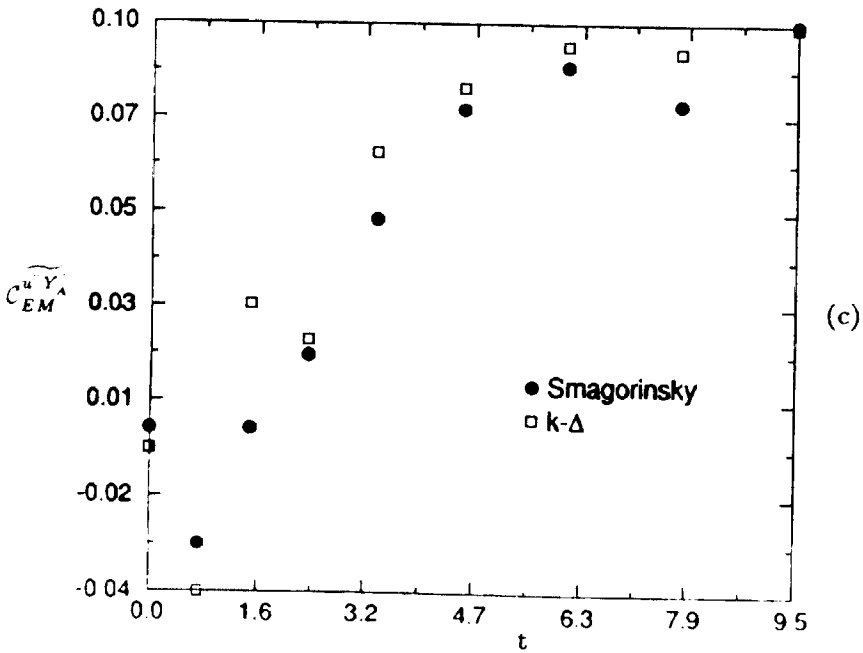

(c)

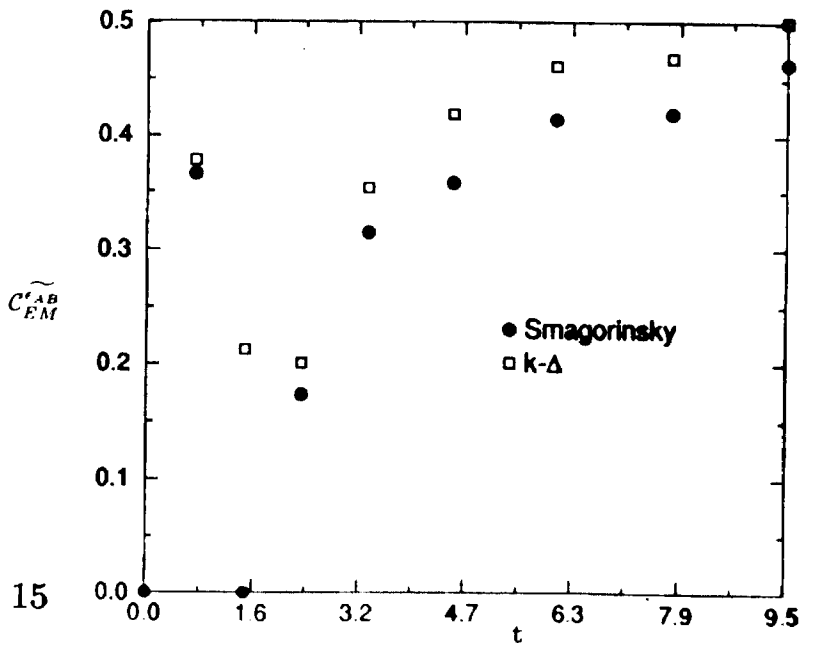

(d)

Figure 15

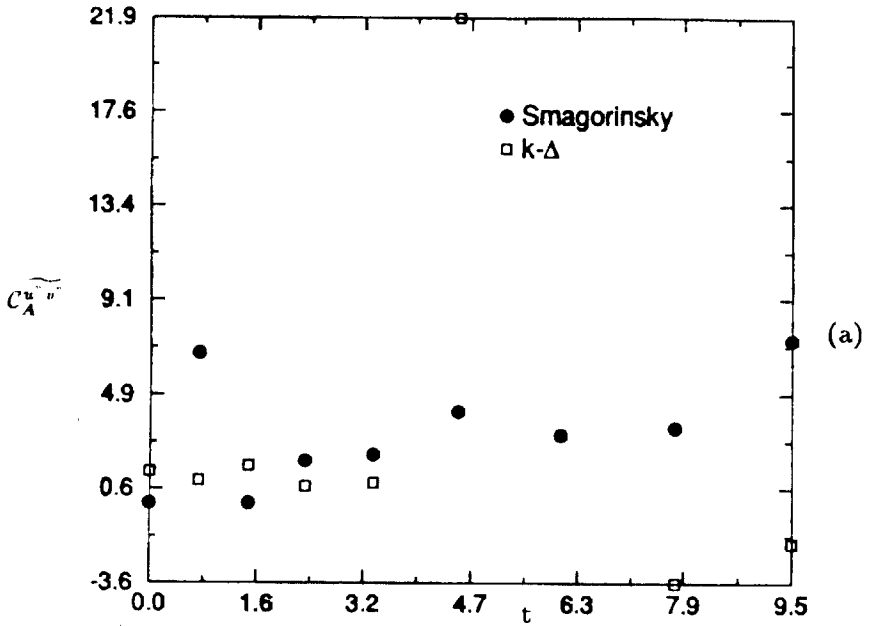

(a)

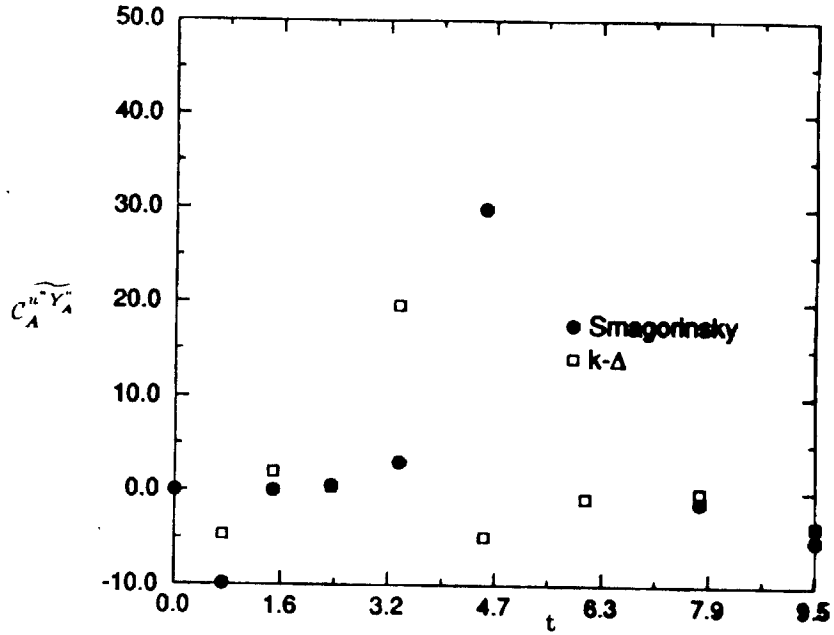

(b)

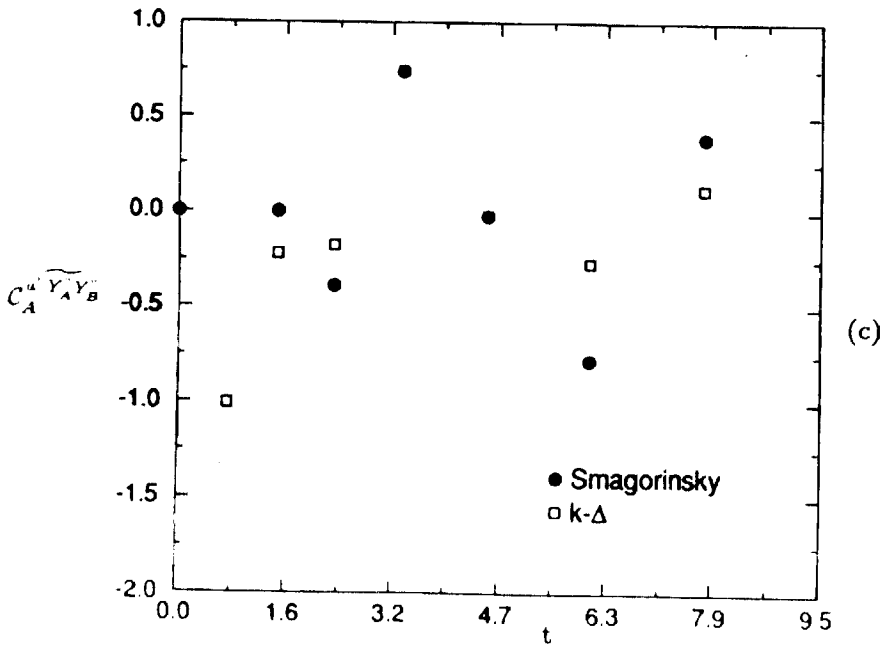

(c)

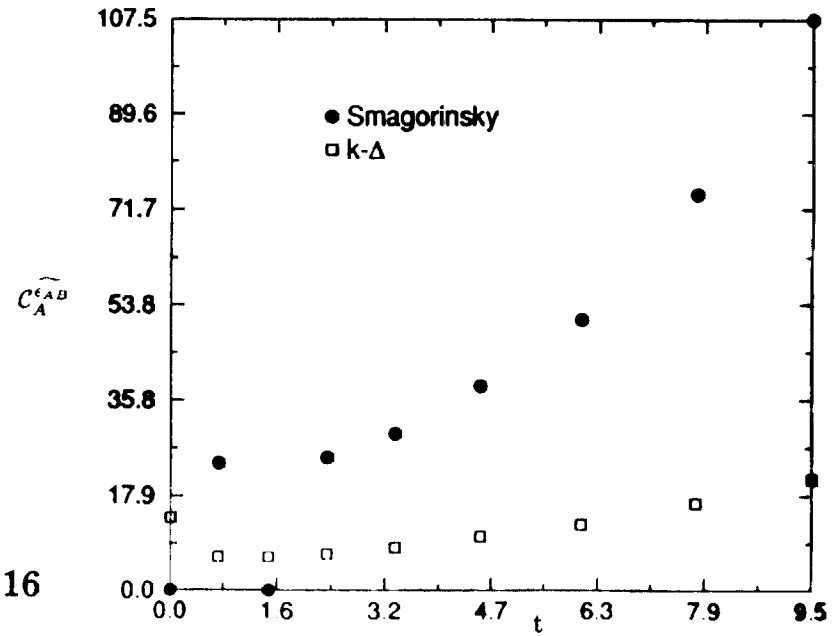

(d)

Figure 16

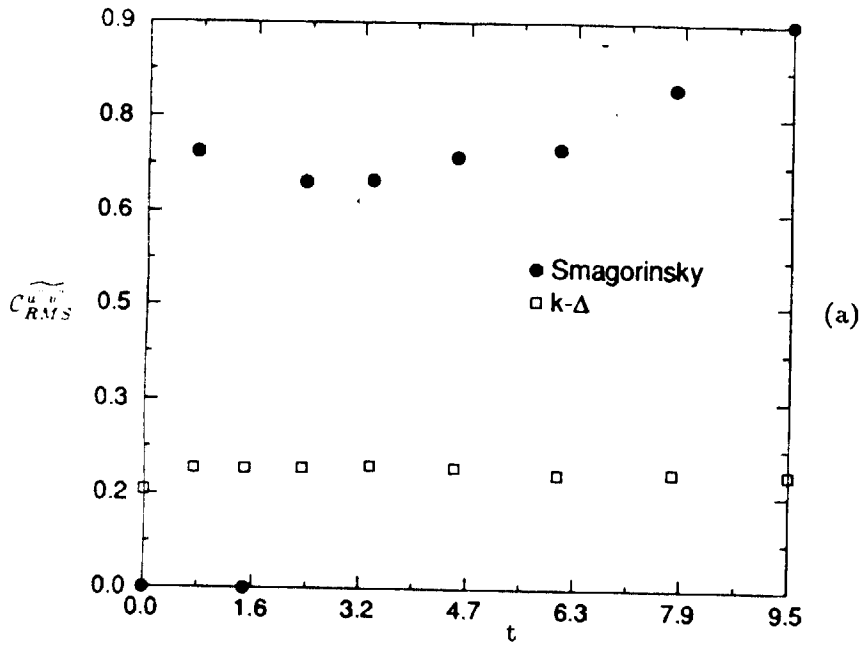

(a)

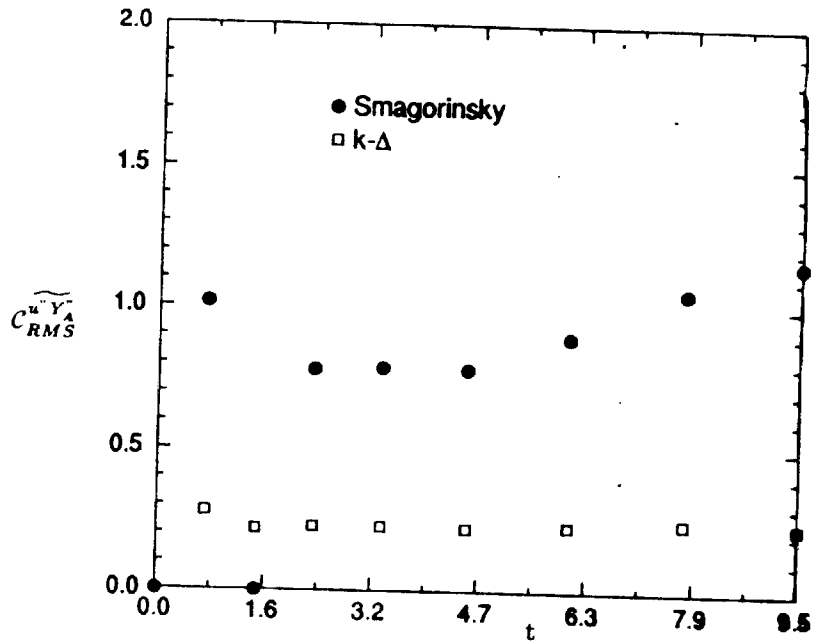

(b)

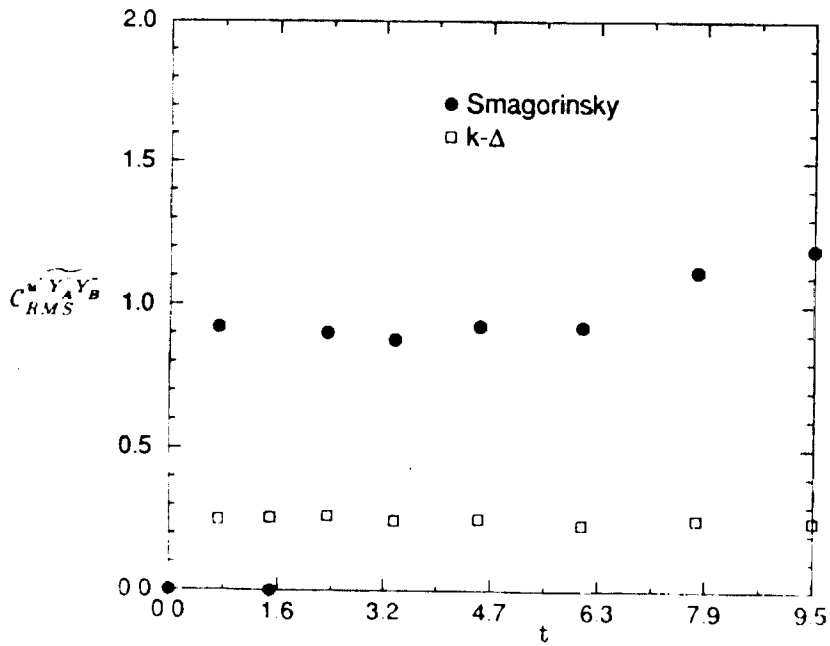

(c)

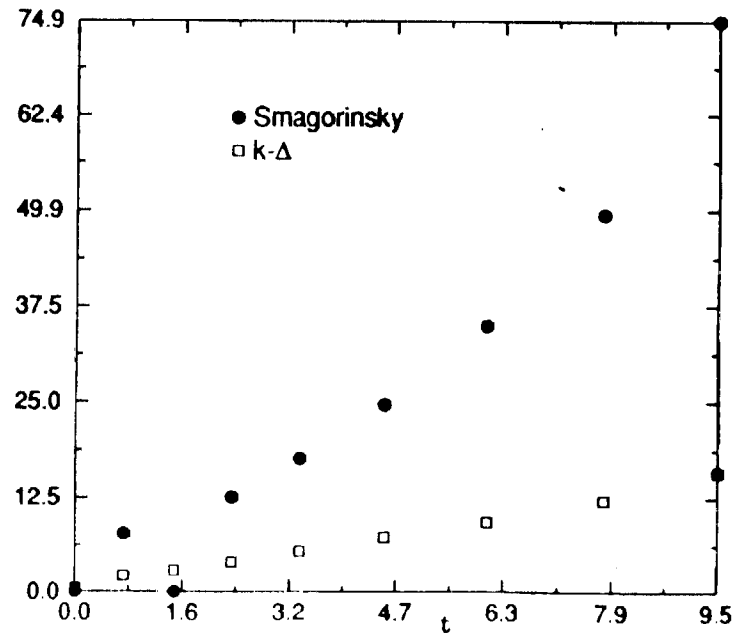

(d)

Figure 17

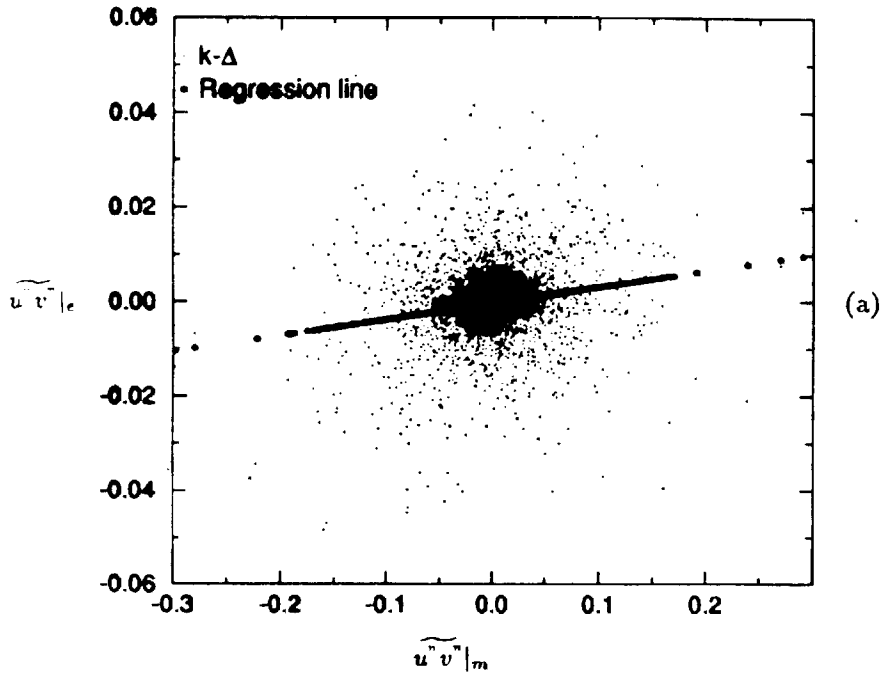

(a)

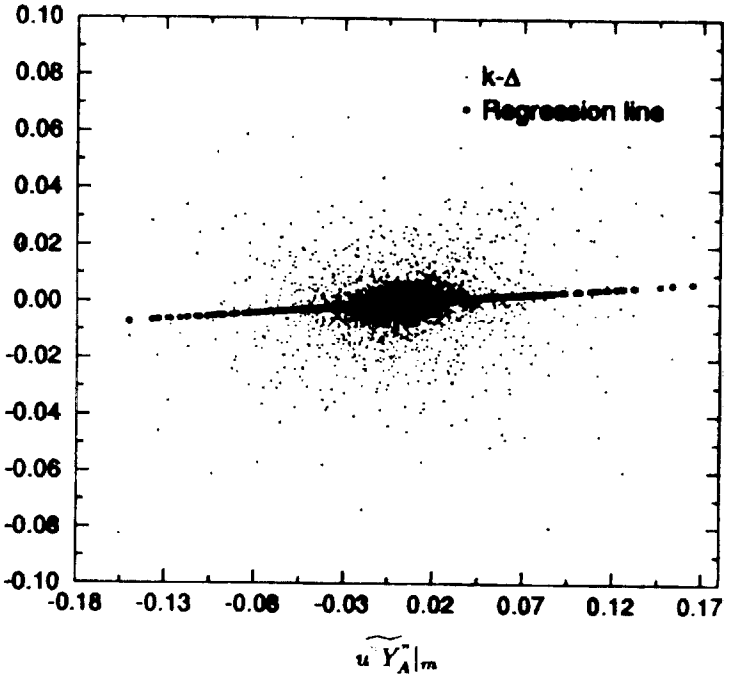

(b)

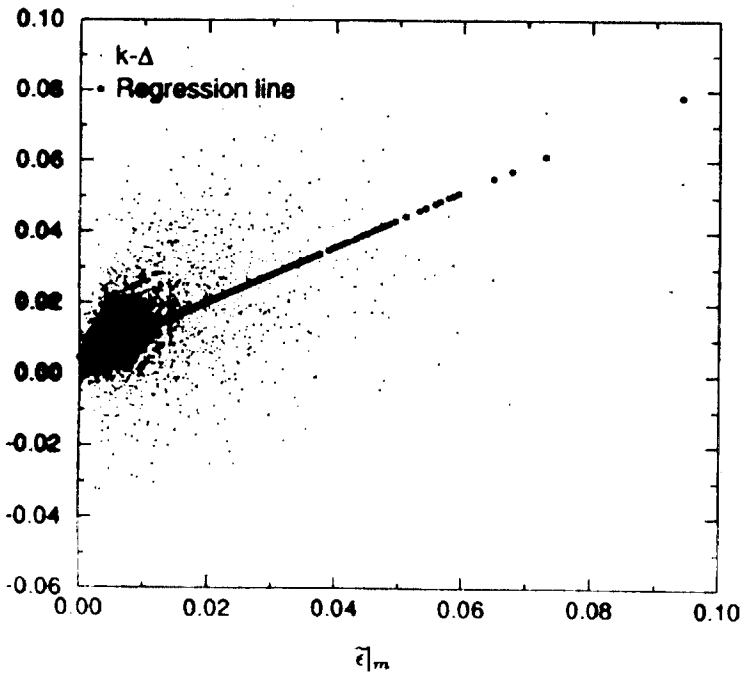

(c)

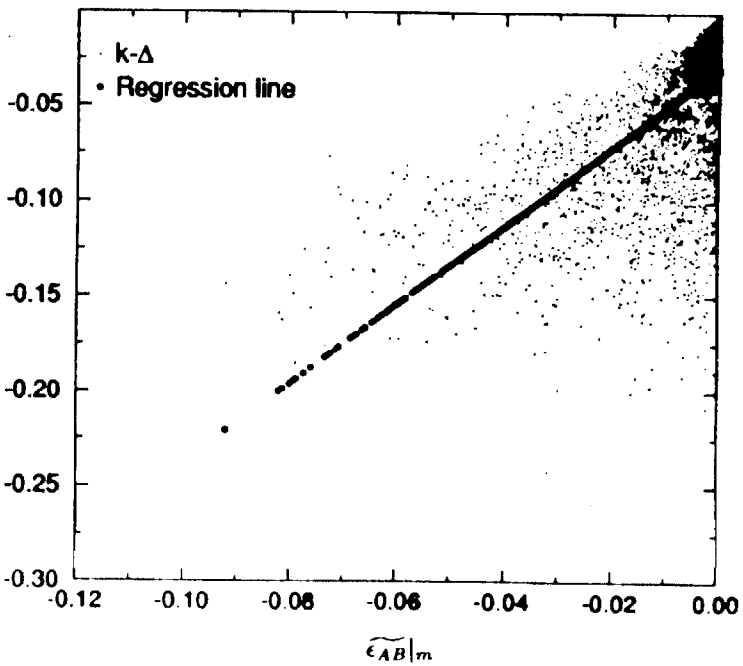

(d)

Figure 18

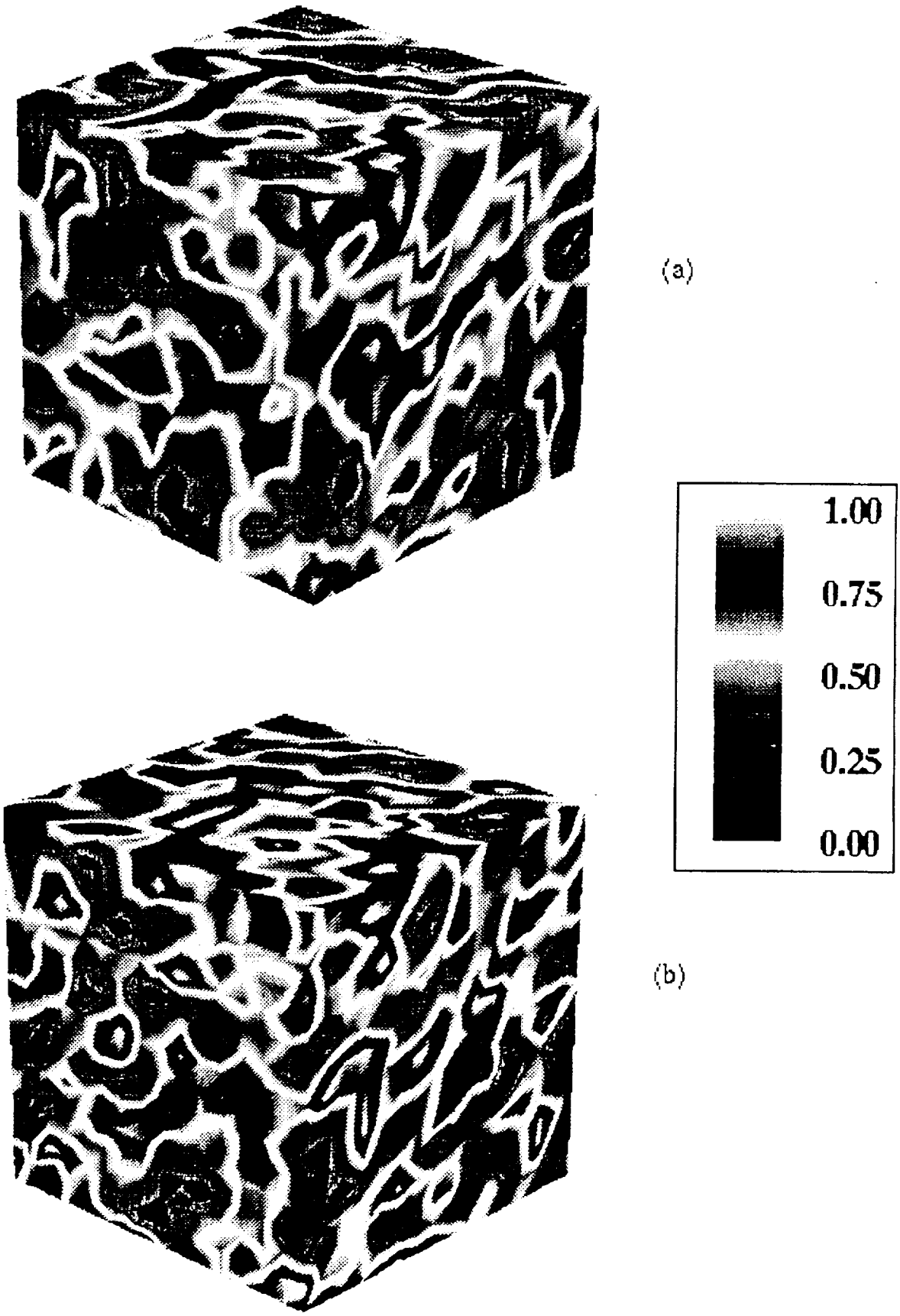

Figure 19

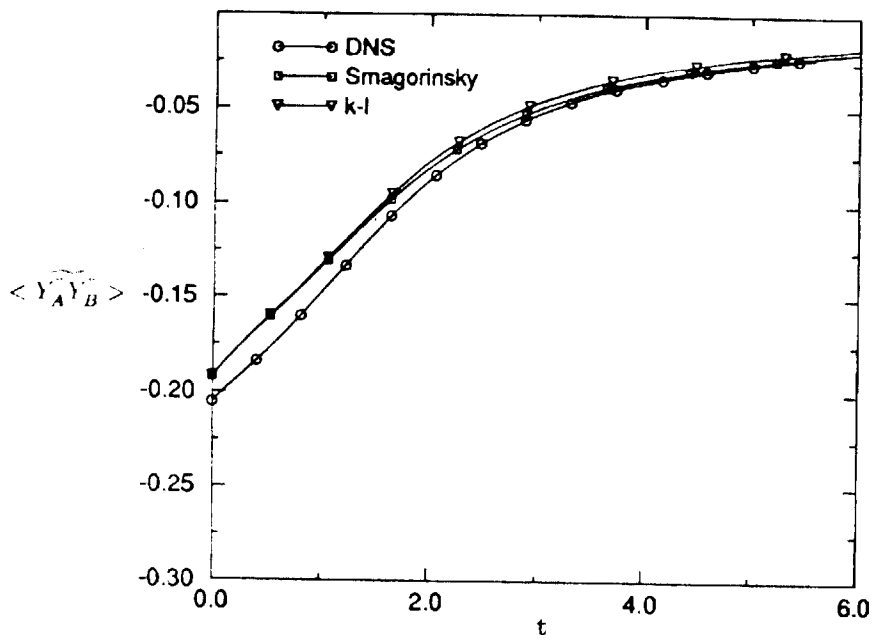

$< \widetilde{Y_A Y_B} >$ (a)

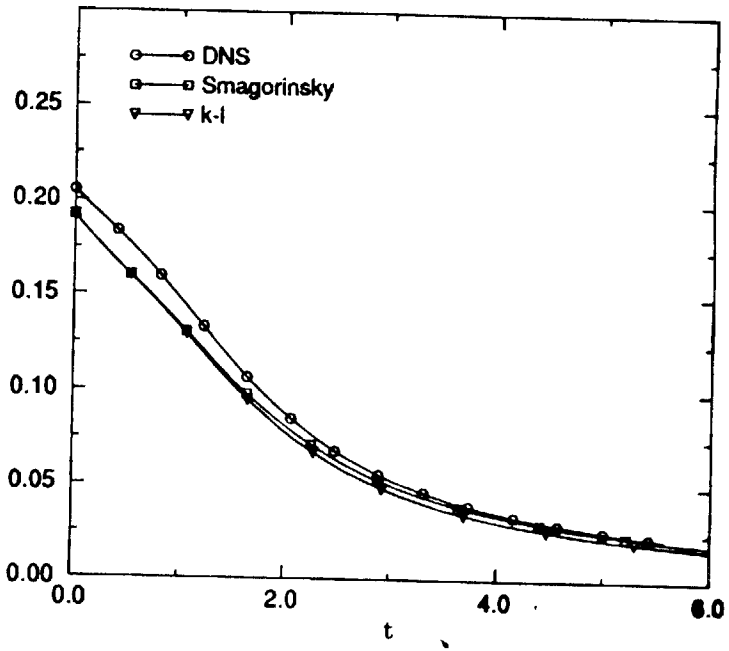

$< \widetilde{Y_A^2} >$ (b)

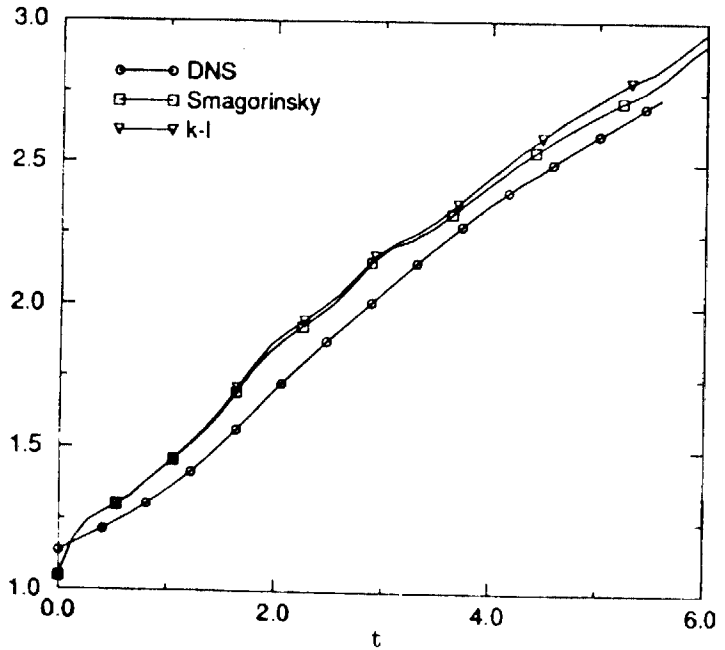

$< \widetilde{Y_A^4} >$ (c)

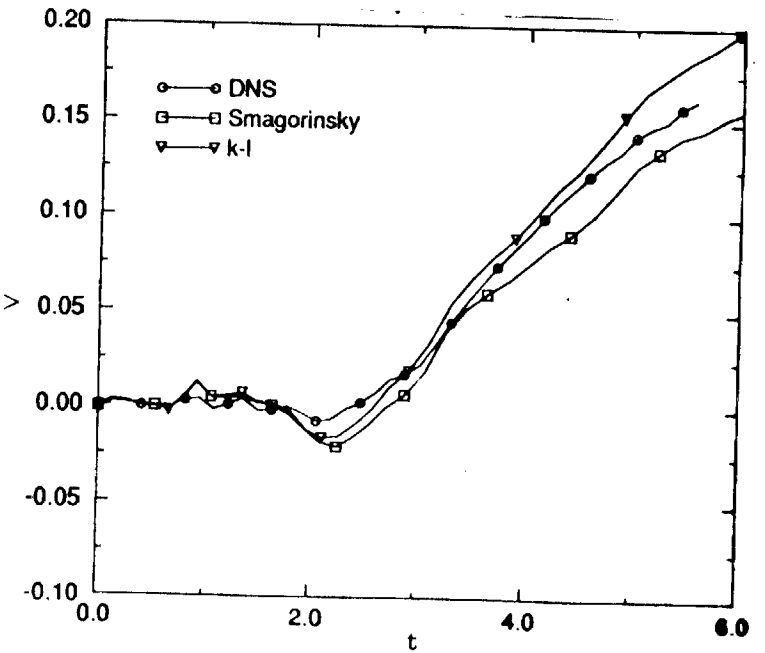

$< \widetilde{Y_A'' Y_B''^2} >$ (d)

Figure 20

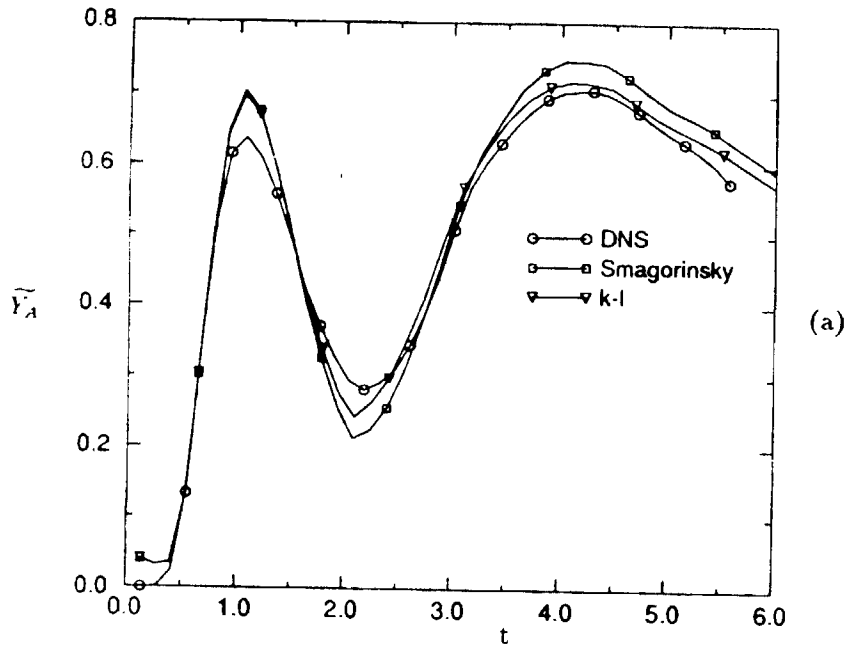

(a)

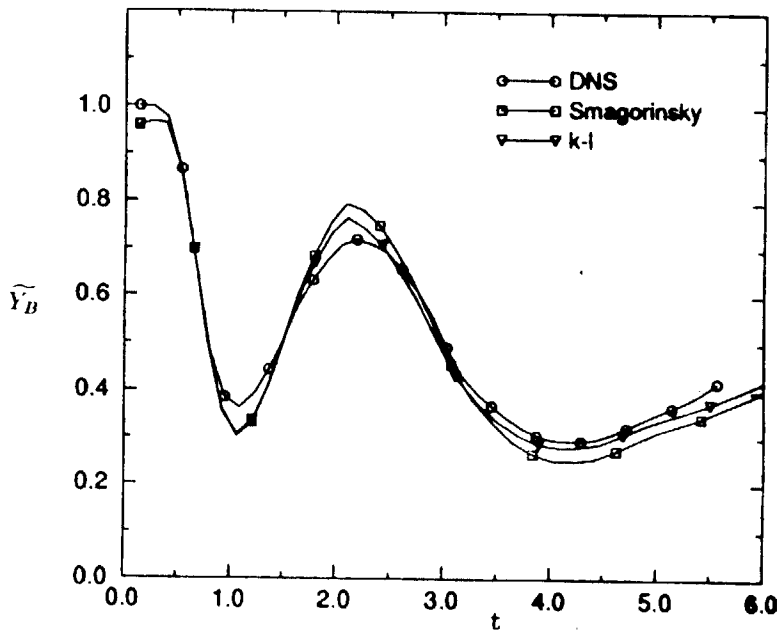

(b)

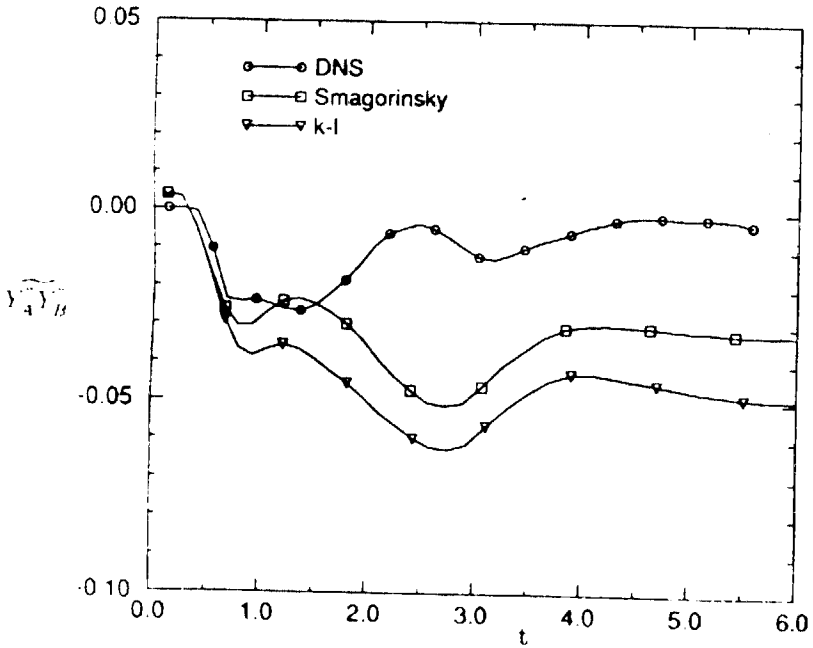

(c)

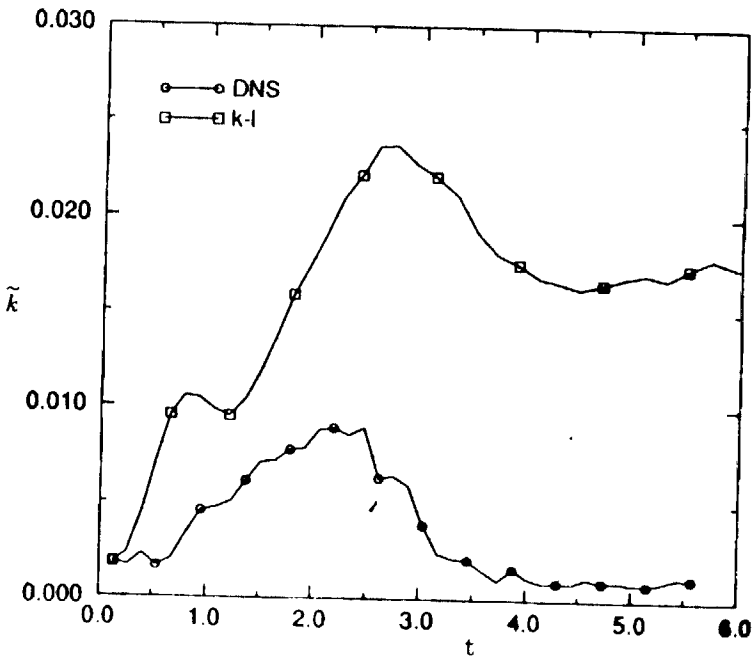

(d)

Figure 21

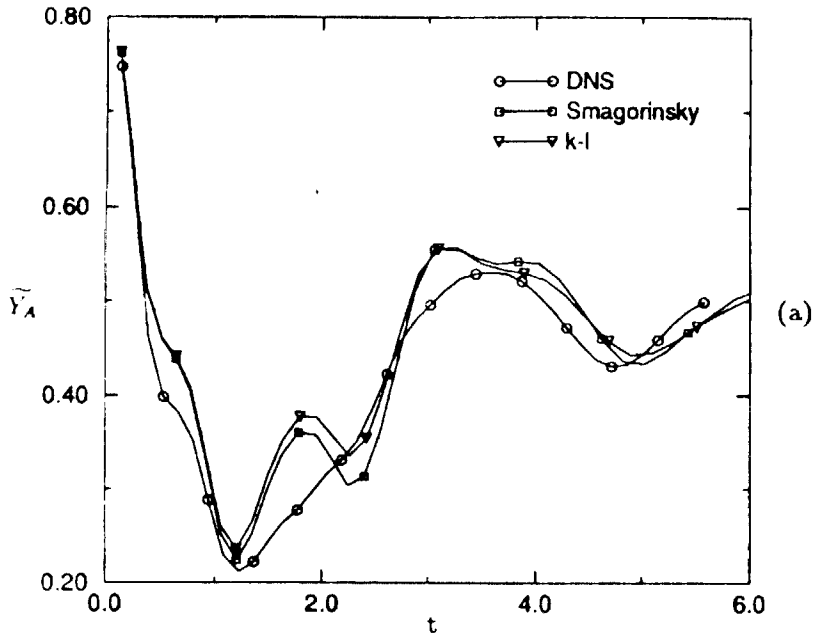

(a)

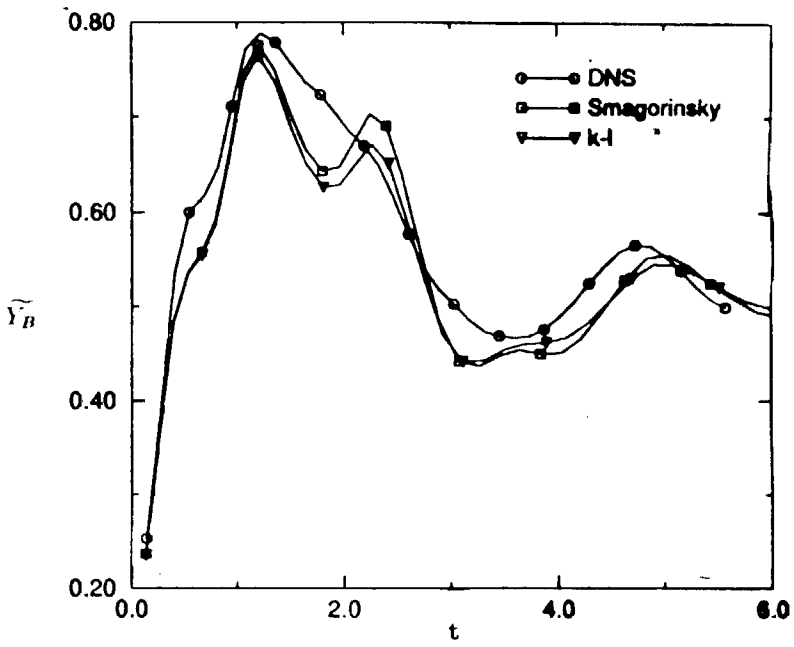

(b)

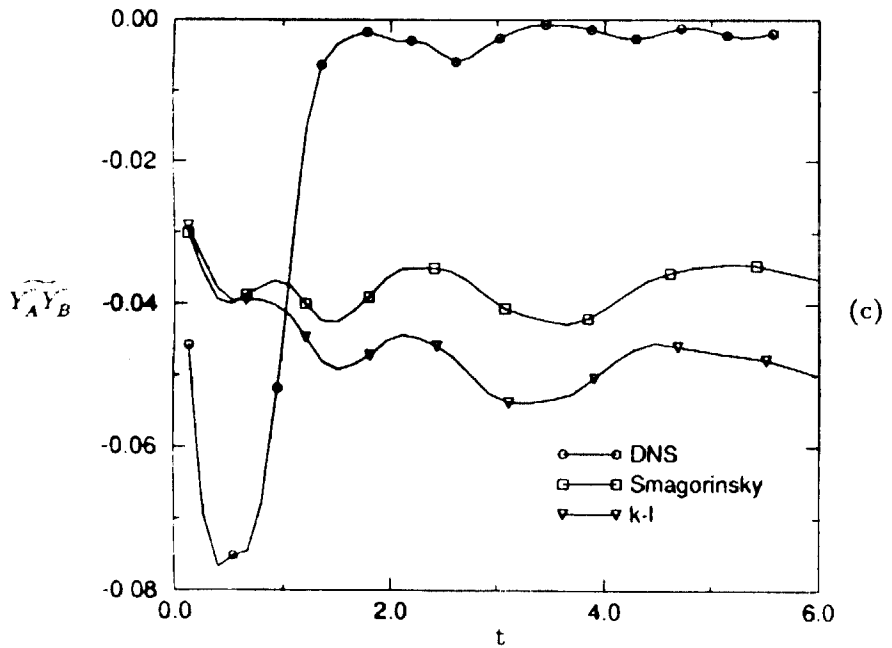

(c)

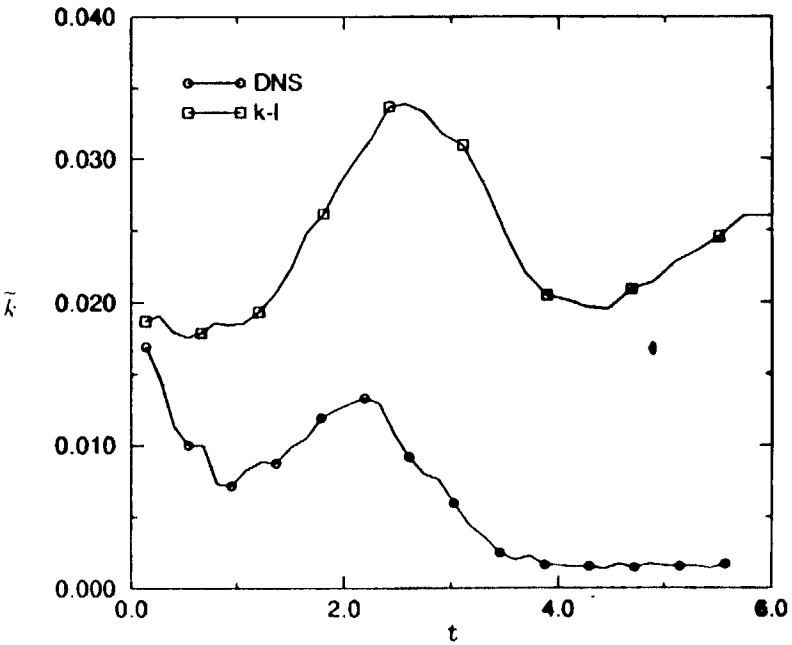

(d)

Figure 22

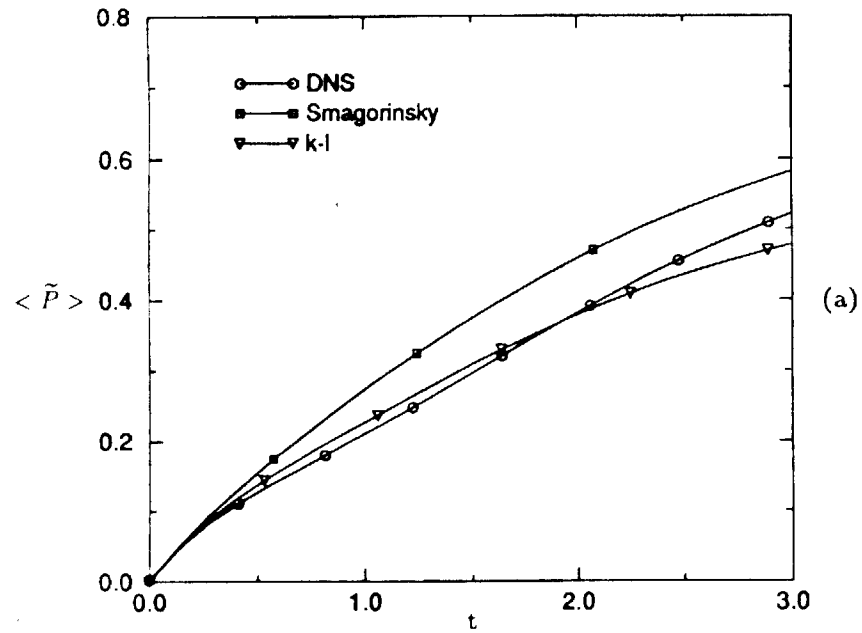
DNS
Smagorinsky
k-l
$< \widetilde{P} >$
t
(a)

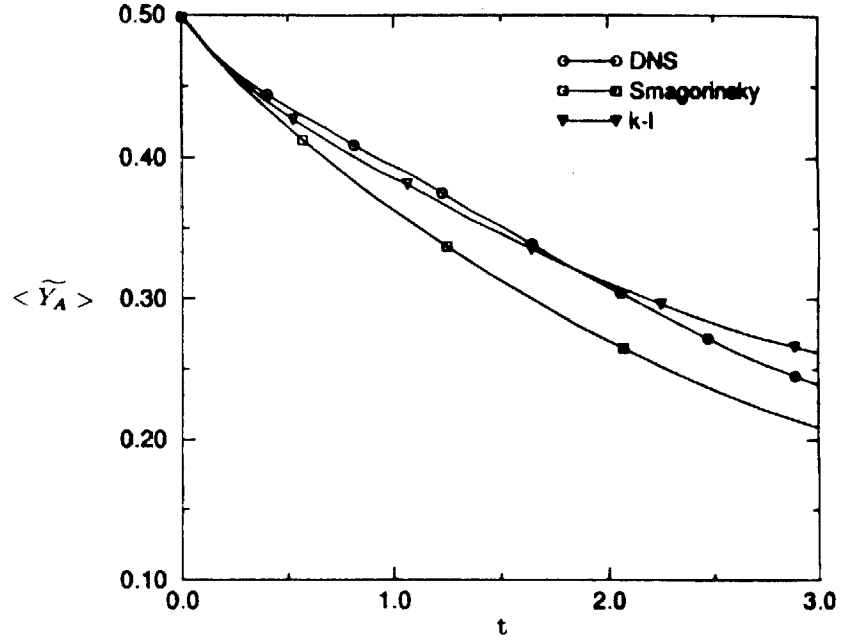
DNS
Smagorinsky
k-l
$< \widetilde{Y_A} >$
t
(b)

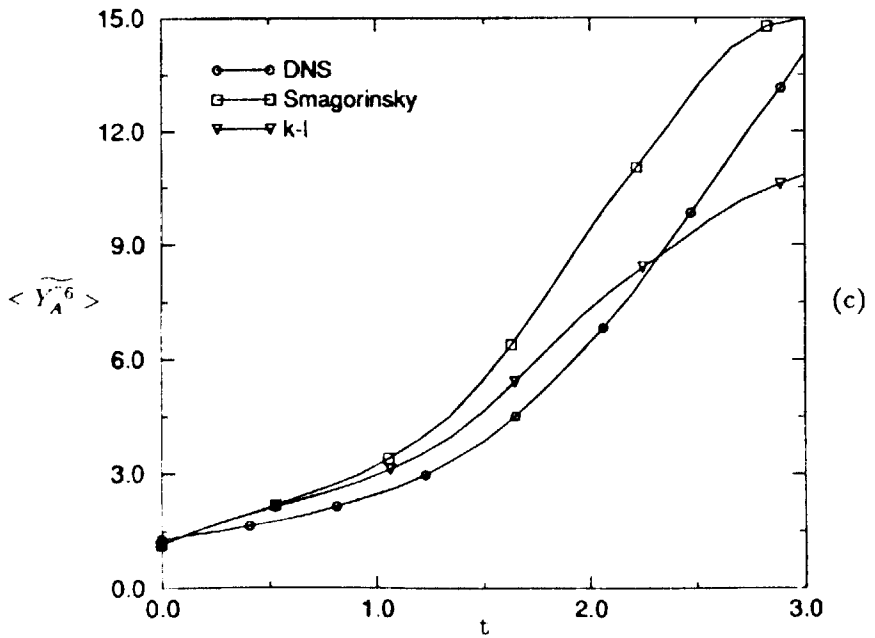
DNS
Smagorinsky
k-l
$< \widetilde{Y_A''^6} >$
t
(c)

Figure 23

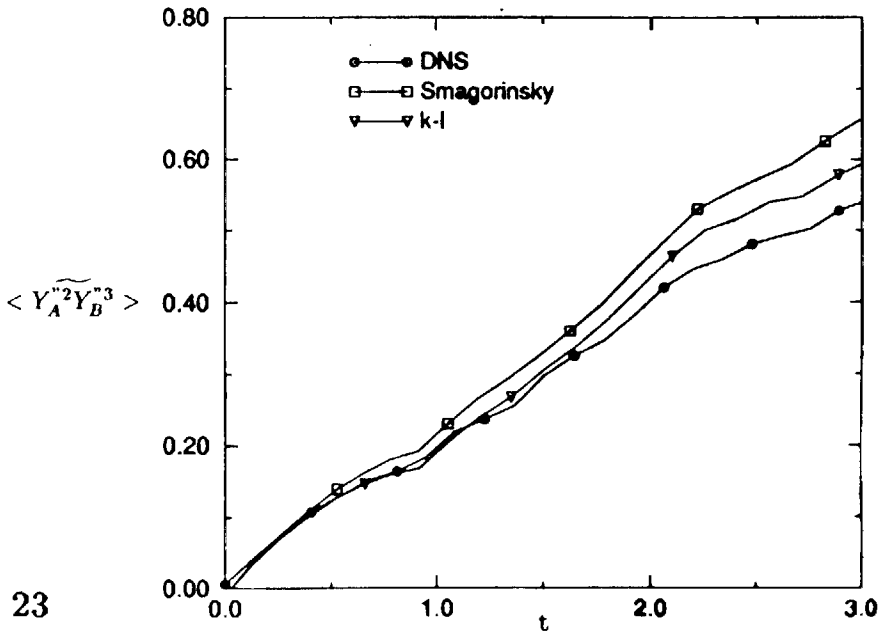
DNS
Smagorinsky
k-l
$< \widetilde{Y_A''^2 Y_B''^3} >$
t
(d)

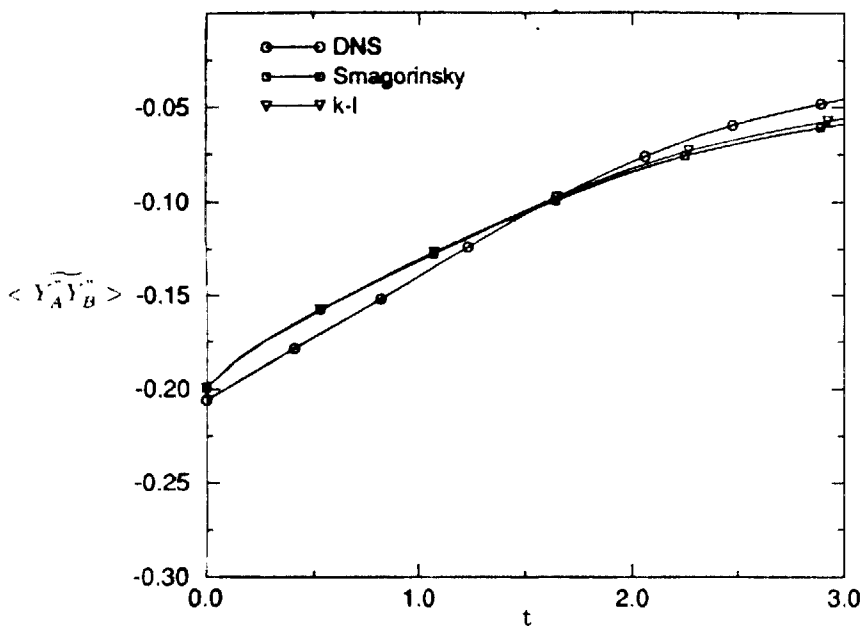

$< \widetilde{Y_A''} \widetilde{Y_B''} >$ (a)

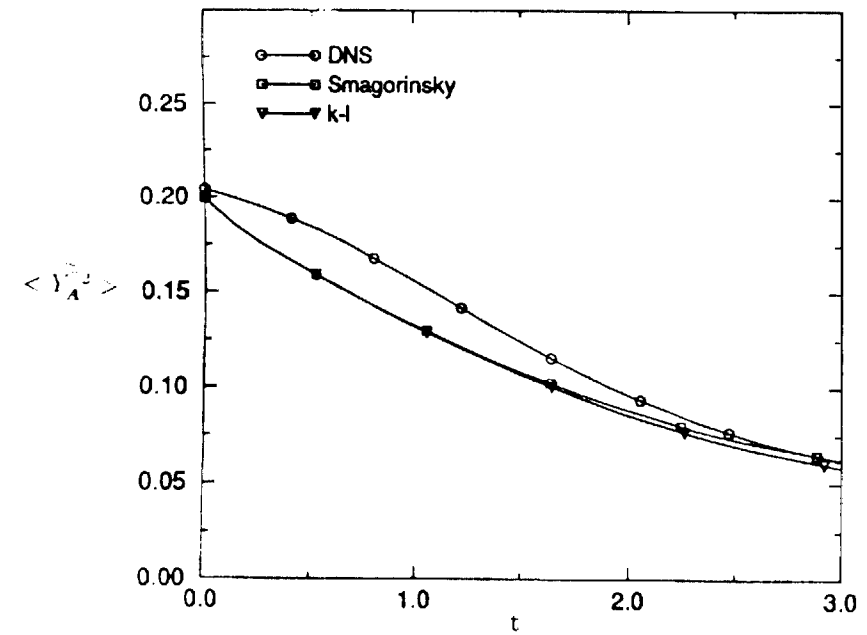

$< \widetilde{Y_A''^2} >$ (b)

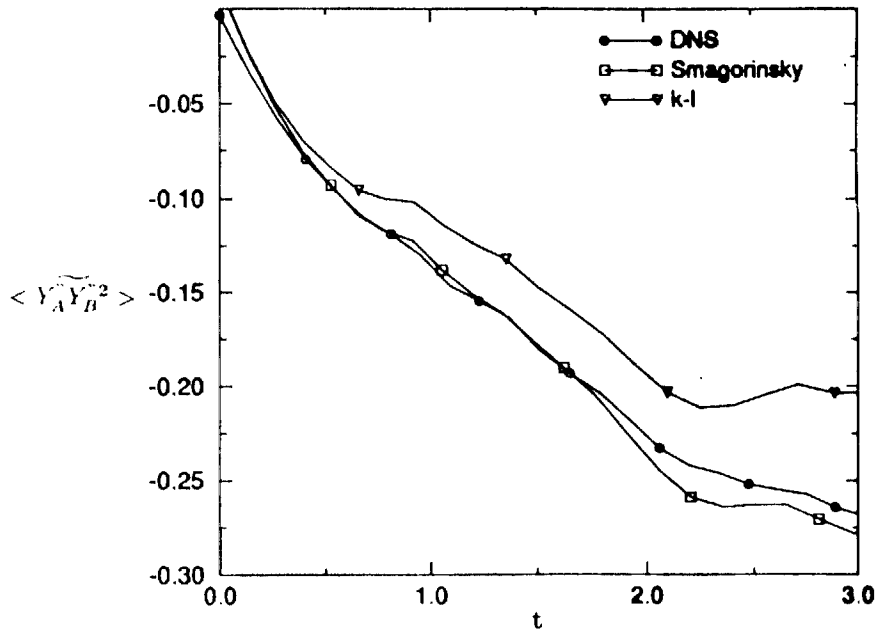

$< \widetilde{Y_A''} \widetilde{Y_B''^2} >$ (d)

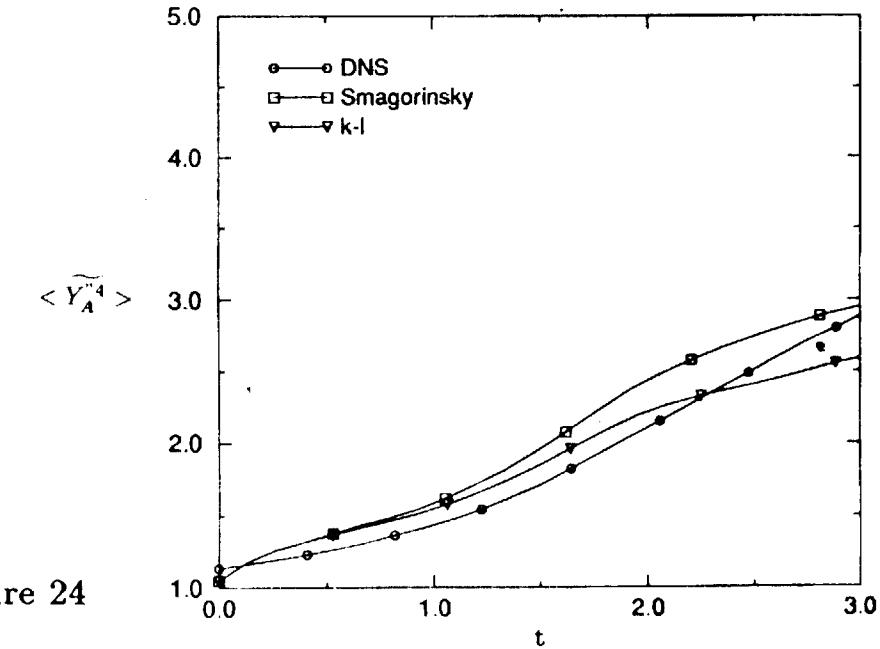

$< \widetilde{Y_A''^4} >$ (c)

Figure 24

(a)

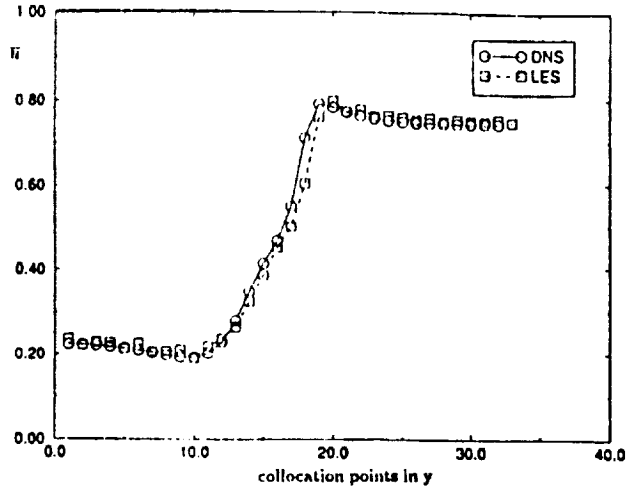

(b)

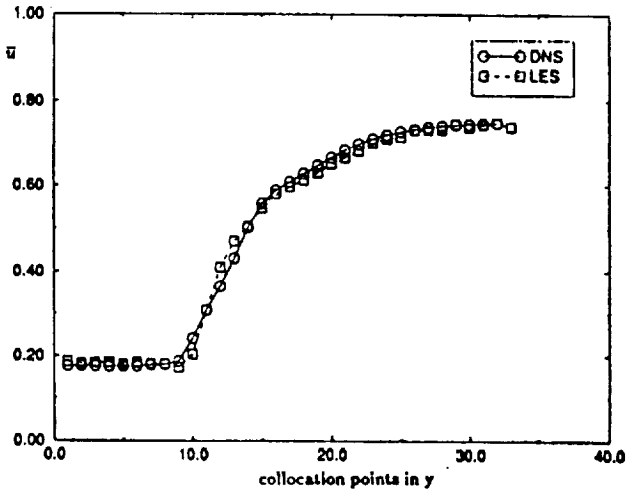

(c)

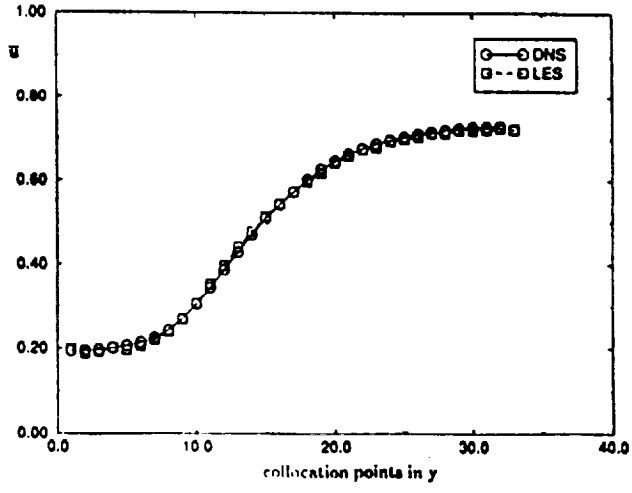

Figure 25

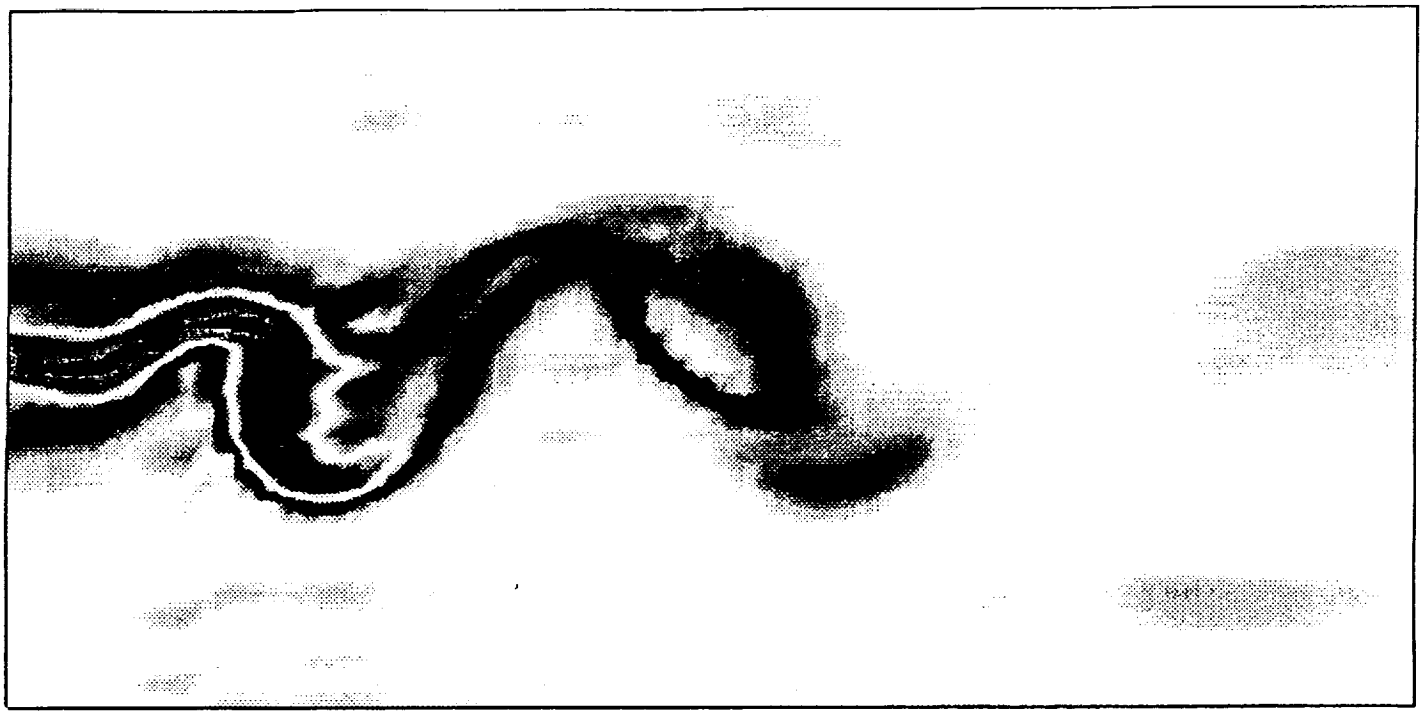

(a)

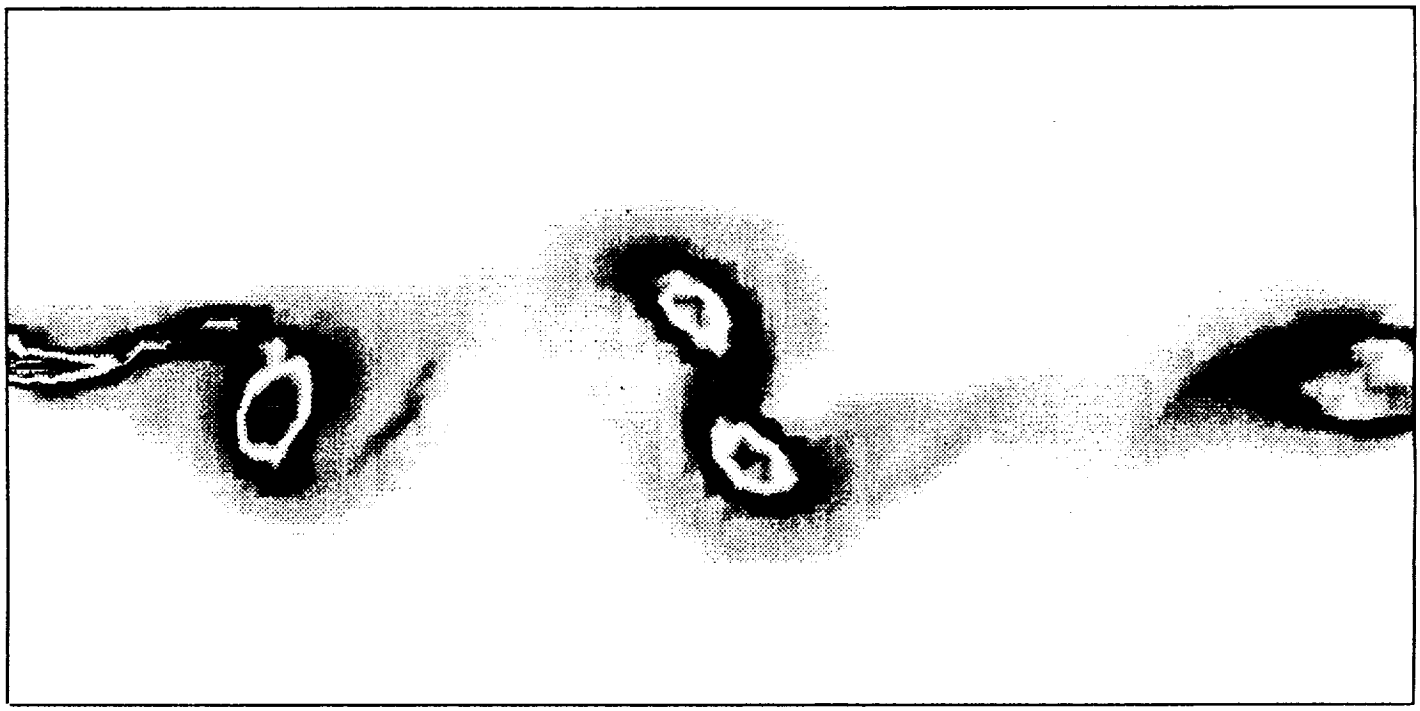

(b)

Figure 26

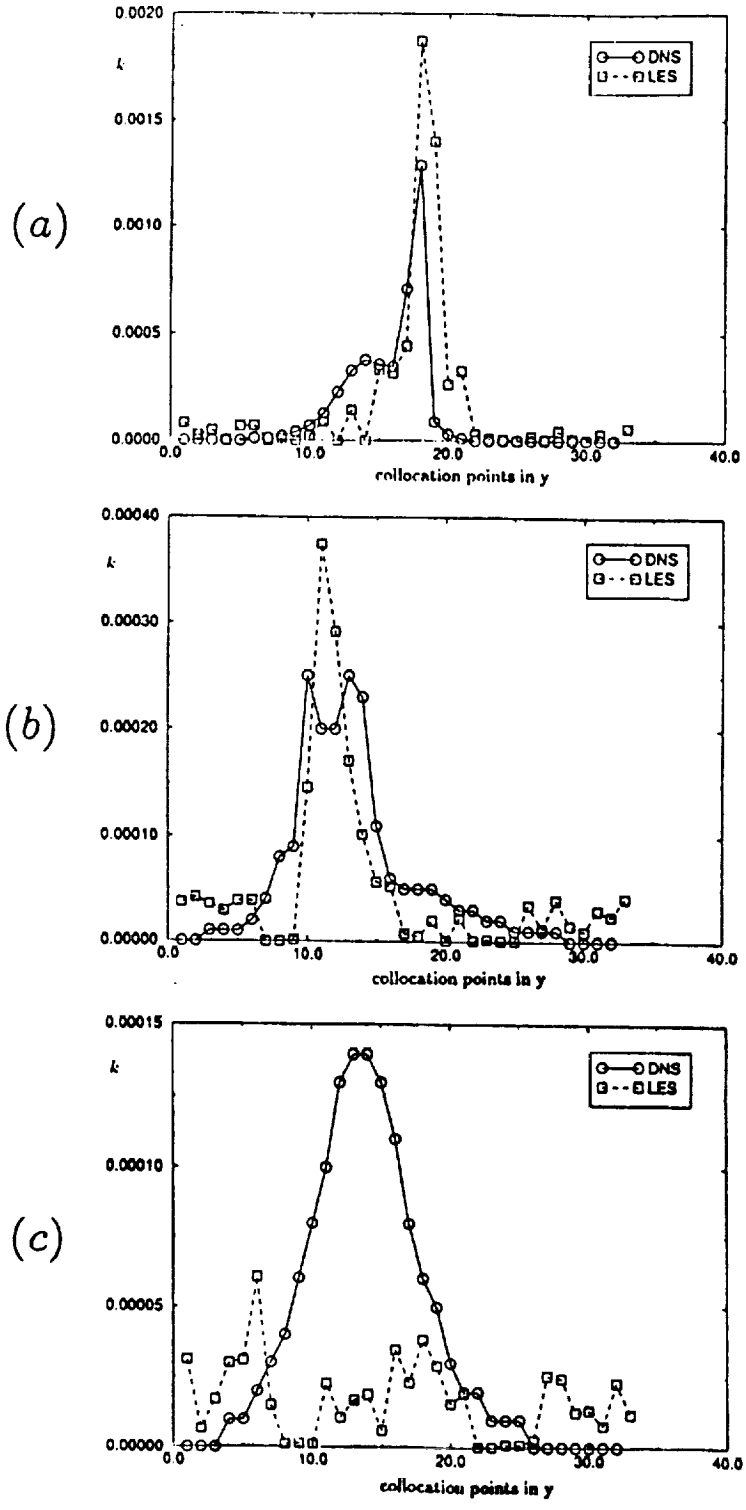
(a)
0.0020
k
0.0015
0.0010
0.0005
0.0000
DNS
LES
0.0
10.0
20.0
30.0
40.0
collocation points in y
(b)
0.00040
k
0.00030
0.00020
0.00010
0.00000
DNS
LES
0.0
10.0
20.0
30.0
40.0
collocation points in y
(c)
0.00015
k
0.00010
0.00005
0.00000
DNS
LES
0.0
10.0
20.0
30.0
40.0
collocation points in y

Figure 27

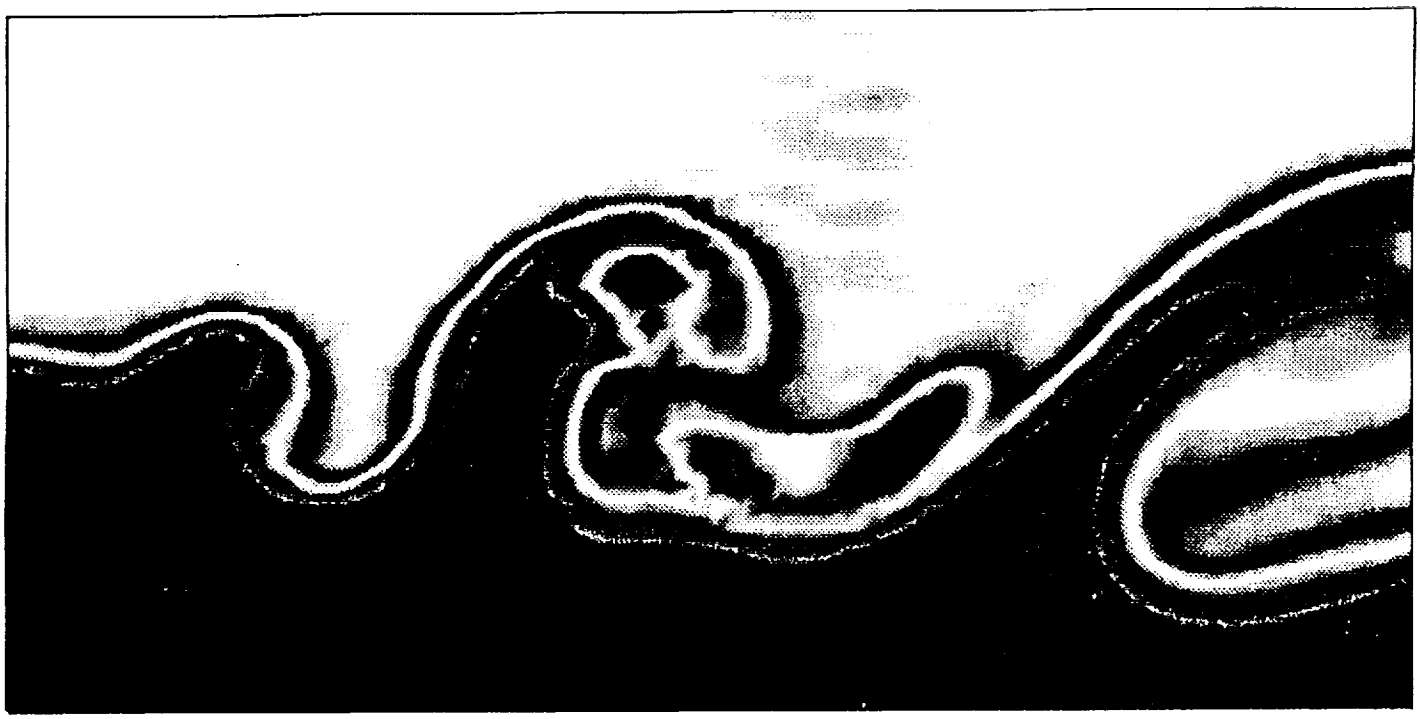

(a)

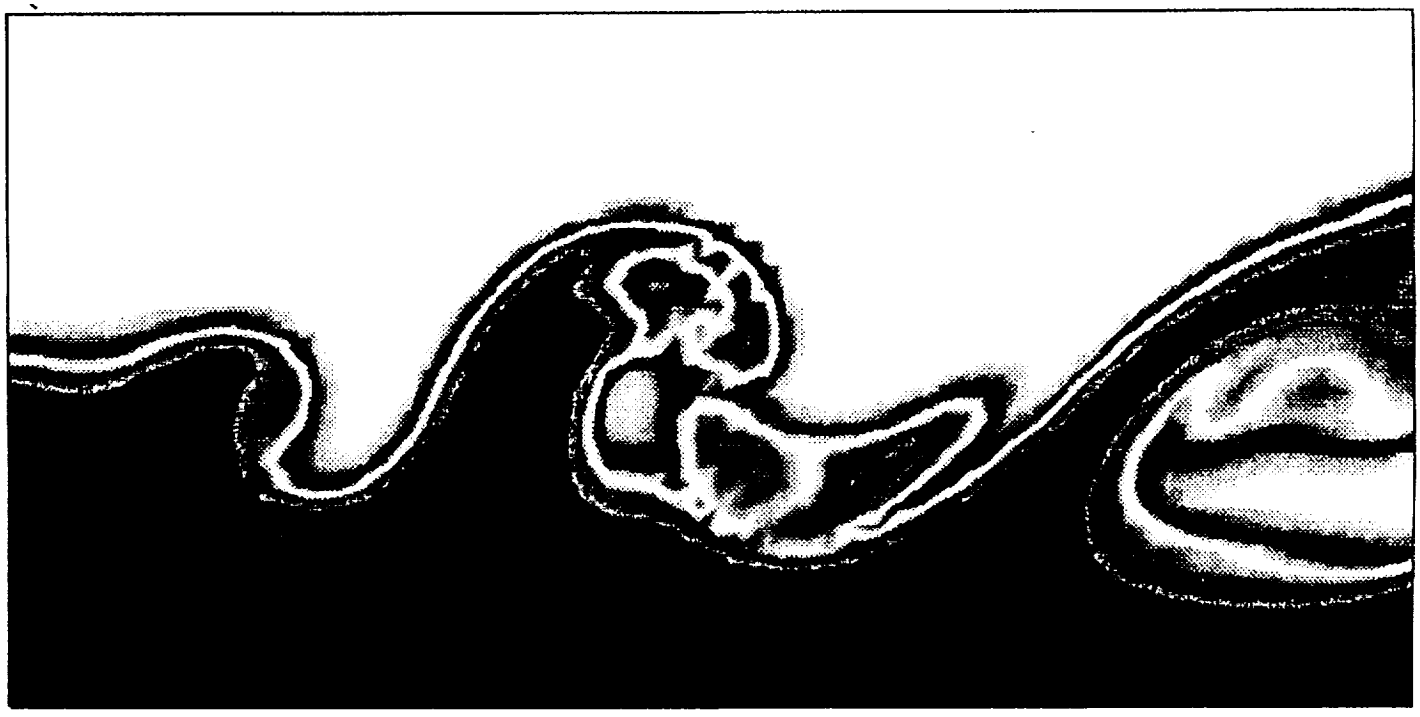

(b)

Figure 28

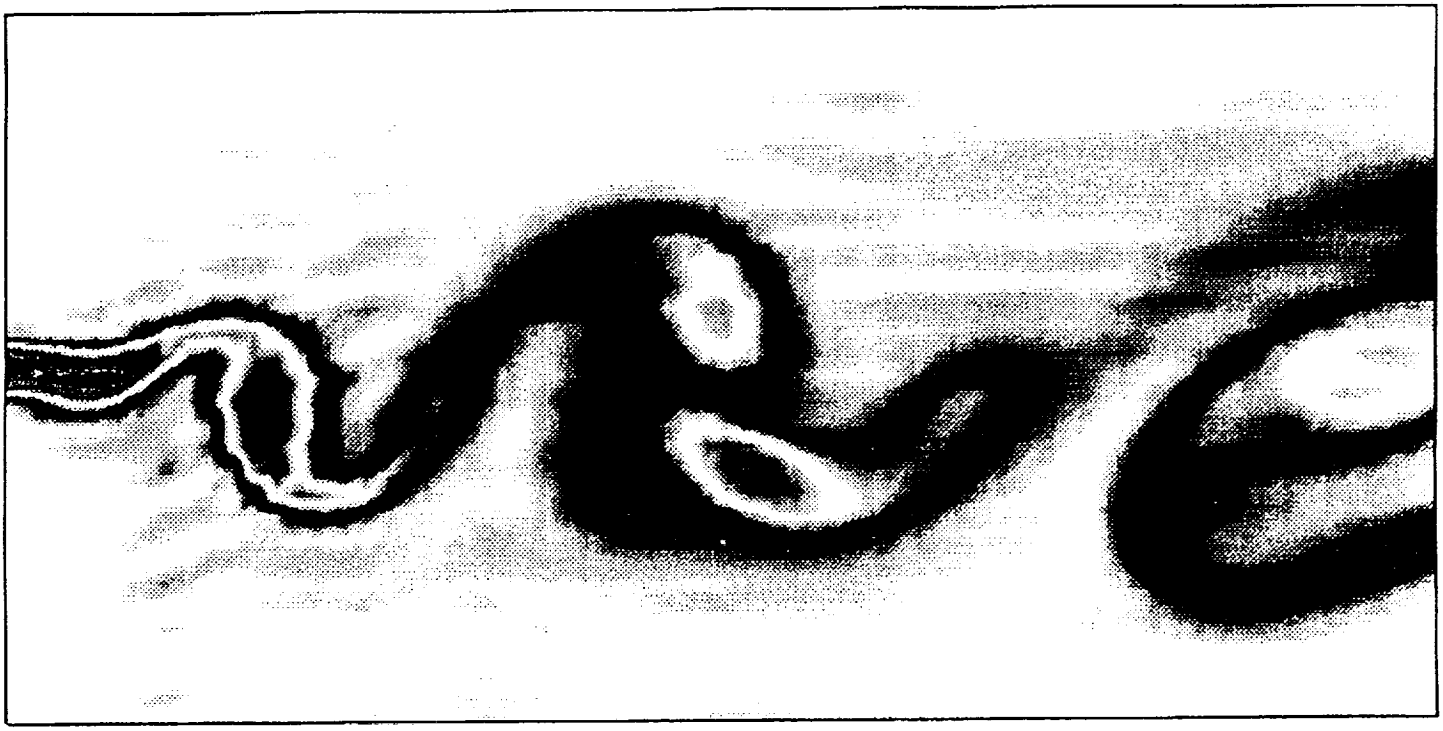

(a)

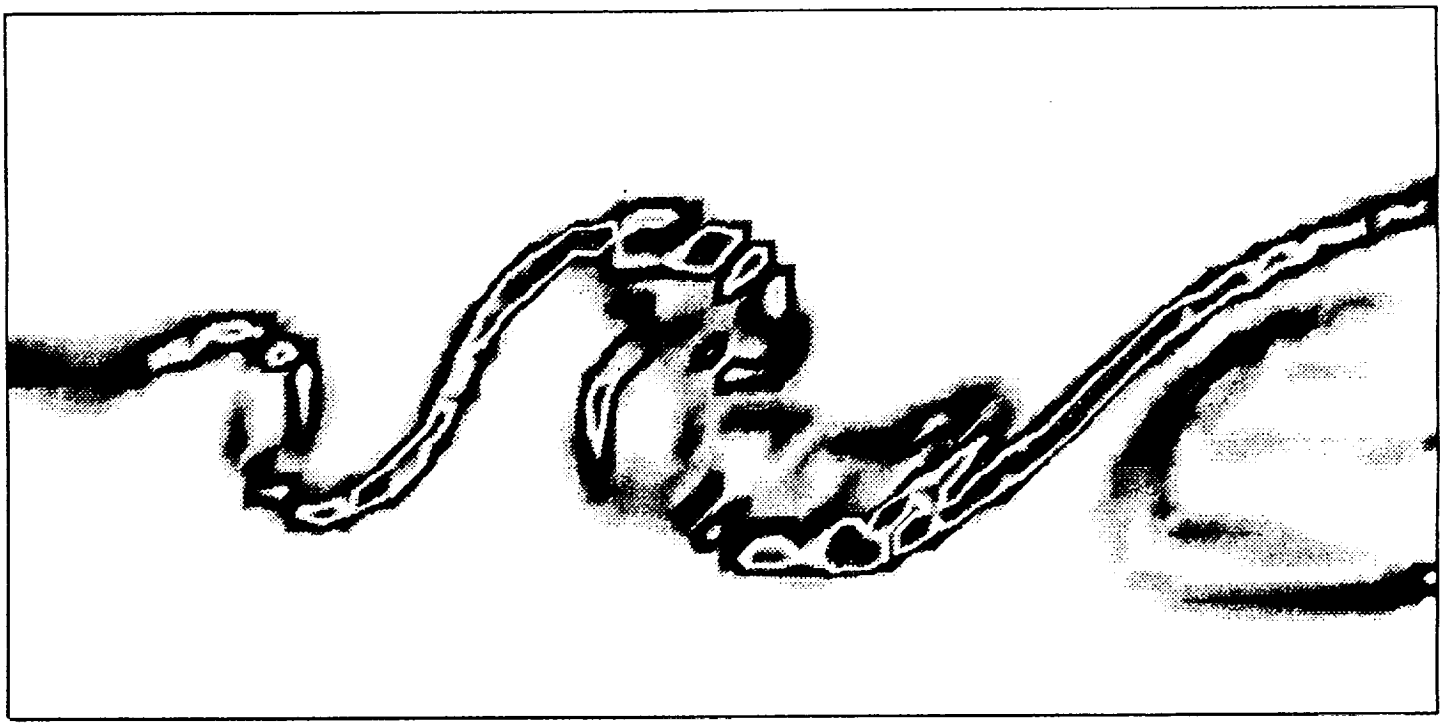

(b)

Figure 29

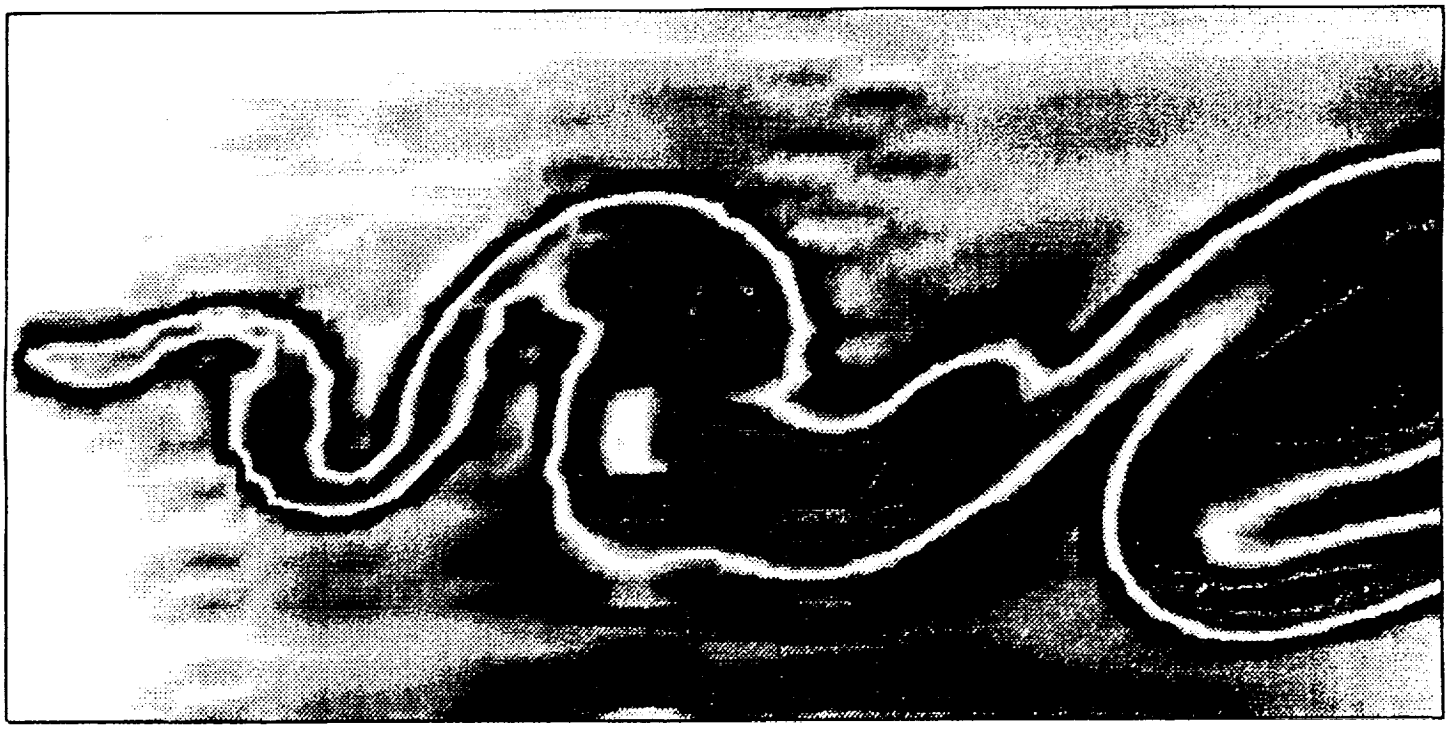

(a)

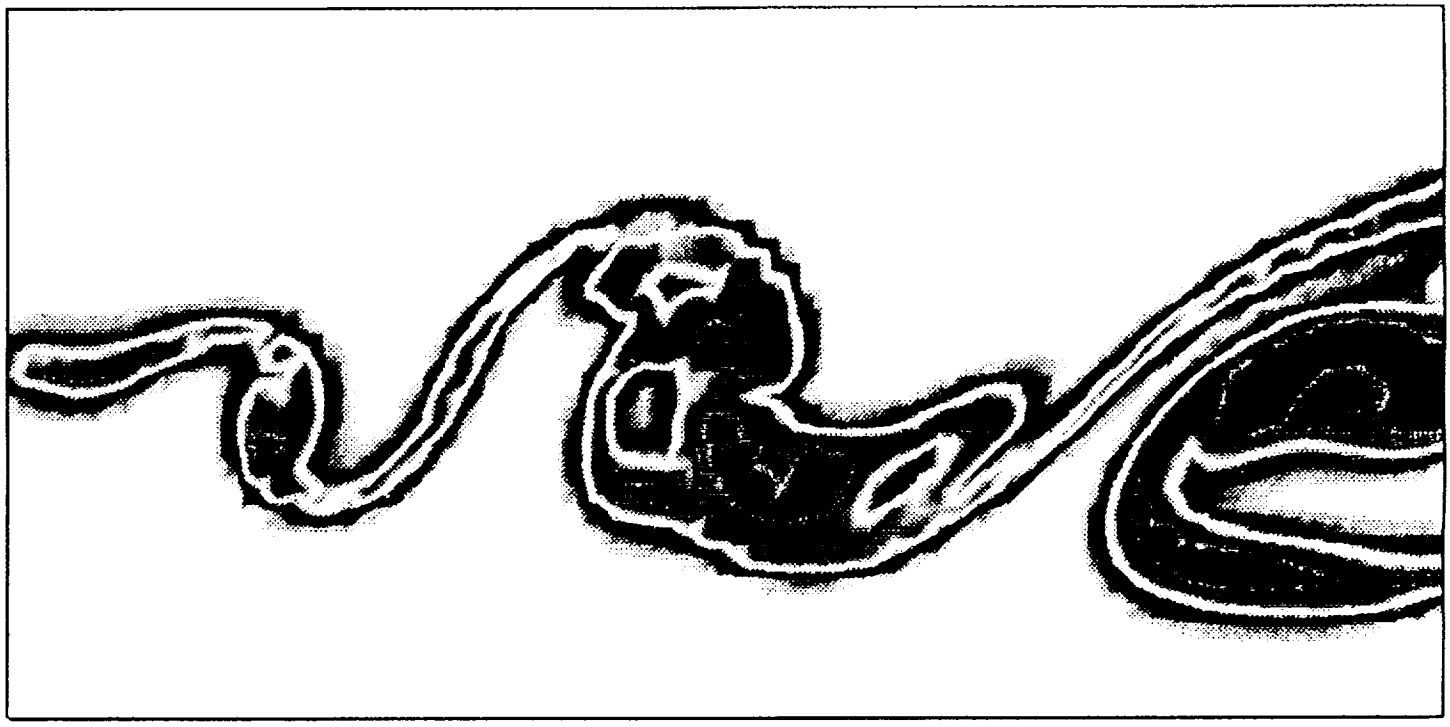

(b)

Figure 30

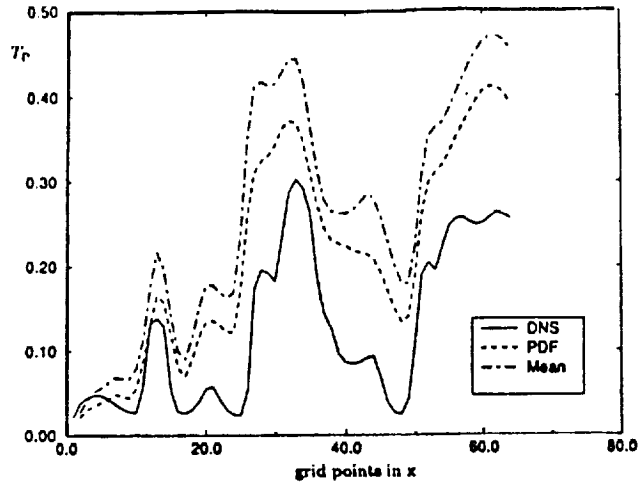

Figure 31

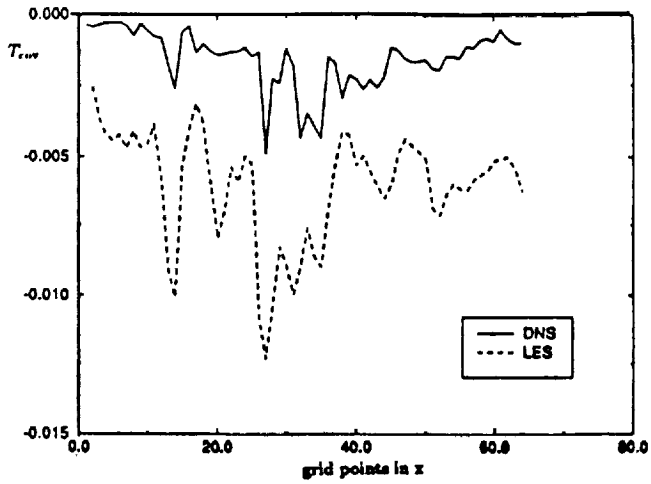

Figure 33

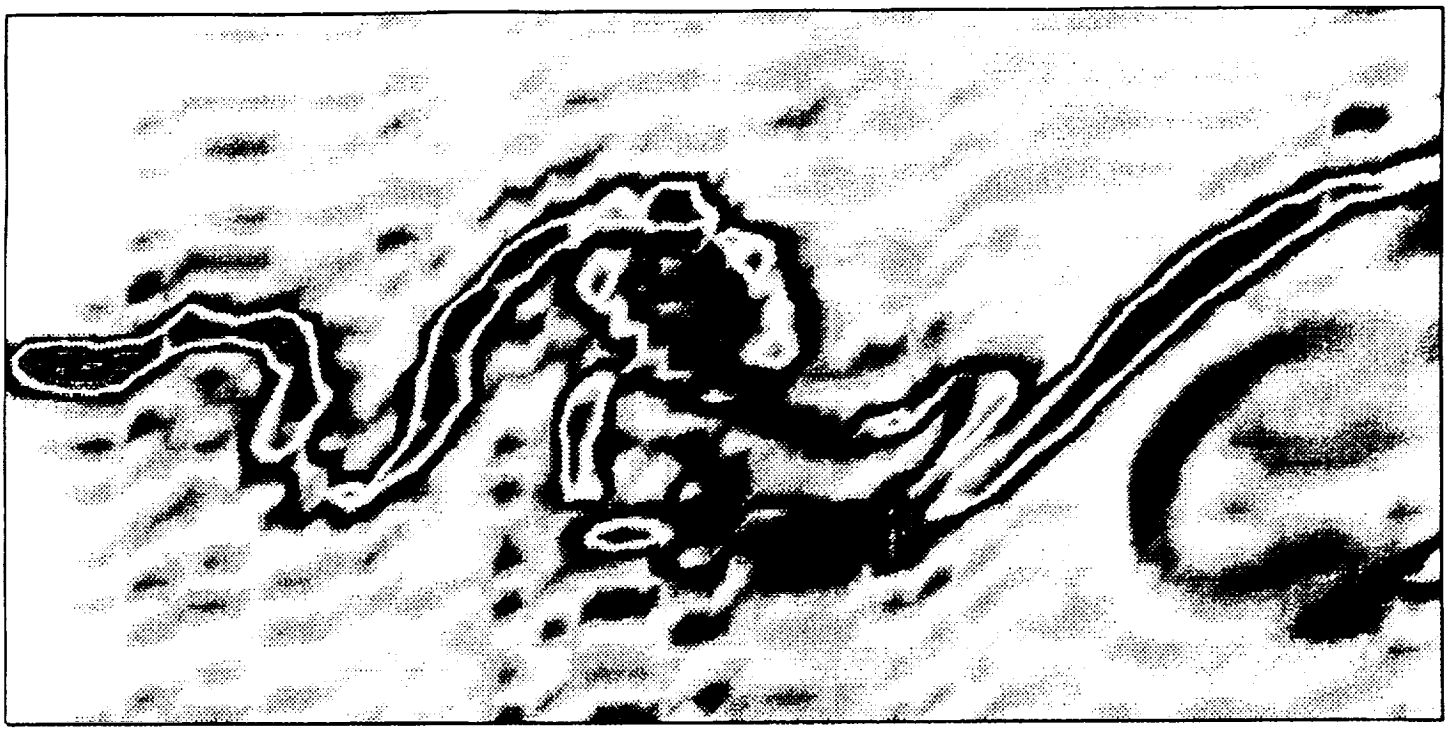

(a)

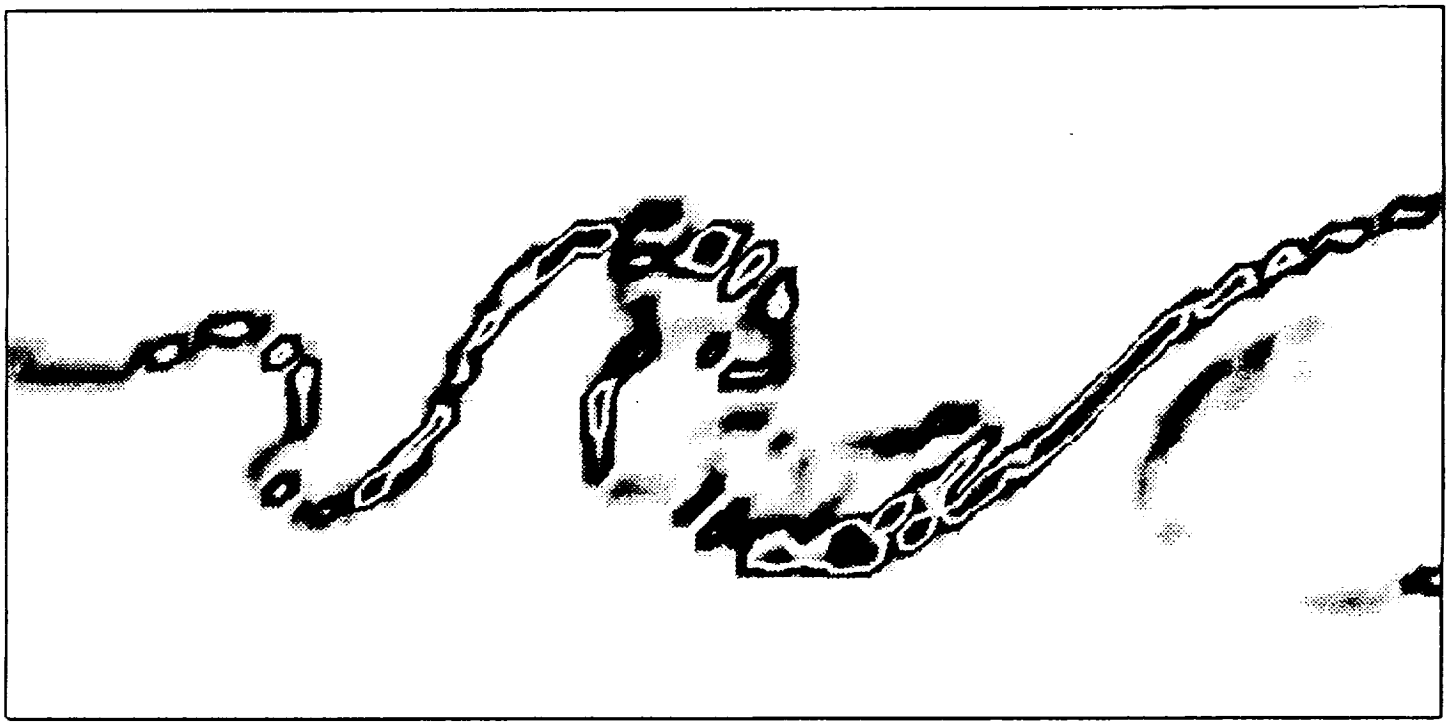

(b)

Figure 32

Appendix I

Combust. Sci. and Tech., 1991, Vol. 78, pp. 33-67
Photocopying permitted by license only

© Gordon and Breach Science Publishers S.A.
Printed in United Kingdom

Effects of Compressibility and Heat Release in a High Speed Reacting Mixing Layer

P. GIVI, C. K. MADNIA, C. J. STEINBERGER *Department of Mechanical and Aerospace Engineering, State University of New York, Buffalo, NY 14260*

M. H. CARPENTER and J.P. DRUMMOND *Theoretical Flow Physics Branch, NASA Langley Research Center, Hampton, VA 23665*

(Received July 17, 1990; in final form March 14, 1991)

Abstract—Results are presented of direct numerical simulations of a two-dimensional temporally developing high speed mixing layer under the influence of a second-order non-equilibrium chemical reaction of the type $A + B \rightarrow Products + Heat$. Simulations are performed with different magnitudes of the convective Mach number and with different chemical kinetics parameters for the purpose of examining the isolated effects of the compressibility and the heat released by the chemical reaction on the structure of the layer. A full compressible code is developed and utilized, so that the coupling between mixing and chemical reaction is captured in a realistic manner.

The results of numerical experiments indicate that at the initial stages of the layer's growth, the heat release results in a slight enhanced mixing, whereas at the intermediate and the final stages, it has a reverse influence. The effect of compressibility is the same in all stages of the development; increased compressibility results in a suppressed mixing and, thus, in a reduced reaction conversion rate. Mixing augmentation by heat release is due to expansion of the layer caused by the exothermicity, and mixing abation is caused by suppression of the growth of the instability modes due to increased heat release and/or compressibility.

Calculations are performed with a constant rate kinetics model and an Arrhenius prototype, and the results are shown to be sensitive to the choice of the chemistry model. In the Arrhenius kinetics calculations, the increase of the temperature due to chemical reaction is substantially higher than that of the constant rate kinetics simulations. This results in a more pronounced response of the layer in all stages of the growth, *i.e.*, an increased thickening of the layer at the initial phase of growth, followed by subdued thickening at later stages.

Key words: Supersonic combustion, Turbulent reacting flows, Direct numerical simulations, Compressible shear flows.

1 INTRODUCTION

Within the past five years, there has been a renewed interest in the analysis of high speed flows, both reacting and non-reacting. This interest has been, to a large extent, motivated by the need for the development of airbreathing vehicles capable of cruising at hypersonic speeds. This need in view of the goals of U.S. government in constructing such vehicles in the near future has resulted in a dramatic increase in research activities (both fundamental and applied) in the area of supersonic combustion. Of particular interest are the reactive systems of supersonic combustion ramjet (scramjet) engines (Waltrup and Billing, 1986; White *et al.*, 1987; Drummond, 1991; Drummond *et al.*, 1991 Givi and Riley, 1991). According to recent surveys of airbreathing technology for hypersonic applications, in the combustor of a scramjet engine the fuel is injected at near sonic conditions into a supersonic air stream and combustion occurs in a mixing zone inside the combustor. The analysis of such a high temperature turbulent shear flow is complicated by the interaction between fluid mechanical and chemical effects, where the reactants first mix and then combine to release heat which in turn alters the structure of the flow.

A basic understanding of the complex physical phenomena associated with high speed combustion requires a detailed knowledge of the effects of mixing and chemical

reactions, and the coupling amongst them. Analyses must be done first in a simple configuration so that the effects of the important physical phenomena can be somewhat isolated and studied in detail. After the establishment of a basic understanding, it is then possible to make use of the knowledge gained for the purpose of design and for optimization of the actual applied processes.

The exact processes of mixing and non-equilibrium chemical reactions in an actual scramjet engine are far too complex to be investigated in a single study. Within the past decade, there has been much effort in research activities focusing on different aspects of high speed combustion, and the scientific community in this area has benefited substantially from the knowledge gained by such investigations (see Drummond, 1991 for a recent review). These activities have been concentrated on both analytical/computational and experimental efforts, and the results obtained to date have been invaluable in providing a better understanding of the intricate details of the reacting compressible transport. The outcome of these analyses, together with the findings of ongoing and future scrutinies will undoubtedly result in an even better comprehension of these complicated phenomena.

In these efforts, the results of which are reported here, we have concentrated on some specific issues regarding the transport of high speed chemically reacting flows. Namely, some effects of compressibility and heat release are the major issues under consideration. The approach is based on a computational effort, and among the tools currently in use, we have selected one based on direct numerical simulations (DNS). This approach, belonging to the class of "model free" methodology (in the terminology adopted by Givi, 1989), has proven quite useful for investigating reactive turbulent flows and its implementation for high speed combustion is deemed plausible. This has been convincingly evidenced by the outcome of several recent contributions in non-reacting high speed simulations (Lele, 1989; Mukunda *et al.*, 1991; Sandham and Reynolds, 1989; Soetrisno *et al.*, 1988; Tang *et al.*, 1989).

Since this is a focused (and somewhat a "narrow-minded") investigation of a very complicated phenomenon, we have selected a simple system in which each of the desired effects can be optimally elucidated. The system adopted is composed of an unsteady two-dimensional shear layer under the influence of a non-equilibrium irreversible chemical reaction. Due to limitations of the computational methodology, many simplifying assumptions regarding the physics of the flow and the transport of the aerothermochemical variables are made. These idealizations make the problem computationally more tractable, without disallowing the explication of desired physical phenomena.

In the next section, a description of the problem is provided together with a presentation of the non-dimensional grouping of the variables characterizing the physics of the problem. In Section 3, the results of simulations are given with a discussion on the actual physics portrayed by such results. The conclusions of this study are summarized in Section 4.

2 DESCRIPTION OF THE PROBLEM

The problem under study is a compressible two-dimensional temporally evolving mixing layer (Figure 1(a)). Within the "temporal" framework, the direction of the flow on the top stream is toward the right with a velocity U_x. The stream on the bottom half of the layer flows to the left with the same speed $(-U_x)$. The region of shear created by the velocity difference across the layer resembles that formed in a laboratory "spatially developing" layer (Dimotakis, 1989), and the temporal layer

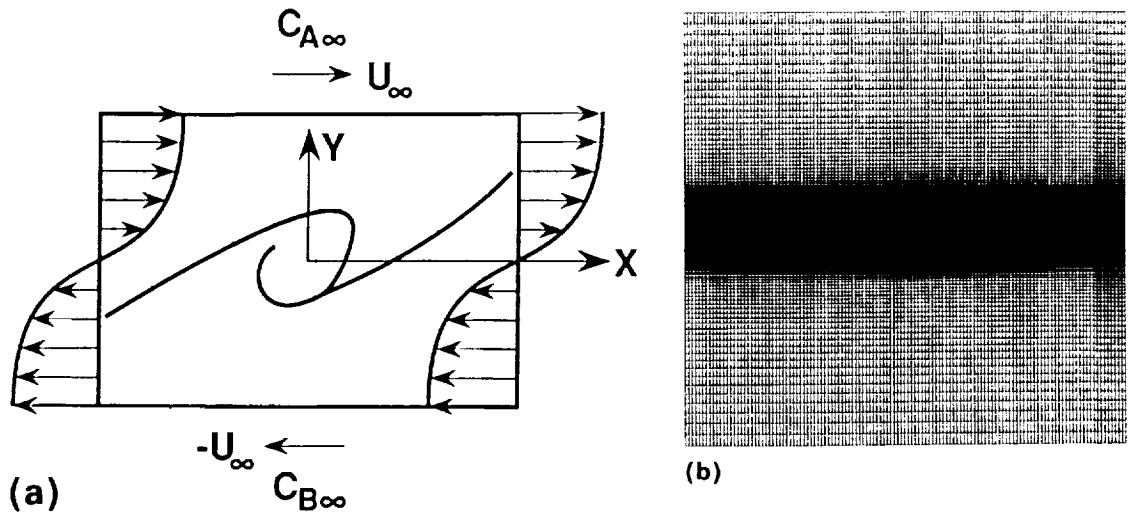

FIGURE 1 (a) Schematic diagram of a temporally evolving mixing layer. (b) The grid.

exhibits many features similar to those of a spatially developing one; namely, the formation of large scale coherent structures and their subsequent influence on the outcome of chemical reactions (Givi, 1989). The exception is the asymmetric mechanism of the mixing procedure in the spatial case (Dimotakis, 1986, Ghoniem and Ng, 1987, Grinstein *et al.*, 1986, Korczak and Hu, 1987, Lowery and Reynolds, 1986 and Givi and Jou, 1988 among others; see Givi, 1989 for a review) which cannot be captured in temporal simulations. Since this aspect of shear mixing is not the subject of the present investigation, provides a proper justification for the simulations in the format prescribed here. Further justifications of simulating temporally developing mixing layers, is provided in many analogous previous works (*e.g.*, Claus, 1986, Givi *et al.*, 1986, Metcalfe *et al.*, 1987, Riley *et al.*, 1986, McMurtry *et al.*, 1989 among others).

The speed in both streams is large enough so that compressibility effects cannot be ignored. A parameter which characterizes this effect is the magnitude of the free stream Mach numbers. For unity temperature and density ratios of free stream flows, the Mach number is the same in two streams and is the same as the "convective Mach number, M_c" identified and widely utilized in characterizations of spatially developing compressible mixing layers (Papamoschou and Roshko, 1988, Dimotakis, 1989).

The reacting species are introduced into the layer at the free streams. The chemical reaction occurring within the flow is idealized to a simple irreversible second-order form of $A + B \rightarrow Products + Heat$. Reactant A is introduced on the top stream, and reactant B on the bottom stream. The two species are assumed to have identical thermodynamical properties, and the mass diffusion is assumed to obey the Fick's law. Moreover, the assumption of a calorically perfect gas is made with a constant ratio of the specific heats.

The flow field is initialized with a hyperbolic tangent streamwise velocity with a specified initial vorticity thickness ($\delta_\omega|_0$). At the initial time, species A is assumed to cover the top half of the layer, and species B the bottom half. The initial temperature, pressure and the density are assumed uniform throughout the field and the size of the computational box in the two directions (L_x, L_y) is large enough to accommodate for the growth of the layer. In all the simulations $L_x/(\delta_\omega|_0) = L_y/(\delta_\omega|_0) \approx 100$.

The chemical reaction between the two species is characterized by the kinetics mechanism employed in the simulations. It is assumed that the rate of reactant conversion is given by a single-step model of the type:

$$\omega = K_f C_A C_B, \tag{1}$$

where C_A and C_B denote the concentrations of the two reacting species, and are assumed equal at free streams, *i.e.*, $C_{A_\infty} = C_{B_\infty} = C_\infty$. K_f is the parameter measuring the extent of reaction. This parameter is normalized to form the definition of the Damköhler number:

$$Da_f = \frac{K_f C_\infty}{U_\infty / \delta_\omega|_0}. \tag{2}$$

Two chemistry models are employed in the simulations, one with constant rate kinetics (*i.e.* constant K_f), and the other with an Arrhenius model in which K_f varies with the temperature, represented by the following equation:

$$K_f = A_f \exp\left(-\frac{Ze}{T}\right), \tag{3}$$

where T represents the temperature normalized with respect to its free stream value, T_∞, A_f is the pre-exponential factor, and Ze is the Zeldovich number defined by:

$$Ze = \frac{E}{RT_\infty}. \tag{4}$$

Here, E is the activation energy, and R is the universal gas constant. In the Arrhenius kinetics calculations, the pre-exponential factor A_f replaces K_f in the definition of the Damköhler number (Eq. 2).

Combustion exothermicity is measured by the energy liberated by the chemical reaction ΔH^0. The magnitude of this energy is parameterized by a non-dimensional heat release parameter Ce defined by:

$$Ce = \frac{-\Delta H^0}{C_p T_\infty}, \tag{5}$$

where C_p is the specific heat. In this form, $Ce = 0$ corresponds to a non-heat releasing chemical reaction.

The governing equations of the compressible reacting flow field are solved by a new version of the SPARK computer code originally developed by Drummond (1987, 1988). This new version, in comparison to the original form, has the capability of employing several high order finite difference schemes for solving the governing transport equations of compressible reacting flow fields. The numerical algorithm employed in this code is tailored for full compressible simulations, so that all the important aspects of compressibility (Chu and Kovasznay, 1958; Kovasznay, 1957) are captured. In its current form, the code is capable of implementing several ad-

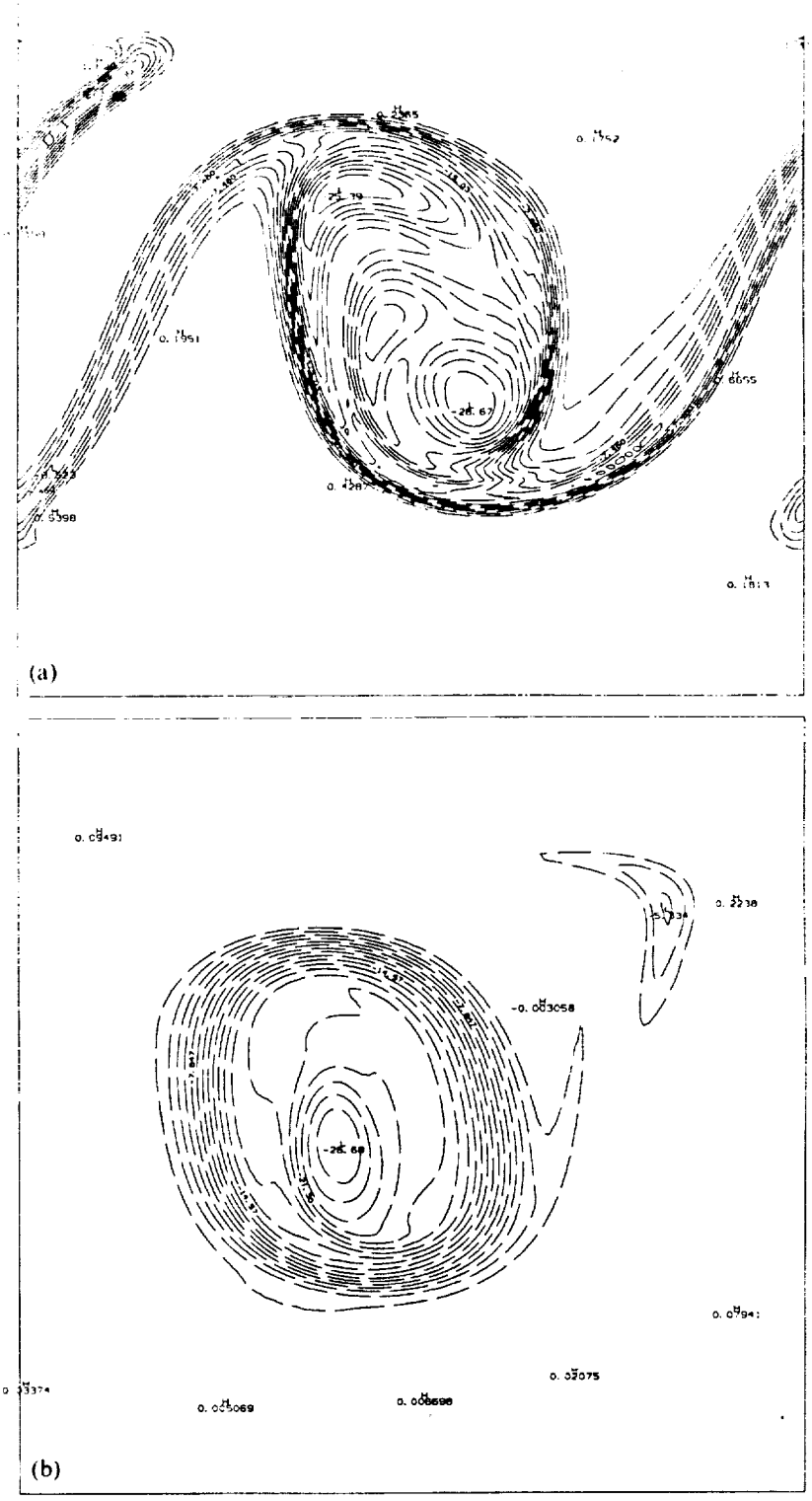

FIGURE 2 Plots of vorticity contours at different time realizations, $M_c = 0.2$, $Ce = 0$. (a) $t^* = 6$, (b) $t^* = 8$.

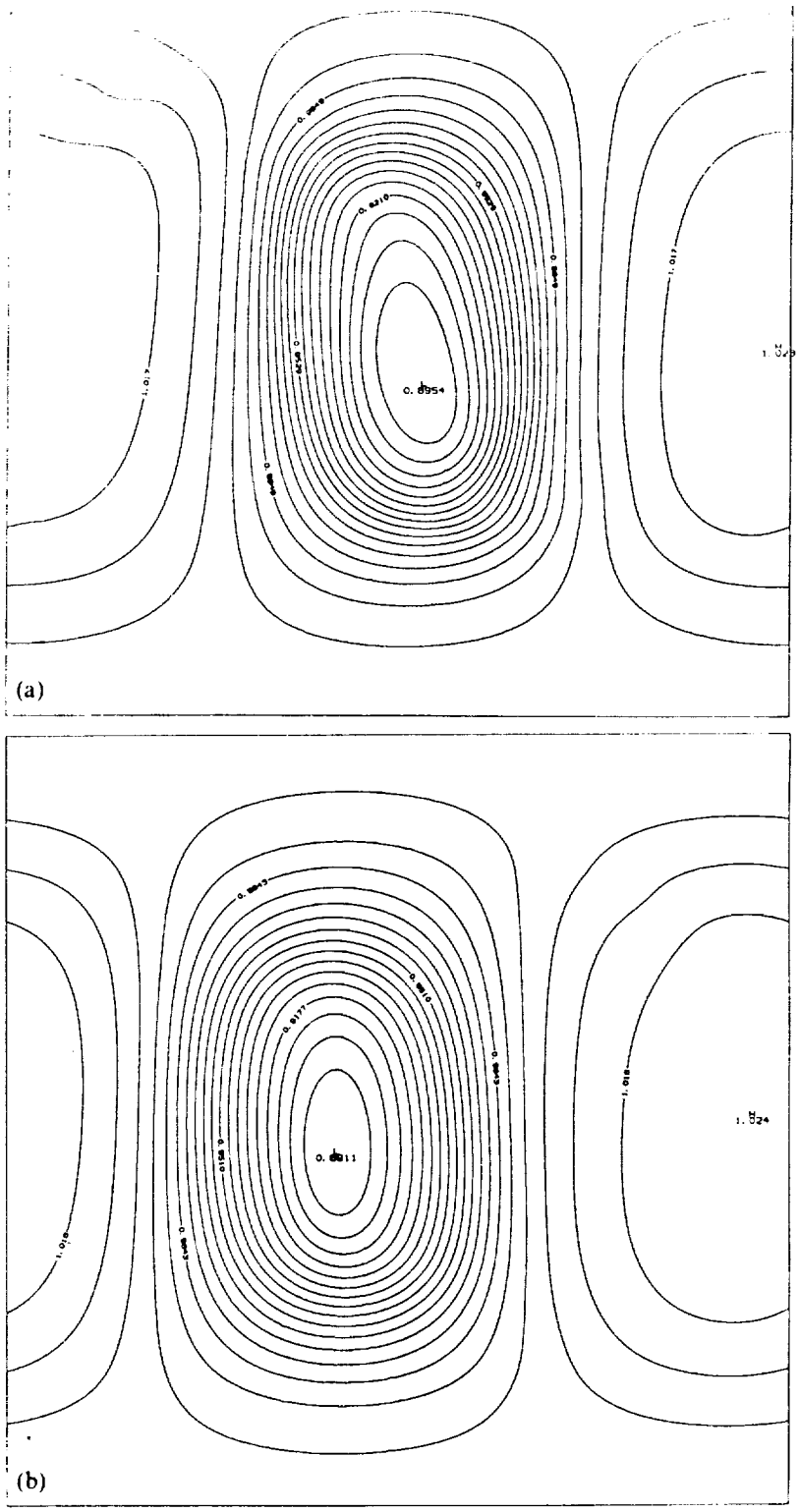

FIGURE 3 Plots of pressure contours at different time realizations, $M_c = 0.2$, $Ce = 0$. (a) $t^* = 6$, (b) $t^* = 8$.

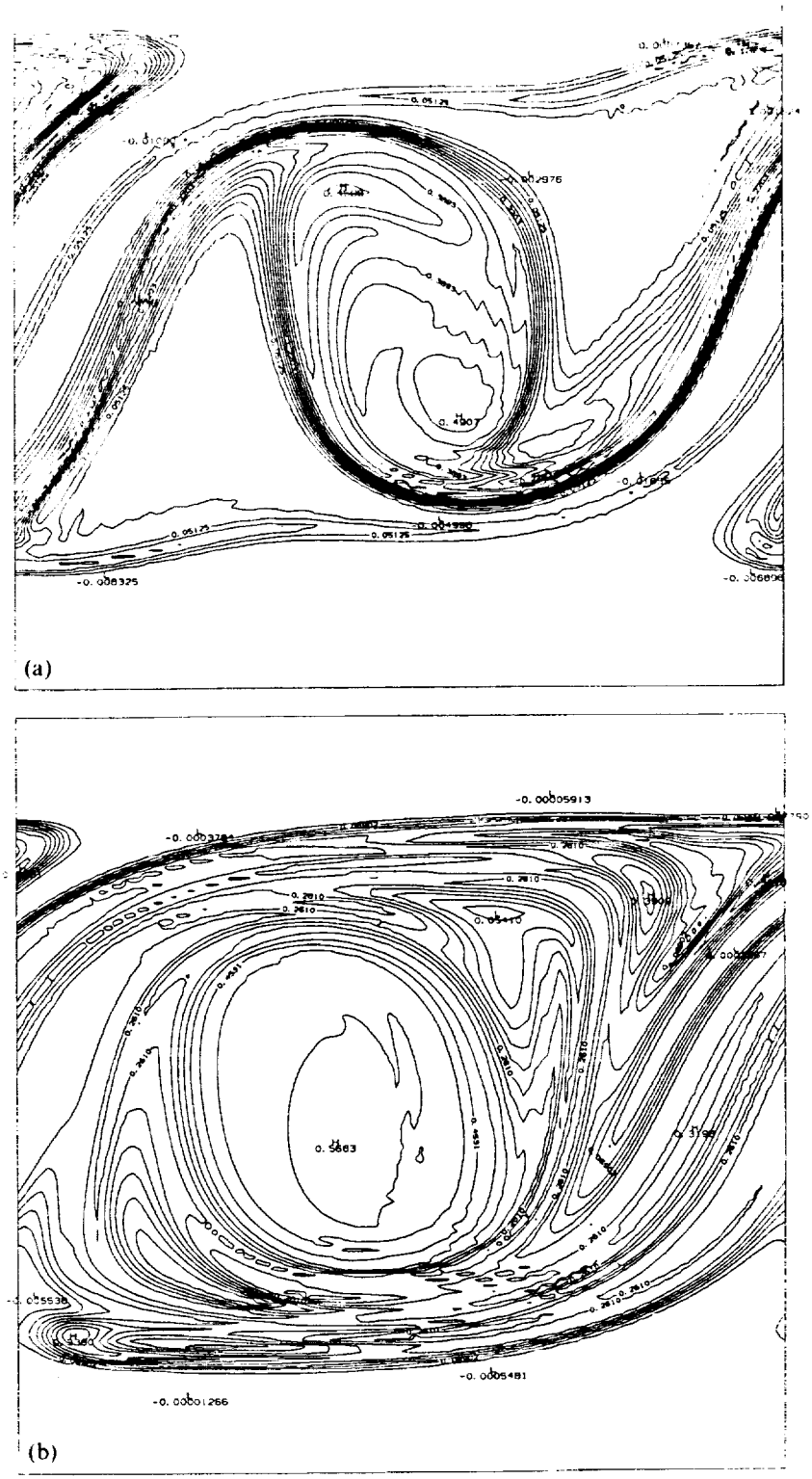

FIGURE 4 Plots of product mass fraction contours at different time realizations, $M_c = 0.2$, $Ce = 0$. (a) $t^* = 6$, (b) $t^* = 8$.

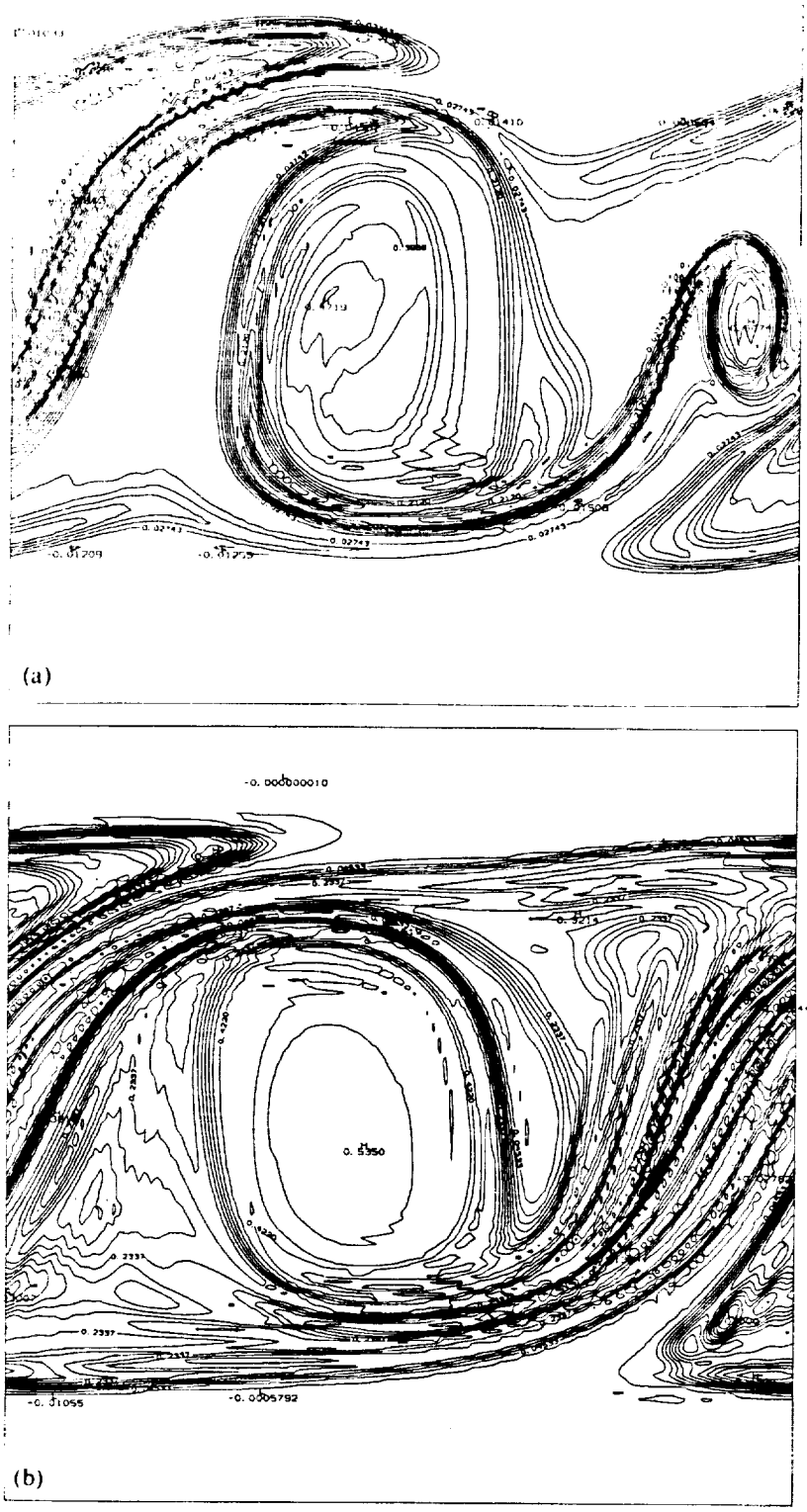

FIGURE 5 Plots of product mass fraction contours at different time realizations, $M_c = 0.4$, $Ce = 0$. (a) $t^* = 6$, (b) $t^* = 8$.

vanced numerical algorithms for this purpose (Carpenter, 1988, 1989, 1990). Among the available options, we selected to utilize the scheme suggested by Gottlieb and Turkel (1976). This scheme provides a fourth order accuracy in evaluating the spatial derivatives and a second order truncation in the temporal discretziation. The results of some rigorous tests by Carpenter (1990) and Steinberger (1991) show that with proper resolution, this algorithm is comparable with schemes based on spectral type approximations (Canuto *et al.*, 1987) and is suitable for discretization of the equations considered here. These equations have been given in a number of previous publications (Drummond, 1988, Carpenter, 1989; also see Williams, 1985), and will not be repeated here. A special care was taken in generating a fine resolution grid, so that the essential features of the reacting compressible field are not concealed by numerical errors.

3 PRESENTATION OF THE RESULTS

Calculations are performed with different values of the convective Mach number M_c, and the heat release parameter Ce, in order to assess the influence of these parameters on the structure of the layer. In this assessment, all the other non-dimensional parameters have been kept constant to isolate the effects of compressibility and exothermicity. The simulations were performed on a domain discretized with 256×256 grid points, and some on a 128×128 mesh for accuracy checks. A constant grid size distribution was employed in the streamwise direction, *i.e.* constant ΔX, but in the cross stream, the grids were unequally spaced with a heavy mesh concentration near the center of the layer ($Y = 0$) covering the region dominated by large scale structures. A schematic of the grid orientation for 128×128 simulations is shown in Figure 1(b). The routine utilized for grid generation is described in detail by Drummond (1988), and will not be discussed here. With the resolution attained, it was possible to perform simulations with a Damköhler number of $Da_l = 100$, and a Reynolds number of 250 based on the initial vorticity thickness, initial density and the free stream velocity. The magnitudes of the Prandtl and the Schmidt numbers were assumed to be equal to unity, resulting in an identical value for the Reynolds and the Peclet numbers. The results of these simulations, together with a discussion of their implications are presented in this section.

For the purpose of flow visualization, the plots of the vorticity contours at different computational times ($t^* = tU_x/L_x$) are presented in Figure 2. In these plots (and those to be presented later), the contours are drawn on a stretched mesh with constant ΔY, so that the structures and the scales of transport are displayed clearly. This figure shows the time development of the vorticity for a case with no heat release at a convective Mach number of $M_c = 0.2$. The growth of instability modes in this layer is represented by the formation of large scale two-dimensional structures. These structures are formed initially in the form of single vortex rollups, followed by the pairing of the neighboring vortices to form a large vortex at later times. The results portrayed by this figure are similar to those of previous simulations of temporally evolving mixing layers (*e.g.*, Riley and Metcalfe, 1980; Givi *et al.*, 1986). The main difference between the results presented here and those of previous simulations is the procedure by which the perturbations are added to the mean flow. The perturbations introduced in the present simulations are generated by numerical truncation and round-off errors, whereas in previous works explicitly-added harmonic forcing were the primary source of perturbations.

The corresponding plots of the contours of the normalized pressure and the product

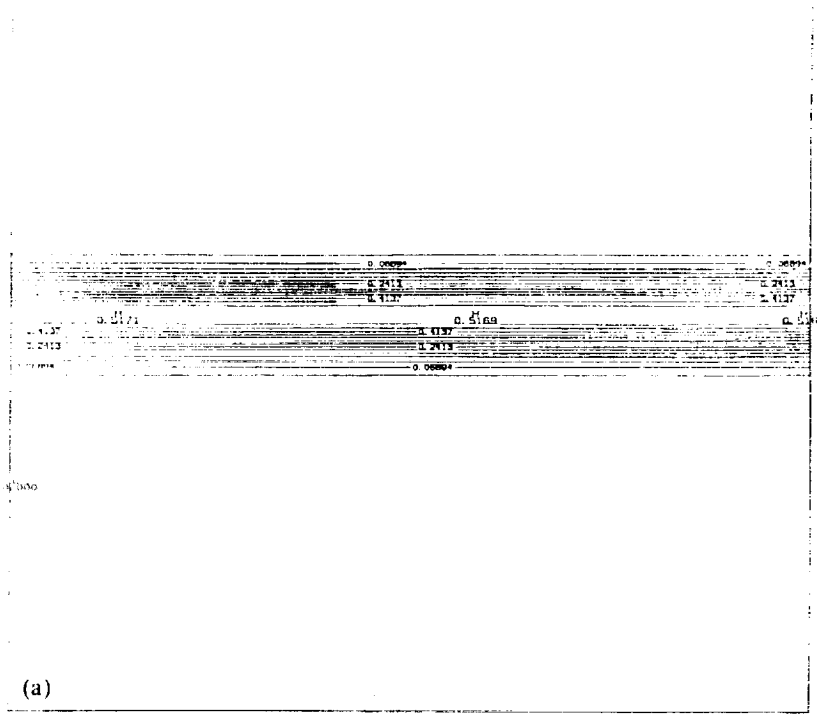

(a)

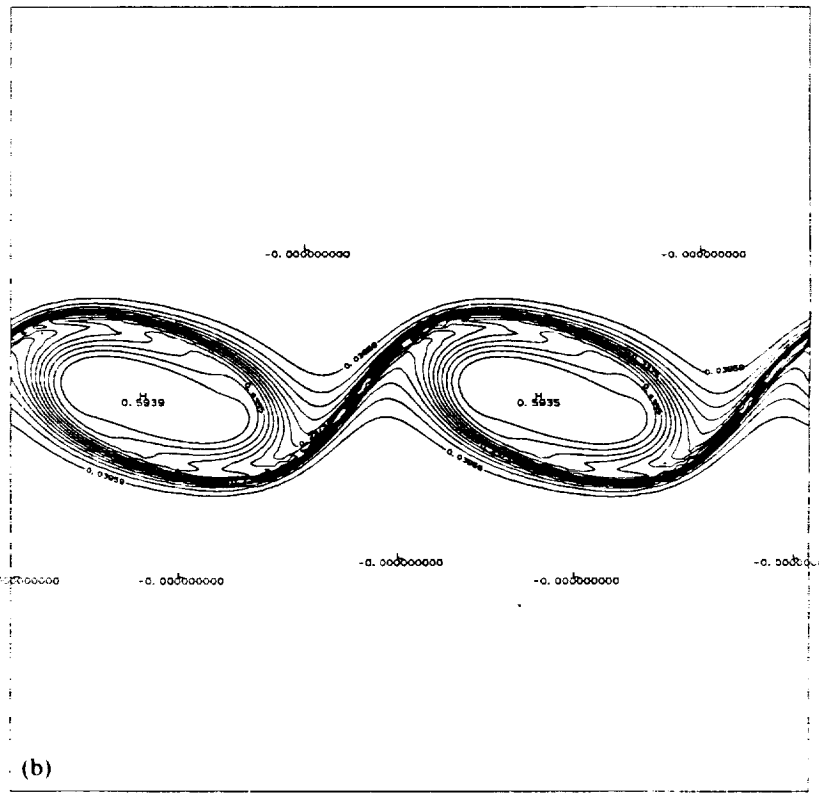

(b)

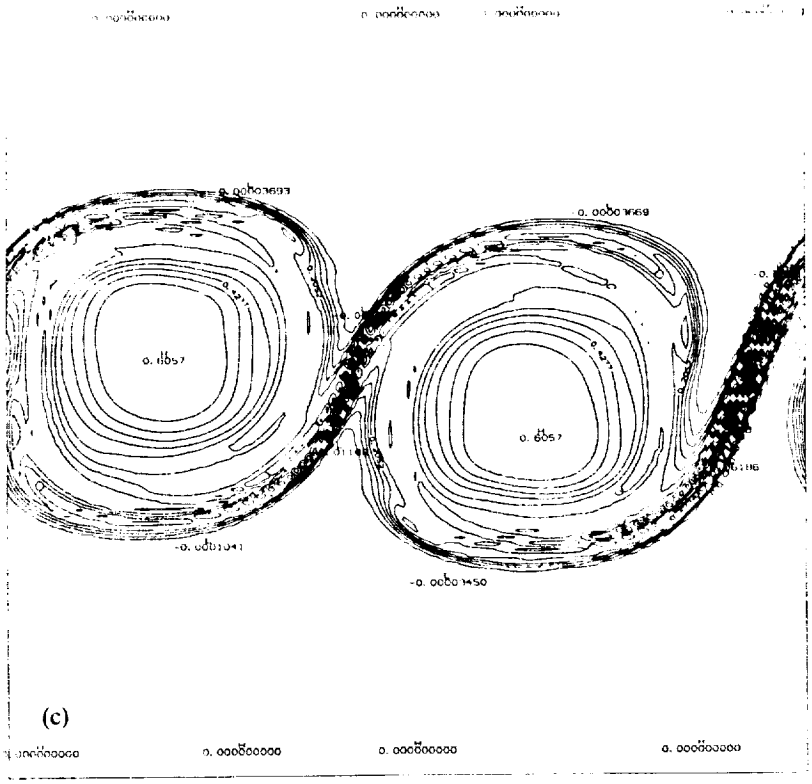

FIGURE 6 Plots of product mass fraction contours at different time realizations, $M_c = 0.8$, $Ce = 0$. (a) $t^* = 6$, (b) $t^* = 8$, (c) $t^* = 10$.

mass fraction for this case are shown, respectively, in Figures 3 and 4. Figure 3 portrays the pressure response to the formation of large scale structures. As these structures are formed, provincial regions of pressure maxima and minima occur. A comparison between Figures 2 and 3 indicates that the location of pressure minima is at the core of the vortices where the magnitude of the absolute vorticity is the highest, and the colony of pressure maxima coincides with the saddle points where the absolute vorticity is at a minimum. The formation of large scale structures results in a direct enhancement of the combustion product formation, as displayed in Figure 4. It is shown that with the development of the large scale vortices, the fluids from the two streams are brought into contact, and the chemical reaction occurs at the mixing zone with a maximum magnitude of the product mass fraction at the core of the vortices. A comparison between Figures 2 and 4 reveals the similarity of the transport of the vorticity and the product mass fraction. This is to be expected since in this case, enhanced mixing (caused by the convolution of coherent vortices) corresponds directly to an increased combustion and thus an increased product formation.

The roles played by the compressibility on reaction conversion rate can be quantitatively assessed by examining the magnitude of the product mass fraction. The plots of the contours of this fraction for different values of the convective Mach numbers (keeping heat release rate at $Ce = 0$) are shown on Figures 5–7 at different time realizations. A glimpse at these figures suggests a reverse relation between the magnitude of the convective Mach number and the extent of large scale mixing and subsequent product formation. As M_c increases, it takes longer for the background perturbations to grow and the layer becomes more sluggish in responding to such

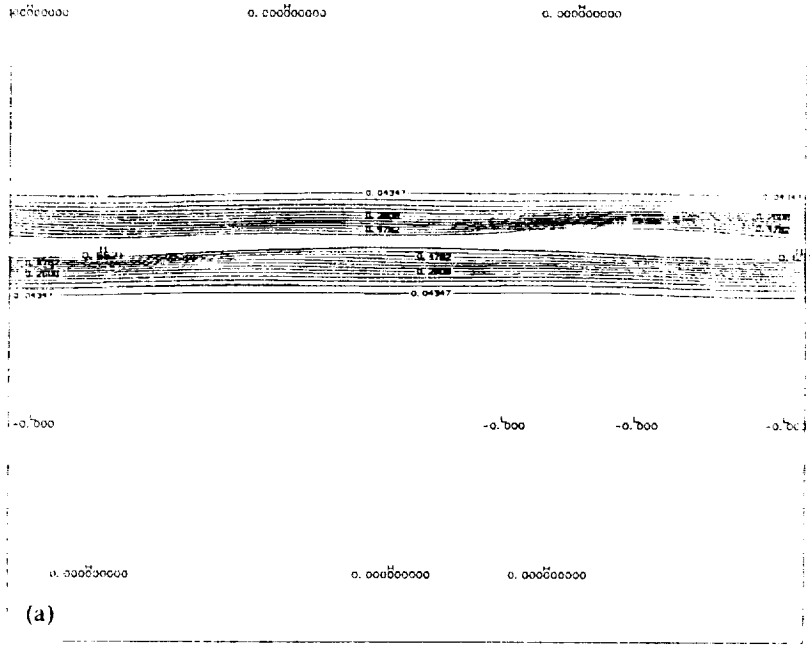

(a)

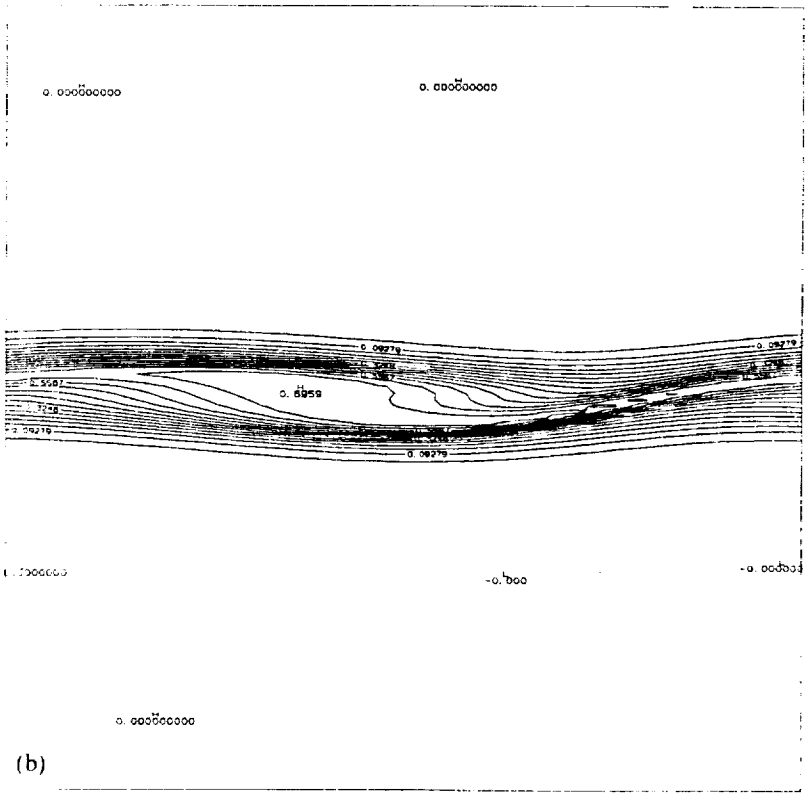

(b)

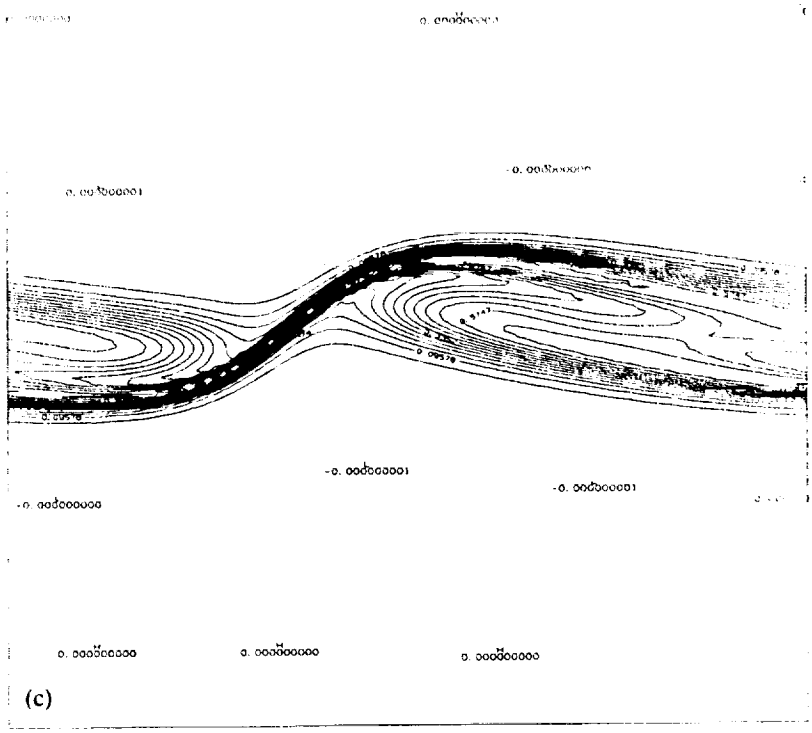

FIGURE 7 Plots of product mass fraction contours at different time realizations, $M_c = 1.2$, $Ce = 0$. (a) $t^* = 6$, (b) $t^* = 8$, (c) $t^* = 10$.

perturbations. The trend is enhanced as the Mach number is increased and at the largest Mach number employed, the rate of growth of the layer and the amount of products formed are the smallest.

The response of the shear layer to increased compressibility can be further appraised by examining the statistical and the integral properties of some appropriate parameters which characterize the flow. For this purpose, the profiles of some of the key parameters which include global information about the flow are presented in Figures 8–9. In Figure 8, the profiles of the normalized vorticity thickness are presented versus the normalized time for different values of the convective Mach number. The general trend observed in this figure indicates the reduction of the rate of growth of the layer as the Mach number is increased. This is to be expected, in view of the contour plots shown earlier; increased compressibility infers reduced mixing and reduced broadening of generated vorticity. The same is also true in the time variation of the normalized total product mass fraction, as evidenced in Figure 9.

A statistical examination of the fluid mechanical variables at selected computational times is presented in Figures 10–11. These figures present the cross stream variations of the mean and the mean square of the streamwise velocity. The knowledge of these quantities is relevant for turbulence closure, and it is the prediction of these quantities that is of main interest to turbulence modelers*. With the approximation of temporal evolution, the flow is homogeneous in the spatial direction X, and the

*Even though these simulations deal with a purely two-dimensional flow without any three-dimensional transport essential for turbulence analysis.

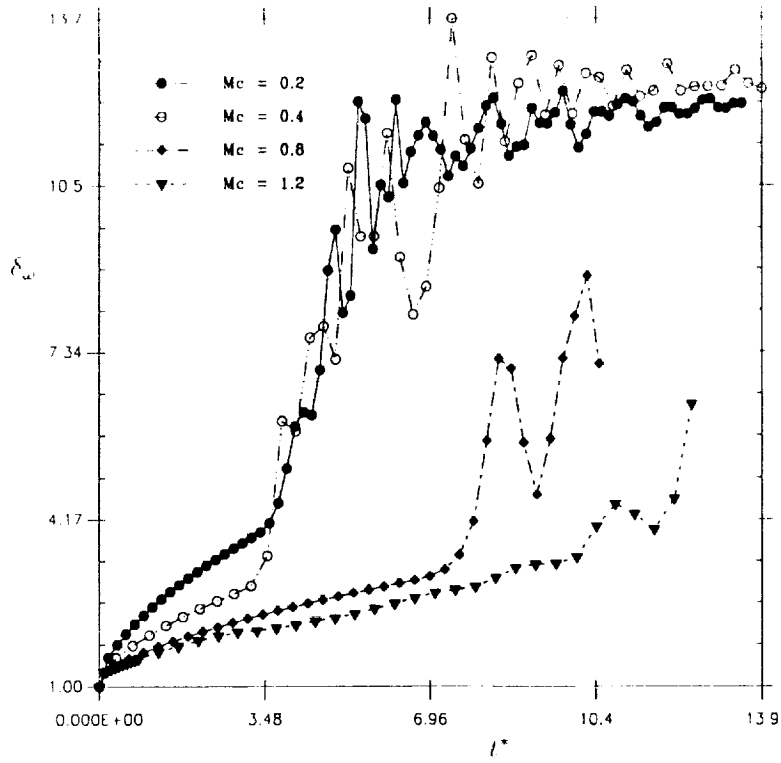

FIGURE 8 Normalized vorticity thickness versus normalized time for different values of the convective Mach number.

statistical information is obtained by sampling the data at the grid points in this direction. In this way, the ensemble mean and the mean square of a transport variable (say ϕ) are obtained by:

$$\langle \phi(Y) \rangle = \frac{1}{N} \sum_{i=1}^{N} \phi_i(Y), \tag{6}$$

$$\langle \phi'^2(Y) \rangle = \frac{1}{N} \sum_{i=1}^{N} (\phi_i - \langle \phi \rangle)^2. \tag{7}$$

Here $\langle\ \rangle$ denotes ensemble average, and the subscript i and the parameter N indicate, respectively, the grid index and the total number of grid points in the X direction.

The profiles of normalized streamwise component of the average velocity are shown in Figure 10 at different times. The most significant feature displayed in this figure is the steepness of the mean velocity profiles at high Mach numbers. Again, in view of the contour plots of the vorticity and the product mass fraction this is to be expected, and the increase in the velocity steepness (caused by the reduced growth rate), implies lesser rate of mixing and, thus, decreased product formations. This trend can also be described by examining the profiles of the mean square of the same variables as shown in Figure 11 for $t^* = 6$. Note the double hump characteristics of the mean square velocity profile at low Mach numbers, with the local maxima (at the humps) corresponding to the regions of maximum velocity gradients. Also, note that as the magnitude of the convective Mach number is increased, the amplitude of the

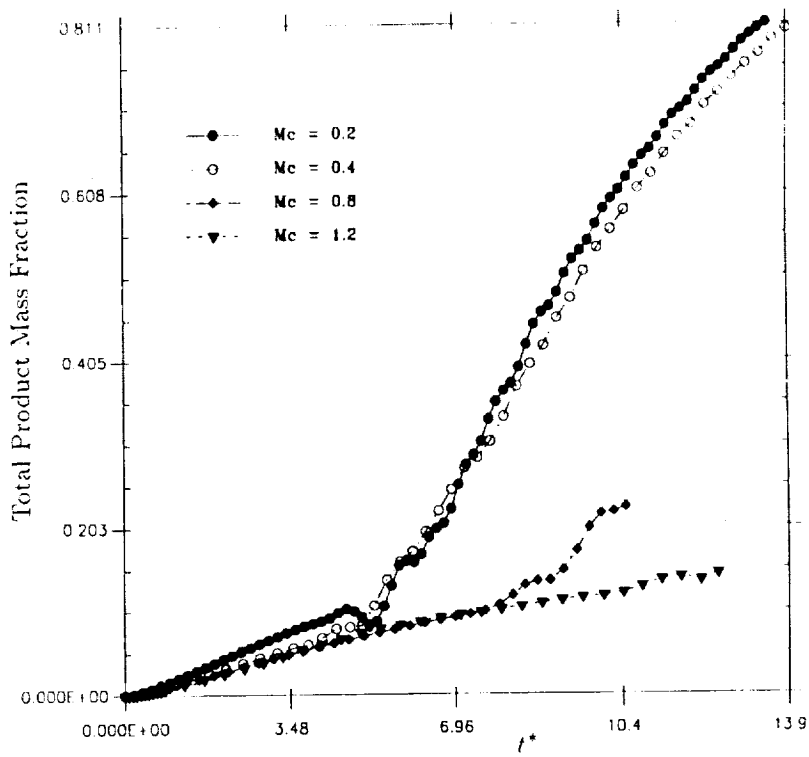

FIGURE 9 Normalized total product mass fraction versus normalized time for different values of the convective Mach number.

fluctuations decreases, and at $M_c = 0.8$ and $M_c = 1.2$, this amplitude becomes very small.

Another interesting characteristic of the increased compressibility is captured by examining the plots of pressure contours at high convective Mach numbers. A time sequence of instantaneous pressure, portraying the evolution of the layer for convective Mach numbers of 0.4, 0.8, and 1.2 are depicted in Figures 12–14. The pressure response in Fig. 12 is very similar to that presented for $M_c = 0.2$ case (Figure 3), indicating the regions of pressure maxima and minima at the braids and the cores of the vortices. At higher convective Mach numbers, however, it is observed that the increased compressibility results in steepness of the gradients of instantaneous pressure and the formation of "eddy shocklets". These shocklets are initiated at the shear zone of the layer, and extend to the outer region of the flow near the boundaries. A ratiocination for the formation of these shocklets is provided by noting the increased compressibility within the domain in high convective Mach numbers. In these cases, the layer is dominated by regions of supersonic and subsonic flows, and in order for the flow to adapt to high pressures at the braids, it must go through a shocklet to make the proper adjustment. Furthermore, it is observed in these figures that as the structures are formed, the regions of high compressibility tend to push the shocklets backward. This is evidenced by the pressure contours at small time intervals in Figures 13–14, which show that the shocklets tend to rotate in an opposite direction to the large scale vortical structures. Finally, note that the currents do not necessarily have to be supersonic at the free streams, and compression occurs within the flow as a result of the formation of large scale structures. This point is more clearly demonstrated by examining the contour plots of the instantaneous Mach numbers in Figures 15–16 (corresponding to some of the cases presented in Figures 13–14). It can be observed

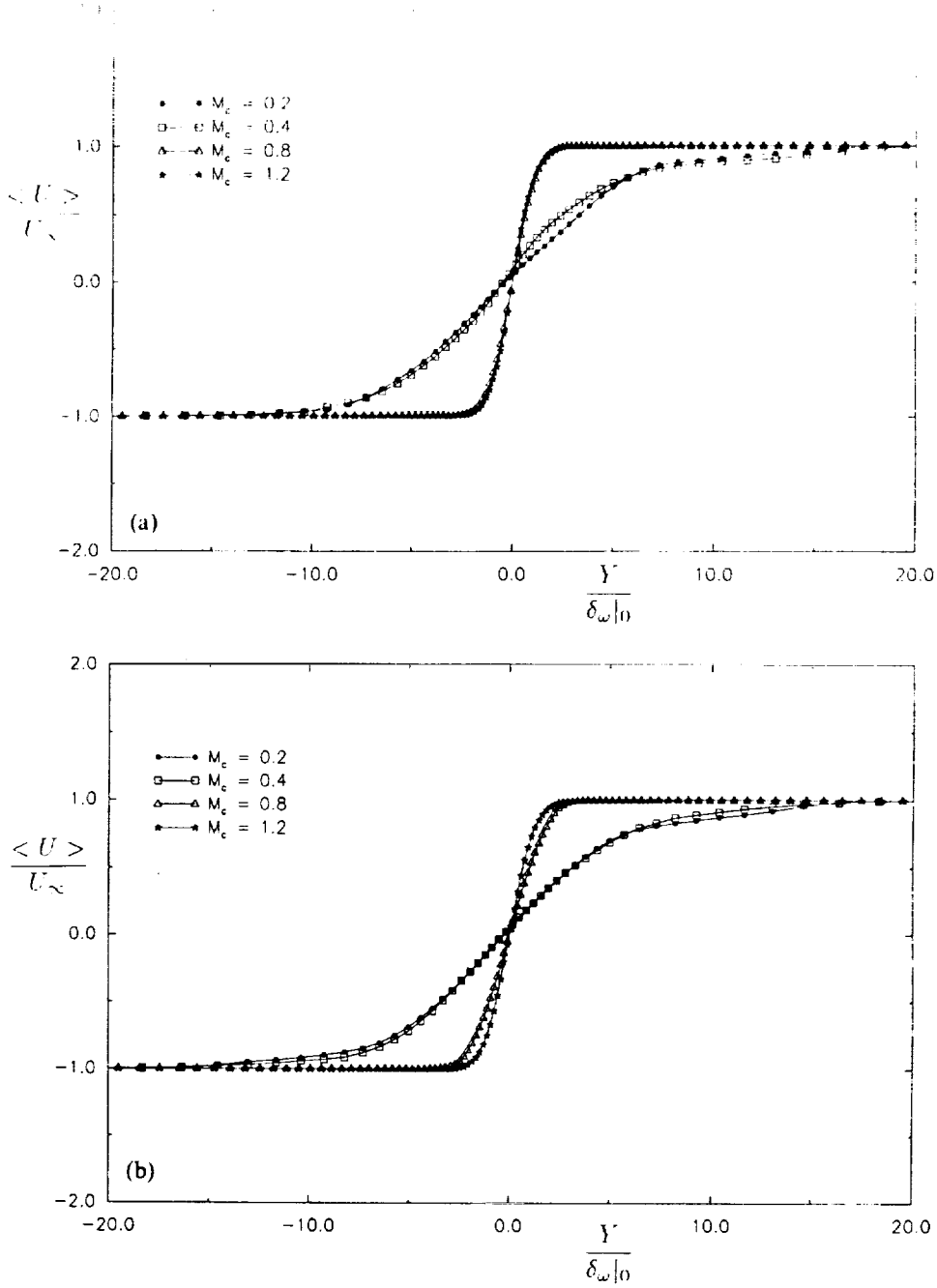

FIGURE 10 Profiles of normalized mean velocity $\langle U \rangle / U_\infty$ versus $Y/\delta_\omega|_0$ for different values of the convective Mach number. (a) $t^* = 6$, (b) $t^* = 8$.

from these figures that for the case of $M_c = 0.8$ (*i.e.* subsonic free streams) the flow at the interior is dominated with localized regions of supersonic ($Ma > 1$), and subsonic ($Ma < 1$) flows. These adjustment from supersonic to subsonic conditions is provided by the formation of eddy shocklets. The strength of these shocklets become stronger as the convective Mach number is increased (*i.e.* as the effects of compressibility become more pronounced).

The results of our simulations are consistent with those of experimental measurements (*e.g.*, Samimy and Elliot, 1990) in that as the compressibility increases, the

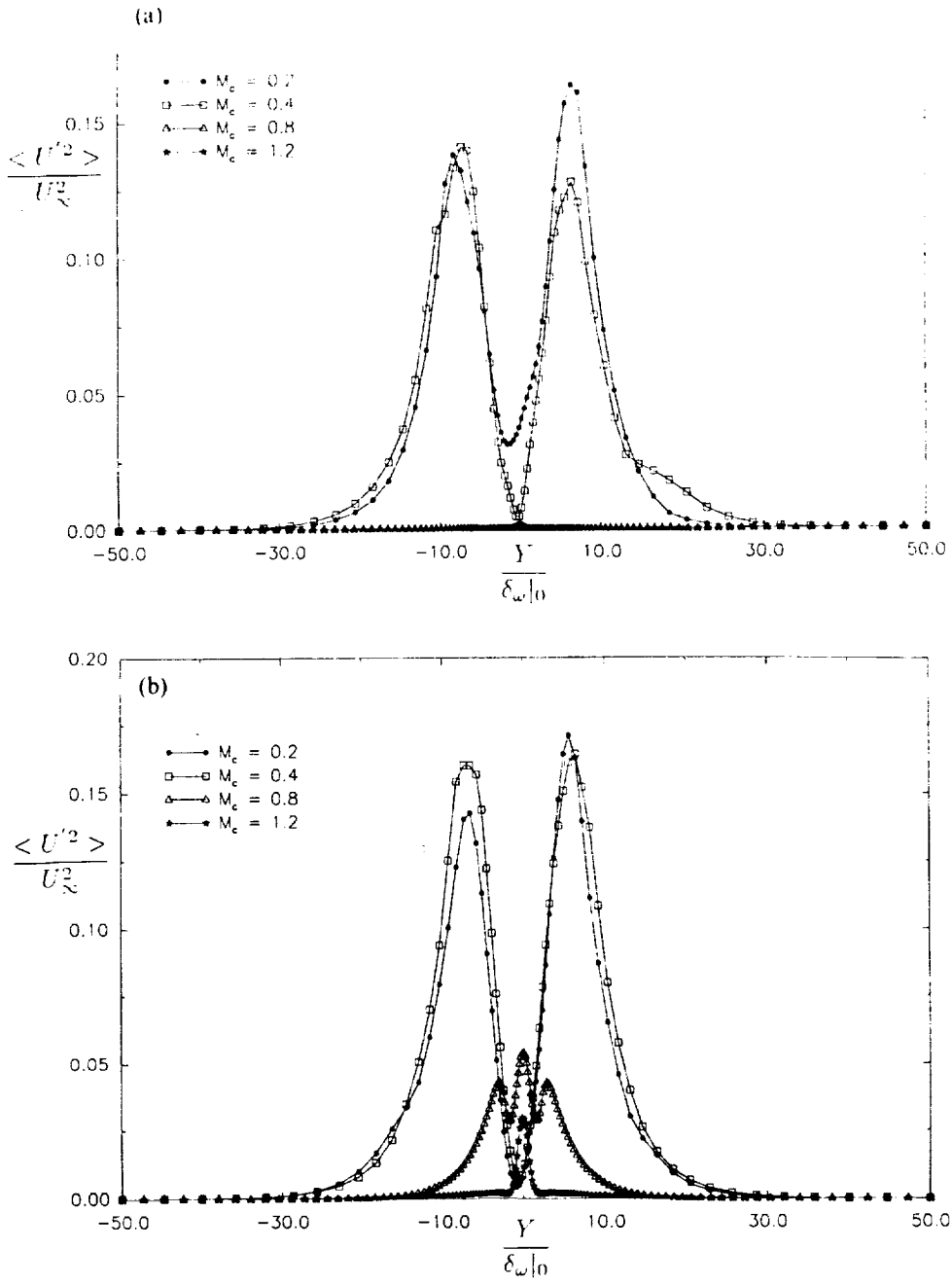

FIGURE 11 Profiles of normalized mean square velocity $\langle U'^2 \rangle / U_\infty^2$ versus $Y/\delta_\omega|_0$ for different values of the convective Mach number. (a) $t^* = 6$, (b) $t^* = 8$.

magnitudes of the turbulence fluctuations decrease. However, the eddy shocklets have not been observed in any of the experiments on compressible shear layers, to date. This could be a consequence of computational limitations in that the simulations are restrictively two-dimensional, whereas the laboratory flow is dominated by small scale three-dimensional transport. Whether or not these shocklets are formed in a flow under the influence of such transport is to be determined in future three-dimensional simulations.

The effects of heat release can be also assessed by following the same procedure as

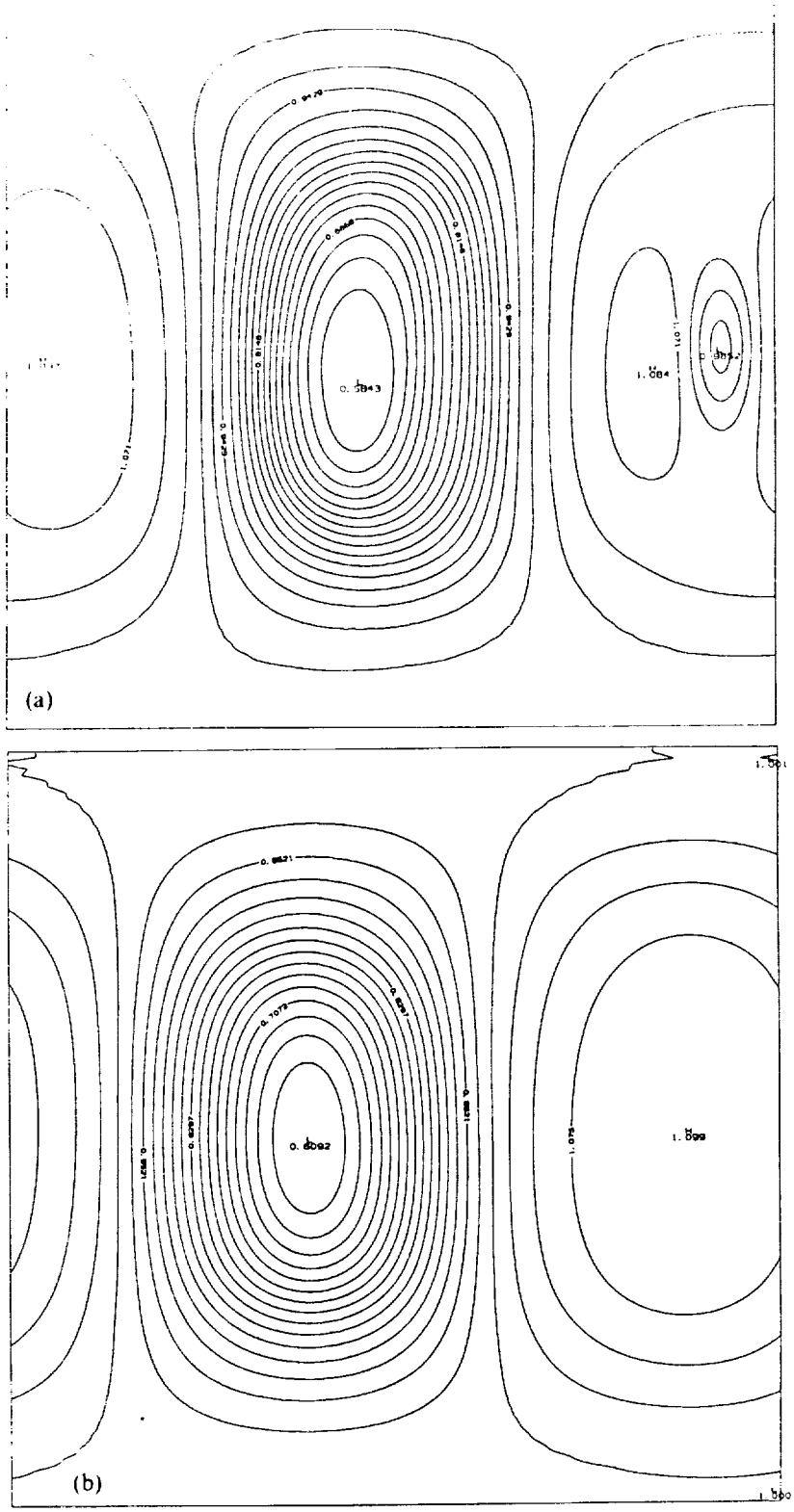

FIGURE 12 Plots of pressure contours at different time realizations, $M_t = 0.4$, $Ce = 0$. (a) $t^* = 6$, (b) $t^* = 10$.

outlined above. In the following discussions, results are presented of simulations for constant rate kinetics with $Mc = 0.2$ and heat release values of $Ce = 0$, $Ce = 1.5$, and $Ce = 6$; and one set of Arrhenius simulations with $Ce = 1.5$ and $Ze = 10$. The results of these simulations are portrayed by the plots of the vorticity thickness versus the normalized time for all four cases (Figure 17). This figure shows that the onset of formation of large scale structures is quickest for the non-heat releasing mixing layer and as the effects of chemistry become more pronounced, the response of the layer becomes more sluggish. For example note that for the $Ce = 0$ case, the layer responds to instabilities fairly rapidly, and after the initial thickening there is a jump in the magnitude of the thickness at $t^* \approx 3$. This jump indicates the formation of vortical structure as shown previously in Figure 2. An increase of the magnitude of the heat release ($Ce = 1.5$), results in a delay of the vortex rollup, and the jump in the vorticity thickness does not occur until $t^* \approx 7$. Further increase in the magnitude of the heat release results in additional delays, and as can be seen for the cases of $Ce = 6$ and $Ce = 1.5$ (with Arrhenius model), the effects of instabilities do not become apparent at all. In these cases, the effect of exothermicity is most pronounced; vorticity rollup does not occur and the only cause of vorticity thickening is due to molecular diffusion. The contour plots of the vorticity in both of these cases form parallel lines (not shown here) which indicate the lack of formation of vortical structures. At larger times, the layer becomes too "thick" to respond to perturbations within the flow, and proceeding in time does not produce any substantial enhancement in mixing except, of course, that facilitated by diffusion. The main reason for the severe retardation of mixing for the Arrhenius case in comparison with that of constant kinetics model is due to the kinetics model employed in the simulations. With the application of the Arrhenius reaction model, the rate of increase of temperature is substantially more than that of constant rate kinetics, even though the magnitude of the heat release parameter (as defined here) is kept fixed. This increase in the local (and global) magnitude of the temperature postpones the growth of the instabilities, and for the case of $Ze = 10$ (as employed here), the layer does not accommodate for the growth of the instability modes to form large scale coherent vortices.

The influence of the heat release on the compositional structure of the flame is displayed by examining the amount of normalized total product mass fraction of the layer as a function of time. This is shown in Figure 18. An examination of this figure shows the influence of heat release on all stages of the development of the layer. At initial times, the effect of heat release is a somewhat enhanced product formation, whereas at intermediate and final stages a reverse scenario holds. At the initial stages, the effect of heat release is to expand the fluid at the cores of the layer. Therefore, it is expected to have a larger mixing zone and thus a slightly larger amount of products formed. However, as the heat release increases and the layer thickens, the rate of growth of instability modes becomes subdued, postponing the rate of formation of large scale vortices. After the initial stages, the non-heat releasing simulations predict a sharp increase in the product formation and as the magnitude of the heat release is increased, the time at which such structures are formed gets delayed. The lowest rate of product formation is for $Ce = 6$ simulations in which, as discussed before, the only mechanism of mixing is through diffusion. This mechanism of reduced product formation is also evidenced by a comparison between the contour plots of the product mass fraction with heat release (Figure 19), and those without heat release (Figure 4).

Further influences of heat release become evident by examining its effect on statistical quantities. In Figure 20 the normalized profiles of mean streamwise velocity component are presented at different times. This figure shows that at early times, the local volume expansion of the fluid caused by exothermicity yields a less steep gradient

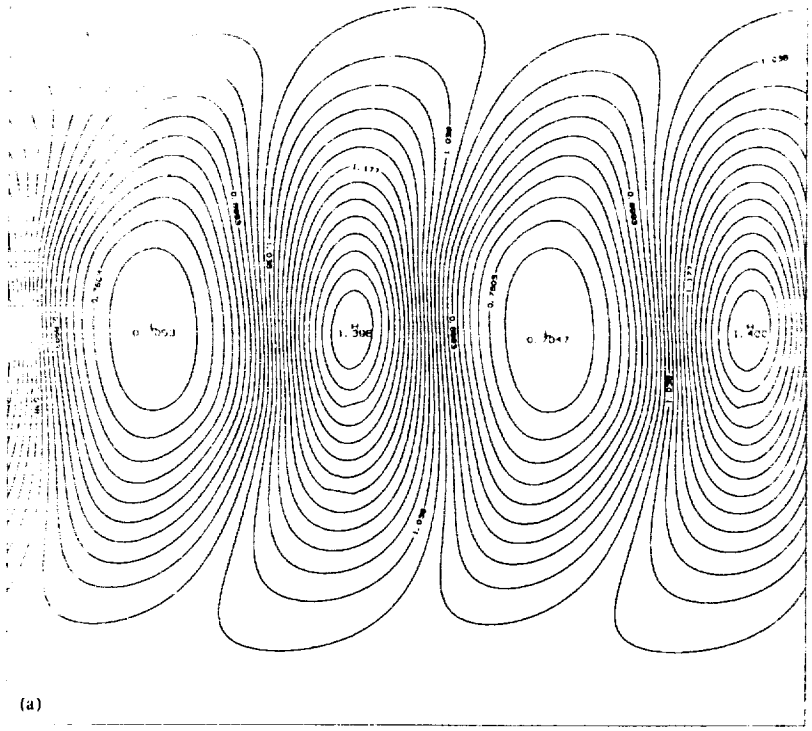
(a)

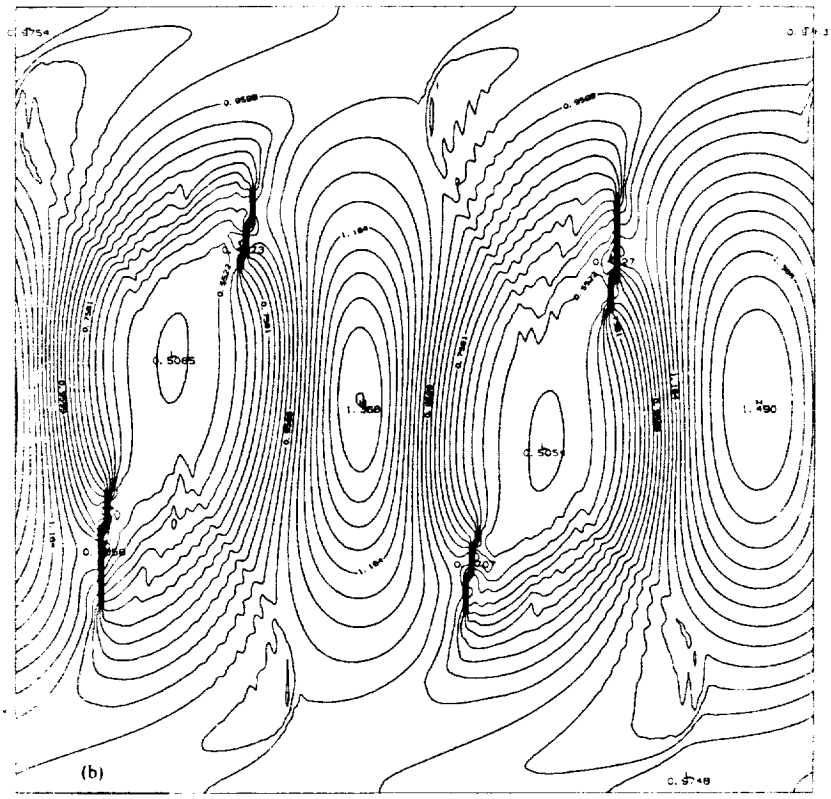
(b)

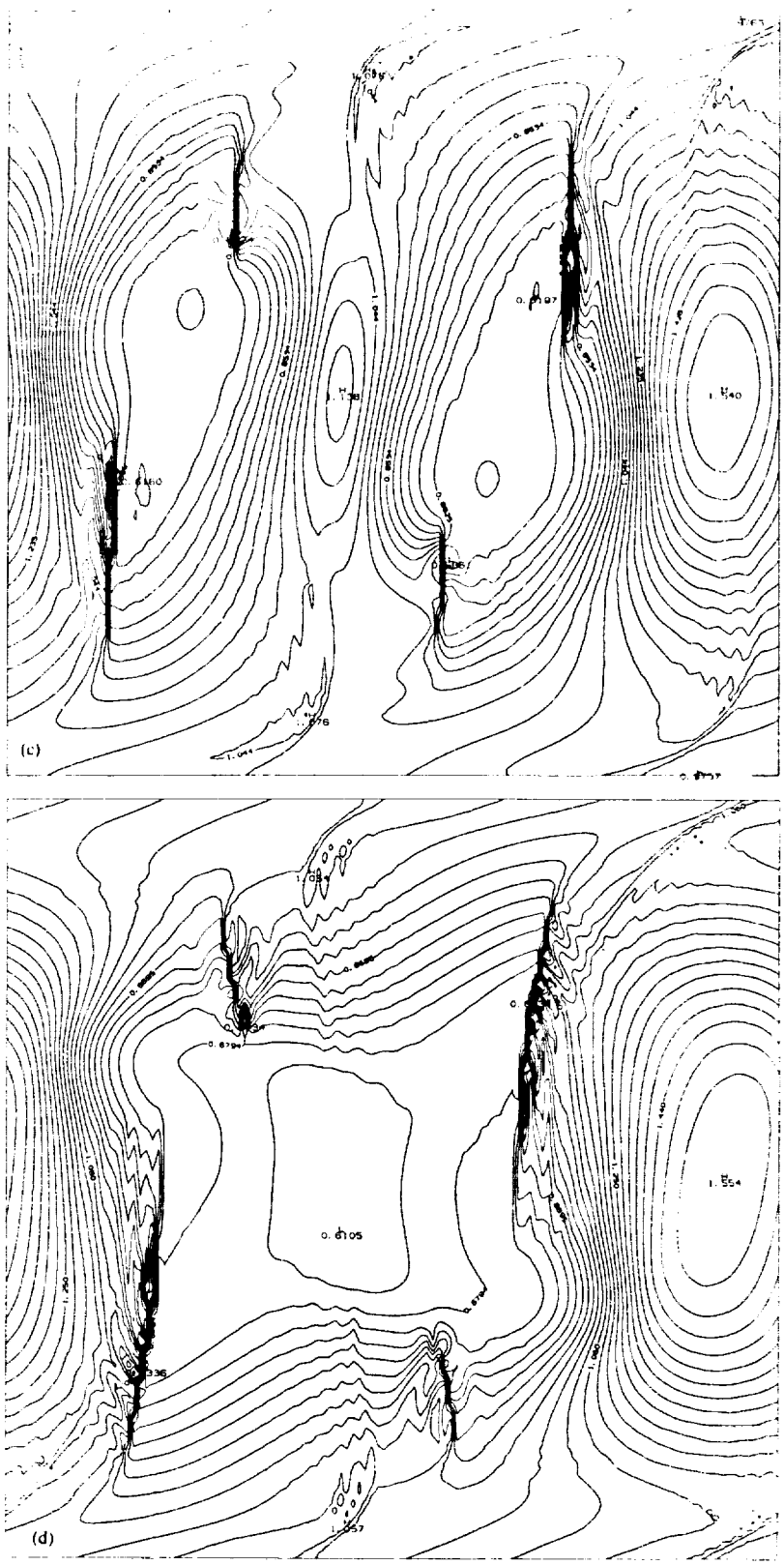

FIGURE 13 Plots of pressure contours at different time realizations, $M_c = 0.8$, $Ce = 0$. (a) $t^* = 8$, (b) $t^* = 10$, (c) $t^* = 10.26$, (d) $t^* = 10.51$.

C-2

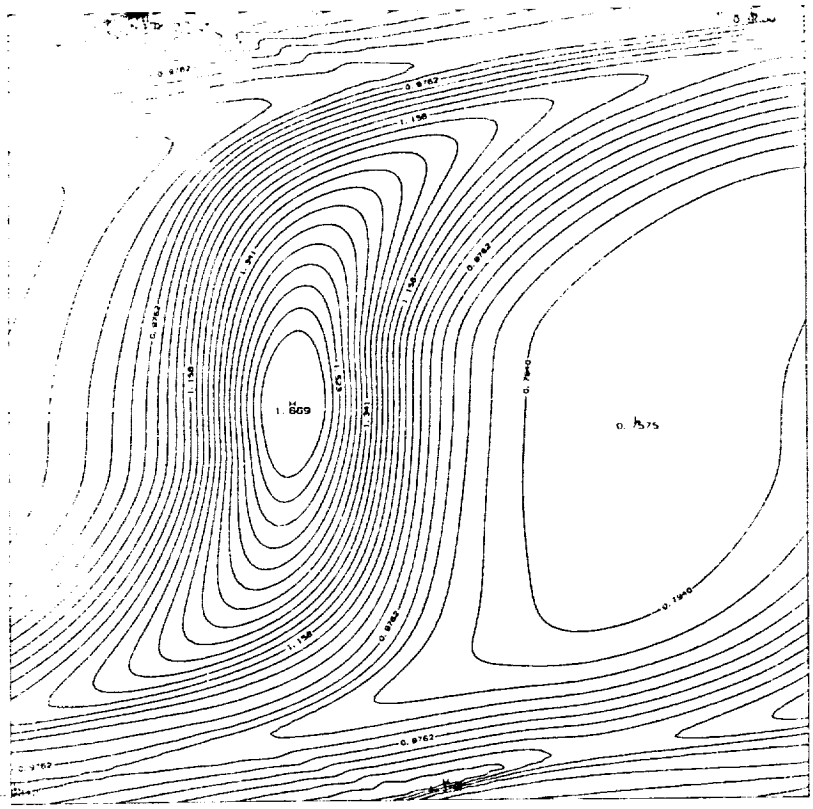

(a)

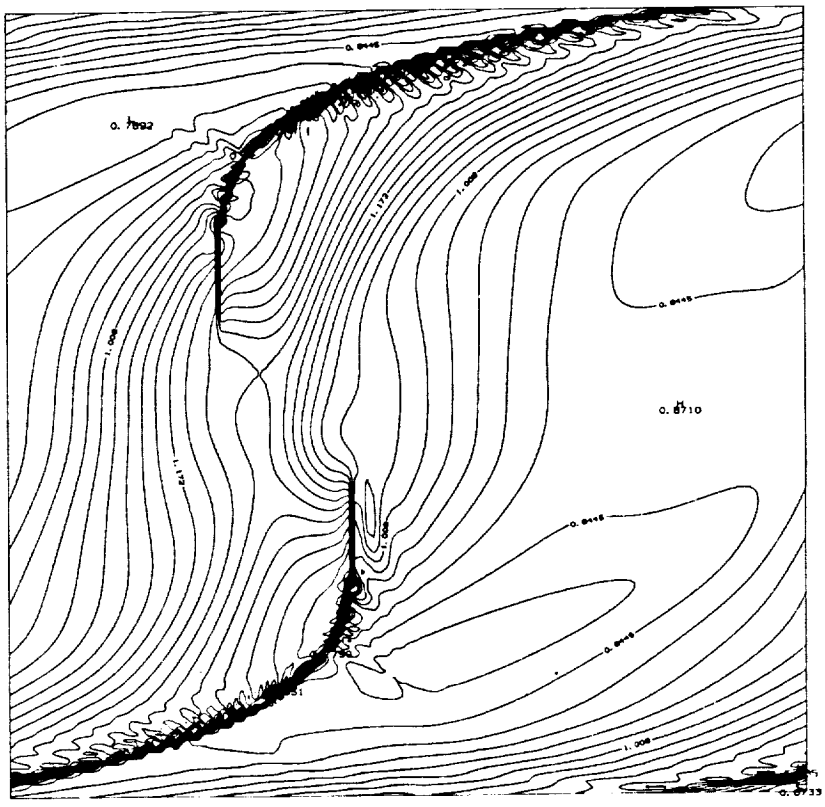

(b)

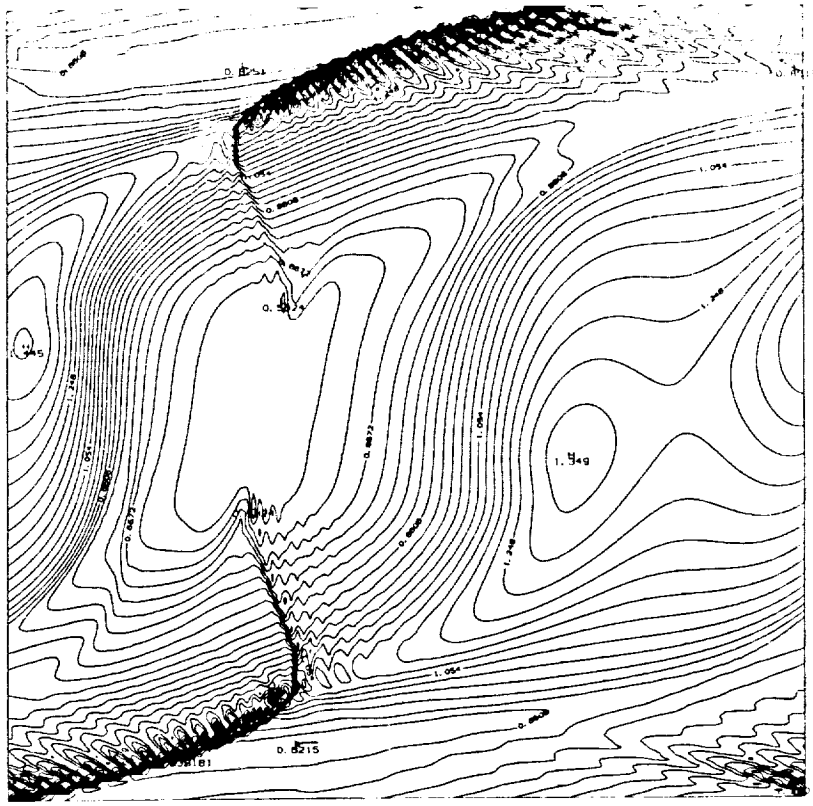

(c)

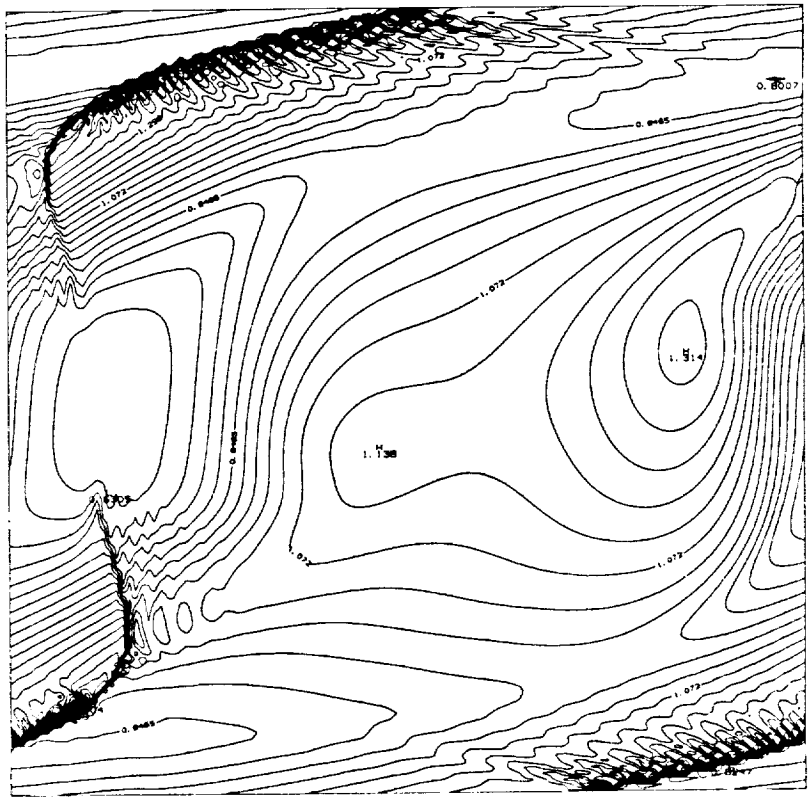

(d)

FIGURE 14 Plots of pressure contours at different time realizations, $M_c = 1.2$, $Ce = 0$. (a) $t^* = 10$, (b) $t^* = 10.85$, (c) $t^* = 11.66$, (d) $t^* = 12.5$.

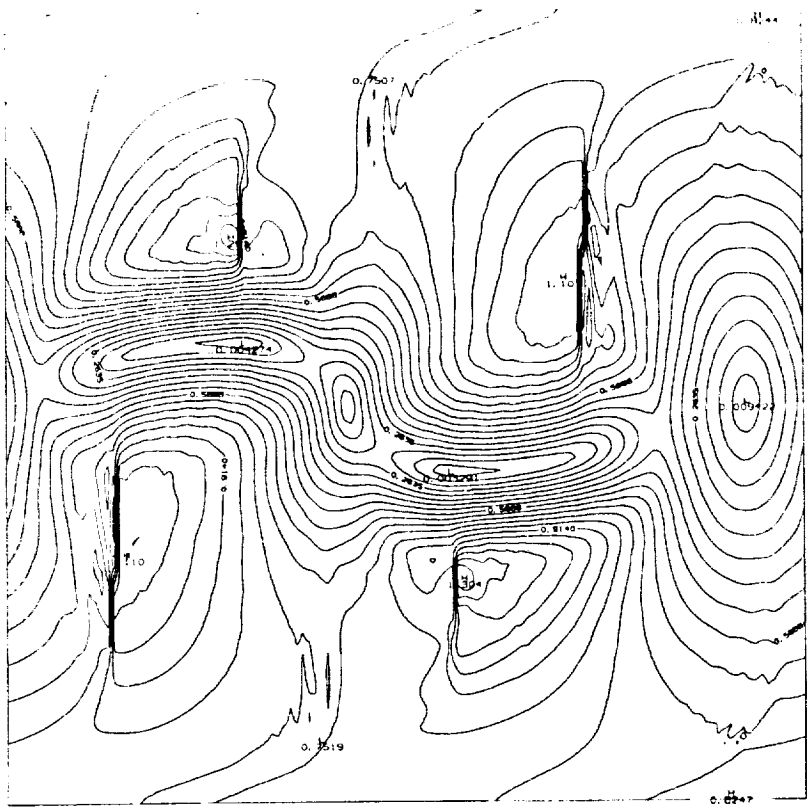

FIGURE 15 Plot of Mach number contours at $t^* = 10.26$, $M_c = 0.8$, $Ce = 0$.

for the higher heat release rates, whereas at final times increased heat liberation results in a relatively more steep gradient of the velocity and, therefore, less mixing. This has a substantial influence on the two-dimensional turbulence transport, as indicated by the cross stream variations of the mean square velocity presented in Figure 21. As shown in this figure, as the flow develops the magnitude of fluctuation is maximum for the non-heat releasing mixing layer and, as the exothermicity becomes dominant, the amplitude of the fluctuation decreases. For the most significant heat release cases ($Ce = 6$ and the Arrhenius model), the amplitude of the mean square velocity is very close to zero indicating virtually no turbulence fluctuations.

In view of some of the earlier works on DNS of low speed temporally evolving reacting mixing layers, there are some points that need to be discussed. These points are related, in particular, to the work of McMurtry *et al.* (1989) and Givi *et al.* (1986). In the former, the simulations of a variable density flow with constant kinetics were undertaken, whereas in the latter, an incompressible layer under the influence of an Arrhenius reaction was the subject of main consideration. In the present contribution, the response of the layer to heat release for the case of constant rate kinetics is consistent with the findings of McMurtry *et al.* (1989). The major difference between present calculations and those of McMurtry *et al.* is the procedure by which the hydrodynamic equations are treated. In this previous work, a low Mach number approximation was made, and all the transport equations were filtered to remove the acoustic field. This approximation does not allow for simulating flows with high Mach numbers and/or high heat release rates. Nevertheless, the general trend of the results suggest mixing suppression at elevated heat release rates. It is encouraging to note that similar trends are also observed in full compressible simulations in the present

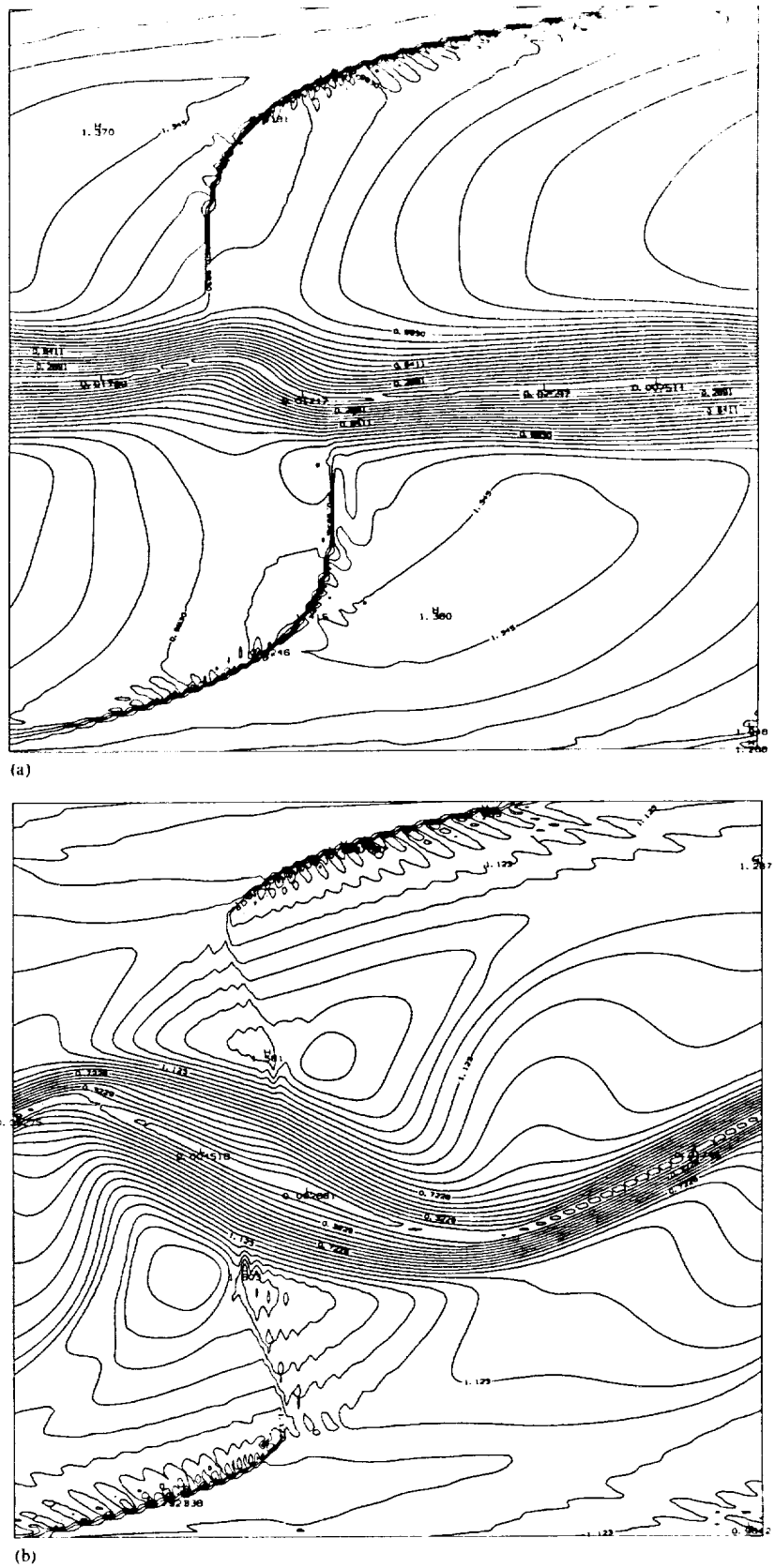

FIGURE 16 Plots of Mach number contours at different time realizations, $M_c = 1.2$, $Ce = 0$. (a) $t^* = 10.85$, (b) $t^* = 11.66$.

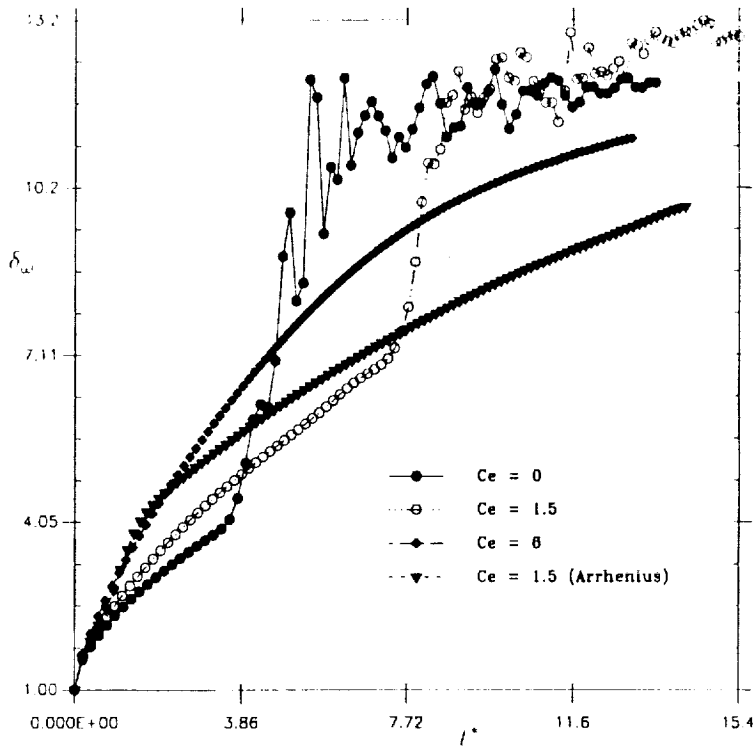

FIGURE 17 Normalized vorticity thickness versus normalized time for different values of the heat release parameter.

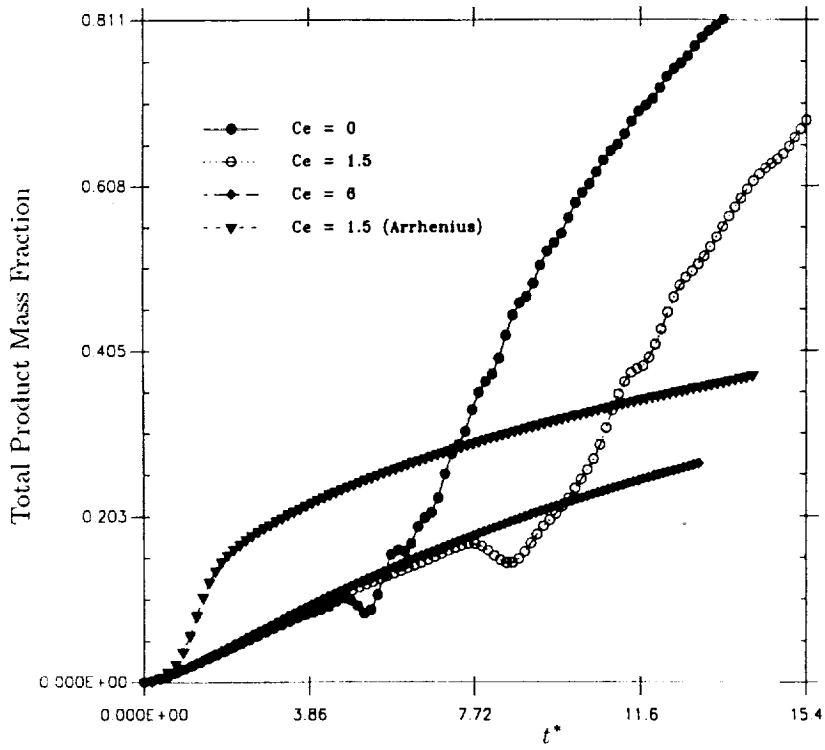

FIGURE 18 Normalized total product mass fraction versus normalized time for different values of the heat release parameter.

contribution. However, in comparison with calculations of Givi *et al.* (1986), the present simulations do not allow the examination of the effects of high stretch rates. This is primarily due to accounting for the effects of variable density in present simulations which were neglected in the previous work. As displayed by the results, the heat release and the associated density variations result in a substantial modification of the mixing procedure. In the range of parameters considered, the layer does not form large scale structures and, therefore, the magnitude of the stretch rate does not become high enough to quench the flame. This indicates the importance of the density field in the analysis of flame quenching (Buckmaster *et al.*, 1986) which was ignored previously (also see the useful comments of Boris in Givi *et al.* (1986) in this regard). In order to investigate the extinction phenomenon, future Arrhenius simulations are required in which the effects of heat release are somewhat less dominant. This can be facilitated by simulating flows with lower values of the heat release and for various magnitudes of the Damköhler and the Zeldovich numbers. Some various combinations of these parameters are required in future simulations to address this important aspect of the non-equilibrium chemistry in detail. This issue is the subject of current investigation.

4 SUMMARY AND CONCLUSIONS

A high order finite difference algorithm is employed for direct numerical simulations of a high speed reacting temporally growing unforced mixing layer. Within the framework of temporal approximation, periodic boundary conditions are employed in the streamwise direction eliminating the need for providing boundary condition in this direction of the flow. With such an approximation, the effects of large scale structures and the subsequent coupling between mixing and reaction in the unsteady compressible flow are simulated without addressing the asymmetric mixing phenomena which are observed in typical laboratory shear layers. With the accuracy of the numerical algorithm (second order in time, and fourth order in space), together with fine resolutions (both temporally and spatially), it was possible to perform accurate simulations of the reacting field with moderate values of the Reynolds, Peclet, Damköhler, Zeldovich, heat of reaction, and the convective Mach number. A full compressible code was implemented in order to allow for a reasonable and accurate simulation of the high speed reacting field. The main objective of the simulations was to examine the isolated effects of compressibility and the heat generated by the chemical reactions. A simplified reaction mechanism with idealized kinetics schemes was employed. Namely a finite-rate reaction of the type $A + B \rightarrow Products + Heat$ was the main subject under investigation. Two types of kinetics mechanisms were employed, one with constant rate kinetics, and another with an Arrhenius model. In both cases, the magnitudes of the Reynolds, Prandtl, Schmidt and Damköhler numbers were kept fixed, but the values of the convective Mach number and the heat release parameter were varied. In the constant rate reaction case, the Damköhler number is the only parameter which describes the chemistry, whereas in the Arrhenius model the Zeldovich number also is an important non-dimensional quantity to be considered.

The results of numerical experiments allowed a reasonable assessment of the roles played by the compressibility and the heat release. It was shown that both these factors have significant influences on the outcome of mixing, and modify the procedures by which the reacting species mix and convert to product species. This, in turn, influences the hydrodynamic transport within the flow and modifies the process

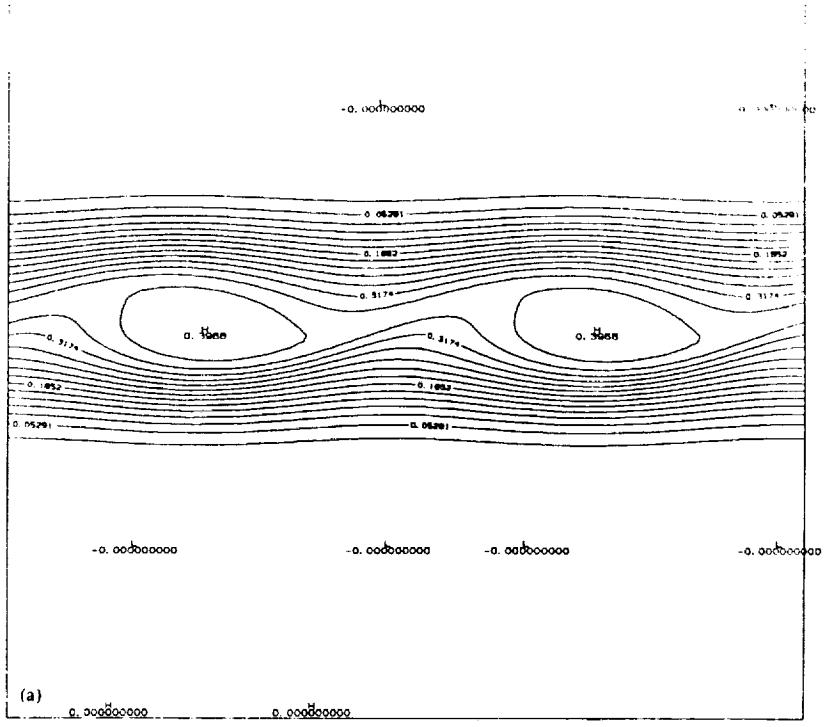

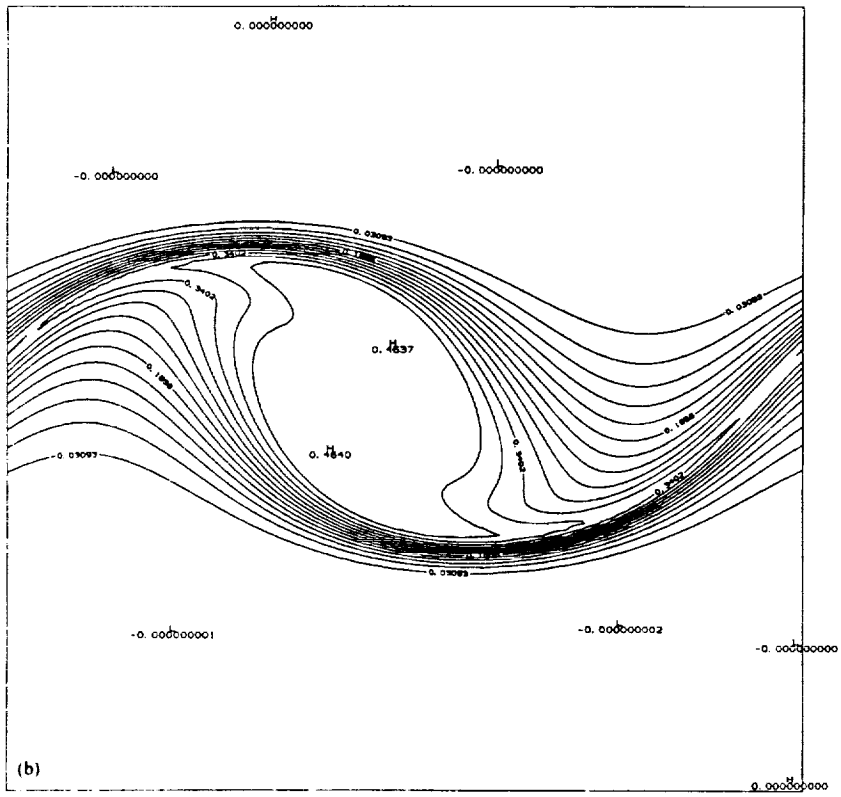

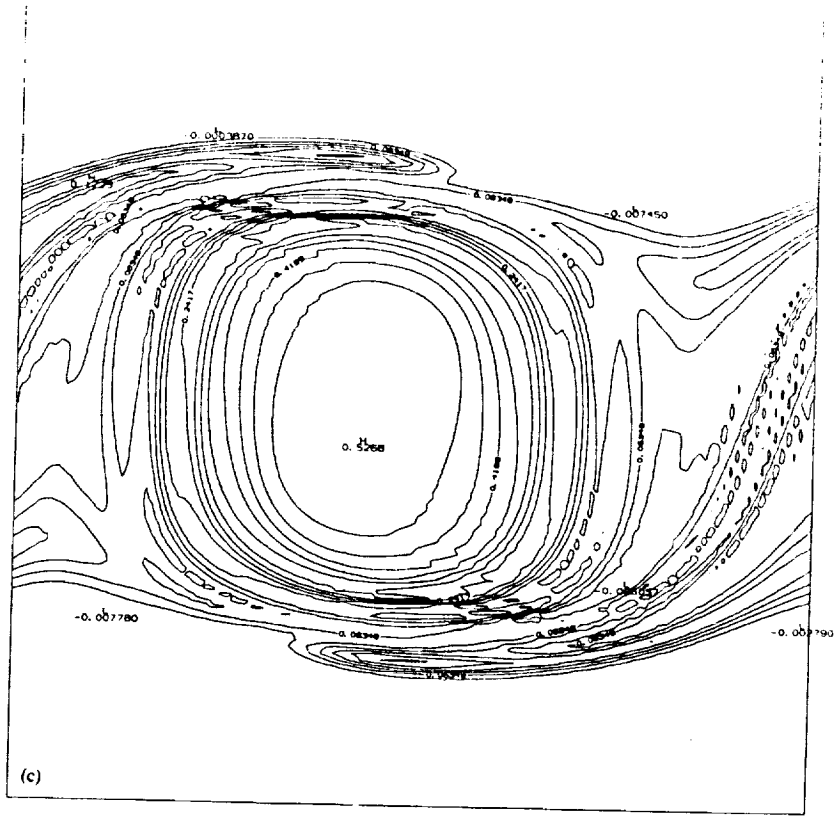

FIGURE 19 Plots of product mass fraction contours at different time realizations, $M_c = 0.2$, $Ce = 1.5$ (a) $t^* = 6$, (b) $t^* = 8$, (c) $t^* = 10$.

by which the unsteady large scale vortical structures develop. These influences are captured in the numerical simulations by a careful examination of the global structures, as well as various integral and statistical properties.

In the range of parameters considered, it is concluded that heat release and compressibility generally result in decreased mixing with the exception of a slight increase in mixing caused by volumetric expansion at high heat release rates. This is noted by the response of the layer to increased heat release and compressibility. As the magnitudes of the heat release parameter and the convective Mach numbers are increased, the layer becomes less responsive to background perturbations and it takes longer for the instability perturbations to grow. This is evidenced by both flow visualization, and by examining the statistical characteristics of the flow. The contour plots of various fluid mechanical and chemical quantities indicate that at low heat release rates, the instability modes grow at a faster rate, and the large scale coherent vortical structures are formed quicker. As the magnitude of the convective Mach number is increased, the layer becomes less sensitive to such perturbations. As a result, the layer grows at a slower rate and less mixing occurs. This is quantitatively demonstrated by examining the temporal variation of the vorticity thickness at different convective numbers which present a reasonable assessment of the effects of compressibility on mixing. Another feature of the increased compressibility is the formation of eddy shocklets as a consequence of increased compression after the formation of large scale structures (even though these structures are not very distinct at high convective Mach numbers). These shocklets are formed for both subsonic and supersonic free stream flows. As the layer is compressed, the flow in the low pressure

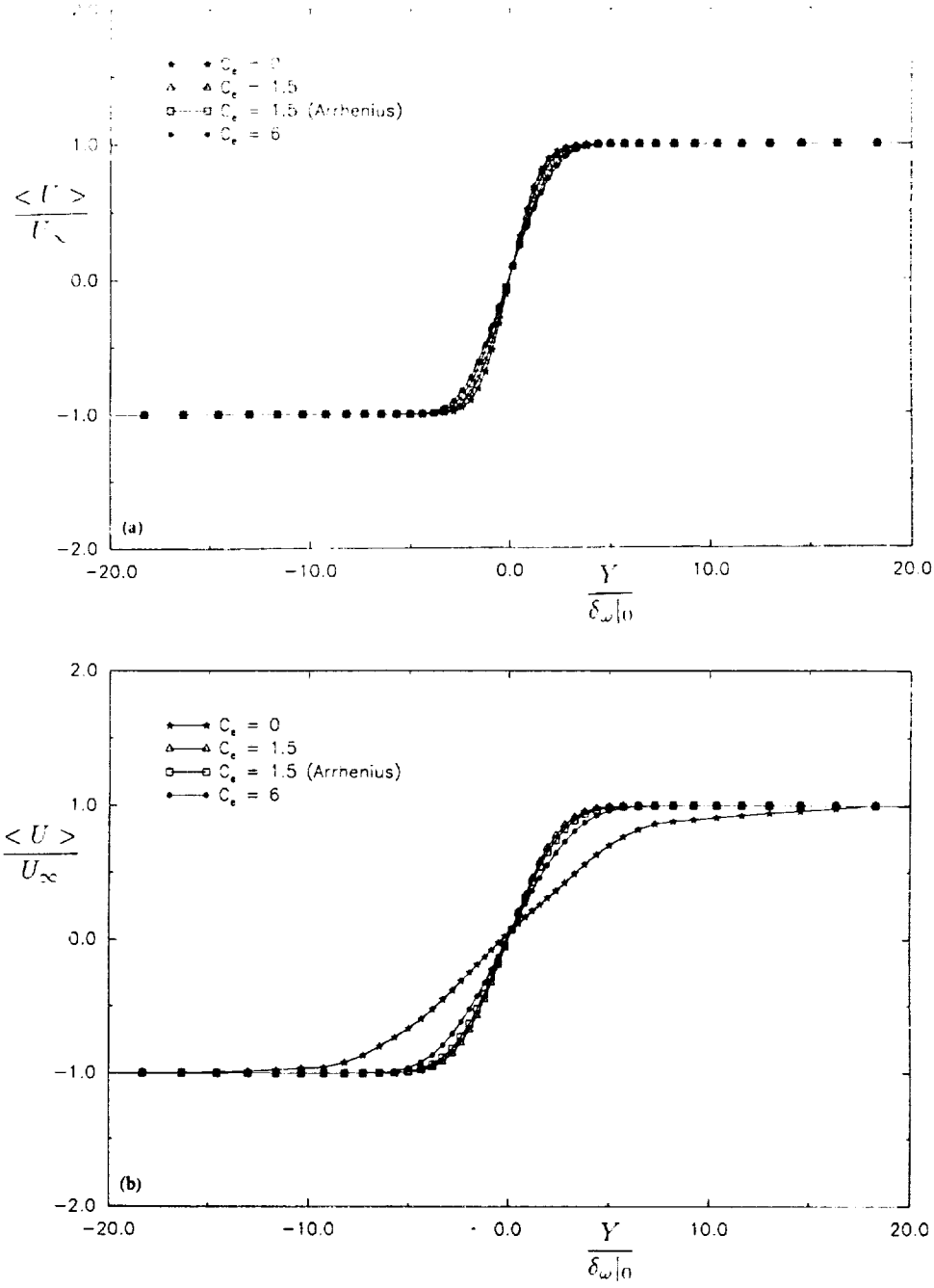

regions outside of the mixing core goes through a shock in order to adapt to the high pressure regions at saddle points at the braids of the vortical structures. These shocklets rotate in an opposite direction to the motion of large scale structures.

The heat release influences the formation of large scale structures and the subsequent evolution of the layer in two different ways. At the initial stages of mixing, the effect of heat release is to increase the volumetric expansion of the fluid. This results in thickening of the layer and in increasing the amount of products formed. After the initial stage, however, the heat release has a reverse influence. As the magnitude of heat release is increased, the layer becomes less responsive to the growth of perturba-

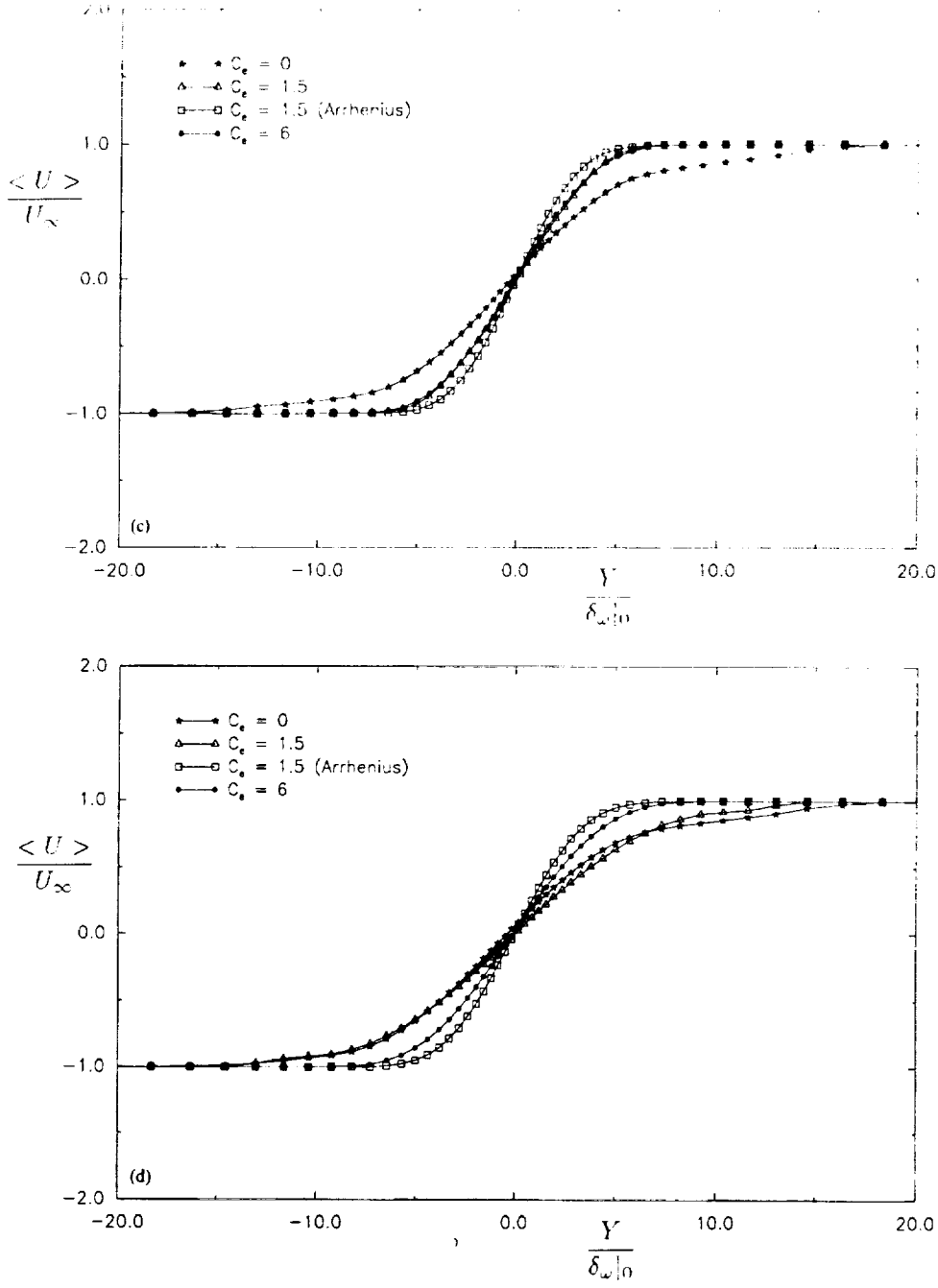

FIGURE 20 Profiles of normalized mean velocity $\langle U \rangle / U_\infty$ versus $Y/\delta_\omega|_0$ for different values of the heat release parameter. (a) $t^* = 3$, (b) $t^* = 6$, (c) $t^* = 8$. (d) $t^* = 10$.

tion, and it takes longer for the instability modes to grow. This delays the formation of coherent vortices at high heat release and yields a substantial decrease in the magnitude of the total products formed. The contour plots of fluid mechanical/chemical quantities provide a valuable flow visualization tool in displaying the effect of heat release on the formation (or lack of formation) of large scale structures. The cross stream variations of the mean and the rms of the same quantities also show the augmentation or depression of mixing as a function of the heat release.

Another important feature of the results of reacting flow simulations is the effect

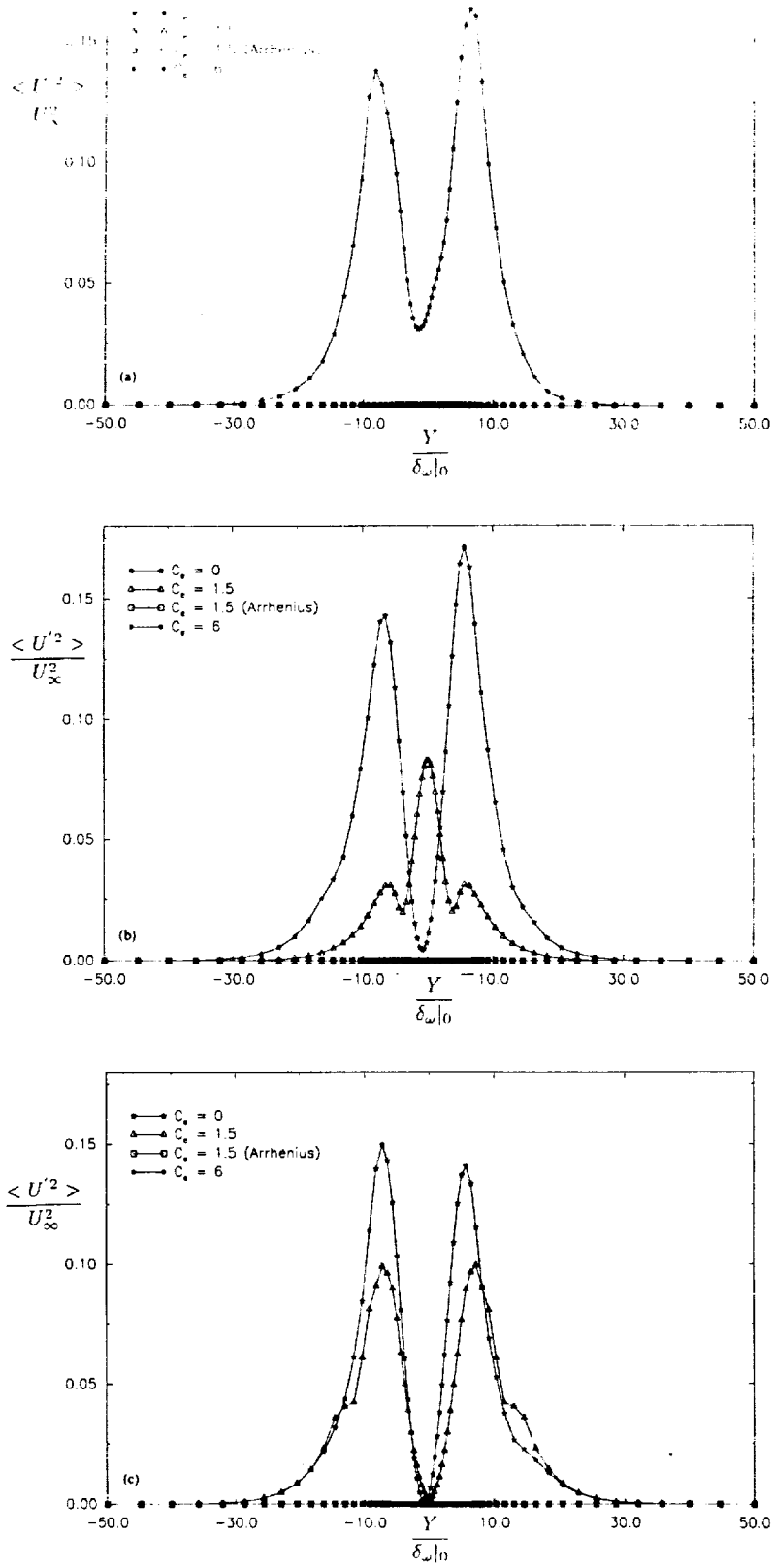

FIGURE 21 Profiles of normalized mean square velocity $\langle U'^2 \rangle / U_\infty^2$ versus $Y/\delta_\omega|_0$ for different values of the heat release parameter. (a) $t^* = 6$, (b) $t^* = 8$, (c) $t^* = 10$.

of kinetics modeling. These results indicate that for the same values of the Damköhler and heat release parameter, the Arrhenius model of the reaction conversion has a more pronounced effect on mixing hindrance. The exponential temperature dependent reaction rate increases the magnitude of the temperature much faster, and therefore enhances the effects of heat liberation. In the case with a Zeldovich number of 10, is shown that the temperature increase at the initial stages of the growth results in a rapid thickening of the layer. At the subsequent stages, the layer does not allow for the growth of instabilities, and large scale coherent structures are never formed within the time range of the simulations. This results in a substantial decrease in the amount of total product formation, and therefore yields a much smaller combustion efficiency. Future simulations with different magnitudes of the Zeldovich numbers, as well as the Damköhler numbers and the enthalpy of formation are required to examine the effects of these parameters on non-equilibrium behavior of the layer.

Much remains to be done in future efforts on DNS of high speed reacting flows. Several recent reviews are available suggesting the future paths and directions to be taken in this important area of research (Drummond, 1991; Givi and Riley, 1991). Some of our ongoing efforts in the analysis of reacting high speed shear layers include the simulations of three-dimensional flows, investigation of non-equilibrium effects and implementations of more complex kinetics mechanisms. In these future efforts, it is planned to examine the effects of secondary instabilities with and without the influences of heat release for different convective Mach number regimes. It is also intended to examine the response of the layer at different values of the Damköhler and Zeldovich numbers in order to make a complementary contribution to the investigations done previously for low speed reacting flows (Givi *et al.*, 1986, Givi and Jou, 1988). Finally, it is planned to include the effects of more complex kinetics mechanisms on the structure of the flow. In these continuation efforts, the influences of multiple Damköhler and Zeldovich numbers on the formation of large scale structures and on small scale three-dimensional random motions are expected to be captured by DNS. Some of our other ongoing efforts are concentrated on the development and implementation of more accurate numerical algorithms for both temporal and spatial discretizations of the transport equations. Two classes of numerical approximations are presently under careful consideration. One is based on compact differencing algorithms of Pade type approximations and the other is based on the spectral-element methods. Both these methods have proven useful for simulating non-reacting and reacting (Carpenter, 1990) and low speed (Givi and Jou, 1988) flows. If such methods prove to be expressively more accurate for simulating reacting high speed flows, without causing significant inconveniences, they will also be employed for future calculations.

ACKNOWLEDGEMENTS

The work at SUNY-Buffalo is supported by NASA Langley Research Center under Grant NAG 1-1122, by the Office of Naval Research under Grant N00014-90-J-4013, and by NASA Lewis Research Center under Grant NAG 3-1011. The computational resources are provided by NAS, NASA Langley and NSF supercomputing facilities. All the calculations were performed on CRAY-2 and CRAY-YMP at NASA Ames Research Center, on CRAY-2 at NASA Langley and on CRAY-2 at the University of Illinois, National Center for Supercomputing Applications.

REFERENCES

Buckmaster, J., Stewart, D. S., Ignatiadis, A. and Williams, A. (1986) On the Wind Generated by a Collapsing Diffusion Flame, *Combust. Sci and Tech.*, **46**, 145.

Canuto, C., Hussaini, M. Y., Quarteroni, A. and Zang, T. A. (1987). *Spectral Methods in Fluid Dynamics*, Springer-Verlag, New York, New York.

Carpenter, M. H. (1988) A Generalized Chemistry Version of SPARK, NASA CR 4196, NASA Langley Research Center, Hampton, VA.

Carpenter, M. H. (1989) Three-Dimensional Computation of Cross-Flow Injection and Combustion in a Supersonic Flow, AIAA Paper AIAA-89-1870.

Carpenter, M. H., (1990) A High-Order Compact Numerical Algorithm for Supersonic Flows, *Proceedings of 12th International Conference on Numerical Methods in Fluid Dynamics*, Oxford, U. K., July 8-12, 1990.

Chu, B. T. and Kovasznay, L. S. G. (1958) Non-Linear Interactions in a Viscous Heat-Conducting Compressible Gas, *J. Fluid Mech.*, **3**, 494.

Claus, R. W. (1986) Direct Numerical Simulations of a Temporally Evolving Mixing Layer Subject to Forcing, NASA TM 88896, NASA Lewis Research Center, Cleveland, Ohio.

Dimotakis, P. E. (1986) Two-dimensional Shear-layer Entrainment, *AIAA J.*, **24** (11), 1791.

Dimotakis, P. E. (1989) Turbulent Shear Layer Mixing, AIAA Paper AIAA-89-0262.

Drummond, J. P. (1987) Numerical Simulation of a Supersonic Chemically Reacting Mixing Layer, Ph.D. Thesis, George Washington University, Washington, D.C.

Drummond, J. P., (1988) A Two-Dimensional Numerical Simulation of a Supersonic, Chemically Reacting Mixing Layer, NASA TM 4055, Langley Research Center, Hampton, VA.

Drummond, J. P. (1991) Supersonic Reacting Internal Flow Fields, Chapter X, in *Numerical Approaches in Combustion Modeling*, AIAA Progress in Aeron. and Astr., editors: E. S. Oran and J. P. Boris, in press.

Drummond, J. P., Carpenter, M. H., and Riggins, D. W. (1991) Mixing and Mixing Enhancement in Supersonic Reacting Flow Fields, Chapter X, in *High Speed Propulsion Systems*, editors: S. N. B. Murthy and E. T. Curran, in press.

Ghoniem, A. F. and Ng, K. K. (1987) Numerical Study of the Dynamics of a Forced Shear Layer, *Phys. Fluids*, **30**(3), 706.

Givi, P. (1989) Model Free Simulations of Turbulent Reactive Flows, *Prog. Energy Comb. Science*, **15**, 1.

Givi, P. and Jou, W.-H. (1988) Direct Numerical Simulations of a Two-Dimensional Reacting, Spatially Developing Mixing Layer by a Spectral-Element Method, *Proceedings of 22nd Symposium (Int.) on Combustion*, The Combustion Institute, Pittsburgh, PA, p. 635.

Givi, P., Jou, W.-H. and Metcalfe, R. W. (1986) Flame Extinction in a Temporally Developing Mixing Layer, *Proceedings of 21st Symposium (Int.) on Combustion*, The Combustion Institute, Pittsburgh, PA, p. 1251.

Givi, P. and Riley, J. J. (1991) Some Current Issues in the Analysis of Reacting Shear Layers: Computational Challenges, chapter in *Major Topics in Combustion*, editors: M. Y. Hussaini, A. Kumar, and R. Voigt, Springer-Verlag, New York, NY, in press.

Gottlieb, D. and Turkel, E. (1976) Dissipative Two-Four Methods for Time-Dependent Problems, *Mathematics of Computations*, **30**, No. 136, 703.

Grinstein, F. F., Oran, E. S., and Boris, J. P. (1986) Numerical Simulations of Asymmetric Mixing in Planar Shear Flows, *J. Fluid Mech.*, **165**, 201.

Korczak, K. Z. and Hu, D. (1987) Turbulent Mixing Layers—Direct Spectral Element Simluations, AIAA paper AIAA-87-0133.

Kovasznay, L. S. G. (1957) Turbulence in Supersonic Flows, *J. Aero. Sciences*, **20** (10), 657.

Lele, S. K. (1989) Direct Numerical Simulation of Compressible Free Shear Layer Flows, AIAA Paper AIAA-89-0374.

Lowery, P. S. and Reynolds, W. C. (1986) Numerical Simulation of a Spatially Developing Forced Plane Mixing Layer, Report TF-26, Department of Mechanical Engineering, Stanford University, Stanford, CA.

Metcalfe, R. W., Orszag, S. A., Brachet, M. E., Menon, S. and Riley, J. J. (1987) Secondary Instability of a Temporally Growing Mixing Layer, *J. Fluid Mech.*, **184**, 207.

McMurtry, P. A., Riley, J. J. and Metcalfe, R. W. (1989) Effects of Heat Release on the Large-Scale Structure in Turbulent Mixing Layers, *J. Fluid Mech.*, **199**, 297.

Mukunda, H. S., Sekar, B., Carpenter, M. H., Drummond, J. P. and Kumar, A. (1991) Studies in Direct Simulation of High Speed Mixing Layers, NASA CR, in press.

Oran, E. S. and Boris, J. P. (1987), *Numerical Simulations of Reactive Flow*, Elsevier Publishing Co., Washington, D.C.

Papamoschou, D. and Roshko, A. (1988) The Turbulent Compressible Shear Layer, *J. Fluid Mech.*, **197**, 453.

Riley, J. J. and Metcalfe, R. W. (1980) Direct Numerical Simulation of a Perturbed, Turbulent Mixing Layer, AIAA Paper AIAA-80-0274.

Riley, J. J., Metcalfe, R. W., and Orszag, S. A. (1986) Direct Numerical Simulations of Chemically Reacting Mixing Layers, *Phys. Fluids*, **29**(2), 406.

Samimy, M. and Elliot, G. S. (1990) Effects of Compressibility on the Mean Flow and Turbulence Characteristics of Free Shear Layers, *AIAA J.*, to appear.

Sandham, N. D. and Reynolds, W. A., (1989) The Compressible Mixing Layer: Linear Theory and Direct Simulation, AIAA paper AIAA-89-0371.

Soetrisno, M., Eberhardt, S., Riley, J. J., and McMurtry, P. A. (1988) A Study of Inviscid, Supersonic Mixing Layers using a Second-Order TVD Scheme, AIAA Paper AIA-88-3676-CP.

Steinberger, C. J., (1991). Mixing and Non-Equilibrium Chemical Reaction in a Compressible Mixing Layer, M.S. Thesis, Department of Mechanical and Aerospace Engineering, State University of New York at Buffalo, Buffalo, New York.

Tang, W., Komerath, N. and Sankar, L. (1989) Numerical Simulation of the Growth of Instabilities in Supersonic Free Shear Layers, AIAA Paper AIAA-89-0376.

Waltrup, P. J. and Billing, F. S. (1986) Liquid Fueled Supersonic Combustion Ramjet: A Research Perspective of the Past, Present and Future, AIAA paper AIAA-86-0158.

White, M. E., Drummond, J. P., and Kumar, A. (1987) Evolution and Application of CFD Techniques for Scramjet Engine Applications, *J. Propulsion and Power*, 3(5), 423.

Williams, F. A. (1985) *Combustion Theory*, Second Edition, The Benjamin Cummings Publishing Co., Inc., Menlo Park, CA.

Appendix II

AIAA-92-0257

MODEL FREE SIMULATIONS OF A HIGH SPEED REACTING MIXING LAYER

Craig J. Steinberger
State University of New York at Buffalo
Buffalo, NY 14260

AIAA 30th Aerospace Sciences Meeting

MODEL FREE SIMULATIONS OF A HIGH SPEED REACTING MIXING LAYER

Craig J. Steinberger *
Department of Mechanical and Aerospace Engineering
State University of New York at Buffalo
Buffalo, NY 14260

Abstract

The effects of compressibility, chemical reaction exothermicity and non-equilibrium chemical modeling in a combusting plane mixing layer were investigated by means of two-dimensional model free numerical simulations. It was shown that increased compressibility generally had a stabilizing effect, resulting in reduced mixing and chemical reaction conversion rate. The appearance of "eddy shocklets" in the flow was observed at high convective Mach numbers. Reaction exothermicity was found to enhance mixing at the initial stages of the layer's growth, but had a stabilizing effect at later times. Calculations were performed for a constant rate chemical rate kinetics model and an Arrhenius type kinetics prototype. The Arrhenius model was found to cause a greater temperature increase due to reaction than the constant kinetics model. This had the same stabilizing effect as increasing the exothermicity of the reaction. Localized flame quenching was also observed when the Zeldovich number was relatively large.

Nomenclature

A_f : Arrhenius law constant
c_v : specific heat at constant volume
C : species concentration
C_e : heat release parameter
Da : Damköhler number
E : activation energy
$\Delta H°$: heat of reaction
K_f : reaction rate constant
l_0 : physical length of computational domain
M_c : convective Mach number
R : universal gas constant
t : time
t^* : normalized time
T : temperature
U : streamwise velocity
$\dot{w}_i$: species production rate of species i
Ze : Zeldovich number
δ_ω : vorticity thickness

Subscripts:
A, B : chemical species
x : in x coordinate direction
y : in y coordinate direction
∞ : free stream

*Research Assistant, Student Member AIAA.

1 Introduction

Research on the subject of compressible reacting mixing layers has been of high priority in recent years. Much of this effort has been devoted to the development of high speed air breathing flight vehicles. This type of vehicle would, according to current proposals, use supersonic combustion ramjet (scramjet) engines for propulsion. In such an engine, fuel is injected into a high speed airflow. The mechanisms of mixing and combustion of this non-premixed, high speed, compressible, reacting flow is of great complexity.[1,2]

The purpose of this study was to investigate the coupling between the hydrodynamic and chemical phenomena that are present in compressible, reacting mixing layers. Although experimental studies have provided useful results, this avenue of research is often difficult and expensive. Numerical simulation has become widely accepted as an alternative and supplement to experimental investigation. Model free simulations have proven especially useful because there is no need to introduce the potential inaccuracies of a turbulence model. An extensive review of current numerical simulation techniques and results for reacting flows is provided by Givi.[3]

1.1 Previous Research

Brown and Roshko[4] found that the turbulent mixing layer is dominated by large scale coherent structures, or vortices. These structures convect at a nearly constant speed and tend to coalesce with neighboring vortices. Papamoschou and Roshko[5] continued these experiments to determine the effect of compressibility on the spreading rate of a supersonic mixing layer. They found that it

is useful to study the flow in reference frame that travels with the flow at the same speed as an average large scale structure. A parameter which quantifies the compressibility in the flow was proposed as the convective Mach number, M_c; defined as the Mach number of the flow with respect to the above mentioned frame of reference. A direct correlation was found between M_c and the stability of the flow. Lele[6] replicated the results of Papamoschou and Roshko[5] by means of direct numerical simulation of a two-dimensional mixing layer. In addition, he noted the appearance of eddy shocklets within the flow for $M_c > 0.7$.

McMurtry, *et al.*[7] studied the effects of an exothermic chemical reaction on the shear layer via direct numerical simulation. In this study, an approximate set of equations that are valid for low Mach number flows was used. It was found that the heat liberated from a chemical reaction causes the layer to grow at a slower rate that of on-heat releasing flow. These results agree with those obtained experimentally. In addition, direct numerical simulations concerned with compressibility and heat release effects on a compressible mixing layer were performed by Givi *et al.*[8]

The phenomenon of flame extinction in non-premixed flames has been the topic of theoretical and experimental study, although direct numerical simulations of such flows have been somewhat limited. Recent reviews of some of the prevalent theories regarding the structure of turbulent non-premixed flames, as well as some of the experimental and numerical work in that field are provided by Bilger[9] and Peters.[10]

1.2 Scope of Present Research

The scope of the present work is to examine the effects of compressibility and chemical reaction exothermicity on a reacting plane mixing layer. An examination is also made of the non-equilibrium effects of the chemical kinetics on the structure of a flame. These are accomplished by direct numerical simulation of an unsteady two-dimensional shear layer. The governing equations are integrated via high order finite difference methods, and no turbulence modeling is employed. Since the focus of this study is the general physics of this type of flow, physical modeling is kept as simple as possible so that the above mentioned hydrodynamic and chemical effects may be isolated. The use of simplifying assumptions has the added advantage of saving considerable amounts of computational resources, without reducing the accuracy or validity of the results.

2 Method of Investigation

A two-dimensional version of the SPARK computer code[11,12] was used to investigate a chemically reacting, compressible, temporally developing mixing layer. The full Navier-Stokes equations as well as the applicable chemical species conservation equations (see[11] or[13] for more detail) were solved via numerical integration. The methods used were the Gottlieb-Turkel finite difference scheme[14] and a dissipative compact parameter method.[15] Both of these algorithms are of fourth order spatial accuracy and second order temporal accuracy.

One of the primary assumptions made in these simulations is that the mixing layer is temporally developing. That is, the reference frame of the simulations is defined to be moving with a velocity equal to that of the mean flow. The advantages of this approximation are twofold. First, with the temporal assumption the inflow and outflow boundary conditions can be assumed to be periodic. The eliminates the problem of specifying downstream boundary conditions. Second, the temporal assumption means that only a relatively small region of the flow is being simulated. This region is then followed in a Lagrangian sense as time progresses. This results in considerable savings in computational resources, which means that the flow may be simulated in greater detail.

The chemical reaction in the flow is assumed to be of a simple, irreversible, second order type of the form

$$A + B \longrightarrow Product + Heat \tag{1}$$

The reaction is characterized by the kinetics mechanism, which is given by the single step model of

$$\dot{w} = K_f C_A C_B \tag{2}$$

where C_A and C_B represent the concentrations of the reacting species and are assumed equal at the free streams, i.e. $C_{A_\infty} = C_{B_\infty} = C_\infty$. K_f is the reaction rate constant, and can be normalized to form the definition of the Damkohler number, Da:

$$Da = \frac{K_f C_\infty}{U_\infty / \delta_\omega|_0} \tag{3}$$

In the present study two types of chemistry models were used; constant rate kinetics (i.e. constant K_f) and an Arrhenius type model in which K_f varies with the temperature. This is written as

$$K_f = A_f e^{-\frac{Ze}{T/T_\infty}} \tag{4}$$

where A_f is the pre-exponential factor and Ze is the Zeldovich number, defined as

$$Ze = \frac{E}{RT_\infty} \tag{5}$$

Here E is the activation energy and R is the universal gas constant. T_∞ is the free stream temperature. When the Arrhenius kinetic model is used, the pre-exponential factor A_f replaces K_f in the definition of Da (Eq. 3).

Combustion exothermicity is measured by the energy liberated by the chemical reaction, $\Delta H°$. The

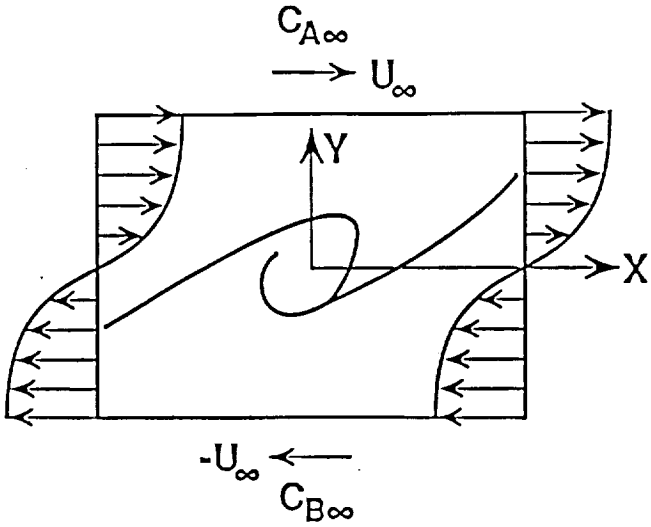

Figure 1: Schematic diagram of a temporally evolving mixing layer.

magnitude of this energy is parameterized by a non-dimensional heat release parameter Ce, defined by:

$$Ce = \frac{-\Delta H^\circ}{c_v T_\infty} \tag{6}$$

Thus, $Ce = 0$ corresponds to a non-heat releasing chemical reaction.

The flow was initialized with a hyperbolic tangent streamwise velocity profile, with reactant A on the top half of the layer with a free stream velocity of $+U_\infty$ and reactant B on the bottom half with a free stream velocity of $-U_\infty$. This flow configuration is shown schematically in Fig. 1. There was no initial fluid motion in the transverse direction, and the pressure was assumed to be initially constant throughout the flowfield. Depending on the problem simulated, the temperature was either assumed to be initially constant or had an initial Gaussian distribution. In most cases, the mixing layer was perturbed by numerical truncation errors. However, when necessary, harmonic forcing was explicitly added to trigger the flow instabilities. For a majority of the simulations, a 128 × 128 point grid was used, with grid compression in the areas of the flow with the sharpest gradients. In those cases where the gradients were too strong for the details of the flow to be resolved, a 256 × 256 point grid was used.

All parameters are normalized when appropriate by initial or free stream conditions. Time is normalized by

$$t^* = \frac{t}{l_0/U_\infty} \tag{7}$$

3 Sample Results

3.1 Effects of Compressibility

The effect of compressibility on the mixing layer was investigated by varying M_c, the convective Mach number over a range of values from $M_c = 0.2$ to $M_c = 1.2$. The vorticity thickness vs. normalized time for different values of M_c is given in Fig. 2. This figure clearly shows that the growth rate of the vorticity thickness is decreased with increased compressibility. Compressibility also affects the time needed for the layer to roll up into a vortex, which is shown in the figure as a jump in vorticity thickness. Valuable information may be obtained from examination of the variation in the transverse direction of the normalized average streamwise component of the velocity and the normalized mean square streamwise velocity fluctuations. The average streamwise velocity profile is shown in Fig. 3. The most significant feature of these curves is the steepness of the mean velocity profiles at high convective Mach numbers. This shows a sharper velocity gradient across the layer, implying a lesser rate of mixing. The degradation of mixing has the effect of retarding the progress of the chemical reaction. The suppression of turbulence fluctuations with compressibility is shown by the profiles of the mean square of the fluctuating velocity in Fig. 4. A marked decrease in the amplitude of the fluctuations can be observed.

Another feature of the increased compressibility is the formation of eddy shocklets as a result of increased compression after the formation of large scale structures. These shocklets are formed for both subsonic and supersonic free stream flows in order to adapt to high pressure at the braids. An example of this can be seen upon examination of Mach number contours, shown in Fig. 5. This phenomenon has not been observed in any of the experiments on compressible shear layers, to date. This might be caused by the fact that the simulations are two-dimensional, whereas a laboratory flow is dominated by small scale three dimensional transport. It is anticipated that future three dimensional simulations will clarify the matter.

3.2 Effects of Reaction Exothermicity

Calculations were also performed to assess how reaction exothermicity affects the mixing layer. Results are presented of simulations for constant rate kinetics with heat release values of $C_e = 0$, 1.5, and 6. One set of calculations was performed using Arrhenius type kinetics with $C_e = 1.5$ and $Ze = 10$.

The results of these simulations presented in the form of plots of the vorticity thickness versus normalized time (Fig. 6). This figure shows that the rate of growth is highest for the no-heat release case ($C_e = 0$), and, as the heat release parameter is increased, the growth of the layer slows. The relatively smooth regions of vorticity thickness growth may be attributed to diffusion

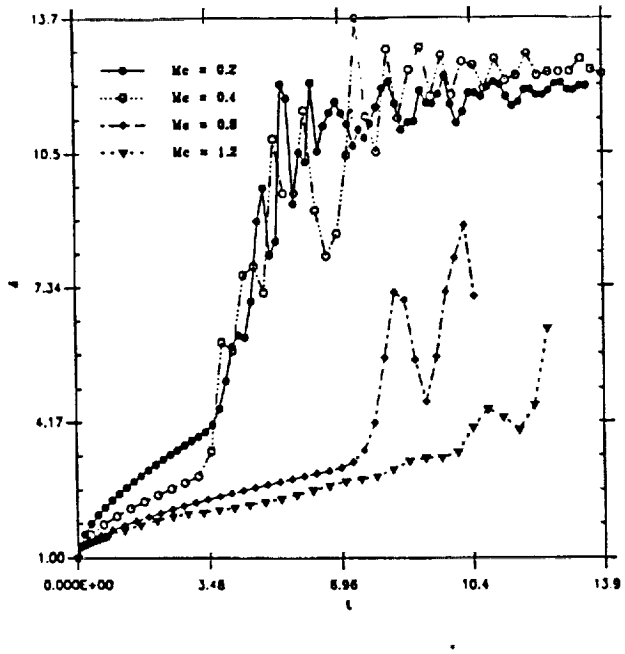

Figure 2: Normalized vorticity thickness versus normalized time for different values of the convective Mach number.

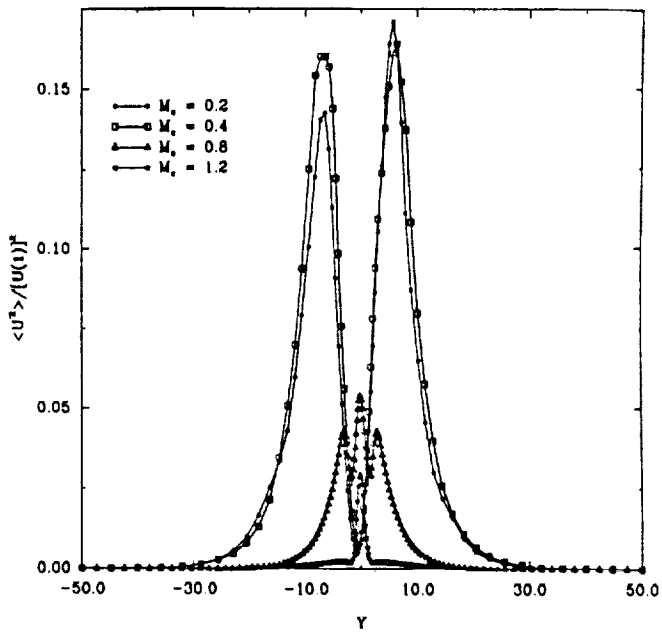

Figure 4: Profiles of normalized mean squared streamwise velocity for different values of the convective Mach number at time $t^* = 8$.

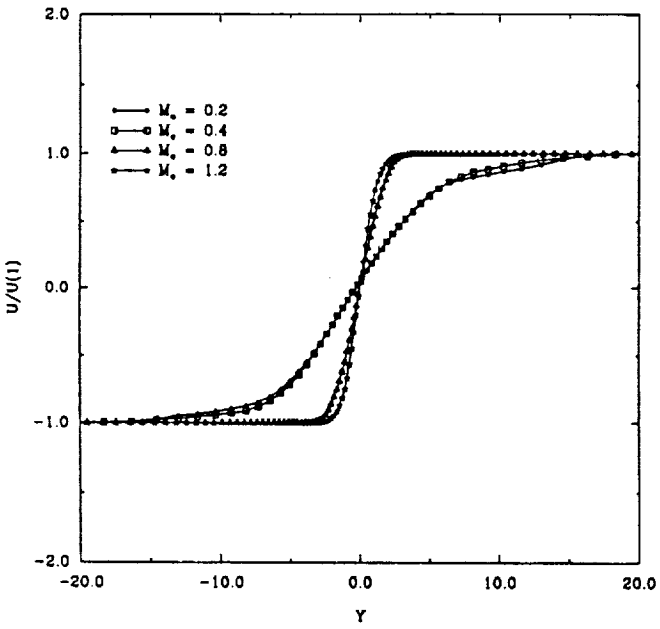

Figure 3: Profiles of normalized mean streamwise velocity for different values of the convective Mach number at time $t^* = 8$.

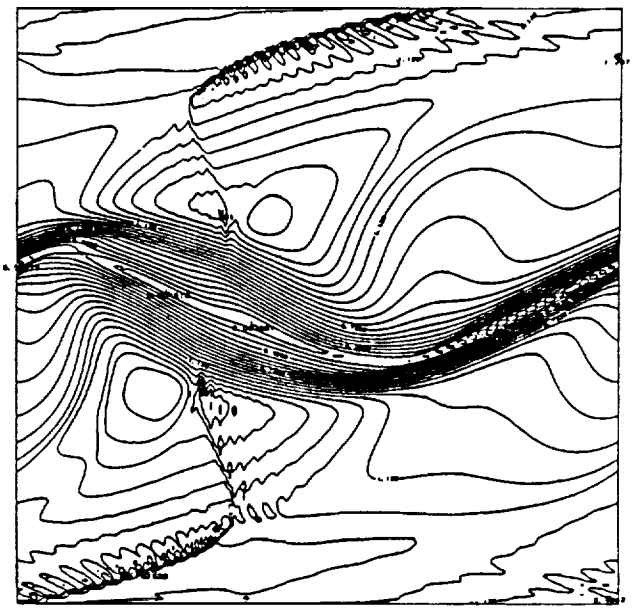

Figure 5: Plot of Mach number contours at time $t^* = 11.66$, $M_c = 1.2$.

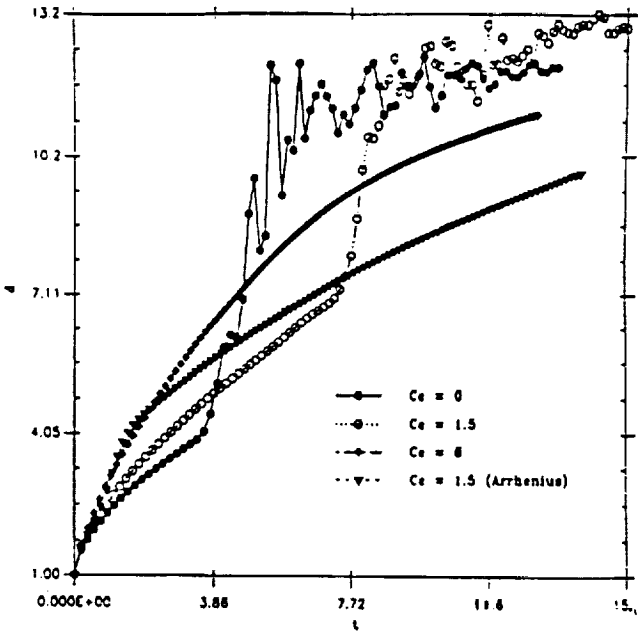

Figure 6: Normalized vorticity thickness versus normalized time for different values of the heat release parameter.

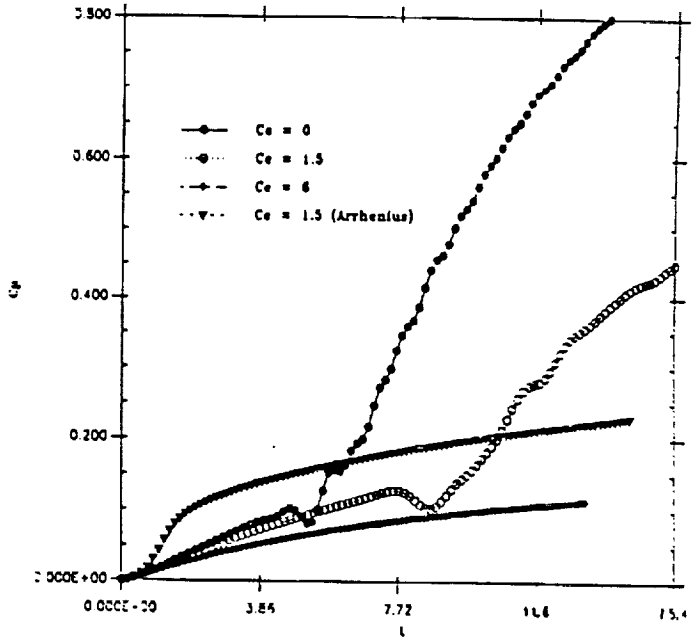

Figure 7: Normalized product thickness versus normalized time for various values of the heat release parameter.

thickening, and a jump in vorticity thickness represents vortex roll-up. For the $C_e = 0$ case, the layer responds to background perturbations fairly quickly, and vortical structures are formed at $t^* \approx 3$. An increase in the magnitude of the heat release results in a delay of vortex roll-up, and the jump in vorticity thickness does not occur until $t^* \approx 7$. Further increase of the heat release parameter results in additional delays, as can be seen for the case of $C_e = 6$. This behavior is also observed for the Arrhenius model with $C_e = 1.5$. In these two cases, the effects of exothermicity are most pronounced; vorticity roll-up does not occur at all, and the only growth in the thickness of the mixing layer is due to molecular diffusion.

The influence of the heat release on the structure of the flame is demonstrated by examining the product thickness of the layer, defined by the normalized total product concentration of the layer as a function of time (Fig. 7). At initial times, the effect of heat release is an enhanced product formation, while the reverse applies at the intermediate and final stages. Initially, the effect of heat release is to expand the fluid at the cores of the layer. A large mixing zone is formed, which results in an enhanced reaction and an increased product formation. This explains the increased initial product thickness. However, as the heat release increases and the layer thickens, the growth of the instability modes become subdued, postponing the formation of the large scale vortices. After initial times, the non-heat release ($C_e = 0$) and $C_e = 1.5$ cases predict a sharp increase in the product thickness. This is caused by the dynamics of the large scale structure formation. The mechanism if roll-up causes the reactants to be entrained into the layer from their prospective free streams. This produces an increase in the extent of mixing, reaction, and product formation. The lack of roll-up in the $C_e = 6$ and Arrhenius cases means the only mixing process is molecular diffusion. Since in these simulations the diffusion mechanism is not as efficient as the roll-up of vortices in the mixing of reactants, the product thickness is correspondingly lower.

3.3 Flame Extinction

Another area of study was the nonequilibrium effects leading to local flame extinction. Simulations were run for large values of the Zeldovich number for an Arrhenius kinetics model and for a constant rate kinetics chemistry model as a control. To obtain the vortex roll-up necessary to this analysis, explicit harmonic forcing was added to the initial conditions of the flow. A forcing amplitude of 0.5% of the mean velocity was used. The most unstable frequencies were found by a linear stability analysis of an equivalent incompressible flow. It was found that if the flow was excited only by the most unstable frequency, two vortices form but they do not pair. If the first subharmonic is added, the vortices undergo pairing.

In the case of large Zeldovich numbers, it was observed from the simulations that, after roll-up and pairing, the flame undergoes local extinction at the braids. This behavior is depicted in contour plots of the reaction

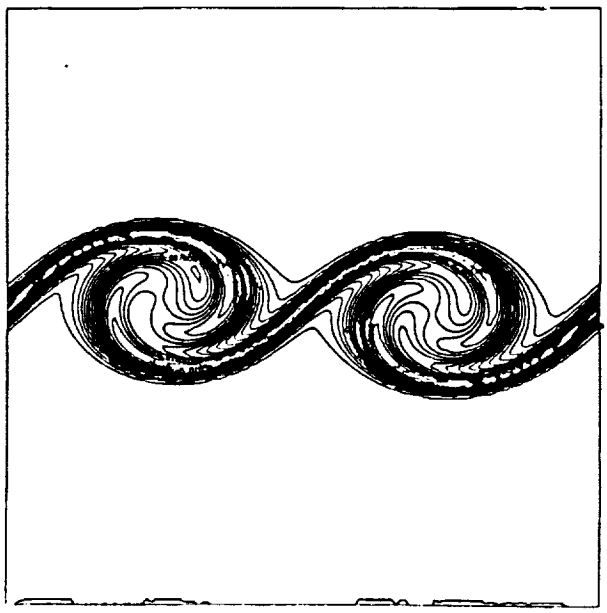

Figure 8: Plot of reaction rate contours, $Ze = 20$, $t^* = 1$.

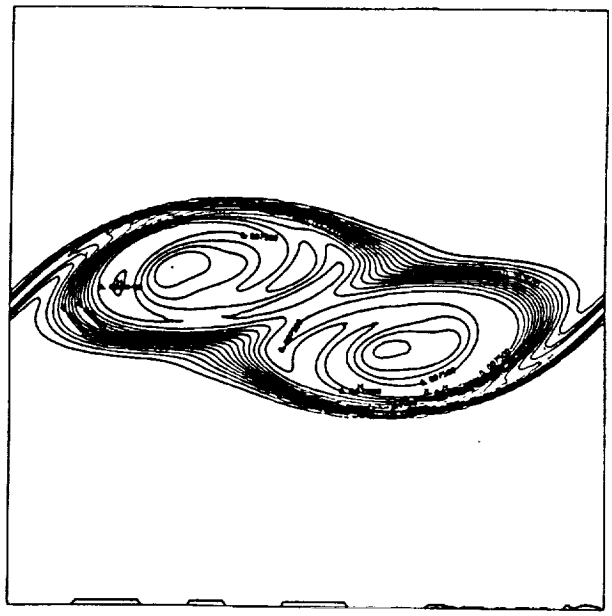

Figure 9: Plot of reaction rate contours, $Ze = 20$, $t^* = 1.5$.

rate at times $t^* = 1$, 1.5, 2.25, and 2.5. These contours are shown in Fig. 8 for time $t^* = 1$, when the vortices have just formed.

The reaction rate is highest along the mixing surface of the layer, that is, in the center of the intervortex braids. The contours at time $t^* = 1.5$ (Fig. 9) portray the behavior at the initial stages of pairing. The reaction rate has begun to decrease in the braids of the emerged vortex. At time $t^* = 2.25$, shown in Fig. 10, the layer has completed the pairing process and strong gradients are observed in the vortex braids. Since the braids are "stretched" as the vortex rotates, they are the area of the highest strain. The flame at the onset of extinction is shown in Fig. 11. Note that the reaction rate has gone to zero at the braids. Product concentration contours (not shown) indicate that very little product exists in these extinguished regions, demonstrating that the flame did not quench due to depletion of reactants. At this point in time, the flame is not continuous, forming what will be called for lack of a better term, a "flame eddy."

This extinction phenomenon has been explained by Peters[10] as follows: At the regions of high strain, the reactants are supplied at a faster rate than they can be consumed by the flame. Thus the local temperature in that area drops and the flame becomes very rich with reactants. As a result, the flame is quenched in that area. If a fast chemistry model or an equilibrium chemistry model is used, the extinction mechanism can not be captured. Investigation of such phenomena requires finite-rate chemistry simulation such as that presented here.

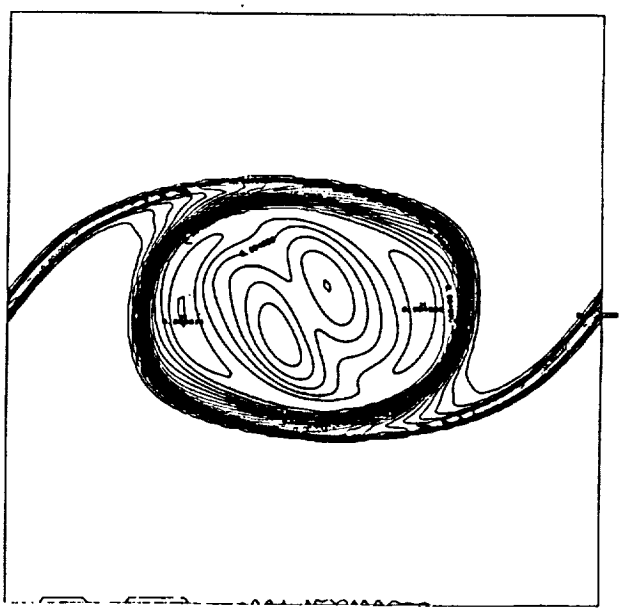

Figure 10: Plot of reaction rate contours, $Ze = 20$, $t^* = 2.25$.

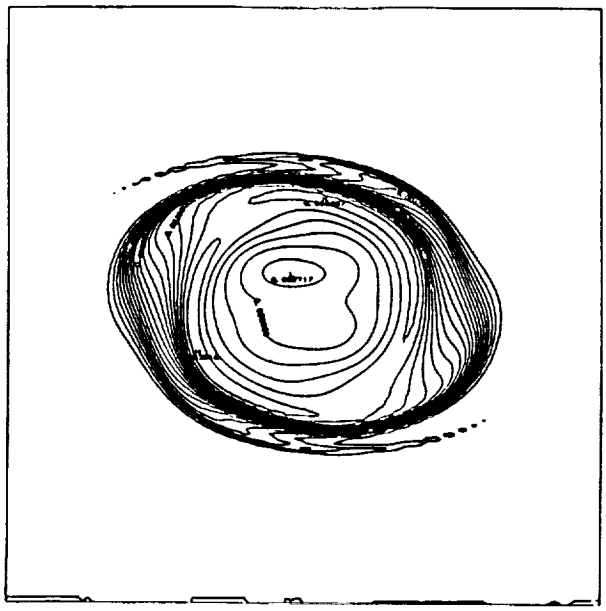

Figure 11: Plot of reaction rate contours, $Ze = 20$, $t^* = 2.5$.

4 Conclusions

Direct numerical simulations of a compressible, temporally developing, reacting plane mixing layer were performed. Several simplifying assumptions were made so that the effects of the variation of isolated parameters could be studied in detail. In particular, the chemical reaction was assumed to be of the general form, $A + B \rightarrow Products + Heat$, and thermodynamic properties were assumed constant and identical for all species.

Studies of various flow phenomena were performed by varying one representative nondimensionalized parameter while keeping all other parameters constant. The convective Mach number, M_c, was used to describe compressibility, the heat release parameter, C_e, represented the exothermicity of the reaction, and the Damköhler number and the Zeldovich number described the rate of the reaction.

The simulations concerning the effect of compressibility on the mixing layer showed a direct correlation between increased compressibility and increased stability (along with reduced turbulence). When the convective Mach number was increased, the rate of growth of the mixing layer, which was measured by the growth of the vorticity thickness, was markedly reduced. Degradation of the development of the streamwise fluctuating velocity and mean velocity profiles was also noted. For high compressibility cases, "eddy shocklets" were observed within the flow. This has been previously reported in two-dimensional simulations, but has not been observed in experiments or in three-dimensional studies to date. An expansion of this work into three dimensions is suggested for future work in this area.

Increased exothermicity was observed to slow the growth of large scale structures. At the initial stages of development, high heat release increased the amount of product formed via volumetric expansion of the core of the layer. However, the heat release caused the layer to be Less responsive to perturbations, reducing the growth of the layer at later stages. The overall effect of increased heat release, therefore, was to stabilize the flow and to decrease the extent and efficiency of the reaction.

The selection of chemical kinetics model was shown to have significant effect on the development of the flow. The introduction of an Arrhenius chemistry model had a stabilizing effect, thus degrading the progress of the reaction. Non-equilibrium chemistry effects due to the chemistry model was also studied. It was found that at high Zeldovich numbers, the flame would be quenched at regions with large local values of the strain rate.

Acknowledgements

The guidance and support of Professor Peyman Givi is gratefully appreciated. This work is sponsored by NASA Langley Research Center under Grant NAG 1-1122 and by NASA Lewis Research Center under Grant NAG 3-1011. All simulations were performed on Cray-2 and Cray YMP supercomputers with resources provided by the NAS program at NASA Ames Research Center, the NCSA at the University of Illinois, and NASA Langley Research Center. Thanks are also due to Drs. Phil Drummond and Mark Carpenter at NASA Langley, and to Dr. Cyrus Madnia at SUNY Buffalo for valuable discussions on the subject.

References

[1] Givi, P. and Riley, J. J., Some Current Issues in the Analysis of Reacting Shear Layers: Computational Challenges, in Voigt, R., Hussani, M. Y., and Kumar, A., editors, *Major Research Topics in Combustion*, Springer-Verlag, 1991, in press.

[2] Drummond, J. P., Supersonic Reacting Internal Flowfields, in Oran, E. S. and Boris, J. P., editors, *Numerical Approaches in Combustion Modeling*, volume 135 of *Progress in Astronautics and Aeronautics*, pp. 365 - 420, AIAA, New York, NY, 1991.

[3] Givi, P., Model Free Simulations of Turbulent Reactive Flows, *Prog. Energy Combust. Science*, 15:1-107 (1989).

[4] Brown, G. L. and Roshko, A., On Density Effects and Large Structure in Turbulent Mixing Layers, *J. Fluid Mech.*, 64:775-816 (1974).

[5] Papamoschou, D. and Roshko, A., Observations of Supersonic Free Shear Layers, AIAA Paper 86-0162, 24th Aerospace Sciences Meeting, Reno, Nevada, 1986.

[6] Lele, S. K., Direct Numerical Simulation of Compressible Free Shear Flows, AIAA Paper 89-0374, 27th Aerospace Sciences Meeting, Reno, Nevada, 1989.

[7] McMurtry, P. A., Riley, J. J., and Metcalfe, R. W., Effects of Heat Release on the Large Scale Structures in a Turbulent Reacting Mixing Layer, *J. Fluid Mech.*, 199:297–332 (1989).

[8] Givi, P., Madnia, C. K., Steinberger, C. J., Carpenter, M. H., and Drummond, J. P., Effects of Compressibility and Heat Release in a High Speed Reacting Mixing Layer, *Combust. Sci. Tech.*, 78:33–68 (1991).

[9] Bilger, R. W., Turbulent Diffusion Flames, *Ann. Rev. Fluid Mech.*, 21:101–135 (1989).

[10] Peters, N., Laminar Diffusion Flamelet Models In Non-Premixed Turbulent Combustion, *Prog. Energy Combust. Sci.*, 10:319–339 (1984).

[11] Drummond, J. P., Two-Dimensional Numerical Simulation of a Supersonic, Chemically Reacting Mixing Layer, NASA TM 4055, NASA Langely Research Center, 1988.

[12] Carpenter, M. H., A Generalized Chemistry Version of SPARK, NASA CR 4196, NASA Langley Research Center, 1988.

[13] Williams, F. A., *Combustion Theory*, The Benjamin/Cummings Publishing Company, Menlo Park, CA, 2nd edition, 1985.

[14] Gottlieb, D. and Turkel, E., Dissipative Two-Four Methods for Time Dependent Problems, *Mathematics of Computations*, 30(136):703–723 (1976).

[15] Carpenter, M. H., A Family of Dissipative Compact Two-Four Schemes, submitted to*Journal of Computational Physics*, 1990.

Appendix III

To appear in *Large Eddy Simulations: Where Do We Stand?*, Editor: Boris Galperin, Springer-Verlag, Heidelberg, FRG (1991).

Technical Report No. 125

On DNS and LES of Reacting Homogeneous Turbulence

by

Cyrus K. Madnia and Peyman Givi

Turbulence Research Laboratory
Faculty of Engineering and Applied Sciences
University at Buffalo/SUNY
Buffalo, NY 14260

March 1991

ON DNS AND LES OF REACTING HOMOGENEOUS TURBULENCE

Cyrus K. Madnia and Peyman Givi
Department of Mechanical and Aerospace Engineering
State University of New York at Buffalo
Buffalo, New York 14260

ABSTRACT

Direct Numerical Simulations (DNS) are performed to investigate the phenomena of mixing in a decaying two-dimensional, homogeneous turbulent flow under non-reacting and reacting unpremixed conditions. In the reacting case, a second order stoichiometric irreversible reaction of the type $A + B \rightarrow Products$ is considered. An infinitely fast chemical reaction rate is assumed without including the effects of non-equilibrium chemistry. The data obtained by DNS is utilized to examine the behavior of the scalar field in a stochastic manner. This involves the extraction of Probability Density Functions (PDF's) of the scalar field from the DNS results. The examination of the data in this manner provides a useful mechanism for assessing the range of validity of PDF methods for turbulence modeling in Reynolds averaged equations, and for subgrid closures in Large Eddy Simulations (LES).

Simulations are performed of flows with various levels of compressibility to examine its effects on the structure of the flow field. In the low compressibility regime, the flow exhibits features similar to those observed in previous incompressible simulations, whereas in the high compressibility case, shocklets are formed. In both cases, the simulated results indicate that the PDF of a conserved Shvab-Zeldovich scalar quantity, characterizing the mixing process, evolves from an initial double-delta distribution to an asymptotic shape that can be approximated by a Gaussian distribution. During this evolution, the PDF can be approximately described by a Beta density and also exhibits features compatible with those predicted by the mapping closure of Kraichnan. The main difference exhibited between the two cases is the time scale of decay of the rms of the scalar by which the PDF is characterized. A discussion of the results is provided with a focus on their relevance towards turbulence modeling and LES closure. A brief review is also provided of recent related contributions in PDF modeling and LES in order to provide a framework for anticipated continuation of the present work.

1. INTRODUCTION

In review of recent computational work on turbulent reacting flows, Drummond (1991), Oran and Boris (1987) and Givi (1989) indicate the need for further development in both the methodology and the implementation of Direct Numerical Simulations (DNS) and Large Eddy Simulations (LES). According to these reviews, the results of previous and ongoing works towards the development of advanced numerical algorithms for simulating reacting turbulent fields have been successful, thus warranting their continued utilization for future implementations. With the broad knowledge gained to date, it is now widely accepted that foreseeable developments in advanced computational facilities will not be sufficient to relax the restriction of DNS to flows having small to moderate variations of the characteristic length and time scales (Rogallo and

Moin, 1981; Reynolds, 1990; Schumann and Friedrich, 1986, 1987, Givi, 1989). Nevertheless, DNS can be (and have been extensively) used to enhance our understanding of the physics of chemically reacting turbulent flows by providing specific information concerning the detailed structure of the flow, and by furnishing a quantitative basis for evaluating the performance of turbulence closures. In this sense, DNS have provided an effective tool for such studies and have established useful guidelines for future investigations.

LES appear to provide a good alternative to DNS for computing flows having ranges of parameters similar to those encountered in practical systems (Reynolds, 1990; Hussaini *et al.*, 1990, Ferziger, 1981, 1983, Schumann and Friedrich, 1987). This approach has a particular advantage over analogous Reynolds-averaging procedures in that only the effects of small-scale turbulence have to be modelled. However, despite their success for the analysis of both incompressible (Ferziger, 1981) and compressible (Erlebacher *et al.*, 1987) flows, they have seldom been employed for calculations of reacting turbulence. This is primarily due to appearance of enormous unclosed terms in the transport equation governing the evolution of the filtered quantities in LES. In these equations, the correlations amongst the scalar variables must be accurately modelled in order to provide a realistic estimate of the reactant's conversion rates.

A methodology which has proven useful for predictions of turbulent reacting flows is based on the Probability Density Function (PDF) or the joint PDF of the scalar variables which characterize the field (O'Brien, 1980; Pope, 1979, 1985, 1990a). A particular advantage of the method is the fundamental property of the probability density, namely that it provides the complete statistical information about the behavior of the variable. This, in comparison with moment methods, provides a unique advantage in that once the distribution of the PDF is known, the mean and higher order moments of the reaction rate (or any other functions of the scalar field) can be directly determined without a need for further closure assumptions. The implementation of PDF methods in conjunction with the Reynolds- and/or Favré-averaged form of the equations of turbulent combustion has proven very successful (For an excellent recent review see Pope (1990a)). During the past 15 years, these methods have been used for simulating a variety of reacting flow configurations and, in many cases, the predicted results have been indicative of the higher accuracy of these methods in comparison with conventional moment methods. Based on this indication, it is safe to state that presently, from the statistical point of view, PDF methods are the most attractive choice for the description of chemically reacting turbulent flows.

A similar scenario may be surmised to be the case when the PDF methods are used in the context of subgrid closures for LES. In this case, the PDF (or the joint PDF) of the scalar variables within the ensemble of grids (identifying the large scales of the flow) may uniquely determine the subgrid average value of the reaction rate (or other functions of the scalar variables). This PDF, in conjunction with an appropriate model for the hydrodynamic fluctuations within the subgrid, may facilitate the implementation of LES for the analysis of reacting turbulence.

Our main goal in this work is to initiate an assessment of the use of PDF methods for their possible future implementation in LES, as well as to further our investigation of the PDF methods in modeling turbulent combustion problems. The approach followed is similar to those previously used in the *a priori* analyses. Namely, the data obtained by DNS are utilized to construct the appropriate PDF's that can be used for either

turbulence modeling or subgrid closures. We are currently in a preliminary stage of our work, especially in tasks directed at subgrid modeling.

In order to establish a framework for the discussion of the results, a review is provided of PDF methods and subgrid closures in Section 2. This review is rather brief and is presented solely for the purpose of providing a reference for the remainder of the chapter. However, the reader is referred to other collective works and survey articles which discuss these statistical methods in greater detail. Also, the discussion on PDF methods focuses on the treatment of scalar quantities alone, without including the treatment of scalar-velocity PDF's. The specification of the problem under current scrutiny is provided in Section 3, in which the relevance of some of the characteristic variables are expressed, together with a description of the geometrical configuration and the initialization procedure. The results of simulations are presented in Section 4, in which we place an emphasis on the use of stochastic methods for modeling of the mixing phenomenon. This chapter ends in Section 5, where we summarize our findings, and also provide some speculations and suggestions for future work, some of which are currently under way.

2. BACKGROUND REVIEW

2.1. PDF METHODS:

In the majority of previous work on the computational treatment of turbulent combustion, statistical methods have generally been employed. These methods involve the representation of physical variables in a stochastic sense, and in conjunction with appropriate transport equations, predict the approximate behavior of the flow field. In the framework of such methods, the physical quantities are treated as *random* variables, and the transport equations describing the evolution of these quantities are used in such a way as to yield their stochastic variations. At present, two general types of strategies are identified which can be utilized for statistical treatment of turbulent combustion problems (Libby and Williams, 1980): (1) the moment method, and (2) the Probability Density Function (PDF) method. In the first approach, "averages" (or "means") of the relevant physical variables are introduced, and the governing transport equations are subsequently averaged. These averages are generally defined in such a way to yield the desired mathematical properties and are usually introduced in the form of time-, ensemble-, or Favré-averages. The second approach, the PDF approach, relies directly on the PDF of these variables by which the desired moments can be obtained.

Moment methods usually involve the determination of the statistical means by virtue of solving transport equations for the various unclosed moments of the equations. These equations provide, in a sense, a description of the variables at one level higher than the equations for the mean values (first moments). This results in explicit transport equations for the second order moments. These equations, however, are still not in a closed form, due to the appearance of the unclosed third order correlations which require further modeling. Regardless of the degree of truncation of the higher moments, the closure problem always remains, and transport equations at any level require modeling at higher orders.

The primary advantage of moment methods is their relative ease of use in engineering applications. Most models suggested in the literature can be implemented directly into computer codes developed for laminar flows. This allows the engineer to

economically obtain approximations to combustion problems for many different sets of flow conditions. The results obtained in this way have, in many cases, exhibited good agreement with experimental measurements. This has been a major factor in justifying the use of moment methods in turbulent combustion and it appears that these methods will remain popular for engineering applications for the near future.

The closure based on the second approach, the PDF method, has proven very useful in the theoretical description of turbulent reactive flows (Hawthorne *et al.*, 1949). The philosophy of this approach is to consider the transport of the PDF's rather than the finite moments of the statistical variables. The key advantage of the method is the fundamental property of the PDF, namely that the mean reaction rate (and any other functions of the scalar) can be evaluated directly from the PDF. Representing the scalar field involving σ species by $\Phi = (\phi^1, \phi^2, \ldots, \phi^\sigma)$, and the reaction conversion rate of species α by $\omega_\alpha(\Phi)$, the mean of this rate (denoted by $< >$) can be written as:

$$< \omega_\alpha >= \int_{-\infty}^{+\infty} \mathcal{P}_1(\underline{\Xi})\omega_\alpha(\underline{\Xi})d\underline{\Xi} \tag{1}$$

In this equation, $\underline{\Xi}$ represents the scalar space and $\mathcal{P}_1(\underline{\Xi})$ is the PDF of the scalar variable at a point, defined so that:

$$\mathcal{P}_1(\underline{\Xi})d\underline{\Xi} = \text{Probability } (\underline{\Xi} \leq \Phi \leq \underline{\Xi} + d\underline{\Xi}) \tag{2}$$

where $d\underline{\Xi} = (d\xi^1, d\xi^2, \ldots, d\xi^\sigma)$ denotes an elemental hypervolume at $\underline{\Xi}$.

The scalar PDF, $\mathcal{P}_1(\underline{\Xi})$, defined in Eqs. (1)-(2), is in its simplest form in that it contains information only about the scalar variables, Φ. Also, it governs the probability distribution only at a single point. However, it contains much more information than is required to determine the mean value of any functions of the random variables Φ. Therefore, its evaluation in comparison to direct evaluation of $< \omega_\alpha >$ (if it could have been done) is understandably more difficult. Nevertheless, since $\mathcal{P}_1(\underline{\Xi})$ includes all the statistical information about the scalars, its determination is in many ways more useful than that of the mean values.

A systematic way of evaluating a PDF is to obtain and solve a transport equation governing its evolution. A transport equation for $\mathcal{P}_1(\underline{\Xi},\ \underline{\Xi} = \xi^1, \xi^2, \ldots, \xi^\sigma)$ can be constructed by relating the PDF to $\Phi(\underline{x}, t)$ in terms of Dirac-delta functions (Pope, 1979, 1985, 1990a; O'Brien, 1980, 1981, 1986):

$$\mathcal{P}_1(\underline{\Xi}) =< \varrho(\underline{x}, t) > \tag{3}$$

where ϱ is the single-point fine grained density defined by:

$$\varrho = \prod_{\alpha=1}^{\alpha=\sigma} \delta(\xi^\alpha - \phi^\alpha) \tag{4}$$

From the appropriate conservation equations for the scalar field and Eqs. (1)-(4) one can obtain transport equation describing the evolution of the PDF. Limiting the formulation to that of a constant density Fickian diffusion flow, we have (see O'Brien, 1980 for a complete derivation):

$$\frac{\partial \mathcal{P}_1}{\partial t} + < \underline{V} \cdot \nabla \varrho > = -\frac{\partial}{\partial \xi^\alpha}(\omega_\alpha \mathcal{P}_1) + \Gamma < \nabla^2_{\underline{x}} \phi^\alpha \frac{\partial \varrho}{\partial \xi^\alpha} > \tag{5}$$

Here, $\underline{V}$ is the velocity field and Γ is the diffusion coefficient of the species. From this equation, it can be seen that the effects of reactivity and diffusivity (the terms on the RHS) are to transport the PDF into the composition space ($\underline{\Xi}$), whereas the convective transport is a physical space phenomenon. Furthermore, it is shown that the influences of $\omega_\alpha(\Phi)$ in the composition space appear in closed form. However, models are needed for the closures of the molecular mixing term (second term on the RHS) and the turbulent convection term (second term on LHS).

Since the term that includes the interaction between the scalar variables through the reaction rate ω_α appears in a closed form in Eq. (5), in what follows we limit the discussion to the transport of a single reacting scalar (i.e. $\sigma = 1$) which is being convected by the velocity field. In this frame, the diffusive transport may be expressed as (O'Brien, 1980, 1981):

$$< \nabla^2_{\underline{x}} \phi \frac{\partial \varrho}{\partial \xi} > = \frac{\partial}{\partial \xi} Lim_{\underline{x}_2 \to \underline{x}_1} \nabla^2_{\underline{x}_2} [E(\xi_2|\xi_1)\mathcal{P}_1(\xi_1)] \tag{6}$$

Here, $E(\xi_2|\xi_1)$ represents the expected value of the scalar at $\underline{x}_2$ from its known value at $\underline{x}_1$. This equation explicitly reveals a fundamental difficulty associated with the PDF formulations, namely that the transport equation for a one-point PDF ($\mathcal{P}_1(\xi, \underline{x}, t)$) requires information about the second point, $\underline{x}_2$. In general, n-point PDF's, $\mathcal{P}_n(\xi_1, \xi_2, \ldots, \xi_n, \underline{x}_1, \underline{x}_2, \ldots, \underline{x}_n, t)$ require information about the $n+1$th point, $\underline{x}_{n+1}$. This is further demonstrated by considering the transport of $\mathcal{P}_n$ in the compositional space (Ievlev, 1970, 1973; Kuo and O'Brien, 1981):

$$\frac{\partial \mathcal{P}_n}{\partial t} + \sum_{q=1}^{n} \frac{\partial}{\partial \xi_{(q)}}[\omega(\xi_{(q)})\mathcal{P}_n] = \sum_{q=1}^{n} \frac{\partial}{\partial \xi_{(q)}}(C^{(q)}\mathcal{P}_n) \tag{7}$$

where:

$$C^{(q)} = \Gamma Lim_{\underline{x}_{n+1} \to \underline{x}_{(q)}} \nabla^2_{\underline{x}_{n+1}} [E(\xi_{n+1}|\xi_1, \xi_2, \ldots, \xi_n, \underline{x}_1, \underline{x}_2, \ldots, \underline{x}_n)] \tag{8}$$

and $E(\xi_{n+1}|\xi_1, \xi_2, \ldots, \xi_n, \underline{x}_1, \underline{x}_2, \ldots, \underline{x}_n)$ is the expected value of ξ_{n+1} at the point $\underline{x}_{n+1}$ based on all the values of $\xi_1, \xi_2, \ldots, \xi_n$ at $\underline{x}_1, \underline{x}_2, \ldots, \underline{x}_n$. The dependence of $C^{(q)}$ on the $n+1$th point in the transport equation for $\mathcal{P}_n$ indicates the need for a closure model which relates $\mathcal{P}_{n+1}$ to $\mathcal{P}_n$.

Despite the attractiveness of the PDF methods in obtaining a closed representation of the reaction term, there is another difficulty with the implementation of the method. This difficulty is caused by the increase of the dimensionality of the PDF as the number of scalars and/or the number of statistical points increase. This imposes a severe limit on the maximum number n in the equation for $\mathcal{P}_n$. The majority of previous work on PDF's have closed the equations at the first level ($n = 1$), and only recently has closure at the $n = 2$ level been attempted. Both these closures are reviewed in detail by Givi (1989).

2.2. LES AND SUBGRID CLOSURES:

Despite the present capability of modern supercomputers in allowing calculations with more than one million grid points, the range of length and time scales that can be resolved by DNS is substantially smaller than those of turbulent flows of practical interest. In DNS the largest computable scales are limited by the size of the computational domain and the "turn-over" time of the large scale structures; the smallest resolvable features are limited by the molecular length and the time scales of the viscous dissipation and chemical reactions. DNS therefore, in comparison to turbulence modeling, find its greatest application in basic research problems in which the scales of the excited modes remain within this band of computationally resolved grid sizes. This implies that for an accurate simulation, the magnitudes of the viscosity and the diffusivity must be large enough to damp out the unresolved scales, and the size of the computational time step must be kept small enough to capture the correct temporal evolution of the turbulent flame. In this context, since the instantaneous behavior of the flow variables is directly simulated at all spatial points at every instant, the computed data can actually be used to provide a quantitative basis for evaluating the validity of turbulence models and for assessing the performance of subgrid closures in LES.

The limitations associated with DNS may be alleviated, to an extent, by pre-filtering the transport equations (Aldama, 1990), a practice implemented in LES. This is effectively equivalent to eliminating the scales smaller than those resolvable within a given mesh. In this way, the variables can be represented on the number of grid points that are available for the simulations. This filtering procedure facilitates the simulations of flows with larger parameter ranges on a coarser grid. The disadvantage is that some modeling is required for the closure of the scales excluded by filtering. The selection between DNS and LES (and turbulence modeling for that matter) is dependent on the type of flow being considered, on the range of physical parameters that characterize the turbulent field, and the degree of desired accuracy.

A straightforward implementation of LES involves the decomposition of the transport variables into "large scale" and "subgrid scale" components. The former is related to the large scale eddies in the turbulent field, whereas the latter is the component containing the small scale fluctuations. The pre-filtering of the variable $\Phi(\underline{x},t)$ is performed by means of the convolution integral (Ferziger, 1977, Aldama, 1990):

$$\widetilde{\Phi}(\underline{x},t) = \int\int\int_{\Delta} F\ell(\underline{x}-\underline{x}')\Phi(\underline{x}',t)d\underline{x}' \tag{9}$$

where $F\ell$ is an appropriate filter function with a characteristic length Δ, and the integration is over the entire flowfield. The remaining portion of Φ from the filtered quantity is defined as the subgrid-scale field and is represented by:

$$\Phi''(\underline{x},t) = \Phi(\underline{x},t) - \widetilde{\Phi}(\underline{x},t) \tag{10}$$

The magnitude of pre-filtered averaged $\widetilde{\Phi}$ and its subgrid component Φ'', are obviously dependent on the filter type (function $F\ell$) and its size Δ (for reviews see Ferziger, 1981, 1982, 1983). The simplest choice would be a box filter with:

$$F\ell(\underline{x}-\underline{x}') = \begin{cases} 1, & \text{if } |\underline{x}-\underline{x}'| \leq \Delta; \\ 0, & \text{Otherwise.} \end{cases} \tag{11}$$

where $\Delta = (\Delta_x, \Delta_y, \Delta_z)$ represents the dimensions of the box, and the length in each direction should be larger than the original grid spacing in that direction. Other types of filters have also been suggested in the literature, each of which with computational and physical advantages as well as limitations (see Aldama, 1990 and Schumann and Friedrich, 1986, 1987).

Implementation of LES as a practical tool involves a combination of DNS for the filtered portion of the transport variable $\widetilde{\Phi}$, and modeling of the subgrid-scale portion, Φ''. The transport equations for the large scale components are obtained by filtering the instantaneous transport equations by means of implementing the filter defined by Eq. (9). In the resulting filtered equations, analogous to those in Reynolds averaged, the equations representing the large scale field contain unclosed terms involving the fluctuation of the subgrid components. The methodology practiced to date in dealing with these fluctuations is very similar to that employed in Reynolds averaging procedures. One may be able to develop and solve transport equations for the moments of fluctuations (Ferziger, 1981). These equations, analogously, contain some higher order moments which are needed to be modelled. The number of these terms are usually more than the corresponding ones that appear in Reynolds averaged transport, because some items that are zero in the Reynolds averaging approach are non-zero when filtering is used. Correspondingly, the tasks required for modeling the subgrid fluctuations would be somewhat more complicated than those in turbulence modeling. Nevertheless, since the small scales of turbulence are believed to exhibit a more "universal" character is the main reason to anticipate that the approach based on subgrid modeling would be more promising than the procedures based on ensemble averaging closures.

Within the past two decades, there have been many attempts to fine-tune the models by optimizing the closure for subgrid fluctuations and the type of filtering to identify the large scale components of the variables. In most of these efforts, the closure of hydrodynamic fluctuations has been the subject of major concern. There has also been some results for the passive scalar simulation and modeling of velocity-scalar correlations. However, no attempts have been made for the treatment of reacting scalars and the treatment of scalar-scalar interactions. This is probably due to the consensus among the researchers in this field that until an accurate subgrid model is constructed to represent the evolution of non-reacting scalar variables, the extension to reactive flow simulations will be a difficult task.

With the new developments and progress in PDF methods and the advantages offered by such schemes over moment methods, one may anticipate that these methods may also prove useful in LES. In this case, the influences of the chemical reactions and the subgrid scalar-scalar correlations can be included by means of considering the PDF's of the fluctuating scalars within the computational grid. The advantage of using these methods for the subgrid closure is apparent since once these PDF's are known, any statistical quantity related to scalar fluctuations can be subsequently determined. This determination, although an ambitious task, is not impossible. The obvious and simplest choice is to follow an approach based on guessed PDF methods. Similar to Reynolds averaging, the first two subgrid moments of the scalar variables can be solved by LES and then the shape of the PDF can be parameterized based on these two moments. This parameterized approximate distribution can be appraised by a comparison with the "exact" shape constructed via DNS results. Similar to common practice in *a priori* assessments (Erlebacher *et al.*, 1987), the PDF distribution can be specified

by performing two sets of calculations; one with a coarse mesh, the other with a fine mesh. The results obtained from the fine mesh simulations can be used to construct the PDF distribution which in turn may be used in extensive subsequent simulations on the coarse mesh. In this setting, calculations with large transport parameters which otherwise could not be simulated on the coarse grids, are possible.

A more direct, but substantially more complicated procedure involves the solution of transport equation for the PDF's of the subgrid scalars rather than assuming their form. This approach, like its counterpart in turbulence modeling, has the advantage that the effect of scalar-scalar correlations appear in a closed form. However, models are needed for the molecular diffusion within the subgrid, and one has to resort to mixing models (a subject of current intense research) for providing the closure. The approach based on guessed PDF methods is feasible and is within the reach of present day computers. The approach based on solving the transport equation for the subgrid scale PDF might require extensive computational resources (Pope, 1990a). These models must initially be developed in a simple flow. A homogeneous flow is an excellent configuration for this purpose, and will be discussed in the next section. After the establishment of a successful model, it may be utilized for simulating more complicated flows. The extent of this utilization is dependent on the available computational resources and on the performance of the model in rigorous trials.

3. DESCRIPTION OF THE PROBLEM

The subject of our DNS is a two-dimensional homogeneous box flow under the influence of a binary chemical reaction of the type $A + B \rightarrow Products$. To impose homogeneity, periodic boundary conditions are employed in all directions of the flow, identifying the box as a homogeneous member of a turbulent universe. This periodicity allows the mapping of all the aerothermochemical variables from the physical domain into a Fourier domain, thus allowing the implementation of spectral methods for numerical simulations. The flow field is assumed to be homogeneous and isotropic, and is initialized in a similar manner to that of Passot and Pouquet (1987). This involves the superposition of a "random" velocity to a zero mean velocity and also includes random initial density, temperature, and Mach number fluctuations. These fluctuations have certain energy spectra, and the ratio between the compressible and the incompressible kinetic energy can be varied to assess the effects of compressibility. The specification of the fluctuating field with a random field is to mimic a "probabilistic" turbulent field in the context of "deterministic" DNS. This approach is similar to that followed in previous direct simulations of turbulent reacting flows (Riley *et al.*, 1986; Givi and McMurtry, 1988; McMurtry and Givi, 1989). In a laboratory flow, these fluctuations appear as the result of interactions with the surrounding universe. Such interactions do not exist in the isolated homogeneous flow considered in our simulations. Therefore, in order to introduce the "noise," which plays a central role in laboratory turbulence, these perturbations are randomly superimposed to initialize the fluctuating field for DNS. The generated turbulence field is of decaying nature, i.e. there is no artificial forcing mechanism to feed energy to the small wave numbers. While it is more desirable to have a stationary turbulence field to focus only on the behavior of the scalar field (Eswaran and Pope, 1988; McMurtry and Givi, 1989), it is not clear how to implement such a forcing mechanism in the compressible case without modifying the behavior at low wave numbers.

The scalar fields are defined to be square waves with the two species out of phase and at stoichiometric conditions. The species field is assumed to be dynamically passive, in that turbulence influences the consequent transport of the scalar field with the neglect of reverse influences. In the non-reacting case, the trace of only one of these reactants is considered, whereas in the reacting case, the transport of an appropriate Shvab-Zeldovich variable is assumed to portray the reactant's conversion rate. This is possible by assuming an infinitely fast chemical reaction rate, and by assuming that the reactants have identical thermochemical properties. In this framework, the effects of non-equilibrium chemistry are neglected; the inclusion of such effects are postponed for future investigations.

The computational package employed in simulations is based on the modification of a code developed by Erlebacher *et al.* (1987). This code is based on a spectral collocation algorithm with Fourier trial functions. All the variables are spectrally approximated on N^2 collocation points, where N represents the number of collocation points in each of the directions. The spatially homogeneous flow evolves in time, and at each time step N^2 defines the sample data size for the purpose of statistical analysis. A third order accurate Runge-Kutta finite difference scheme is employed for temporal discretization. For a trustworthy simulation, the magnitudes of the Reynolds and Peclet numbers must be kept at moderate levels and the size of the time step should be kept small. The code is capable of simulating both two- and three- dimensional flows and we have performed both such simulations. In the presentation of our results in the next section, however, we limit our discussion to that of a two-dimensional flow.

4. PRESENTATION OF RESULTS

Computations are performed on a domain with a normalized dimension of 2π in each of the directions of the flow. With the available computational resources, a resolution of 256×256 collocation grid is attainable. With this resolution, the magnitude of the Taylor microscale Reynolds numbers that could be simulated is in the range, $Re_\lambda \approx 20 \sim 30$. Simulations are performed with a wide spectrum of compressibility levels; here we only report the results obtained by use of two extreme cases: one with a low compressibility level, or pseudo incompressible, and the other with a relatively high level. In the former, the initial value of the normalized density rms is very small, i.e. $\rho_{rms} = \sqrt{< \rho'^2 >}/\rho_0 \approx 0$, whereas in the latter, this value is of order unity. The compressibility level was monitored by adjusting the initial values of the following parameters (Passot and Pouquet, 1987): (1) the rms of the Mach number, $M_t = \sqrt{< M'^2 >}$, and (2) the ratio of the compressible energy to that of the total kinetic energy, χ. Below, we limit the discussion to the results obtained for two cases. In what follows, we refer to pseudo incompressible simulations in which the following values are used initially: $M_t = 0.2$, $\chi = 0.01$, and to compressible simulations in which at the initial time $M_t = 0.6$, $\chi = 0.2$.

The compressibility effects can be manifested by both flow visualization and by considering the global behavior in an integral sense. In the former, the contour plots of the relevant variables constructed from the DNS results show the qualitative behavior, whereas in the latter, the ensemble averages of the simulated results portray the quantitative response. To demonstrate this, in Figs. 1 and 2 we present the contour plots of the density for the pseudo incompressible case and for the compressible case, respectively. A prominent difference between the two cases is the formation of steep

gradients in the high compressible case which are not observed in the pseudo incompressible simulations. The regions of high gradients are referred to as shocklets, and consistent with the previous simulations of Passot and Pouquet (1987), appear when the initial levels of density and Mach number fluctuations are high. The effects of increased compressibility can be quantitatively demonstrated by examining the temporal variations of the maxima and minima of the divergence of the velocity, the fluctuating Mach number and the ratio of the compressible to the total kinetic energy. These are presented in Figs. 3-6. In Figs. 3 and 4 the temporal variations of the minimum and maximum values of the divergence of the instantaneous velocity ($\nabla \cdot \underline{V}$) are presented for the pseudo incompressible and for the compressible cases, respectively. Note that in the low compressible flow, the minimum and maximum values are approximately mirror image of each other (with respect to $\nabla \cdot \underline{V} = 0$). In the high compressible case, however, the maximum and minimum divergence curves are asymmetric. The minimum value of divergence occurs at the normalized time of $t \approx 0.7$. This time corresponds to the onset of formation of the shocklets, and indicates severe compression within the flow. It must be mentioned that the capture of these shocklets by means of global numerical methods (without any artificial dissipation) is rather difficult. With 256×256 collocation points, this was the strongest shock that we were able to capture, and a lower resolution would result in a significant oscillation in the magnitude of the velocity divergence after the appearance of the shock. One must be careful not to confuse these numerical oscillations with compression and expansion waves.

The effects of compressibility are further quantified in Figs. 5-6. For the pseudo incompressible flow, Fig. 5, the magnitude of M_t decreases monotonically, whereas in the compressible case, Fig. 6, the decrease in M_t is interrupted by plateaux. The locations of these plateaux coincide with those corresponding to a rise in the compressible kinetic energy and the local minima of the velocity divergence. Therefore, these locations correspond to the times at which shocklets can be formed in the flow. In the pseudo incompressible flow, the magnitude of χ remains fairly constant, indicating that the initial low level of compressibility remains low at all times.

With the development of the flow, the species field would consequently evolve. To visualize the flow, the contour plots of species A are presented in Fig. 7. Parts (a) and (b) of this figure correspond to the zero and the infinitely fast reaction rate cases, respectively. This figure exhibits the effects of random motion on the distortion of the scalar field and the mixing of the two initially segregated reactants (the contours form parallel lines at $t = 0$). The effects of chemical reaction are to increase the steepness of the scalar gradients and to reduce the instantaneous values of the reactants, as indicated by a comparison between parts (a) and (b) of the figure. The quantitative behavior of the scalar development is depicted in a statistical sense by means of examining the evolution of the PDF's of the conserved Shvab-Zeldovich variable $\mathcal{J}$. This variable is normalized and defined within the region $[0, 1]$. Correspondingly, its PDF, $\mathcal{P}_1(\mathcal{J})$ is always bounded in this region. The temporal variation of $\mathcal{P}_1(\mathcal{J})$ is presented in Fig. 8. It is shown in this figure that at the initial time, the PDF is approximately composed of two delta functions at $\mathcal{J} = 0, 1$, indicating the two initially segregated reactants A and B. At later times, it evolves through an inverse-like diffusion in the composition space. The heights of the delta functions decrease and the PDF is redistributed at other $\mathcal{J}$ values in the range $[0, 1]$. At even later times, the PDF becomes concentrated around the mean value. Proceeding further in time results in a sharper peak at this

mean concentration, and the PDF can be approximated by a Gaussian distribution. This Gaussian type behavior has been observed in previous simulations of Givi and McMurtry (1988), and Eswaran and Pope (1988), and also has been corroborated in a number of experimental investigations.

An interesting character of these PDF's is that throughout their evolution, the simulated results compare remarkably well with that of a Beta density. This is also shown in Fig. 8 by a comparison between the Beta density and the DNS generated PDF's. The Beta density is parameterized with the same first two moments as those of the DNS. Therefore, in all the figures, the results are presented with respect to a time scale (t^*) proportional to the decay of the variance of the scalar $\mathcal{J}$. Higher order moments of the DNS data for the variable $\mathcal{J}$ also show good agreements in comparison with those predicted by the Beta density. This is demonstrated in Figs. 9 and 10, where the normalized kurtosis (μ_4) and superskewness (μ_6) are presented of the random variable $\mathcal{J}$ and the reactant A, respectively. At time zero, these moments are close to unity and monotonically increase as mixing proceeds. For the Shvab-Zeldovich variable $\mathcal{J}$, the magnitudes of the kurtosis and superskewness resulting from the Beta density asymptotically approach the limiting values of 3 and 15, respectively. These correspond to the normalized fourth and sixth moments of a Gaussian distribution as the variance of $\mathcal{J}$ tends to zero (as $t^* \rightarrow \infty$). The DNS generated results are very close to those of the Beta distribution throughout the simulations. However, the limiting value for variance of $\mathcal{J}$ approaching zero can not be obtained in the simulations due to obvious numerical difficulties. In the reacting case, the moments of the scalar A are consistently higher than those of the conserved scalar, but portray similar trends in both Beta density and DNS generated results.

The trends shown above are also observed in the compressible simulations. The profiles of the PDF's and those of the higher order moments and their comparisons with the corresponding parameterized Beta density are presented in Figs. 11-13. Again, the comparison is remarkably good. The main difference between these results and those of pseudo incompressible simulations is the time scale of the decay of the variance by which the PDF is evolved.† This time scale can not be incorporated into the PDF description in the format employed here. The single-point nature of these PDF's do not allow for any information about the length scales (or any other scales requiring two-point statistics) of turbulence. For a systematic inclusion of the length scale into the PDF and quantitative description of the differences between the results in the two cases, one is required to consider the evolution of the PDF's at two points (at least). Employing the results of DNS to evaluate (or to generate) models for more than one-point-level closures (O'Brien, 1985; Eswaran and O'Brien, 1989) has proven to be a challenging task, and is the subject of current research (Jiang and Givi, 1991).

The results of these simulations indicate that the approximation of a Gaussian PDF for the final stages of mixing of a conserved scalar is well justified. This corroborates the results of laboratory experiments (e.g. Miyawaki *et al.*, 1974; Tavoularis and Corrsin, 1981) and those of other numerical simulations (e.g. Eswaran and Pope, 1988; Givi and McMurtry, 1988). The numerical experiments performed here, however, are similar to most of the laboratory investigations in that they include the results of only one

† This is not illustrated in the figures clearly, since the time is scaled by the rate of variance decay.

experimental realization. Future numerical experiments using different initializations and/or with better numerical resolution and including three dimensional effects would be logical extensions of this work.

In addition to the Beta distribution approximations, the DNS results also compare very well with the mapping closure recently introduced by Kraichnan (see Chen *et al.*, 1989 and Kraichnan, 1990). This closure has the property of allowing the relaxation of the PDF of a conserved scalar property to an asymptotic Gaussian distribution. Pope (1990b) has utilized this closure for the prediction of PDF evolution in an isotropic homogeneous turbulent flow with an initial double delta distribution (similar to the condition imposed here). He showed that in the context of a one point PDF, the results obtained by this closure compare favorably with the DNS results. However, again there is no length scale information built into the model, and only the evolution of the PDF without any information regarding the time scale of evolution can be predicted. Madnia and Givi (1991) have extended this model for predicting the decay rate of a reacting scalar in homogeneous turbulence. The generated results obtained by applying this model for the prediction of the decay rate of a reacting scalar for the cases considered in DNS are shown in Figs. 14 and 15. In these figures, the DNS generated results and those predicted by a Beta density are also shown. The two PDF's (by the mapping closure, and the Beta density) are constructed in such a way to yield the same first two normalized moments of the Shvab-Zeldovich variable as those of DNS. In this context, the predicted results of the decay by both models show good agreements. The agreement for the mapping closure model is rather surprising, considering that this closure was developed for an isotropic, fully three-dimensional turbulent flow. This is probably due to matching of the normalized first two moments. A better test of the model would be its utilization at two-point level, and its comparison with DNS generated results. Also, the agreement between the mapping closure results and those of DNS worsens as the compressibility level is increased. This again is understandable in that Kraichnan's model was developed for a purely incompressible flow without including any compressibility effects.

With the construction of the DNS database, the results are used to construct the PDF's of the scalar quantities within the subgrid. Since the major riddle in PDF modeling is associated with the closure of the diffusion term and not the chemical reaction term, we limit the analysis to that of the generated PDF's of the conserved Shvab-Zeldovich variable. The construction of the PDF's is implemented by placing a coarse (n^2) mesh over the physical space occupied by the fine mesh (N^2). This mesh can be considered as the one to be potentially used in LES. In this way, it is assumed that the LES predicts the averaged results at the centers of the n^2 mesh, and the fluctuations within the coarse grids are to be modelled by an appropriate PDF closure. The actual LES in this case would correspond effectively to simulations with a homogeneous box filter in which the values of the filtered means are constant. This is somewhat analogous to the procedure followed by Schumann (1989). The main difference is the mechanism by which the fluctuations are to be considered. Schumann (1989) simply neglected such effects, but with consideration of the PDF, it may be possible to account for such effects, albeit statistically. Within each cell of the coarse mesh, we have the values of the scalar quantities at $N_\phi = (N/n)^2$ equally spaced points. This means that there is an ensemble of N_ϕ sample points at each location to construct the PDF's. This construction is implemented by statistical sampling of N_ϕ number of data points. The

domain of the scalar property $\phi \in [\phi_{min}, \phi_{max}]$ is divided into a number of bins of size $\Delta\phi$, and the number of scalar variables within each of these bins are counted. The PDF of the variable ϕ, denoted by $\mathcal{P}(\xi)$ is calculated in the interval $\xi \leq \phi \leq \xi + d\xi$, $d\xi \equiv d\phi$, from the definition of the probability:

$$\mathcal{P}(\xi)d\xi = \text{Probability } (\xi \leq \phi \leq \xi + d\xi) \tag{2'}$$

which translates into:

$$\begin{aligned} \mathcal{P}(\xi)d\xi &\equiv \text{Probability Density} \\ &= \frac{\text{Number of elements in the interval } \xi \leq \phi \leq \xi + d\xi}{N_\phi} \end{aligned} \tag{12}$$

The value of N_ϕ is a measure of the width of the filter, in that it determines the scale at which the fluctuations of the scalar field are not accounted for deterministically, but are included in a probabilistic manner by the PDF's. Consequently, the shapes of these distributions are dependent on the magnitude of the sample size N_ϕ. If this value is too small, then there will be a large scatter in the data. If it is too large, then the PDF's correspond to those appropriate for Reynolds averaging and not LES. In this primeval implementation, we have not yet performed an actual LES (using a PDF subgrid closure). Rather, we have focused only on constructing the shapes of the PDF's from the DNS results. These PDF's can again be quantified by the magnitudes of their moments to provide a reasonable *a priori* assessment of the closure for future actual LES.

With the 256^2 available total data, there is a limit on the magnitude of the ensemble data for an *a priori* assessment. Our experience indicated that an ensemble of about 32^2 was the lowest acceptable limit for a meaningful statistical analysis. Therefore, the domain was broken into 8×8 squares, within each the PDF's were constructed. There was also some analysis with 4×4 squares for better statistics. However, since this is very close to the Reynolds averaging limit, the generated results will not be considered in the forthcoming discussions.

The PDF's constructed from this ensemble showed that as the mixing proceeds, all the PDF's tend to have an asymptotic Gaussian distribution. This is to be expected, since a subset constructed from a large random set with a probability distribution tends to portray the same statistical behavior. However, the results showed that for all the cases considered, the PDF's tend to have an evolution similar to that of the Beta density. This is demonstrated in a sample plot of the distributions in Fig. 16 for both pseudo incompressible and compressible simulations. In this figure, the PDF's within one of the coarse grids are compared with that of a Beta density with the same two first moments as those within the subgrid. The comparison is fairly good, considering the size of sampled data. The overall deviation from the Beta density and the Gaussian distribution in all the subgrids can be quantified by measuring the norms of the deviation of higher moments. The L_2 norms of the fourth moments for the pseudo incompressible and the compressible simulations are shown in Figs. 17 and 18, respectively. Note that at the initial time, the deviation from a Beta distribution is very small and increases with progress in time, but not substantially. At final times, the DNS data are closer to that of a Gaussian distribution, but the magnitudes of the second moments are not

small enough for the Beta density to approach a Gaussian distribution. Similar overall trends are also observed for the compressible simulations.

With the results of the analysis, albeit primitive, it is speculated that the approach based on PDF parameterization from its first two moments may prove serviceable for LES, at least for a conserved scalar. However, the approach requires the accurate input of the first two moments of the subgrid which must be provided by modelled LES transport equations. In the absence of a better alternative, the Beta density may prove useful, and the generated results can be used to estimate the maximum reaction conversion rate in the infinitely fast chemistry limit. However, the generalization to include finite rate kinetics may not be very straightforward, since the first two moments (including the covariance of the scalar fluctuations) must be known (or modelled) *a priori*. By the same token, the extension to more complex kinetics with the inclusion of non-equilibrium effects, which are very important for practical applications, remains to be a challenging task.

An improvement of the procedure obviously involves the solution of a transport equation for the PDF (rather than its parameterization with its moments). However, the computational burden may be prohibitive due to the increased dimensionality of the subgrid PDF transport equations. An estimate of the computational requirements indicates that the cost associated with the implementation of LES procedure involving the stochastic solution of the PDF transport equation may be of the same order as that of DNS on the fine grids, unless the ratio of the fine to coarse grid is large. In this regard, the tradeoff between LES and DNS depends on other factors, such as the physical complexity and computational resources.

5. CONCLUDING REMARKS

A spectral collocation algorithm has been employed to study the mechanism of mixing and reaction in a non-premixed, decaying two-dimensional homogeneous turbulent flow. The evolution of the species field in a one-step stoichiometric reaction of the type $A + B \rightarrow Products$ was the subject of the investigation. Calculations were performed for zero-rate and infinitely fast rate chemistry in both pseudo incompressible and relatively high compressible flows. The effects of compressibility are delineated by the formation of thin shocklets and can be quantified by a global examination of the data. Mixing and the reaction conversion rate (in the reacting case) are characterized by examining the evolution of a Shvab-Zeldovich conserved scalar quantity extracted from the DNS. The results show that the PDF of this scalar variable evolves from an initial double-delta function distribution to an asymptotic shape which can be approximated by a Gaussian distribution. During this evolution, a Beta density qualitatively describes the DNS generated PDF's in both pseudo incompressible and compressible simulations. This is quantitatively demonstrated by a good agreement between the values of the higher order moments of the PDF's calculated from the DNS data and those predicted by the Beta approximation. The generated results also compare very well with those predicted with the mapping closure of Kraichnan. The decay of the mean of the reacting scalar determined by DNS compares very well with that predicted by this model and that obtained via the use of the Beta density. This trend is observed in both pseudo incompressible and compressible simulations. The main difference is the time scale of the decay of the variance of the PDF's.

The Beta density seems to also predict the behavior of the fluctuating field within the subgrid for a conserved scalar quantity. Therefore, it may provide a reasonable means of parameterizing the subgrid fluctuations in a stochastic sense. The procedure, however, requires the input of the first two moments of the variable within the subgrid, and these must be provided by modelled LES transport equations. Also, the generalization to include finite rate kinetics may not be very straightforward, since these moments must be modelled *a priori*. An improvement of the procedure involving the solution of a transport equation for the PDF is possible, but may not be practical due to the increased dimensionality of the modelled subgrid PDF transport equations. From the computational point of view, it is recommended to assess the applicability of such a procedure in (yet) simpler flows, before its implementation in simulating more complex flows.

In comparing the DNS results with those of predictions, the first two moments of the Shvab-Zeldovich variable must be matched. This is because single-point PDF's do not include information about the frequency scales of turbulence. Therefore, the evolution of the length scale, or any other parameter requiring two-point information, must be introduced in an *ad hoc* manner (here, such information is provided via DNS). Future validation studies of the PDF's by DNS need to consider the evolution of multi- (at least two-) point statistics. O'Brien (1985) has already employed a two-point formulation in the statistical description of homogeneous turbulent flows. The preliminary results obtained by such formulations are in good agreement with experimental data (Eswaran and O'Brien, 1989). However, a comparison between the predicted results and the DNS data, similar to the ones reported here for single point PDF's is recommended.

Future work should also deal with finite rate chemistry with the inclusion of non-equilibrium effects, and also on examining the extension of PDF methods in dealing with the subgrid closures in LES of such flows.

Acknowledgements: This research is sponsored by NASA Langley Research Center under Grant NAG-1-1122, by the Office of Naval Research under Grant N00014-90-J-4013 and by the National Science Foundation under Grant CTS-9057460. Computational resources are provided by NAS at NASA Ames Research Center and by the NCSA at the University of Illinois.

References:

Aldama, A. A. (1990), *Filtering Techniques for Turbulent Flow Simulations*, Lecture Notes in Engineering, vol. 56, Editor: Brebbia, C. A. and Orszag, S. A., Springer-Verlag, New York, NY.

Chen, H., Chen, S. and Kraichnan, R. H. (1989), *Phys. Rev. Lett.*, vol. 62, p. 2657.

Drummond, J. P. (1991), in *Numerical Approaches in Combustion Modeling*, Chap. X, AIAA Prog. in Aeron. and Astr., Editors: Oran, E. S. and Boris, J. P., in press.

Erlebacher, G., Hussaini, M. Y., Speziale, C. G. and Zang, T. A. (1987), *NASA CR 178273*, ICASE Report 87-20, NASA Langley Research Center, Hampton, VA.

Eswaran, V. and O'Brien, E. E. (1989), *Phys. Fluids A*, vol. 1(3), p. 537.

Eswaran, V. and Pope, S. B. (1988), *Phys. Fluids*, vol. 31(3), p. 506.

Ferziger, J. H. (1977), *AIAA Journal*, vol. 15(9), p. 1261.

Ferziger, J. H. (1981), Stanford University Report No. TF-16, Department of Mechanical Engineering, Stanford University, Stanford, CA.

Ferziger, J. H. (1982), in *Recent Contributions to Fluid Mechanics*, Editor: Haase, W., Springer-Verlag, New York.

Ferziger, J. H. (1983), in *Computational Methods for Turbulent, Transonic and Viscous Flows*, p. 93, Editor: Essers, J. A., Hemisphere Publishing Co., New York, NY.

Givi, P. (1989), *Prog. Energy Comb. Sci.*, vol. 15, p. 1.

Givi, P. and McMurtry, P. A. (1988), *AIChE Journal*, vol. 34(6), p. 1039.

Hawthorne, W. R., Wedell, D. S. and Hottel, H. C. (1949) , Third Symposium on Combustion, Flames and Explosion Phenomena, The Combustion Institute, Pittsburgh, PA, p. 266.

Hussaini, M. Y., Speziale, C. G. and Zang, T. A., (1990), in *Whither Turbulence? Turbulence at the Crossroads*, Editor: Lumley, J. L., Lecture Notes in Physics, vol. 357, p. 354, Springer-Verlag, New York, NY.

Ievlev, V. M. (1970) *Izv. Akad. Navk. S.S.S.R. Mekh. Zhidk. Gaza*, vol. 5, p. 91.

Ievlev, V. M. (1973) *Dokl Akad. Navk. S.S.S.R.*, vol. 208, p. 1044 (also, *Sov. Phys.-Dokl.*, vol. 18, p. 117 (1973).

Jiang, T.-L. and Givi, P. (1991), work in progress.

Kraichnan, R. H. (1990), *Phys. Rev. Lett.*, vol. 65, p. 575.

Kuo, Y. Y. and O'Brien, E. E. (1981), *Phys. Fluids*, vol. 24, p. 194.

Libby, P. A. and Williams, F. A. (1980), Editors, *Turbulent Reacting Flows*, Topics in Applied Physics, vol. 44, Springer-Verlag, New York, NY.

Madnia, C. K. and Givi, P. (1991), work in progress.

McMurtry, P. A. and Givi, P. (1989), *Comb. Flame.* vol. 77, p. 171.

Miyawaki, O., Tsujikawa, H., and Uraguchi, Y. (1974), *J. Chem. Eng. Japan*, vol. 7, p. 52.

O'Brien, E. E. (1980), in *Turbulent Reacting Flows*, vol. 44, Topics in Applied Physics, Chap. 5, p. 185, Editors: Libby, P. A. and Williams, F. A., Springer-Verlag, New York, NY.

O'Brien, E. E. (1981), *AIAA Journal*, vol. 19, p. 366.

O'Brien, E. E. (1985), in *Frontiers in Fluid Mechanics*, Editors: Davis, S. W. and Lumley, J. L., p. 113, Springer-Verlag, New York, NY.

O'Brien, E. E. (1986), *Physico Chemical Hydrodynamics*, vol. 7(1), p. 1.

Oran, E. S. and Boris, J. P. (1987), *Numerical Simulations of Reactive Flow*, Elsevier Publishing Co., Washington, D. C.

Passot, T. and Pouquet, A. (1987), *J. Fluid Mech.*, vol. 181, p. 441.

Pope, S. B. (1979), *Phil. Trans. Royal Soc. London*, vol. 291 (1384), p. 529.

Pope, S. B. (1985), *Prog. Energy Comb. Sci.*, vol. 11, p. 119.

Pope, S. B. (1990a), Proceedings of Twenty-Fourth Symposium (Int.) on Combustion, The Combustion Institute, Pittsburgh, PA., in press.

Pope, S. B. (1990b), "Mapping Closures for Turbulent Mixing and Reaction," presented at NASA Langley Research Center on the occasion of the sixtieth birthday of John Lumley. Hampton, Virginia, October 1990.

Reynolds, W. C. (1990), in *Whither Turbulence? Turbulence at the Crossroads*, Editor: Lumley, J. L., Lecture Notes in Physics, vol. 357, p. 313, Springer-Verlag, New York, NY.

Riley, J. J., Metcalfe, R. W., and Orszag, S. A. (1986), *Phys. Fluids*, vol. 29(2), p. 406.

Rogallo, R. S. and Moin, P. (1984), *Ann. Rev. Fluid Mech.*, vol. 16, p. 99.

Schumann, U. (1989), *Atmospheric Environment*, vol. 23(8), p. 1713.

Schumann, U. and Friedrich, R. (1986), Editors, *Direct and Large Eddy Simulation of Turbulence*, Proceedings of the EUROMECH Colloquium No. 199, Munchen, FRG, Sep. 30-Oct. 2, 1985.

Schumann, U. and Friedrich, R. (1987), in *Advances in Turbulence*, Editors: Comte-Bellot, G. and Mathieu, J., Springer-Verlag, New York, NY.

Tavoularis, S., and Corrsin, S. (1981), *J. Fluid Mech.*, vol. 104, p. 311.

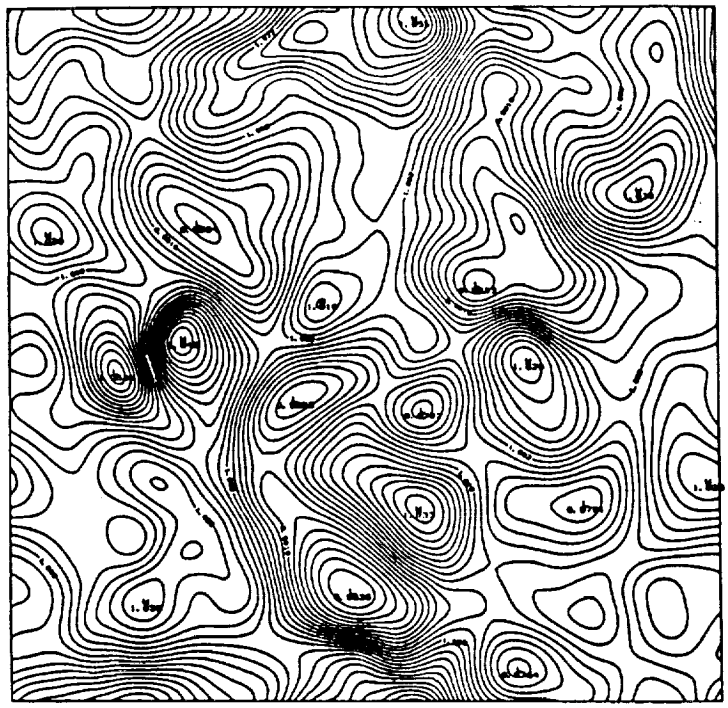

Figure 1. Plot of density contours for the pseudo incompressible case. $t = 6.142$.

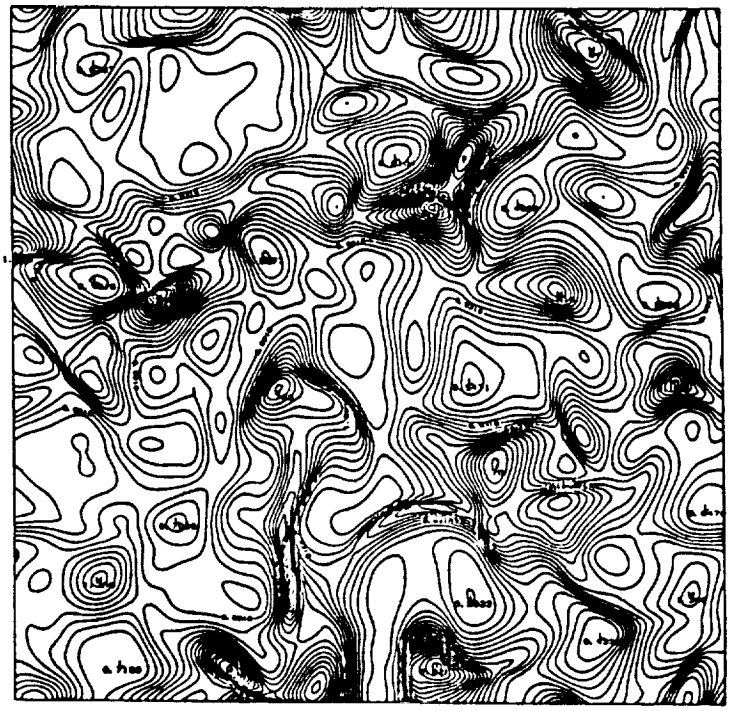

Figure 2. Plot of density contours for the compressible case. $t = 0.686$.

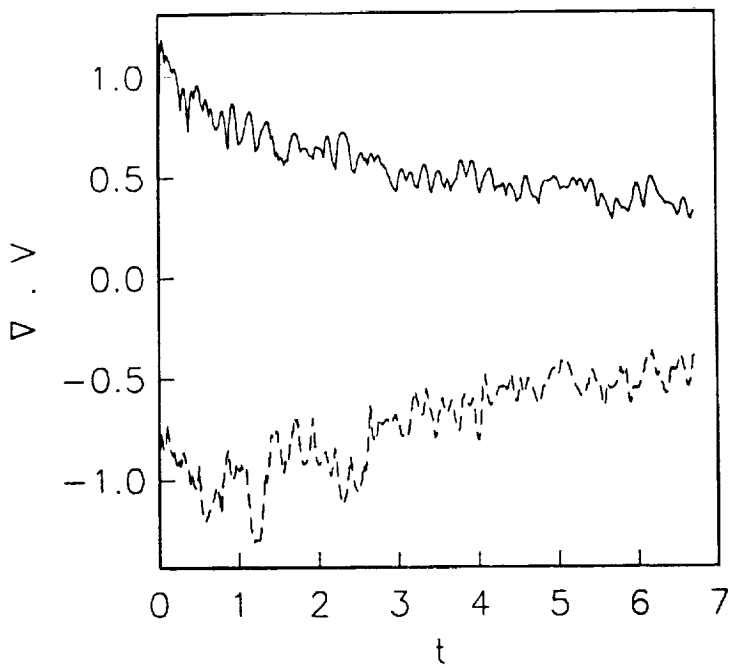

Figure 3. Temporal variation of the minimum and maximum values of velocity divergence for the pseudo incompressible case.

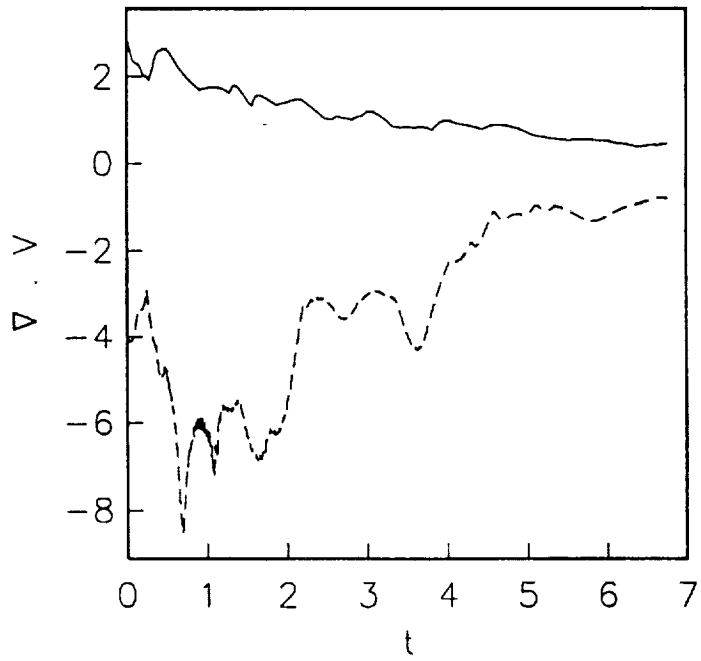

Figure 4. Temporal variation of the minimum and maximum values of the velocity divergence for the compressible case.

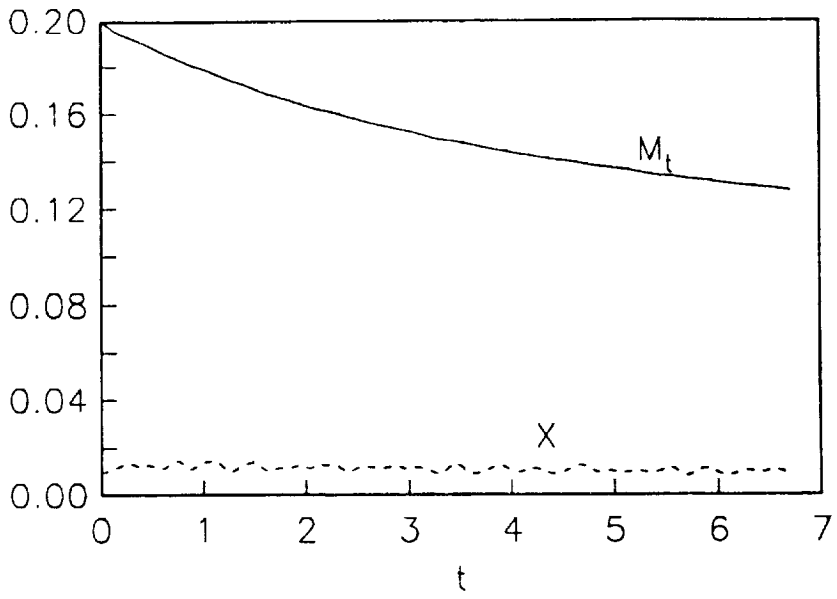

Figure 5. Temporal evolution of M_t (solid line) and χ (dashed line) for the pseudo incompressible case.

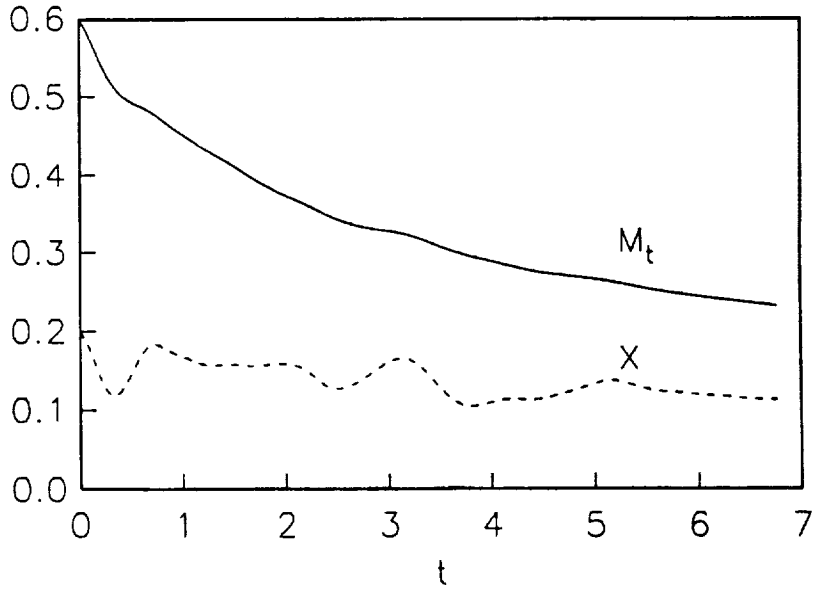

Figure 6. Temporal evolution of M_t (solid line) and χ (dashed line) for the compressible case.

(a)

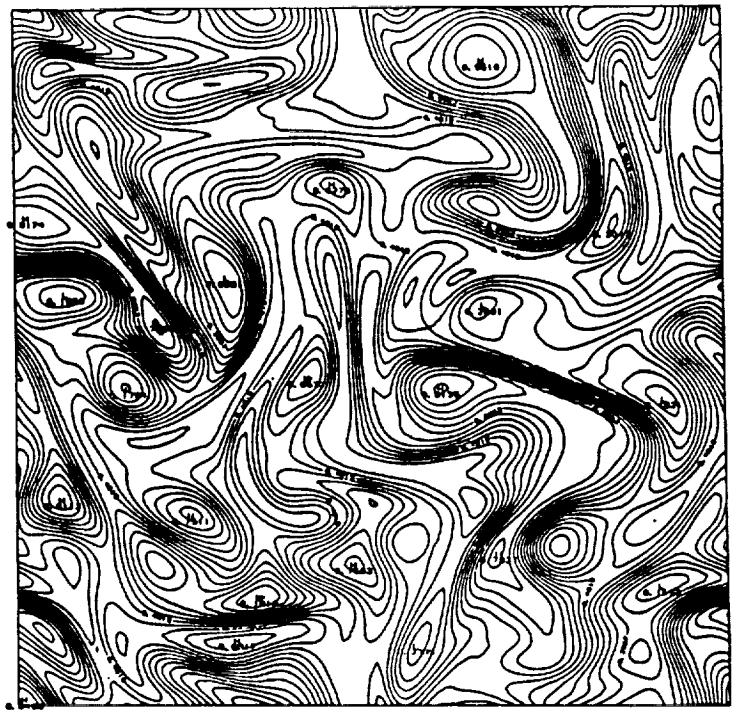

(b)

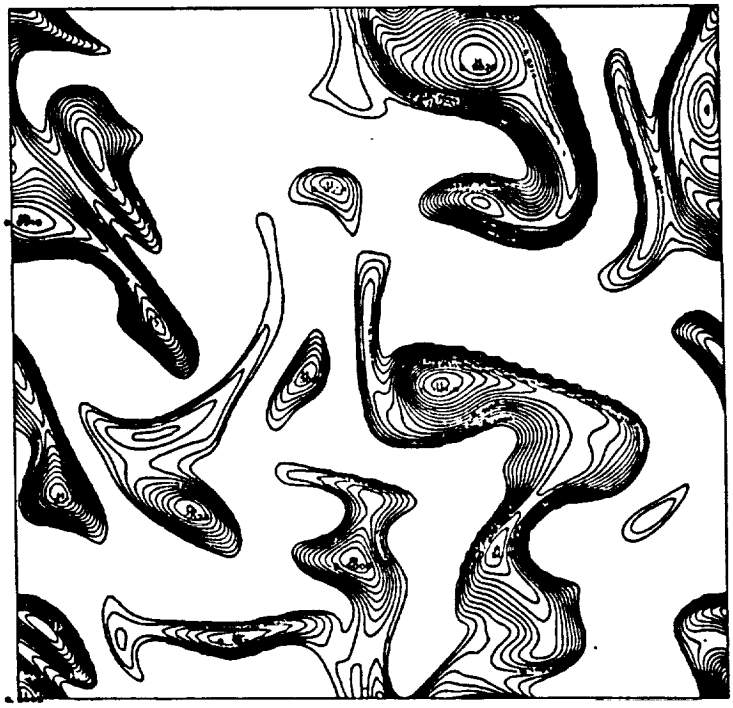

Figure 7. Plot of species A concentration contours at $t^* = 1.0715$. (a) non-reacting case; (b) reacting case.

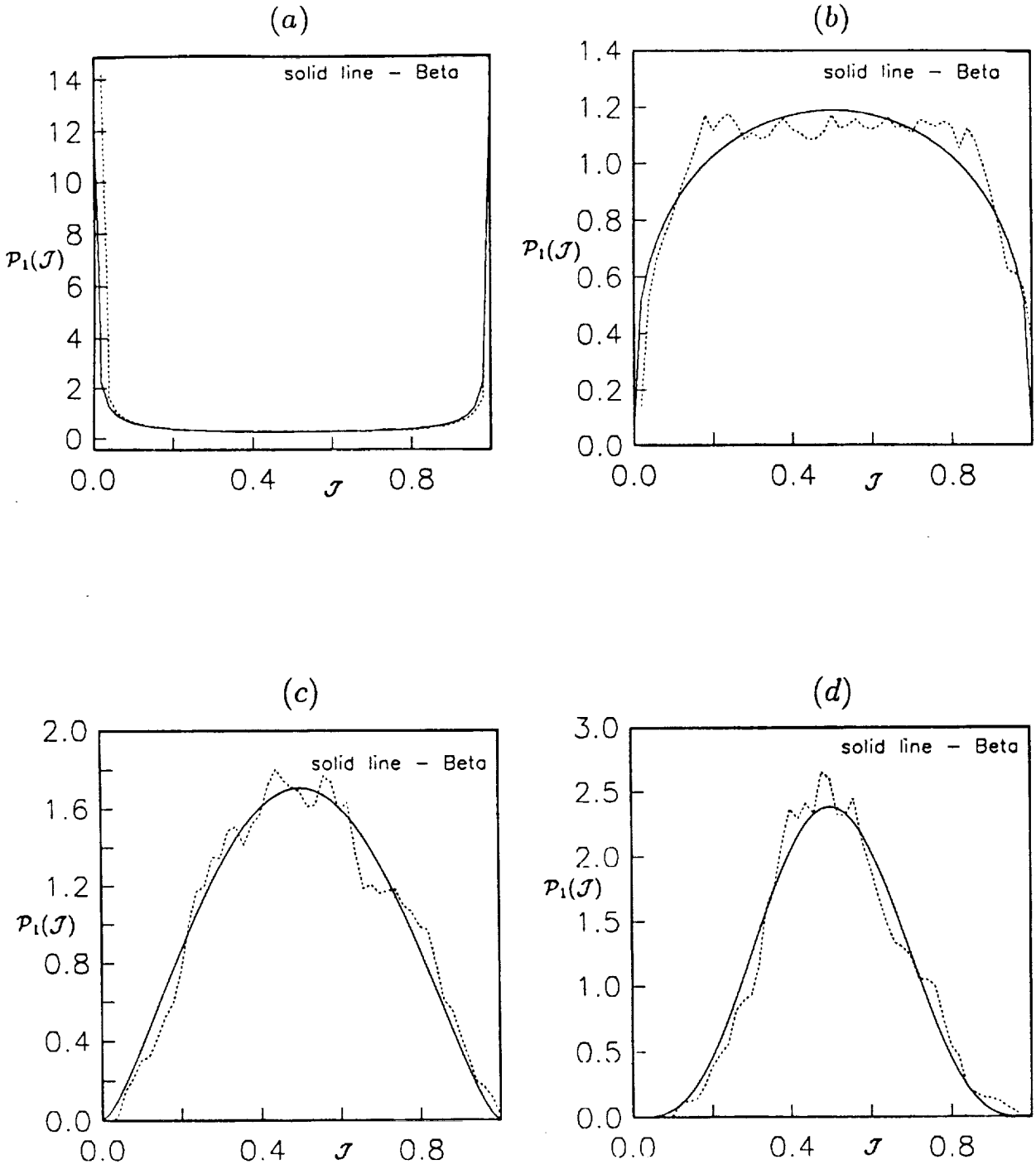

Figure 8. Temporal evolution of $\mathcal{P}_1(\mathcal{J})$ for the pseudo incompressible case. DNS data (dotted line), Beta density (solid line).
(a) $t^* = 0.035$, (b) $t^* = 0.549$, (c) $t^* = 0.800$,
(d) $t^* = 1.0715$.

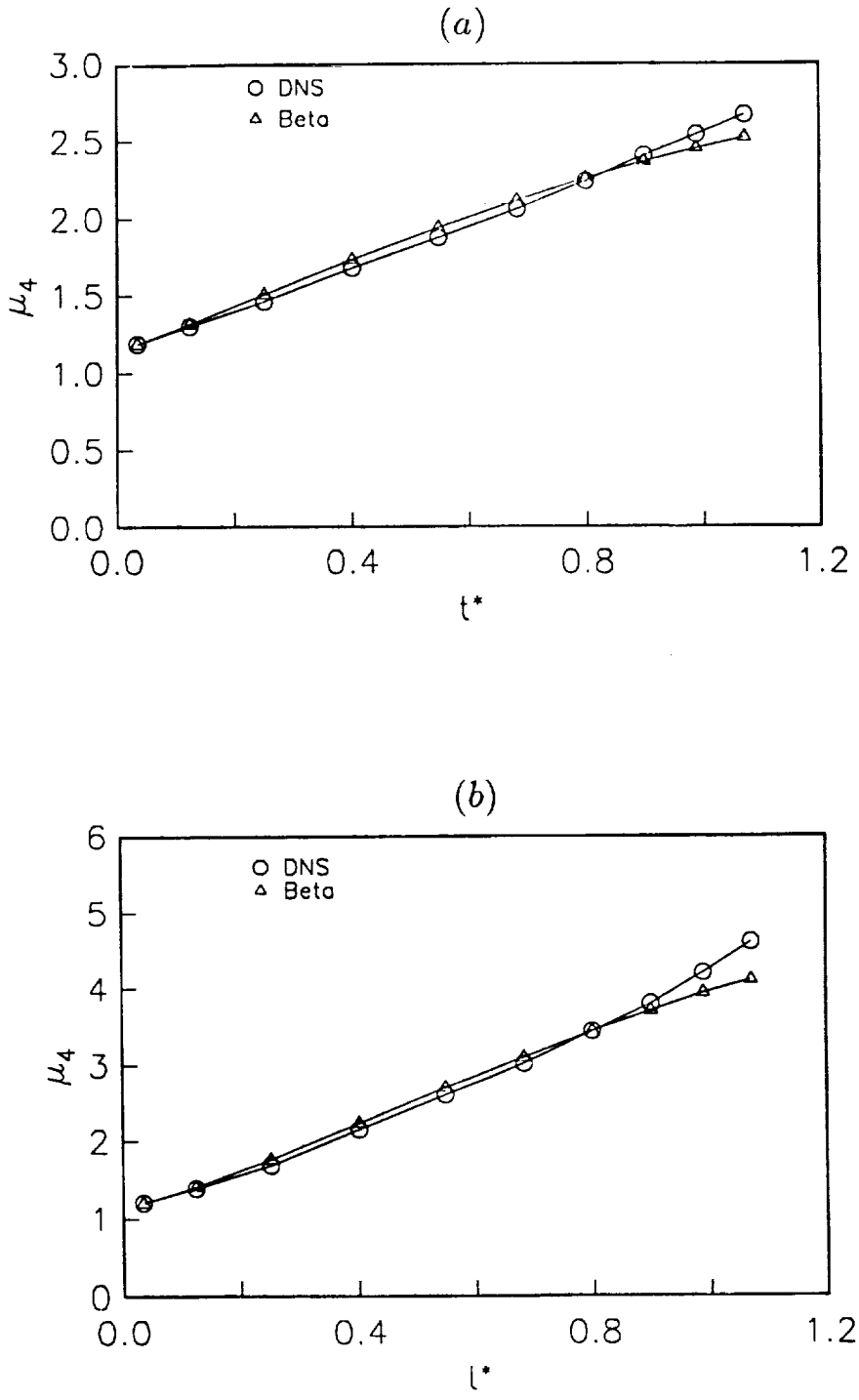

Figure 9. Temporal variation of the kurtosis, μ_4, for the pseudo incompressible case. (a) variable $\mathcal{J}$, (b) Species A in reacting case.

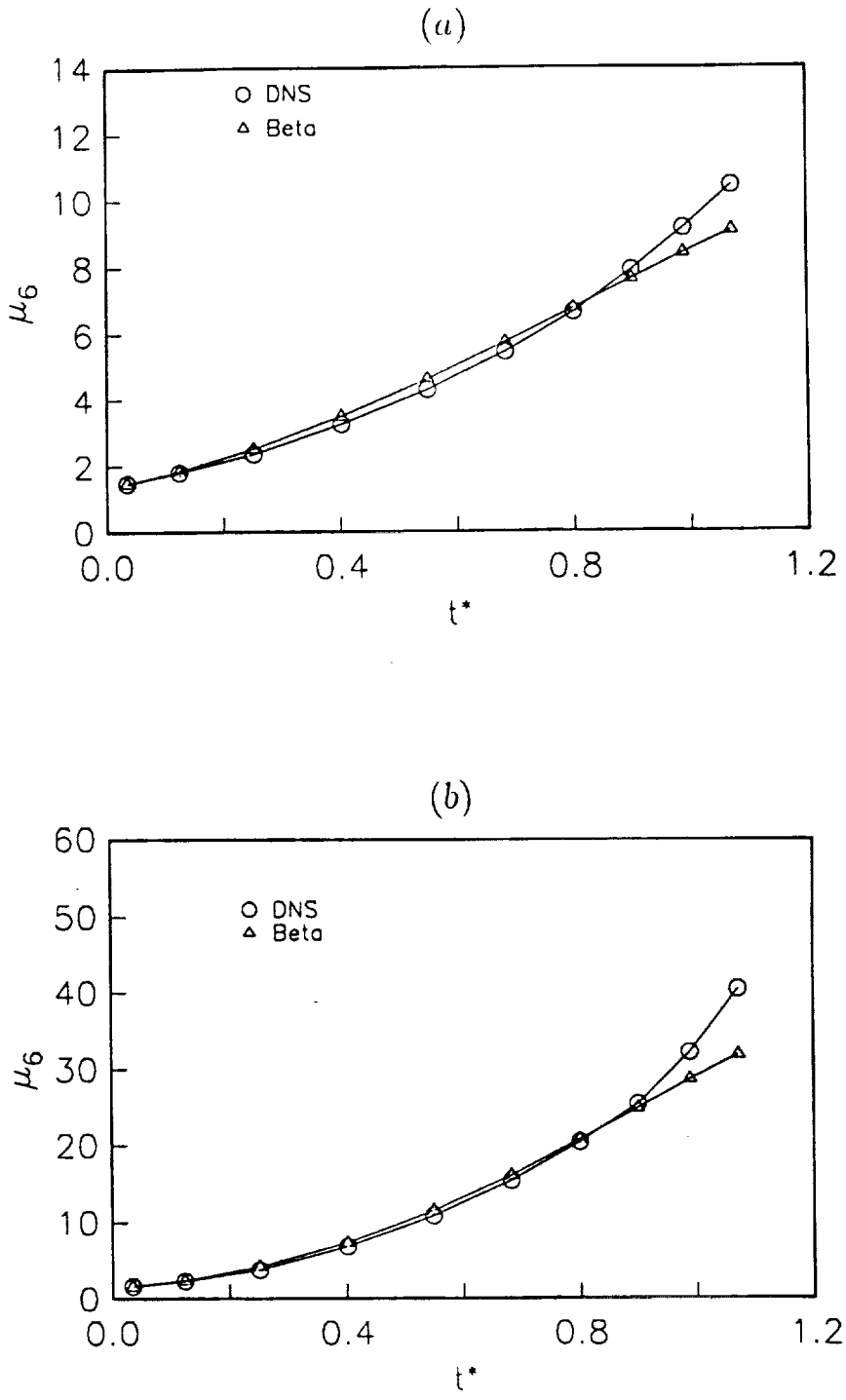

Figure 10. Temporal variation of the superskewness, μ_6, for the pseudo incompressible case. (a) variable $\mathcal{J}$, (b) Species A in reacting case.

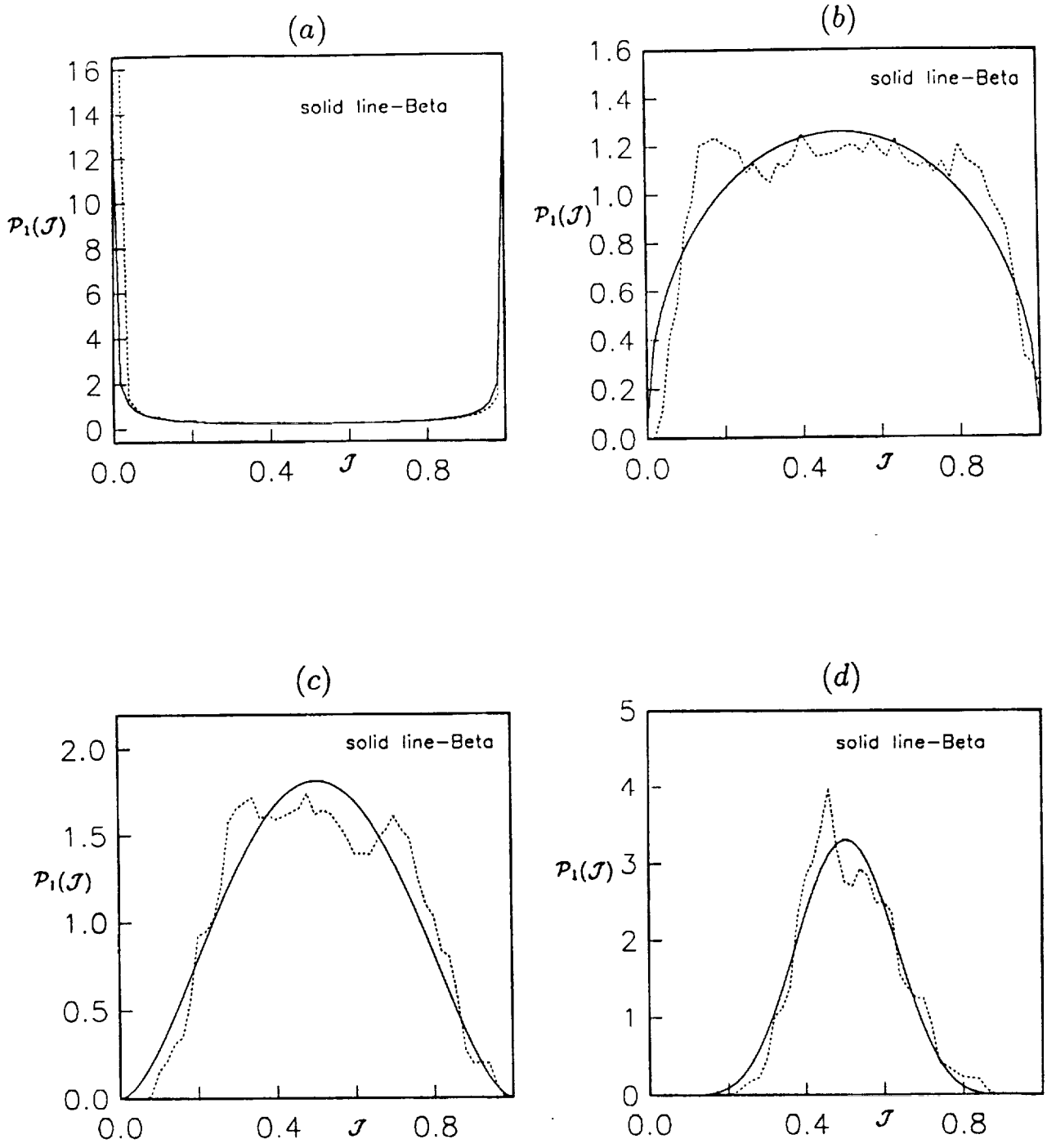

Figure 11. Temporal evolution of $\mathcal{P}_1(\mathcal{J})$ for the compressible case.
DNS data (dotted line), Beta density (solid line).
(a) $t^* = 0.014$, (b) $t^* = 0.587$, (c) $t^* = 0.848$,
(d) $t^* = 1.365$.

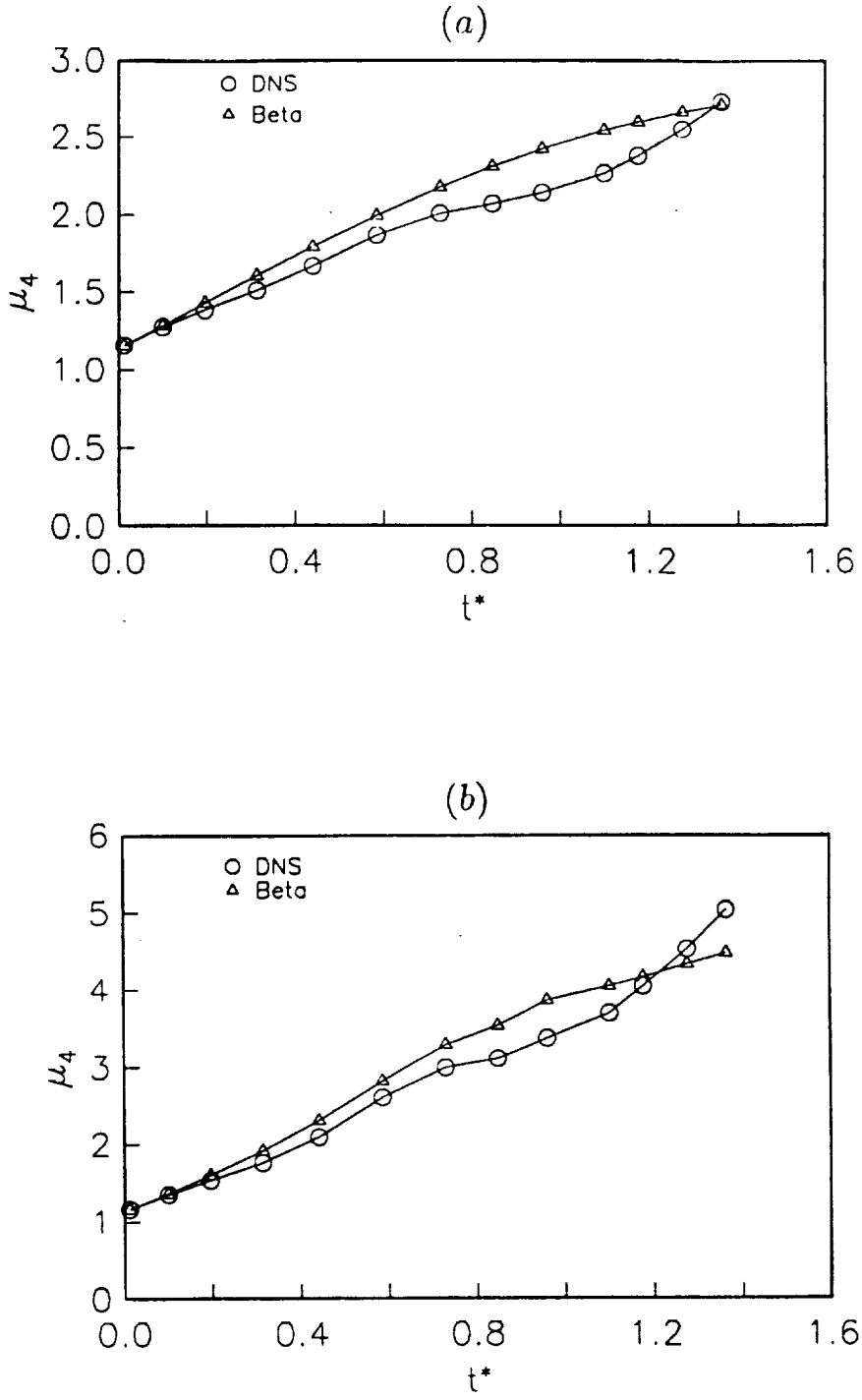

Figure 12. Temporal variation of the kurtosis, μ_4, for the compressible case. (a) variable $\mathcal{J}$, (b) Species A in reacting case.

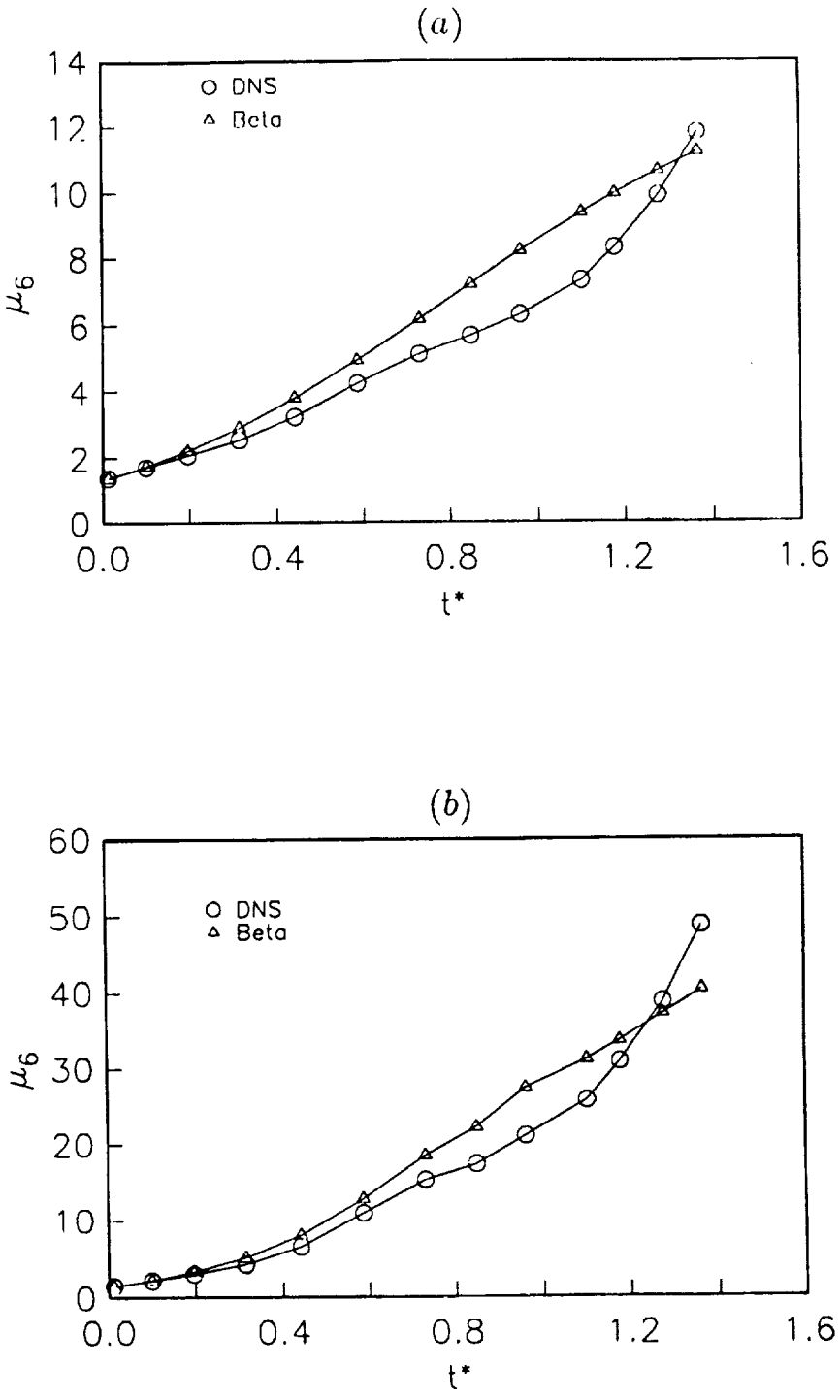

Figure 13. Temporal variation of the superskewness, μ_6, for the compressible case. (a) variable $\mathcal{J}$, (b) Species A in reacting case.

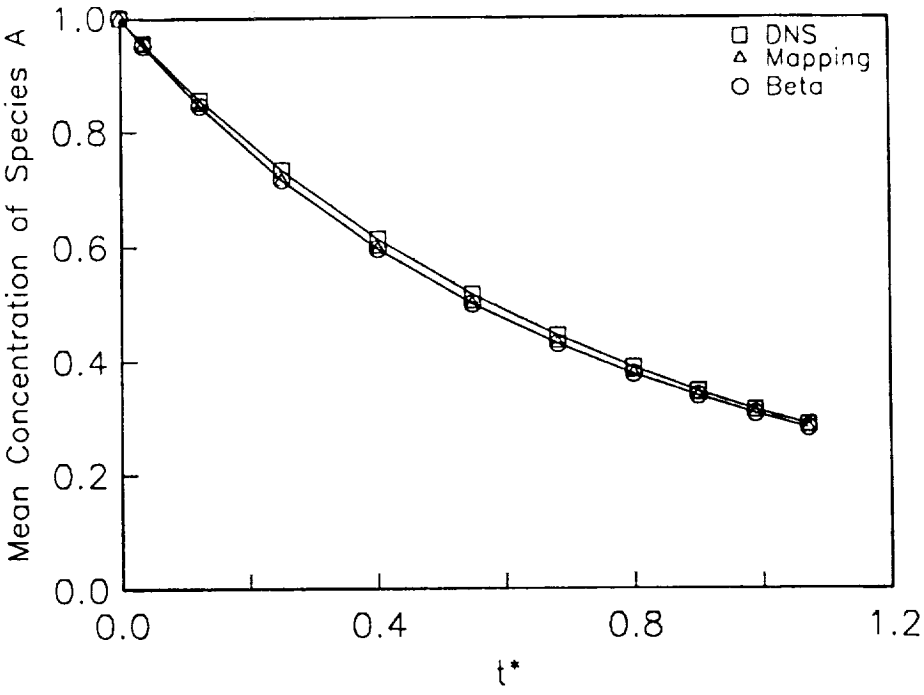

Figure 14. Mean concentration of the reacting species A vs. time for the pseudo incompressible case.

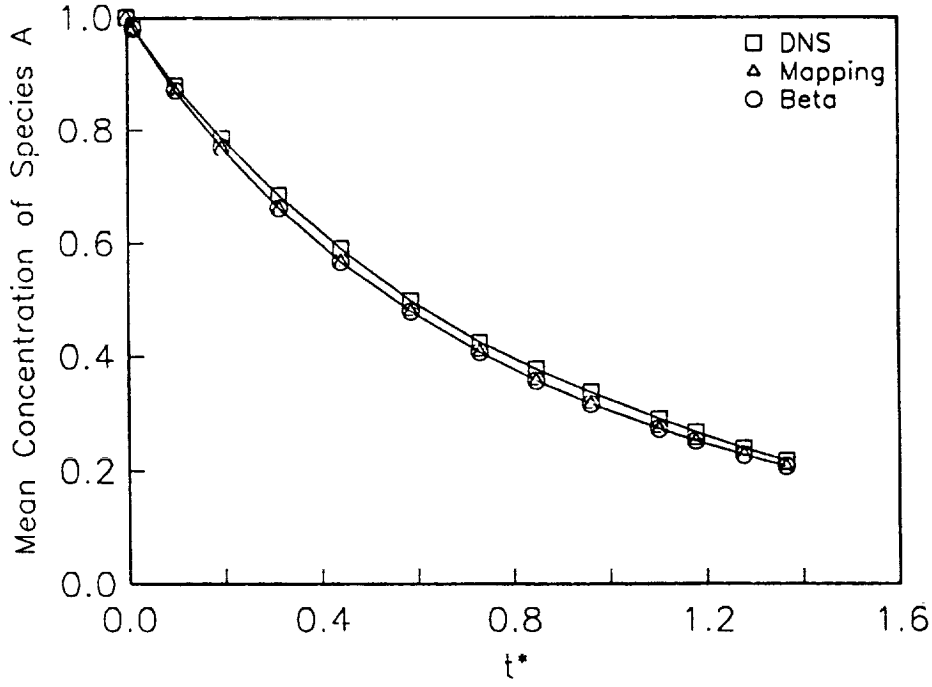

Figure 15. Mean concentration of the reacting species A vs. time for the compressible case.

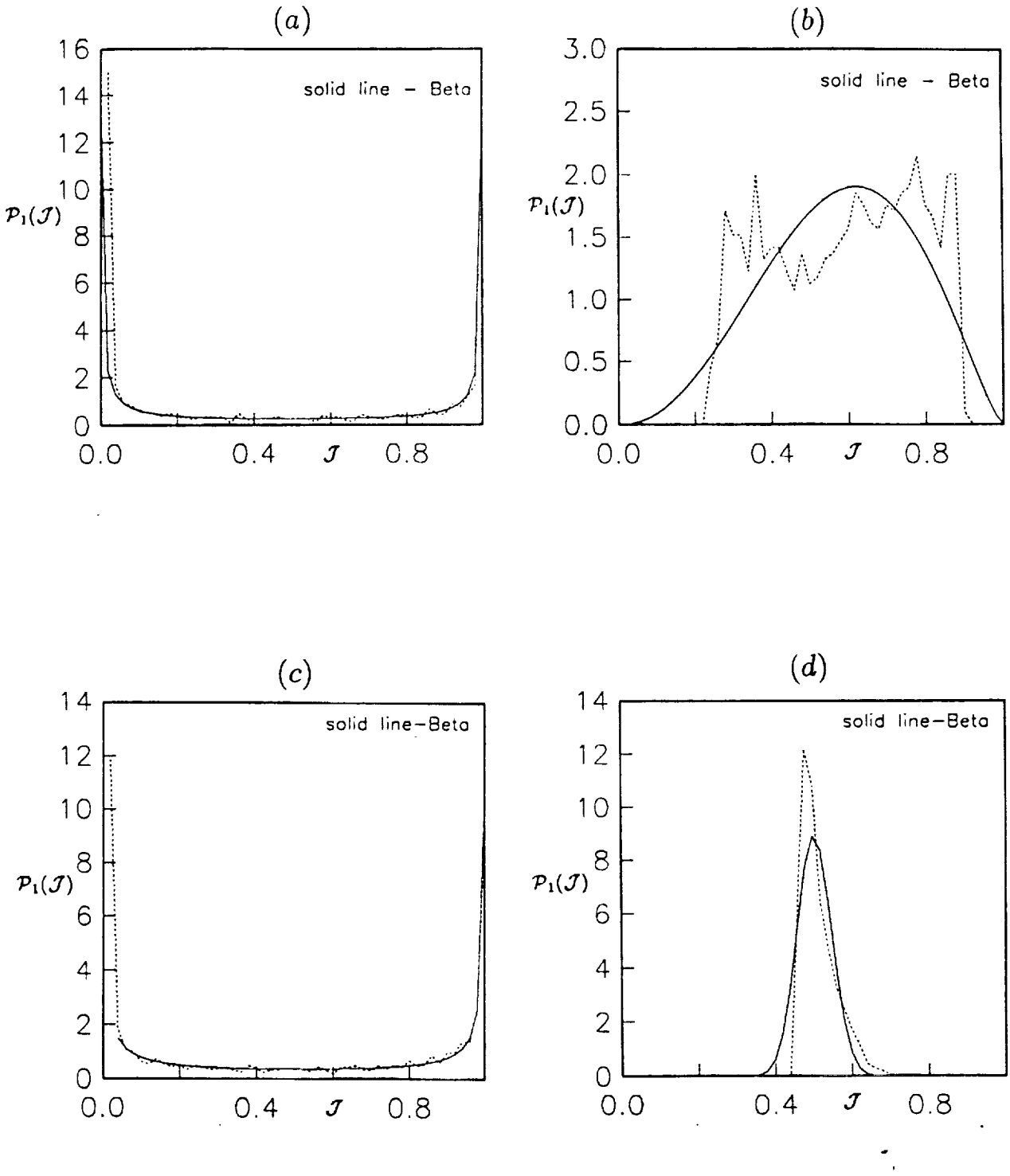

Figure 16. Sample PDF's of the variable $\mathcal{J}$ within the subgrid.
(a) pseudo incompressible case, $t^* = 0.0355$, (b) pseudo incompressible case, $t^* = 0.800$
(c) compressible case, $t^* = 0.101$, (d) compressible case, $t^* = 1.507$.

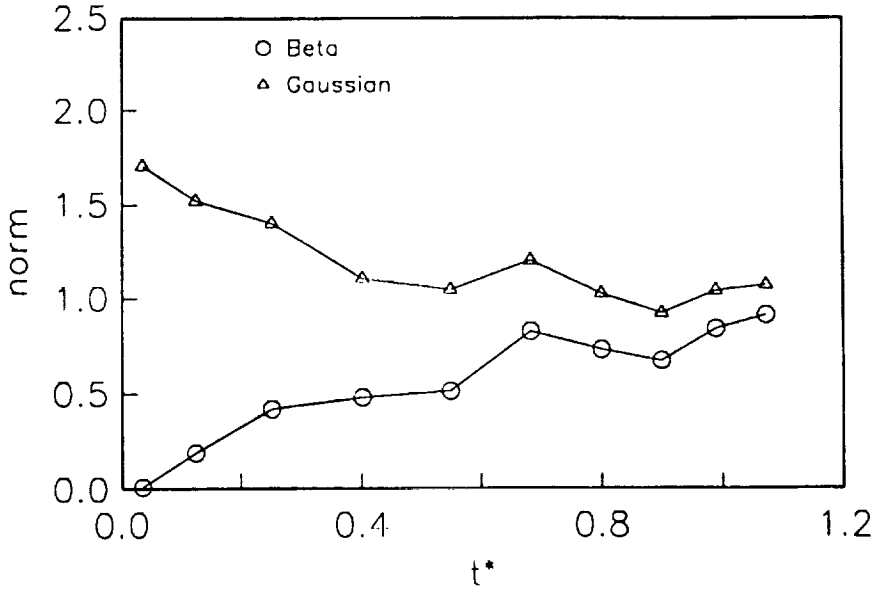

Figure 17. L_2 norm of deviation of the fourth moment vs. time for the pseudo incompressible case.

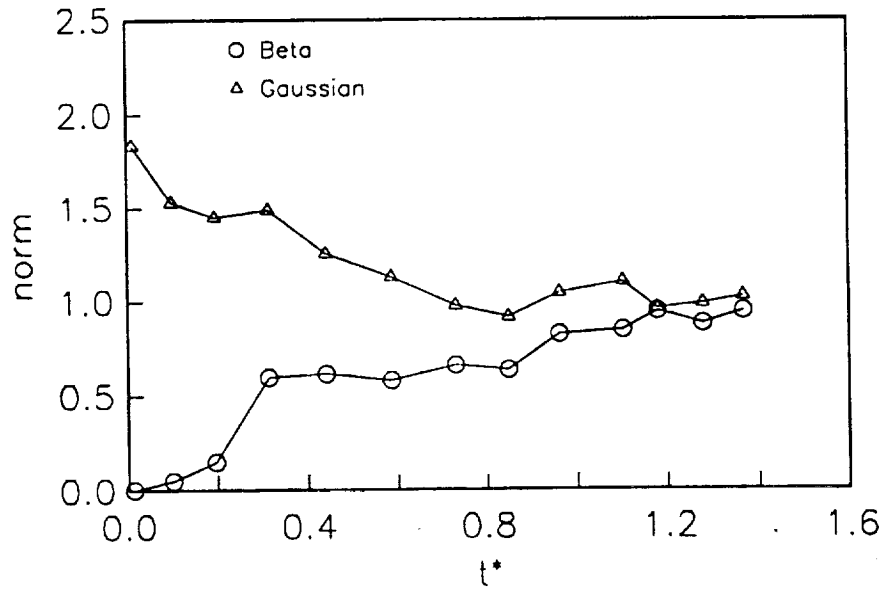

Figure 18. L_2 norm of deviation of the fourth moment vs. time for the compressible case.

Appendix IV

Theoret. Comput. Fluid Dynamics (1992) 4: 79–93

Theoretical and Computational Fluid Dynamics

Reactant Conversion in Homogeneous Turbulence: Mathematical Modeling, Computational Validations, and Practical Applications[1]

C.K. Madnia, S.H. Frankel, and P. Givi

Department of Mechanical and Aerospace Engineering, State University of New York, Buffalo, NY 14260, U.S.A.

Communicated by M.Y. Hussaini

Received 24 March 1992 and accepted 27 July 1992

Abstract. Closed form analytical expressions are obtained for predicting the limiting rate of mean reactant conversion in homogeneous turbulent flows under the influence of a binary reaction of the type $F + rO \rightarrow (1 + r)$ *Product*. These relations are obtained by means of a single-point Probability Density Function (PDF) method based on the *Amplitude Mapping Closure* (Kraichnan, 1989; Chen *et al.*, 1989; Pope, 1991). It is demonstrated that with this model, the maximum rate of the mean reactants' decay can be conveniently expressed in terms of definite integrals of the parabolic cylinder functions. For the cases with complete initial segregation, it is shown that the results agree very closely with those predicted by employing a beta density of the first kind for an appropriately defined Shvab–Zeldovich scalar variable. With this assumption, the final results can also be expressed in terms of closed form analytical expressions which are based on the incomplete beta functions. With both models, the dependence of the results on the stoichiometric coefficient and the equivalence ratio can be expressed in an explicit manner. For a stoichiometric mixture the analytical results simplify significantly. In the mapping closure these results are expressed in terms of simple trigonometric functions. For the beta density model they are in the form of gamma functions. In all the cases considered, the results are shown to agree well with data generated by Direct Numerical Simulations (DNS). Due to the simplicity of these expressions and because of nice mathematical features of the parabolic cylinder and the incomplete beta functions, these models are recommended for estimating the limiting rate of mean reactant conversion in homogeneous reacting flows. These results also provide a valuable tool in assessing the extent of validity of turbulence closures for the modeling of unpremixed reacting flows. Some discussions are provided on the extension of the models for treating more complicated reacting systems, including realistic kinetics schemes and multiscalar mixing with finite rate chemical reactions in more complex configurations.

Nomenclature

a, b, c: some constant.
B: the beta function.
$\mathscr{D}$: the parabolic cylinder function.
Da: the Damköhler number.
F: fuel.
$\mathscr{G}$: the parameter in the mapping closure.

[1] This work was sponsored by the NASA Langley Research Center under Grant NAG-1-1122, and by the Office of Naval Research under Grant N00014-90-J-4013. Computational resources were provided by NCSA at the University of Illinois.

g: half the inverse of the normalized variance of the Shvab Zeldovich variable.
H: the Heaviside function.
$\mathcal{I}$: the incomplete beta function.
$\mathcal{J}$: the Shvab-Zeldovich variable.
O: the oxidizer.
$\mathcal{P}$: the PDF.
r: the stoichiometric coefficient.
t: the physical time.
W: the area weight of the reactant.
y: the dummy variable of integration.
$\mathcal{Y}$: the unmixedness ratio.

Greek Letters

$\beta_1, \beta_2, \ldots$: parameters of the beta density.
γ: the equivalence ratio.
Γ: the gamma function.
δ: the delta function.
ξ: the composition space for the PDF.
φ_0: the composition space for a Gaussian reference field.
τ: the normalized time.
χ: the mapping function.

Subscripts

0: time zero (inlet of plug flow reactor).
G: Gaussian.
st: stoichiometric.

Other symbols

$\langle\ \rangle$: the probability average.
$'$: the fluctuation for the ensemble mean.

1. Introduction

For the past 40 years, since the early work of Hawthorne *et al.* (1949), estimation of the mean reactant conversion rate has been the subject of wide investigations in mathematical modeling of turbulent reacting flows. In unpremixed reacting systems, including diffusion flames, there are two factors by which this rate is influenced: (1) the speed at which the reactants are brought into the reaction zone, and (2) the rate at which they are converted to products through chemical reactions. The relative importance of the two mechanisms is characterized by magnitude of the Damköhler number (Da), which is the ratio of the characteristic frequency of the chemical reaction to that of the hydrodynamics. The role of the Damköhler number in the characterization of reacting flows is very important (Williams, 1985). In the limit of $Da \to \infty$, the rate of reactant consumption is governed by the hydrodynamics, i.e., the reaction is "mixing controlled" and is determined by the speed at which the reactants are brought into an infinitely thin reaction zone (Bilger, 1980). Obviously, with the assumption of an infinitely fast chemistry, it is not possible to account for many interesting issues associated with nonequilibrium effects in unpremixed flames (Libby and Williams, 1980). However, as indicated in the original pioneering work of Toor (1962), and later by O'Brien (1971) and Bilger (1980), it is very important to have a prior estimate of the "limiting" rate of mean reactant conversion in practical modeling of combustion systems. In this limit the problem reduces to the simpler problem of "mixing," in which its analysis is much simpler (Toor, 1962, 1975).

Development of an appropriate turbulence model which can predict the mean rate of reactant conversion has been the subject of extensive investigations (for reviews see Toor, 1975; Brodkey, 1981; Libby and Williams, 1980; Williams, 1985). Amongst the theoretical tools developed, it is now firmly accepted that the approach based on the single-point Probability Density Function (PDF) of the scalar quantities is particularly useful, and this approach has been very popular for modeling the reactant conversion in a variety of turbulent reacting flow systems (Kollmann, 1990; Pope, 1985, 1990, 1991). The advantage of PDF methods is due to their inherent capability to include all the single-

point statistical information pertaining to the scalar field. Therefore, once the PDF (or the joint PDF) of the scalar variables is determined, all the relevant one-point statistics of the field are available without need for additional closures.

The most logical and systematic means of determining the PDF involves the solution of an appropriate transport equation governing its evolution. In this equation, due to the nature of the formulation, the effects of chemical reaction appear in a closed form (Pope, 1976), regardless of its degree of complexity. However, the influences of molecular action cannot be fully described, and can be treated only by means of employing an appropriate closure. As noted by Pope (1991), in most previous applications this problem has been circumvented through the use of the Coalescence/Dispersion (C/D) models. Examples of such models are the early C/D prototype of Curl (1963), the Linear Mean Square Estimation (LMSE) theory (O'Brien, 1980), the closure of Janicka *et al.* (1979), among others (Pope, 1982, 1985; Kosaly and Givi, 1987; Givi, 1989; Dutta and Tarbell, 1989). Despite their advantageous characteristics, the shortcomings associated with the C/D closures in the probabilistic description of scalar transport are well recognized. Namely, none of the aforementioned models predict an asymptotic Gaussian distribution for the PDF of a conserved scalar variable in homogeneous turbulence (Pope, 1982, 1991; Kosaly and Givi, 1987); and those which are capable of doing so (e.g., Pope, 1982), do not predict the initial stages of mixing correctly (Kosaly, 1986; Kosaly and Givi, 1987).

Recent development of the Amplitude Mapping Closure by Kraichnan and coworkers (Kraichnan, 1989; Chen *et al.*, 1989) (see also Pope, 1991) has provided a promising way of alleviating some of the problems associated with the C/D closures. This closure, in essence, provides a means of accounting for the transport of the PDF in composition space, and its validity and physical applicability have been evidenced in a number of comparisons against data generated by means of both direct numerical simulations (Pope, 1990, 1991; Gao, 1991a,b; Madnia *et al.*, 1991b; Jiang *et al.*, 1992) and laboratory experiments (Frankel *et al.*, 1992a). These results suggest that, at least in the setting of an isotropic turbulent flow, this closure has some superior features over all the previous C/D-type models.

Based on this demonstrated superiority, our objective here is to examine further the properties of this closure and to assess its capabilities for applications in modeling of unpremixed turbulent reacting flow systems. In particular, it is intended to provide a reasonably simple recipe that can be used in conjunction with this closure for predicting the limiting rate of mean reactant conversion. However, since this is the first study of this type, and due to mathematical complexities (that soon become apparent), we have made some simplifying assumptions which are indicated here. Firstly, we consider an idealized irreversible binary reaction of the type $F + rO \rightarrow (1 + r)$ *Product* with initially segregated reactants (F and O). In accordance with the discussions above, only the maximum rate of mean reactant conversion is considered. Secondly, the turbulence field is assumed statistically homogeneous. Thirdly, all the chemical species are assumed to have identical and constant thermodynamic properties. Finally, the flow field is assumed isothermal in which the dynamic role of the chemical reaction on the hydrodynamic field is ignored.

With all these assumptions, the reacting system considered is obviously an idealized prototype of conventional combustion systems. However, it does provide a good model for dilute reacting systems in typical mixing controlled plug flow reactors (Toor, 1962, 1975; Bilger, 1980; Hill, 1976; Brodkey, 1981). Moreover, because of the mathematical complexities, even in this simple case, it is deemed necessary to analyze this simplified system before considering more complex scenarios. Nevertheless, the model is capable of accounting for arbitrary values of the stoichiometric coefficients and for any equivalence ratio. This allows the capture of many interesting features, as will be demonstrated.

For the idealized case of initially segregated reactants, the initial marginal PDFs of their concentrations are composed of "delta functions." Therefore, it is speculated that the approach based on an *assumed* probability distribution may also provide a reasonably good closure. Therefore, in addition to the mapping closure, a member of the family of *Pearson* frequencies is also considered. The results obtained by this frequency are compared with those of the mapping closure, and are also assessed against data generated by means of DNS.

In the next section the problem under consideration is outlined along with the mathematical basis by which the single-point PDF methods are used. In Section 2.1 the salient features of the mapping

closure at the single-point level are analyzed including a discussion on the formalities of the closure for our purpose. With this closure, a closed form analytical expression is provided for the limiting bound of the mean reactant conversion. This limiting rate is also predicted by means of the beta density model in Section 2.2. In both these subsections the simplifications for the case of a stoichiometric mixture are made, motivating the use of our final "simple" analytical expressions in practical modeling of stoichiometric plug flow reactors. In Section 3.1 the results predicted by both models are compared against those generated by DNS of a three-dimensional homogeneous turbulent flow. In Section 3.2 some discussions are presented highlighting the implications of these results in turbulence modeling. This paper is drawn to a close in Section 4 with some discussions for possible future extension of the two models for the statistical description of more complicated chemically reacting turbulent flows.

2. Formulation

With the assumptions described in the introduction, the statistical behavior of the reacting field in the reaction $F + rO \rightarrow (1 + r)$ *Product* can be related to the statistics of an appropriate conserved Shvab–Zeldovich mixture fraction, $\mathcal{J}$ (Bilger, 1980). This mixture fraction can be normalized in such a way to yield values of unity in the fuel F stream and zero in the oxidizer O stream. For the purpose of statistical treatment, we define $\mathcal{P}_F(\xi, t)$, $\mathcal{P}_O(\xi, t)$, and $\mathcal{P}_\mathcal{J}(\xi, t)$, respectively, as the marginal PDFs of the concentration of F, the concentration of O, and the Shvab–Zeldovich variable $\mathcal{J}$. For initially segregated reactants with no fuel in the oxidizer stream (and vice versa), the initial conditions for the marginal PDFs of the concentrations of the two reactants are given by

$$\begin{aligned} \mathcal{P}_F(\xi, 0) &= W_F\delta(\xi - F_i) + W_O\delta(\xi), \\ \mathcal{P}_O(\xi, 0) &= W_O\delta(\xi - O_i) + W_F\delta(\xi), \qquad 0 \le \xi \le 1. \end{aligned} \tag{1}$$

Here, F_i and O_i denote the initial concentrations of the two species in the two feeds, and W_F and W_O represent the relative weights of the reactants at the initial time (i.e., the area ratios at the inlet of a plug flow reactor). With the normalized value of the concentrations equal to unity at the feeds, i.e., $F_i = O_i = 1$, the stoichiometric value of the Shvab–Zeldovich variable, $\mathcal{J}_{st}$, is determined from the parameter r. With the assumption of an infinitely fast chemistry, the marginal PDFs of the reactants' concentrations are related to the frequency of the Shvab–Zeldovich variable (Bilger, 1980; Kosaly and Givi, 1987):

$$\begin{aligned} \mathcal{P}_F(\xi, t) &= (1 - \mathcal{J}_{st})\mathcal{P}_\mathcal{J}(\mathcal{J}_{st} + \xi(1 - \mathcal{J}_{st}), t) + \vartheta_F(t)\delta(\xi), \\ \mathcal{P}_O(\xi, t) &= \mathcal{J}_{st}\mathcal{P}_\mathcal{J}(\mathcal{J}_{st}(1 - \xi), t) + \vartheta_O(t)\delta(\xi). \end{aligned} \tag{2}$$

Here, $\xi \ge 0$ and

$$\begin{aligned} \vartheta_F(t) &= \int_{-\infty}^{\mathcal{J}_{st}} \mathcal{P}_\mathcal{J}(\xi, t)\, d\xi, \\ \vartheta_O(t) &= \int_{\mathcal{J}_{st}}^{\infty} \mathcal{P}_\mathcal{J}(\xi, t)\, d\xi = 1 - \vartheta_F(t). \end{aligned} \tag{3}$$

The initial condition for the PDF of the Shvab–Zeldovich variable is given by

$$\mathcal{P}_\mathcal{J}(\xi, 0) = W_F\delta(\xi - 1) + W_O\delta(\xi). \tag{4}$$

Equation (4) implies that $\langle \mathcal{J} \rangle(t = 0) = W_F$. Since $\mathcal{J}$ is a conserved variable, its mean value remains constant, i.e., $\langle \mathcal{J} \rangle(t) = \langle \mathcal{J} \rangle(0) = W_F$. The integration of (2) yields the temporal variation of the statistics of the species field at all times, if the PDFs of $\mathcal{J}$ are known. As indicated above, in the setting of a mixing controlled reaction this PDF provides all the desired statistical properties of the reacting field.

2.1. Amplitude Mapping Closure

The implementation of the amplitude mapping closure involves a mapping of the random field of interest ξ to a stationary Gaussian reference field φ_0, via a transformation $\xi = \chi(\varphi_0, t)$. Once this

relation is established, the PDF of the random variable ξ, $\mathscr{P}(\xi)$, is related to that of a Gaussian distribution. In homogeneous turbulence, the transport equation for this function satisfies (Chen *et al.*, 1989; Pope, 1991)

$$\frac{\partial \chi}{\partial \tau} = -\varphi_0 \frac{\partial \chi}{\partial \varphi_0} + \frac{\partial^2 \chi}{\partial \varphi_0^2}. \tag{5}$$

In this equation, τ is a normalized time within which the scalar length scale information is embedded. The relations between this time and the physical time, i.e., $\tau(t)$, cannot be determined in the context of single-point PDF description and must be provided by external means (Pope, 1990; Jiang *et al.*, 1992). For the case considered here, with the initial PDF of the variable $\mathscr{J}$ given by (4), the corresponding form of the initial mapping is

$$\chi(\varphi_0, 0) = H(\varphi_0 - \varphi^*), \qquad -\infty \le \varphi_0 \le \infty, \tag{6}$$

where H is the Heaviside function and φ^* is a measure of the initial asymmetry of the initial PDF around the ensemble mean of the variable $\mathscr{J}$:

$$\varphi^* = \sqrt{2}\,\mathrm{erf}^{-1}(1 - 2\langle \mathscr{J} \rangle), \tag{7}$$

where "erf" denotes the error function. The mapping function is obtained by solving (5) subject to initial condition (6). The general solution of this equation has the form (Gao, 1991a)

$$\chi(\varphi_0, \tau) = \frac{\sqrt{\mathscr{G}^2 + 1}}{\sqrt{2\pi}\mathscr{G}} \int_{-\infty}^{\infty} \chi(y, 0) \exp\left[-\frac{(\varphi_0 e^{-\tau} - y)^2 (1 + \mathscr{G}^2)}{2\mathscr{G}^2} \right] dy, \tag{8}$$

where $\mathscr{G}(\tau) = \sqrt{\exp(2\tau) - 1}$. Inserting (6) for $\chi(\varphi_0, 0)$ in (8), we have

$$\chi(\varphi_0, \tau) = \tfrac{1}{2}[1 + \mathrm{erf}(a\varphi_0 + b)], \tag{9}$$

where

$$a(\tau) = \frac{1}{\sqrt{2}\mathscr{G}}, \qquad b(\tau) = \frac{-\varphi^* \sqrt{1 + \mathscr{G}^2}}{\sqrt{2}\mathscr{G}}. \tag{10}$$

Finally, the solution for the PDF of $\mathscr{J}$ is determined directly from the mapping relation between the physical field ξ and the Gaussian reference field φ_0:

$$\mathscr{P}_{\mathscr{J}}(\chi(\varphi_0, \tau), \tau) = \mathscr{P}_G(\varphi_0) \left(\frac{\partial \chi}{\partial \varphi_0} \right)^{-1}. \tag{11}$$

Here, $\mathscr{P}_G$ denotes the PDF of a standardized Gaussian distribution, i.e., $\mathscr{P}_G(\varphi_0) = (1/\sqrt{2\pi}) \exp(-\varphi_0^2/2)$. A combination of (11) and (9) yields the final result for the PDF of the Shvab–Zeldovich variable:

$$\mathscr{P}_{\mathscr{J}}(\chi(\varphi_0, \tau), \tau) = \mathscr{G} \exp\left[\frac{(\varphi_0 e^{-\tau} - \varphi^*)^2}{2(1 - e^{-2\tau})} - \frac{\varphi_0^2}{2} \right]. \tag{12}$$

With a combination of (12) and (2), all the pertinent single-point statistics of the reacting field are determined. The most important of these statistics are the ensemble mean values of the reactants' concentrations. These mean values are obtained directly by integrating their respective PDFs. The intermediate steps in deriving these relations are not presented but are provided by Frankel (1992). Here, only the essential steps are presented. For the mean fuel concentration, $\langle F \rangle$, the first part of (2) reads

$$\langle F \rangle(\tau) = \int_{\mathscr{J}_{st}}^{1} F(\xi) \mathscr{P}_{\mathscr{J}}(\xi, \tau)\, d\xi = \int_{\varphi_0(\chi = \mathscr{J}_{st})}^{\infty} F(\chi(\varphi_0, \tau), \tau) \mathscr{P}_G(\varphi_0)\, d\varphi_0, \tag{13}$$

where the lower limit of the last integral corresponds to the value of φ_0 at which χ is equal to the stoichiometric value of the Shvab–Zeldovich variable. Evaluating this limit from (9), equation (13) can be analytically integrated. This is possible by representing the error function in the form of its definition, and performing the resulting definite, double exponential integral. The results after extensive algebraic manipulations yield

$$\langle F \rangle(\tau) = \frac{(1 - 2\mathscr{J}_{st})}{4(1 - \mathscr{J}_{st})} \left[1 + \mathrm{erf}\left(\frac{b/a + c}{\sqrt{2}} \right) \right] + \frac{1}{\pi \sqrt{2} a (1 - \mathscr{J}_{st})} \exp\left(-\frac{b^2}{2a^2} - \frac{c^2}{2} - \frac{bc}{a} \right) \Theta_+. \tag{14}$$

Similar expressions can be obtained for the mean oxidizer concentration:

$$\langle O\rangle(\tau)=\frac{1}{2}\left(1-\frac{1}{2\mathscr{J}_{st}}\right)\left[1-\operatorname{erf}\left(\frac{b/a+c}{\sqrt{2}}\right)\right]-\frac{1}{\pi\sqrt{2}a\mathscr{J}_{st}}\exp\left(-\frac{b^2}{2a^2}-\frac{c^2}{2}-\frac{bc}{a}\right)\Theta_{-}. \tag{15}$$

In these equations, c is related to the stoichiometric coefficient,

$$c=\frac{-1}{a}\operatorname{erf}^{-1}(2\mathscr{J}_{st}-1), \tag{16}$$

and

$$\Theta_{\pm}=\int_0^1 dy\exp\left(-a^2c^2y^2+\frac{y_{\pm}^2}{8y_2}\right)\left[\frac{1}{2y_2}\mathscr{D}_{-2}\left(\frac{y_{\pm}}{\sqrt{2y_2}}\right)-\frac{ac}{\sqrt{2y_2}}\mathscr{D}_{-1}\left(\frac{y_{\pm}}{\sqrt{2y_2}}\right)\right],$$

$$y_2=y^2+\frac{1}{2a^2}, \tag{17}$$

$$y_{\pm}=\mp 2acy^2-\frac{b}{a^2}-\frac{c}{a}.$$

Here, $\mathscr{D}_{-2}$ and $\mathscr{D}_{-1}$ are, respectively, the parabolic cylinder functions of order -2 and -1, belonging to the family of degenerate hypergeometric functions (Abramowitz and Stegun, 1972).

Due to nice properties of the degenerate hypergeometric functions, many of the interesting features of (14) and (15) can be depicted. First, simple manipulation of this equation shows that for a stoichiometric mixture, $\langle\mathscr{J}\rangle=\mathscr{J}_{st}$, both reactants decay at the same rate, i.e.,

$$\frac{\langle F\rangle(t)}{\langle F\rangle(0)=W_F}=\frac{\langle O\rangle(t)}{\langle O\rangle(0)=W_O},$$

and for a nonstoichiometric initial condition, the limits of the concentration values as $\tau,\mathscr{G}\to\infty$, asymptote to

$$\lim_{\tau,\mathscr{G}\to\infty}\langle F\rangle(\tau)=\begin{cases}0, & \mathscr{J}_{st}\geq\langle\mathscr{J}\rangle,\\ \dfrac{\langle\mathscr{J}\rangle-\mathscr{J}_{st}}{1-\mathscr{J}_{st}}, & \mathscr{J}_{st}\leq\langle\mathscr{J}\rangle,\end{cases}$$

$$\lim_{\tau,\mathscr{G}\to\infty}\langle O\rangle(\tau)=\begin{cases}0, & \mathscr{J}_{st}\leq\langle\mathscr{J}\rangle,\\ 1-\dfrac{\langle\mathscr{J}\rangle}{\mathscr{J}_{st}}, & \mathscr{J}_{st}\geq\langle\mathscr{J}\rangle,\end{cases} \tag{18}$$

These limits are obtained by employing the Taylor series expansion of the relevant functions as $\mathscr{G}\to\infty$, and indicate the limiting bound of the concentrations of the unconsumed reactants in both fuel-rich and fuel-lean mixtures. While these limiting behaviors are rather trivial from a physical standpoint, in a computational procedure it must be made sure that they are satisfied. Because of the mathematical properties of the parabolic cylinder functions, these limiting cases can be realized in our computational procedure in a relatively easy manner. It would be very difficult to obtain these limiting behaviors numerically in an integration procedure within the original unbounded domain.

At first glance, (14) and (15) may appear somewhat complicated. However, due to nice mathematical properties of the parabolic cylinder functions (Abramowitz and Stegun, 1972), these equations can be integrated rather easily within the finite domain ($0\leq y\leq 1$). For fuel-lean or fuel-rich mixtures, the integration can only be done by means of employing numerical methods. However, for a stoichiometric mixture, the results simplify further as demonstrated below.

Stoichiometric Mixture. For practical applications in stoichiometric plug flow reactors, the equations simplify considerably. For a stoichiometric mixture, and an initially symmetric PDF around the mean value (i.e., $\langle\mathscr{J}\rangle=\mathscr{J}_{st}=\frac{1}{2}$), both parameters b and c are zero. Under this condition, the first terms on the right-hand sides of (14) and (15) drop. Knowing $\mathscr{D}_{-2}(0)=\mathscr{D}_{-1}(0)=1$, the remaining terms yield

$$\frac{\langle F\rangle(\tau)}{\langle F\rangle(0)}=\frac{\langle O\rangle(\tau)}{\langle O\rangle(0)}=\frac{1}{\pi\sqrt{2}a}\int_0^1\frac{dy}{2y^2+1/a^2}=1-\frac{2\arctan\mathscr{G}(\tau)}{\pi}. \tag{19}$$

The simplicity of this equation is noteworthy and very pleasing. Because of this simplicity, (19) is strongly recommended for engineering predictions of the mean reactant conversion rate in stoichiometric homogeneous flows, such as the plug flow reactors considered in numerous previous investigations (Toor, 1962, 1975; Brodkey, 1981; Hill, 1976; O'Brien, 1971; Kosaly and Givi, 1987).

2.2. The Beta Density Model

For initially segregated reactants, the initial PDF of the Shvab–Zeldovich variable is composed of two delta functions at the extreme limits of the variable. Therefore, it is proposed that the family of Pearson (1895) frequencies may provide a reasonable means of estimating this distribution at all times (Frankel *et al.*, 1991; Girimaji, 1991a). The appropriate form of the Pearson distribution is in this case the beta density of the first kind. This density has been employed in the statistical description of turbulent reacting flows by Rhodes (1975), Jones and Priddin (1978), Lockwood and Moneib (1980), Peters (1984), and Janicka and Peters (1982) amongst others (for recent reviews, see Givi, 1989; Priddin, 1991). For an initially nonsymmetric PDF, the beta density corresponds to Pearson Type I and for the symmetric case to Pearson Type II. The relevance of the latter in modeling of molecular mixing from an initial symmetric binary state has been described by Madnia *et al.* (1991a) and Girimaji (1991a). In both cases the PDF of the Shvab–Zeldovich variable is represented by (Abramowitz and Stegun, 1972)

$$\mathscr{P}_{\mathscr{J}}(\xi) = \frac{1}{B(\beta_1, \beta_2)} \xi^{\beta_1 - 1}(1 - \xi)^{\beta_2 - 1}, \qquad 0 \le \xi \le 1, \tag{20}$$

where $B(\beta_1, \beta_2)$ denotes the beta function, and the parameters β_1 and β_2 are dependent on the mean and the variance of the random variable $\mathscr{J}$. In applications to the mixing controlled reaction considered here, we assume that the PDF of the Shvab–Zeldovich variable always retains a beta distribution. Thus all the statistics of the reacting scalar are subsequently determined. The ensemble mean values are determined by a combination of (20) and (2). Following the same procedure as that described in the section on the mapping closure, after some manipulations the final results can be expressed as (Frankel, 1992)

$$\langle F \rangle(t) = \frac{\mathscr{J}_{st}^{\beta_1}(1 - \mathscr{J}_{st})^{\beta_2 - 1}}{(\beta_1 + \beta_2)B(\beta_1, \beta_2)} + \frac{1}{1 - \mathscr{J}_{st}}\left(\frac{\beta_1}{\beta_1 + \beta_2} - \mathscr{J}_{st}\right)(1 - \mathscr{I}_{\mathscr{J}_{st}}(\beta_1, \beta_2)), \tag{21}$$

$$\langle O \rangle(t) = \frac{\mathscr{J}_{st}^{\beta_1 - 1}(1 - \mathscr{J}_{st})^{\beta_2}}{(\beta_1 + \beta_2)B(\beta_1, \beta_2)} + \left(1 - \frac{\beta_1}{(\beta_1 + \beta_2)\mathscr{J}_{st}}\right)\mathscr{I}_{\mathscr{J}_{st}}(\beta_1, \beta_2), \tag{22}$$

where $\mathscr{I}$ denotes the incomplete beta function (Abramowitz and Stegun, 1972).

Due to nice mathematical properties of the beta function, the final results are cast in terms of its integral. In this case, however, the integral can be expressed in terms of the incomplete beta function. The mathematical properties of this special function are well known, and the expressions above are conveniently amenable to numerical integration (Frankel, 1992). Again, the physical limiting conditions discussed before are realized by (21) and (22). That is, in a stoichiometric mixture, both reactants decay at the same rate; and in lean or rich mixtures, the same limiting conditions as those in (18) are realized.

Stoichiometric Mixture. Again, in the case of an initially symmetric PDF under stoichiometric conditions, the final expressions become simpler. Under this condition, $\beta_1 = \beta_2$, and knowing $\mathscr{I}_{1/2}(x, x) = \frac{1}{2}$, (21) and (22) reduce to

$$\frac{\langle F \rangle(t)}{\langle F \rangle(0)} = \frac{\langle O \rangle(t)}{\langle O \rangle(0)} = \frac{1}{\sqrt{\pi}} \frac{\Gamma(g)}{\Gamma(g + \frac{1}{2})}, \tag{23}$$

where g is half the inverse of the normalized variance of the Shvab–Zeldovich variable, and Γ denotes the gamma function.

3. Results

The final forms of (14), (15), (19), (21), (22), and (23) are gratifying since they provide a relatively simple and effective means of estimating the maximum rate of mean reactant conversion in homogen-

eous reacting flows. As indicated before, the mathematical operations leading to these equations are somewhat involved, but the final results can be conveniently expressed in terms of known special functions. However, since both models are based on single-point PDF descriptions, these equations are not in a complete closed form and are dependent on the parameters g and/or $\mathcal{G}$. In this context this parameter cannot be determined by the model and must therefore be specified by external means (Pope, 1991; Jiang *et al.*, 1992; Frankel *et al.*, 1992a). This deficiency is not particular to the two models considered here, and exists in any single-point statistical description, including all of those based on the C/D models.

The extent of validity of these simple relations can be demonstrated by a comparison between the model predictions and the data obtained by means of DNS. The comparison is made here for several values of $\langle \mathcal{J} \rangle$ and $\mathcal{J}_{st}$ for the purpose of demonstration. In this comparison the magnitudes of the normalized variance of the Shvab–Zeldovich variable are matched with those of DNS. This implies that, for given values of $\langle \mathcal{J} \rangle$ and $\mathcal{J}_{st}$, the parameters g, $\mathcal{G}$, β_1, and β_2 are provided externally from the DNS data. With this provision, the model prediction results can be directly assessed against DNS data.

The DNS procedure is similar to that of previous simulations of this type. For a detailed description we refer the reader to Madnia and Givi (1992). The subject of the present DNS is a three-dimensional periodic homogeneous box flow under the influence of a binary reaction of the type described above. The initial species field is composed of out-of-phase square waves for the two reactants F and O. The computational package is based on the modification of a spectral-collocation procedure using Fourier basis functions developed by Erlebacher *et al.* (1990a) (see also Erlebacher *et al.*, 1987, 1990b). The hydrodynamic field is assumed isotropic, and is initialized in a similar manner to that of Erlebacher *et al.* (1990a) and Passot and Pouquet (1987). The turbulent field is of a decaying nature in that there is no artificial forcing mechanism to feed energy to low wave numbers. The code is capable of simulating flows with different levels of compressibility (Hussaini *et al.*, 1990). Here, only the results obtained for a low compressible case are discussed, since most previous analyses of plug flow reactors have dealt primarily with incompressible flows (Toor, 1975; Hill, 1976; Brodkey, 1981; Leonard and Hill, 1988a,b, 1991). The resolution consists of 96 collocation points in each direction. Therefore, at each time step 96^3 is the sample size for statistical analyses. With this resolution, simulations with a Reynolds number (based on the Taylor microscale) of $Re_\lambda \approx 41$ are attainable. The value of the molecular Schmidt number is set equal to unity.

3.1. Validations

The statistical behavior of the scalar field is depicted by examining the evolution of the PDFs of the Shvab–Zeldovich variable $\mathcal{J}$. These are shown in Figures 1 and 2 at times close to the initial ($t1$) and

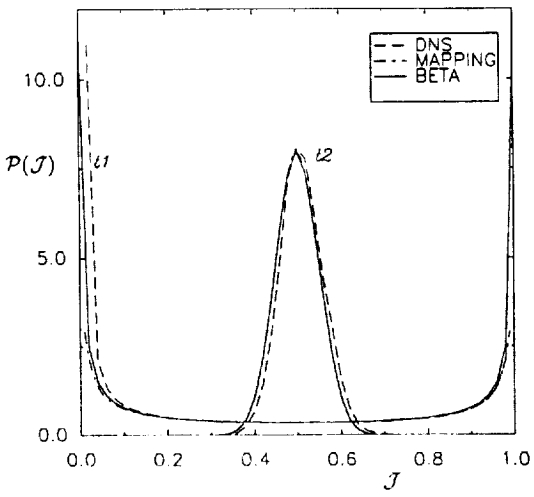

Figure 1. PDF of the Shvab–Zeldovich variable at two times ($t2 > t1$) for the symmetric case ($\langle \mathcal{J} \rangle = \frac{1}{2}$).

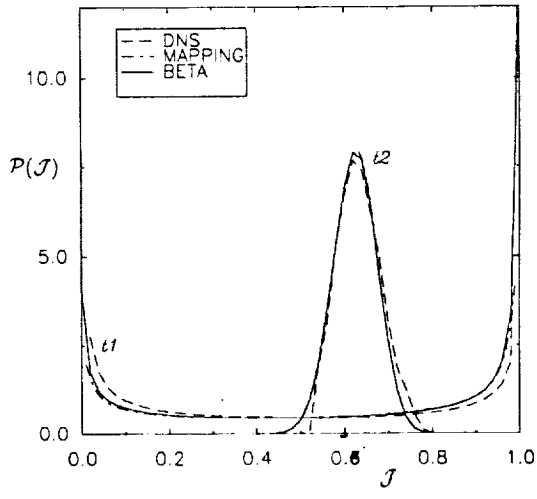

Figure 2. PDF of the Shvab–Zeldovich variable at two times ($t2 > t1$) for the nonsymmetric case ($\langle \mathcal{J} \rangle = 0.625$).

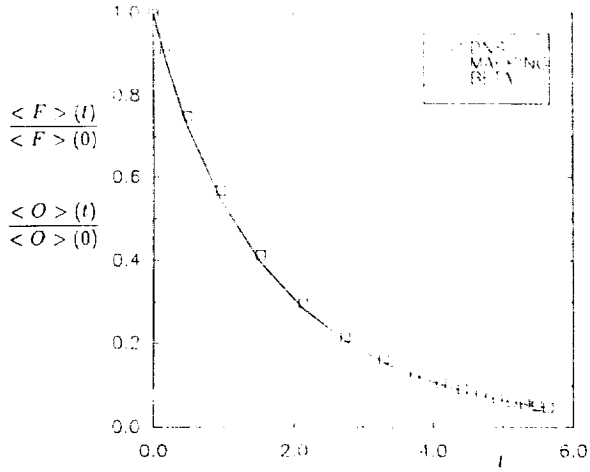

Figure 3. Normalized mean concentration of fuel and the oxidizer for the symmetric case, and $\mathcal{J}_{st} = 0.5$.

the final ($t2$) states. These figures correspond, respectively, to the cases of an initially symmetric ($\langle \mathcal{J} \rangle = \frac{1}{2}$) and nonsymmetric ($\langle \mathcal{J} \rangle = 0.625$) PDFs. At the initial time, the PDF is approximately composed of two delta functions at $\mathcal{J} = 0, 1$ indicative of the two initially segregated reactants, F and O. At later times, the PDF evolves through an inverse-like diffusion in composition space. The heights of the delta functions decrease, and the PDF is redistributed at other $\mathcal{J}$ values in the range [0, 1], and subsequently becomes centralized around the mean value. Proceeding further in time results in a sharper peak at this mean value, and in both cases the PDF can be approximated by a Gaussian distribution near the mean scalar value. The trend for the symmetric case is the same as that presented in earlier DNS studies (Eswaran and Pope, 1988; Givi and McMurtry, 1988). For the nonsymmetric case there are no DNS data in the literature, but the present results verify that the asymptotic PDF can still be approximated by a Gaussian distribution near its mean value.

The PDFs obtained by the mapping closure and those by an assumed beta density are also presented in Figures 1 and 2. In these figures the model PDFs are parametrized with the same first two moments obtained from DNS. In this parametrization only the normalized magnitude of the variance of the models are forced equal to that of the DNS and no attempt was made to account for the departure from the "exact" initial double delta distribution in DNS. With this matching, nevertheless, the results clearly indicate that the model predictions compare very well with the DNS results. Also, both models yield an asymptotic Gaussian-like PDF.

The temporal variation of the ensemble mean of the reactants' concentration by the two models are compared against those of DNS in Figures 3 and 4. These figures correspond to the two cases of

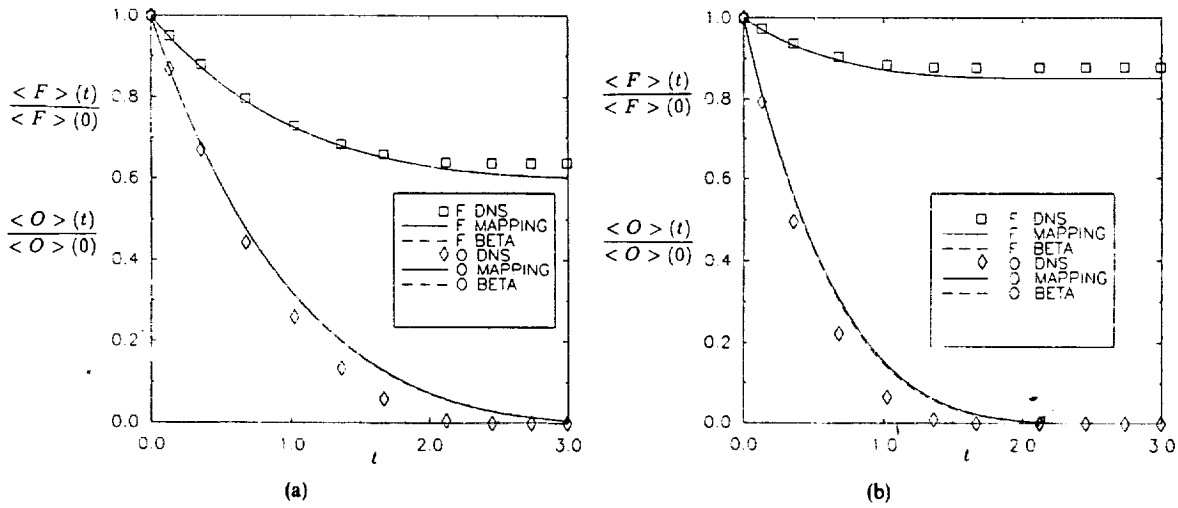

Figure 4. Normalized mean concentration of fuel and the oxidizer for the nonsymmetric case. (a) $\mathcal{J}_{st} = 0.4$, (b) $\mathcal{J}_{st} = 0.2$.

symmetric and nonsymmetric initial PDFs, respectively. In the symmetric case, under stoichiometric conditions, the results are simply obtained from the analytical expressions in (19) and (23). In the nonsymmetric case, numerical integration of (14) and (15) and evaluation of the incomplete beta function in (21) and (22) are necessary. In both cases the agreement of the models with the DNS data is noteworthy. Also, a comparison between parts (a) and (b) of Figure 4 shows that as the magnitude of $\mathcal{J}_{st}$ decreases, the rate of consumption of the oxidizer increases.

The agreements noted above follow from the compatibility of the model PDFs and those of DNS, at least for the case of binary mixing considered here. This finding is not new and has been well documented in previous works, at least those considering an initially symmetric PDF (Pope, 1990, 1991; Madnia and Givi, 1992; Madnia *et al.*, 1991a; Girimaji, 1991a). However, a nice feature of the models is the explicit form of the final equations expressing these statistical quantities. Supported by this quantitative agreement, it is proposed that, in the absence of a better alternative, the relations obtained above be used as an explicit simple means for predicting the maximum rate of mean reactant conversion in homogeneous reacting systems.

Despite the simplicity of these equations and their ease of application, it must be mentioned that these equations predict the rate of mean decay of the reactants' concentration far better than all the previous turbulence closures based on the C/D models (see Givi, 1989). This is particularly advantageous in that this evaluation can be made by a simple algebraic relation, whereas the C/D implementations usually require more expensive numerical simulations (Kosaly and Givi, 1987; McMurtry and Givi, 1989). Even for nonunity equivalence ratios, the numerical integration required by the two models above is considerably less computationally demanding than those of the C/D models. The only input in these models, similar to those in C/D closures, is the variance of the Shvab–Zeldovich variable. This is provided here by means of DNS. In an actual implementation, this variance can be obtained from experimental data or by means of an appropriate turbulence model (Frankel *et al.*, 1992a). The provision of such data is not very difficult since they can be obtained in the setting of a nonreacting flow.

3.2. Applications

The relations obtained here can be used in determining the extent of validity of other conventional closures for predicting the limiting rate of mean reactant conversion in turbulent flows. As an example, here we consider the model based on the famous hypothesis of Toor (1962, 1975), which has received considerable attention in practical modeling of unpremixed homogeneous reacting systems (Bilger, 1980; Brodkey, 1981; Leonard and Hill, 1987, 1988a, b; Kosaly and Givi, 1987; Kosaly, 1987; Givi and McMurtry, 1988; McMurtry and Givi, 1989; Givi, 1989). According to this hypothesis, in an isothermal homogeneous reacting turbulent flow, the decay of the unmixedness, denoted by $\Psi = \langle F'O' \rangle(t)/\langle F'O' \rangle(0)$, where the prime quantities indicate fluctuation from the ensemble mean value, is independent of the magnitude of the Damköhler number. This implies that the normalized unmixedness parameter, defined by

$$\mathcal{Y} = \frac{\Psi(t)|_{Da}}{\Psi(t)|_{Da=0}}, \tag{24}$$

is the same under both reacting and nonreacting conditions, i.e., $\mathcal{Y}(t) = \text{constant} = 1$ for all values of Da. In previous DNS assessments of this hypothesis, it has been shown that for the case of initially segregated reactants this model cannot be employed, and the normalized unmixedness ratio depends on the nature of mixing and the magnitude of the Damköher number (Givi and McMurtry, 1988; McMurtry and Givi, 1989). In particular, it has been demonstrated that even for $Da \to \infty$, while the normalized unmixedness is equal to unity at the initial time, its limiting lower bound depends on the asymptotic frequency of the Shvab–Zeldovich variable. That is, $\mathcal{Y}(t = 0) = 1 > \mathcal{Y}(t) > \mathcal{Y}(t \to \infty) = C$, where C is the lower limiting bound. For an asymptotic Gaussian distribution, it can be easily shown that, for a mixture under stoichiometric conditions, the lower bound limits asymptotes to the constant value $C = 2/\pi$ (Kosaly, 1987; Givi and McMurtry, 1988).

This deviation from unity can be realized by the two models considered. With the mapping closure, under symmetric stoichiometric conditions, from (2), (14), and (15), following the same integration

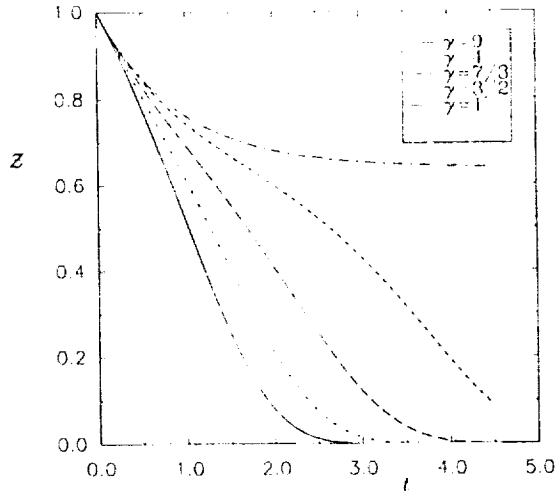

Figure 5. The unmixedness ratio at several values of the equivalence ratio.

procedure as before, it is shown that

$$\mathscr{Y}_{\mathrm{m}} = \frac{\langle F'O' \rangle (Da \to \infty)}{\langle F'O' \rangle (Da = 0)} = \frac{2(\arctan(1/\mathscr{G}))^2}{\pi \arctan(1/\mathscr{G}\sqrt{\mathscr{G}^2 + 2})}. \tag{25}$$

For the beta density model, the corresponding form of the unmixedness ratio for $\beta_1 = \beta_2$ is given by

$$\mathscr{Y}_{\beta} = \frac{2g}{\pi}\left(\frac{\Gamma(g)}{\Gamma(g + \frac{1}{2})}\right)^2. \tag{26}$$

In (25) and (26), the subscripts m and β are added to denote the mapping and the beta density model. It is easy to show that these equations satisfy the correct limiting conditions for a stoichiometric mixture. This is for both the initial time, i.e., the inlet of the reactor,

$$\lim_{[\mathscr{G} \to 0]} \mathscr{Y}_{\mathrm{m}} = \lim_{[g \to 1/2]} \mathscr{Y}_{\beta} = 1, \tag{27}$$

and at large distances from it:

$$\lim_{[\mathscr{G} \to \infty]} \mathscr{Y}_{\mathrm{m}} = \lim_{[g \to \infty]} \mathscr{Y}_{\beta} = C = \frac{2}{\pi}. \tag{28}$$

The latter limiting condition cannot be realized in any of the previously used C/D models, or by means of Toor's models (McMurtry and Givi, 1989; Givi, 1989).

The results based on the applications of Toor's model become less accurate for nonstoichiometric mixtures. For equivalence ratios other than unity, with the depletion of one of the reactants, the unmixedness parameter approaches zero faster. This is demonstrated by the solution of the mapping closure shown in Figure 5 for several values of the equivalence ratio (γ). Note that as the magnitude of this ratio increases above one, the unmixedness ratio goes to zero more rapidly. For an unity equivalence ratio, the correct asymptotic value of $2/\pi$ is realized.

4. Extensions for Modeling of More Complex Reacting Turbulent Flows

Despite the pleasing features of our simple mathematical expressions, there are several restricting assumptions which were necessarily imposed in deriving these equations. Here, we would like to address the ramifications associated with these assumptions, and to provide the means of overcoming them in future extensions of these models.

Firstly, due to the assumption of infinitely fast chemistry, only the *maximum rate* of the mean reactant conversion is obtained. While this rate is very useful in describing unpremixed flames, from both a theoretical standpoint and for practical applications (Givi, 1989; McMurtry and Givi, 1989; Kosaly and Givi, 1987; Toor, 1962, 1975; O'Brien, 1971; Bilger, 1980; Williams, 1985; Dutta and

Tarbell, 1989), the model is not capable of describing some of the important features of the turbulent flames, especially those associated with nonequilibrium effects. The extensions to finite rate chemistry, reversible reactions, nonequilibrium flames, and multistep kinetics systems require numerical integration of the PDF transport equation. For these cases the problem cannot be mathematically reduced to that of keeping track of a single scalar variable (like $\mathcal{J}$), and requires the use of *multivariate* statistical descriptions. For this, the implementation of mapping closure is relatively straightforward since it provides a transport equation for the joint PDFs of the scalar variable in a multivariable sense (Pope, 1991; Gao and O'Brien, 1991). However, it is not presently clear how to devise an efficient computational procedure, typically based on Monte Carlo methods (Pope, 1981), for the numerical treatment of these equations. Some work in this regard is currently under way (Valiño and Gao, 1991; Valiño *et al.*, 1991).

The extension of assumed distributions based on the beta density for treating multiscalars is more straightforward but less trivial to justify. The most obvious means is to implement the multivariate form of the Pearson distributions. The direct analogue of the beta density is the *Dirichlet* frequency (Johnson, 1987; Johnson and Kotz, 1972; Wilks, 1962; Narumi, 1923). For a mixture composed of $N+1$ species, the joint PDF of N concentrations $(\psi_1, \psi_2, \ldots, \psi_N)$ is described in terms of an N-variate density of the form

$$\mathcal{P}(\psi_1, \psi_2, \ldots, \psi_N) = \frac{\Gamma(\beta_1 + \beta_2 + \cdots + \beta_{N+1})}{\Gamma(\beta_1)\Gamma(\beta_2), \ldots, \Gamma(\beta_{N+1})} \psi_1^{\beta_1 - 1} \psi_2^{\beta_2 - 1} \cdots \psi_N^{\beta_N - 1} (1 - \psi_1 - \psi_2 - \cdots - \psi_N)^{\beta_{N+1} - 1} \tag{29}$$

subject to the physical constraint

$$\sum_{i=1}^{N+1} \psi_i = 1. \tag{30}$$

The application of this density in modeling of multispecies reactions has been nicely discussed by Girimaji (1991a). Due to the mathematical properties of the gamma function, this density is pleasing from a mathematical viewpoint and most statistical cross correlations of the random variables $(\psi_1, \psi_2, \ldots)$ can be conveniently obtained by means of simple analytical relations (Frankel, 1992). Some points in this regard have been made by Girimaji (1991b). However, the use of the Dirichlet frequency cannot be justified for modeling of unpremixed reacting flow in a general sense (Frankel, 1992). In fact, there is no way of implementing this density directly for modeling of nonequilibrium flames, involving strong temperature variations. This is simply due to the additivity constraints of this density requiring the unity sum of the normalized random variables (30).

Secondly, the mathematical derivations presented here are only valid for initially segregated reactants. In both models the complete segregation facilitates significant simplifications of the final equations. This assumption is compatible with that made in the majority of previous works on unpremixed reacting flows (Toor, 1975; Brodkey, 1981; Bilger, 1980). For other initial conditions, e.g., partial premixing of the reactants, or non-delta-like distributions, numerical integration of the PDF transport equation is required. Again, an appropriately devised numerical procedure can accommodate such conditions. However, the use of a beta density (or any other assumed distributions) cannot be justified for other complex initial conditions.

Thirdly, the final mathematical expressions are only valid in the setting of a homogeneous flow. Extension to inhomogeneous flow predictions is also straightforward, but requires numerical integration of the modeled equations. Both models can be directly implemented into appropriately devised numerical procedures. The mapping closure can be invoked in the *mixing* step of a fractional stepping procedure, similar to that of typical Monte Carlo procedures (Pope, 1981). The beta density requires modeled transport equations for the low-order statistics of the reacting field. These equations include the required information pertaining to the spatial inhomogeneity of the flow through the parameters $\beta_1, \beta_2, \ldots$. With this information, all the higher-order statistics of the reacting field can be provided by simple analytical means (Girimaji, 1991b; Frankel *et al.*, 1992b).

Finally, in the context of the single-point PDF formulation presented, there is no information pertaining to the evolution of the relevant turbulent length scales. The final expressions can only be presented in terms of other physical parameters (here, through the variance of the Shvab–Zeldovich variable). In the context considered, this parameter has been provided by the DNS data. In a practical

application, this must be provided by external means (turbulence models, experimental data, etc.). Jiang *et al.* (1992) and Frankel *et al.* (1992a) provide further discussions related to this issue.

5. Concluding Remarks

It is demonstrated that the mapping closure of Kraichnan (Chen *et al.*, 1989; Pope, 1991) yields closed-form analytical expressions for predicting the limiting bound of the mean reactant conversion rate in simple chemistry of the type $F + rO \rightarrow (1 + r)$ *Product* in homogeneous, isothermal turbulent flows. It is also shown that, for the case of complete initial segregation, the scalar PDFs generated by this closure can be well approximated by a beta density. This density also provides closed-form analytical expressions for the limiting rate of mean reactant conversion. A nice feature of the mathematical results generated by the two models is their capability of revealing the influence of the stoichiometric coefficient and the equivalence ratio. In both cases the mathematical expressions simplify significantly for a stoichiometric mixture. The prediction results via both models compare favorably with data generated by DNS. This agreement follows from the compatibility of the models' PDFs with those of DNS. The simple final results generated here are superior to those of previous closures based on typical C/D models, and those based on Toor's hypothesis.

These closed-form relations are furnished with the imposition of several restrictive assumptions. The ramifications associated with these assumptions are discussed, and some suggestions for future extensions are provided. Despite these assumptions, it is very encouraging to have physically plausible algebraic relations for the direct estimate of the mean reactant conversion rate in homogeneous turbulent flows, typical of those in plug flow reactors.

Acknowledgments

The original version of the DNS computer code was provided by Dr. Gordon Erlebacher (ICASE, NASA LaRC). The authors are grateful to Dr. Erlebacher for his invaluable assistance in modifying this code. The authors are also indebeted to Dr. J. Philip Drummond (NASA LaRC) and to Mr. Richard S. Miller (SUNY—Buffalo) for their suggestions and many helpful discussions in regard to this work.

References

Abramowitz, M., and Stegun, I.A. (1972). *Handbook of Mathematical Functions and Formulas, Graphs, and Mathematical Tables.* Government Printing Office, Washington, DC.

Bilger, R.W. (1980). Turbulent flows with nonpremixed reactants. In Libby, P.A., and Williams, F.A., editors, *Turbulent Reacting Flows*, pp. 65–113. Springer-Verlag, Heidelberg.

Brodkey, R.S. (1981). Fundamentals of turbulent motion. *Chem. Engrg. Comm.* **8**, 1–23.

Chen, H., Chen, S., and Kraichnan, R.H. (1989). Probability distribution of a stochastically advected scalar field. *Phys. Rev. Lett.* **63**, 2657–2660.

Curl, R.L. (1963). Dispersed phase mixing: I. Theory and effects in simple reactors. *AIChE J.* **9**, 175–181.

Dutta, A., and Tarbell, J.M. (1989). Closure models for turbulent reacting flows. *AIChE J.* **35**, 2013–2027.

Erlebacher, G., Hussaini, M.Y., Speziale, C.G., and Zang, T.A. (1987). Toward the large eddy simulation of compressible turbulent flows. ICASE Report 87-20, NASA Langley Research Center, Hampton, VA. Also available as NASA CR 178273.

Erlebacher, G., Hussaini, M.Y., Speziale, C.G., and Zang, T.A. (1990a). On the large-eddy simulation of compressible isotropic turbulence. In *Proc. 12th Internat. Conf. on Numerical Methods in Fluid Dynamics.*

Erlebacher, G., Hussaini, M.Y., Kreiss, H.O., and Sarkar, S. (1990b). The analysis and simulation of compressible turbulence. *Theoret. Comput. Fluid Dynamics* **2**, 73–95.

Eswaran, V., and Pope, S.B. (1988). Direct numerical simulations of the turbulent mixing of a passive scalar. *Phys. Fluids* **31**, 506–520.

Frankel, S.H. (1992). Ph.D. Thesis, Department of Mechanical and Aerospace Engineering, State University of New York at Buffalo, Buffalo, NY, in preparation.

Frankel, S.H., Madnia, C.K., and Givi, P. (1991). On the modeling of the unmixedness in homogeneous reacting turbulence. *Chem. Engrg. Comm.* **104**, 117–125.

Frankel, S.H., Jiang, T.J., and Givi, P. (1992a). Modeling of isotropic reacting turbulence by a hybrid mapping-EDQNM closure. *AIChE J.* **38**, 535–543.

Frankel, S.H., Madnia, C.K., and Givi, P. (1992b). Modeling of the reactant conversion rate in a turbulent shear flow. *Chem. Engrg. Comm.* **113**, 197–209.

Gao, F. (1991a). An analytical solution for the scalar probability density function in homogeneous turbulence. *Phys. Fluids A* **3**, 511–513.

Gao, F. (1991b). Mapping closure and non-Gaussianity of the scalar probability density functions in isotropic turbulence. *Phys. Fluids A* **3**, 2438–2444.

Gao, F., and O'Brien, E.E. (1991). A mapping closure for multispecies Fickian diffusion. *Phys. Fluids A* **3**, 956–959.

Girimaji, S.S. (1991a). Assumed β-pdf model for turbulent mixing: validation and extension to multiple scalar mixing. *Combust. Sci. Technol.* **78**, 177–196.

Girimaji, S.S. (1991b). A simple recipe for modeling reaction-rates in flows with turbulent-combustion. AIAA paper AIAA-91-1792.

Givi, P. (1989). Model free simulations of turbulent reactive flows. *Progr. Energy Combust. Sci.* **15**, 1–107.

Givi, P., and McMurtry, P.A. (1988). Non-premixed reaction in homogeneous turbulence: direct numerical simulations. *AIChE J.* **34**, 1039–1042.

Hawthorne, W.R., Wedell, D.S., and Hottel, H.C. (1949). Mixing and combustion in turbulent gas jets. In *Proc. 3rd Symp. on Combustion, Flames and Explosion Phenomena*, pp. 266–288. The Combustion Institute, Pittsburgh, PA.

Hill, J.C. (1976). Homogeneous turbulent mixing with chemical reaction. *Ann. Rev. Fluid Mech.* **8**, 135–161.

Hussaini, M.Y., Speziale, C.G., and Zang, T.A. (1990). The potential and limitations of direct and large eddy simulations. In Lumley, J.L., editor, *Whither Turbulence? Turbulence at the Crossroads*, pp. 354–368. Lecture Notes in Physics, vol. 357. Springer-Verlag, Berlin.

Janicka, J., and Peters, N. (1982). Prediction of turbulent jet diffusion flame lift-off using a pdf transport equation. In *Proc. 19th Internat. Symp. on Combustion*, pp. 367–374. The Combustion Institute, Pittsburgh, PA.

Janicka, J., Kolbe, W., and Kollmann, W. (1979). Closure of the transport equation for the probability density function of turbulent scalar field. *J. Nonequil. Thermodyn.* **4**, 47–66.

Jiang, T.-L., Givi, P., and Gao, F. (1992). Binary and trinary scalar mixing by Fickian diffusion-some mapping closure results. *Phys. Fluids A* **4**, 1028–1035.

Johnson, M.E. (1987). *Multivariate Statistical Simulation.* Wiley, New York.

Johnson, N.L., and Kotz, S. (1972). *Distributions in Statistics: Continuous Multivariate Distributions.* Wiley, New York.

Jones, W.P., and Priddin, C.H. (1978). Predictions of the flowfield and local gas composition in gas turbine combustors. In *Proc. 17th Internat. Symp. on Combustion*, pp. 399–409. The Combustion Institute, Pittsburgh, PA.

Kollmann, W. (1990). The pdf approach to turbulent flow. *Theoret. Comput. Fluid Dynamics* **1**, 249–285.

Kosaly, G. (1986). Theoretical remarks on a phenomenological model of turbulent mixing. *Combust. Sci. Technol.* **49**, 227–234.

Kosaly, G. (1987). Non-premixed simple reaction in homogeneous turbulence. *AIChE J.* **33**, 1998–2002.

Kosaly, G., and Givi, P. (1987). Modeling of turbulent molecular mixing. *Combust. Flame* **70**, 101–118.

Kraichnan, R.H. (1989). Closures for probability distributions. *Bull. Amer. Phys. Soc.* **34**, 2298.

Leonard, A.D., and Hill, J.C. (1987). A simple chemical reaction in numerically simulated homogeneous turbulence. AIAA paper AIAA-87-0134.

Leonard, A.D., and Hill, J.C. (1988a). Direct numerical simulation of a homogeneous turbulent reacting flow. AIAA paper AIAA-88-3624.

Leonard, A.D., and Hill, J.C. (1988b). Direct numerical simulation of turbulent flows with chemical reaction. *J. Sci. Comput.* **3**, 25–43.

Leonard, A.D., and Hill, J.C. (1991). Scalar dissipation and mixing in turbulent reacting flows. *Phys. Fluids A.* **3**, 1286–1299.

Libby, P.A., and Williams, F.A., editors (1980). *Turbulent Reacting Flows.* Topics in Applied Physics, vol. 44. Springer-Verlag, Heidelberg.

Lockwood, F.C., and Moneib, H.A. (1980). Fluctuating temperature measurement in a heated round free jet. *Combust. Sci. Technol.* **22**, 63–81.

Madnia, C.K., and Givi, P. (1992). On DNS and LES of homogeneous reacting turbulence. In Galperin, B., and Orszag, S.A., editors, *Large Eddy Simulations of Complex Engineering and Geophysical Flows.* Cambridge University Press, Cambridge, in press.

Madnia, C.K., Frankel, S.H., and Givi, P. (1991a). Direct numerical simulations of the unmixedness in homogeneous reacting turbulence. *Chem. Engrg. Comm.* **109**, 19–29.

Madnia, C.K., Frankel, S.H., and Givi, P. (1991b). Mathematical modeling of the reactant conversion rate by single-point pdf methods. In *Proc. Fall Technical Meeting of the Combustion Institute, Eastern Section*, Ithaca, NY.

McMurtry, P.A., and Givi, P. (1989). Direct numerical simulations of mixing and reaction in a nonpremixed homogeneous turbulent flow. *Combust. Flame* **77**, 171–185.

Narumi, S. (1923). On the general form of bivariate frequency distributions which are mathematically possible when regression and variation are subjected to limiting conditions, I. *Biometrika* **15**, 77–88.

O'Brien, E.E. (1971). Turbulent mixing of two rapidly reacting chemical species. *Phys. Fluids* **14**, 1326.

O'Brien, E.E. (1980). The probability density function (PDF) approach to reacting turbulent flows. In Libby, P.A., and Williams, F.A., editors, *Turbulent Reacting Flows*, pp. 185–218. Springer-Verlag, Heidelberg.

Passot, T., and Pouquet, A. (1987). Numerical simulation of compressible homogeneous flows in the turbulent regime. *J. Fluid Mech.* **181**, 441–466.

Pearson, K. (1895). Contributions to the mathematical theory of evolution: II. Skew variations in homogeneous material. *Philos. Trans. Roy. Soc. London Ser. A* **186**, 343–414.

Peters, N. (1984). Laminar diffusion flamelet models in non-premixed turbulent combustion. *Progr. Energy Combust. Sci.* **10**, 319–339.

Pope, S.B. (1976). The probability approach to modelling of turbulent reacting flows. *Combust. Flame* **27**, 299–312.

Pope, S.B. (1981). A Monte Carlo method for the pdf equations of turbulent reactive flow. *Combust. Sci. Techol.* **25**, 159–174.

Pope, S.B. (1982). An improved turbulent mixing model. *Combust. Sci. Technol.* **28**, 131–145.

Pope, S.B. (1985). PDF methods for turbulent reacting flows. *Progr. Energy Combust. Sci.* **11**, 119–192.

Pope, S.B. (1990). Computations of turbulent combustion: progress and challenges. In *Proc. 23rd Internat. Symp. on Combustion*, pp. 591–612. The Combustion Institute, Pittsburgh, PA.

Pope, S.B. (1991). Mapping closures for turbulent mixing and reaction. *Theoret. Comput. Fluid Dynamics* **2**, 255–270.

Priddin, C.H. (1991). Turbulent combustion modelling—a review. In Johansson, A.V., and Alfredsson, P.H., editors, *Advances in Turbulence 3*, pp. 279–299. Springer-Verlag, Berlin.

Rhodes, P.R. (1975). A probability distribution function for turbulent flows. In Murthy, S.N.B., editor, *Turbulent Mixing in Non-Reactive and Reactive Mixing*, pp. 235–241. Plenum, New York.

Toor, H.L. (1962). Mass transfer in dilute turbulent and nonturbulent systems with rapid irreversible reactions and equal diffusivities. *AIChE J.* **8**, 70–78.

Toor, H.L. (1975). The non-premixed reaction: $A + B \rightarrow Products$. In Brodkey, R.S., editor, *Turbulence in Mixing Operations*, pp. 123–166. Academic Press, New York.

Valiño, L., and Gao, F. (1991). Monte Carlo implementation of the mapping closure for turbulent reacting flows. In *Fluid Dynamics Division Meeting of the American Physical Society*, Phoenix, AZ.

Valiño, L., Ros, J., and Dopazo, C. (1991). Monte Carlo implementation and analytic solution of an inert-scalar turbulent-mixing test problem using a mapping closure. *Phys. Fluids A* **3**, 2191–2198.

Wilks, S.S. (1962). *Mathematical Statistics*, 2nd edn. Wiley, New York.

Williams, F.A. (1985). *Combustion Theory*, 2nd edn. Benjamin/Cummings, Menlo Part, CA.

Appendix V

Chem. Eng. Comm. 1992, Vol. 113, pp. 197–209
Reprints available directly from the publisher.
Photocopying permitted by license only.

Printed in the United States of America

MODELING OF THE REACTANT CONVERSION RATE IN A TURBULENT SHEAR FLOW

S.H. FRANKEL, C.K. MADNIA, and P. GIVI

Department of Mechanical and Aerospace Engineering
State University of New York
Buffalo, NY 14260
U.S.A.

(Received August 6, 1991; in final form December 12, 1991)

Results are presented of direct numerical simulations (DNS) of a spatially developing shear flow under the influence of an infinitely fast chemical reactions of the type $A + B \rightarrow Products$. The simulation results are used to construct the compositional structure of the scalar field in a statistical manner. The results of this statistical analysis indicate that the use of a Beta density for the probability density function (PDF) of an appropriate Shvab–Zeldovich mixture fraction provides a very good estimate of the limiting bounds of the reactant conversion rate within the shear layer. This provides a strong justification for the implementation of this density in practical modeling of non-homogeneous turbulent reacting flows. However, the validity of the model cannot be generalized for predictions of higher order statistical quantities. A closed form analytical expression is presented for predicting the maximum rate of reactant conversion in non-homogeneous reacting turbulence.

KEYWORDS Direct numerical simulations Turbulent shear flows Beta density Probability density function Unmixedness.

INTRODUCTION

In our previous work (Madnia *et al.*, 1991a) we have demonstrated that the Beta density provides a very good means of approximating the probability distribution of a conserved scalar quantity in homogeneous turbulent flows. The versatility of this density enables it to predict the evolution of a conserved scalar variable in a statistically homogeneous field, in a manner that is in accord with both DNS and experimental measurements. Despite this positive feature, some questions pertaining to the generality of this density for more realistic flow configurations remained unanswered.

In this work, we intend to address some of these remaining questions. Specifically, we shall make a comparative assessment of the behavior of this model, and provide an estimate of the degree of its validity in the context of more general conditions than previously considered. For this purpose, we have selected a configuration of particular interest in the design of diffusion controlled reactors; namely, a spatially developing parallel mixing layer under the influence of harmonic perturbations. The flow field which develops in this setting is dominated by large scale coherent structures and exhibits non-homogeneous features. This

inhomogeneity plays a dominant role in the mechanism of mixing in turbulent flows and is very suitable for promoting mixing and chemical reactions. Because of this property, this configuration has been widely utilized in numerous investigations on turbulent reacting flow phenomena (see Givi and Riley (1992) for a recent review).

We shall follow an analogous approach to that of our previous work (Madnia *et al.*, 1991a) in assessing the model's behavior. However, there are fundamental differences between the works in formulating the problem and in implementing the numerical procedure involved in the DNS. The configuration considered here is non-homogeneous. Therefore, both the procedure of statistical sampling and the numerical algorithm used in the DNS are different from the homogeneous simulations of Madnia *et al.* Also, the mathematical operations leading to the estimate of the reactant conversion rate are substantially more elaborate. However, analytical solutions can be attained with the aid of the mathematical properties of the Beta Function and the Incomplete Beta Function. With these, the generated results can be directly compared with those of DNS.

DESCRIPTION

The problem under consideration is that of a spatially evolving mixing layer containing initially segregated reacting species A and B in the two free streams. Species A is introduced into the upper, high-speed stream and species B enters on the lower, low-speed side. The chemical reaction between the two species is assumed to be single step, irreversible and infinitely fast. The magnitude of the Mach number is assumed negligible. Therefore, the flow is considered incompressible. The two species are assumed thermodynamically similar with identical diffusion coefficients. Within the framework of these approximations, the flow is mathematically described by the conservation equations of mass, momentum, and a species conservation equation for the trace of a conserved Shvab–Zeldovich variable $\mathcal{J}$, which characterizes the compositional structure of the flow. These equations are parameterized by the Reynolds number, the Peclet number, and the velocity ratio across the layer.

The computational package employed in the DNS is based on a hybrid pseudospectral-spectral element algorithm developed by Givi and Jou (1988) and McMurtry and Givi (1991). The pseudospectral routine, which is based on Fourier collocation, is used in the cross stream direction together with free slip boundary conditions. The spectral-element discretization is employed in the streamwise direction. This involves the decomposition of the domain in this direction into an ensemble of macro finite elements. Within each of these elements, the dependent flow variables are approximated spectrally by means of Tchebysheff polynomials of the first kind. The hybrid procedure employed in this way is very attractive in that it combines the accuracy of spectral discretization with the versatility of finite element methods. Therefore, it is convenient for accurate simulations of the complex spatially developing flow under consideration

here. For a detailed description of this hybrid method for DNS of turbulent shear flows, the reader is referred to McMurtry and Givi (1991).

The flow field is initialized at the inflow by a hyperbolic tangent mean velocity distribution, upon which low amplitude perturbations are superimposed in order to promote the formation of coherent vortices. The initialization of the Shvab–Zeldovich variable at the inflow is such that it takes on the values of zero and one in the streams containing B and A, respectively. The disturbances on the mean flow correspond to the most unstable mode of the hyperbolic tangent profile (Michalke, 1965) and its first two subharmonics. The amplitude of the fluctuating velocity is set equal to 6% of the mean velocity. This amplitude corresponds to that measured in typical shear layer experiments. The magnitudes of the phase shifts between the modes of the instability waves are randomly selected from a random seed with a top hat PDF of zero mean and a specified variance. The implementation of these phase shifts is the only mechanism to introduce randomness into an otherwise deterministic simulation. This is to partially mimic the random "commotions" which are present in the "universe," into an isolated two-dimensional simulation. At the outflow, a weak condition of zero second derivative is applied for all the dependent variables. This boundary condition cannot be justified in a rigorous mathematical sense and can be specified only in an *ad hoc* manner. This was done in order to facilitate implementation of the Dirichlet boundary conditions in the finite element procedure employed here. Moreover, the results of extensive numerical tests showed that the effects of the approximate boundary conditions are confined within the last computational element. This is consistent with that found previously by Korczak and Hu (1987). Therefore, the solution in the last computational domain can be ignored.

With the solution of the unsteady transport equations, the DNS data are extremely useful in visualizing the instantaneous behavior of the flow. The results of these direct simulations can also provide an assessment of the statistical behavior of the flow. This is due to the availability of flow information at all the computational grid points and at all times. Therefore, statistical sampling can be done quite easily by ensemble averaging of the instantaneous data gathered over many realizations.

In our simulations the instantaneous data of the Shvab–Zeldovich variable, obtained from the DNS, are used for statistical analysis. A total of 3200 realizations were employed in the sampling. With this ensemble, the magnitudes of the mean and the variance of the Shvab–Zeldovich variable are calculated at all the grid points. These statistical quantities are of primary interest for turbulence modeling. Based on the knowledge of these first two moments, a Beta density is assumed for the PDF of the Shvab–Zeldovich variable. The ensemble mean values of the product concentration and the unmixedness are calculated subsequently via this density. These modeled quantities are then compared with those obtained directly from the DNS data. At the majority of grid points the Beta density is asymmetric. Nevertheless, analytical solutions for the statistics of the reacting field are possible and have recently been obtained by Madnia *et al.* (1991b). The derivations of the equations are rather involved. Here, we only

present the final results for the normalized mean product concentration $\langle C_p \rangle$ and that of the unmixedness Ψ^2:

$$\langle C_p \rangle = \langle C_p \rangle(x, y) = 1 - \theta_1 - \theta_2 \tag{1}$$

$$\Psi^2 = \Psi^2(x, y) = -\theta_1 \theta_2 \tag{2}$$

where:

$$\theta_1 = \frac{1}{2^{\alpha+\beta-1}(\alpha+\beta)} \frac{\Gamma(\alpha+\beta)}{\Gamma(\alpha)\Gamma(\beta)} + \frac{\alpha-\beta}{\alpha+\beta}(1 - I_{\mathcal{J}_{st}}(\alpha, \beta)) \tag{3}$$

$$\theta_2 = \frac{1}{2^{\alpha+\beta-1}(\alpha+\beta)} \frac{\Gamma(\alpha+\beta)}{\Gamma(\alpha)\Gamma(\beta)} + \frac{\beta-\alpha}{\alpha+\beta} I_{\mathcal{J}_{st}}(\alpha, \beta) \tag{4}$$

Here, Γ is the Gamma function, and α and β are related to the first two moments of the random field (Frankel *et al.*, 1991). $I_{\mathcal{J}_{st}}(\alpha, \beta)$ is the Incomplete Beta Function, and $\mathcal{J}_{st}$ denotes the stoichiometric value of the Shvab–Zeldovich variable, $\mathcal{J}$. For unity normalized concentrations at the free streams, $\mathcal{J}_{st} = 0.5$. The results predicted by these equations shall be compared with those generated by DNS for a quantitative assessment of the closure.

PRESENTATATION OF RESULTS

Computations were performed in a domain of size $13\delta \times 34\delta$, where δ denotes the vorticity thickness at the inlet of the flow. There are 65 Fourier modes in the cross-stream direction and 42 finite elements are used for the streamwise discretization. A fifth order Tchebysheff polynomial is employed to approximate the variables within each element. This discretization is equivalent to, at least, a fifth order accurate finite difference technique even if the spectral convergence is not considered. This results in a total number of 211 points in the streamwise direction. A second-order Adams-Bashforth finite difference scheme was utilized for temporal discretization. With the computationally affordable 211×65 grid resolution available, accurate simulations with $Re = Pe = 200$ (where these normalized quantities are defined based on the velocity difference across the layer, and the initial vorticity thickness) are possible (Givi, 1989). These values are somewhat smaller than those of a fully developed laboratory turbulent shear layer, but are sufficiently high to promote the growth of instability waves.

In order to visualize the flow evolution, a time series of DNS generated snapshots of the instantaneously normalized product concentration are shown in Figure 1. This figure depicts the way in which the small amplitude perturbations manifest themselves in the formation of large scale coherent vortices downstream of the splitter plate. The forcing associated with the most unstable mode alone would cause the initial roll-up of these vortices. The perturbations corresponding to the first subharmonic mode result in a second roll-up in the form of merging neighboring vortices, and the presence of the second subharmonic generates a

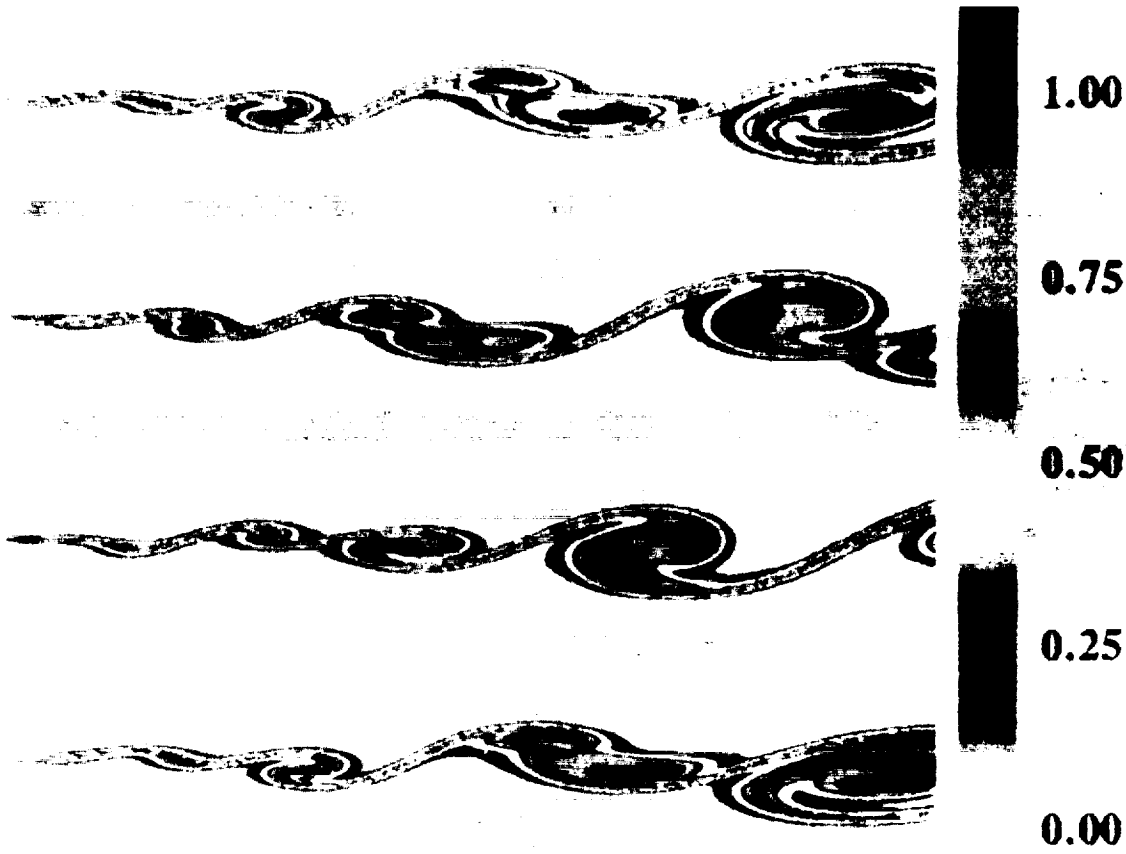

FIGURE 1 Time sequence of contour plots of instantaneous product concentration. (See color Plate I.)

third roll-up (second merging) at a region near the outflow. The roll-up and the subsequent pairings of these vortical structures engulf the unreacted species from the two streams into the mixing zone. The dynamics of the vortical evolution in this process reflect the two main mechanisms of mixing enhancement. Large concentrations of vorticity, that are approximately of one sign, bring the fluid from the two free streams into the large scale structures. Within these structures, the fluid elements are subject to further straining, and diffusion between the two fluids results in final mixing at the molecular scale. With these processes, along with the assumption of infinitely fast chemistry, the rate of product formation is naturally enhanced by the dynamics of vortical evolution.

The ensemble average of the product concentration, formed as a result of the mechanisms just described, is presented in Figure 2(a). The statistical averaging process was performed over a time span approximately equal to the residence time of the flow within the domain of computational consideration. This analysis was performed after the effects of the initial transients were washed away at the outflow. A comparison between Figures 1 and 2(a) reveals the essential deficiencies of the ensemble averaged results. Note that, all the detailed intricacies of the dynamics of flow evolution are masked by the averaging. While these ensemble-averaged results are of main interest for practical applications,

FIGURE 2 Contour plots of mean product concentration generated by (a) DNS, (b) the model. (See color Plate II.)

they are not capable of describing many of the interesting features of turbulence transport. The results depicted in Figure 2(a) are the best that one can expect to generate from a turbulence closure in a statistical sense.

To demonstrate the capability of the model based on the Beta density, in Figure 2(b), the average product concentration obtained by means of Eqs. (1)–(4) is presented. A comparison of this figure with Figure 2(a) reveals a remarkable similarity between the two results. For a more quantitative comparison, the cross stream variation of this product concentration and those of the negative of the unmixedness are presented at two streamwise locations in Figures 3–4. Also the streamwise variation of the total product, T_p, is presented in Figure 5. In all these figures, the comparisons between the model predictions and the DNS results are noteworthy.

The agreements demonstrated by the comparisons noted above provide a reasonable justification for recommending Eqs. (1)–(4) as working relations in routine engineering predictions. However, these relations are advocated only for statistical predictions of low order moments. The physics of the mixing phenomenon in a spatially developing shear flow is far too complex to be *completely* described by the Beta density. The highly intermittent nature of the mixing process exhibits features that cannot be fully captured by this density (Givi, 1989). To demonstrate this point quantitatively, in Figures 6–7 the cross stream variations of the third and fourth centralized moments of the Shvab Zeldovich variable calculated from the Beta density are compared with those generated by

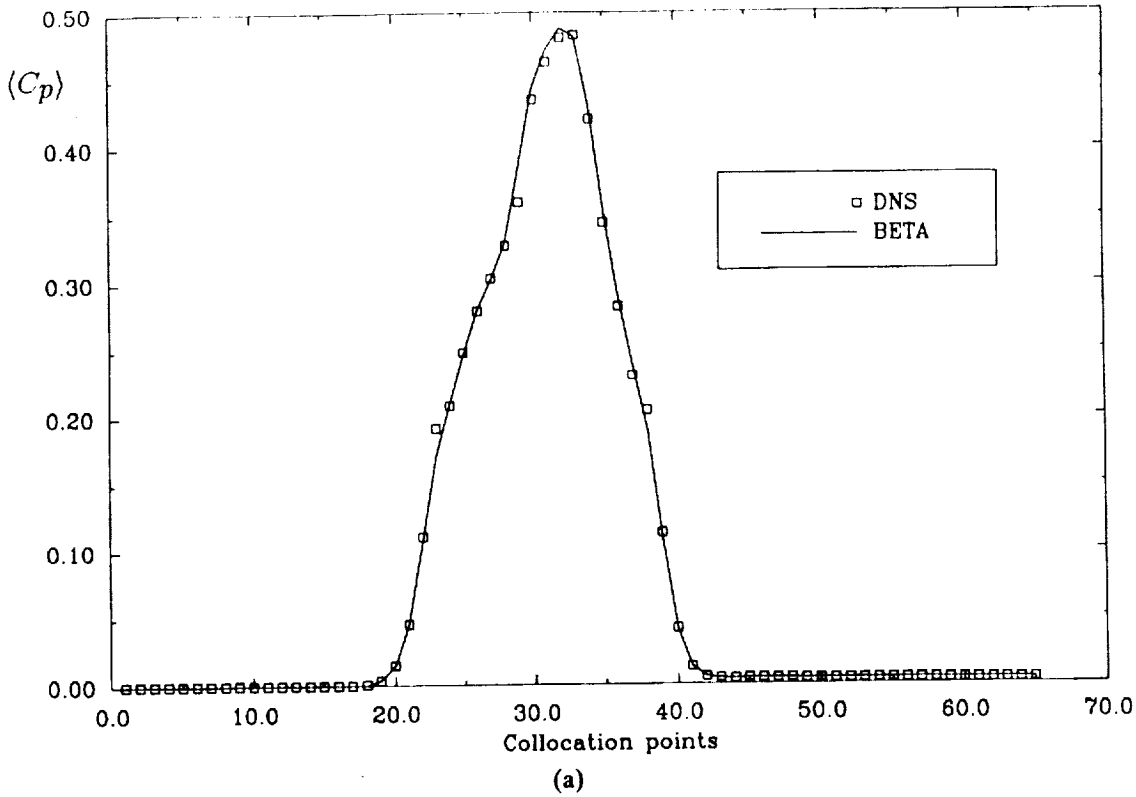

(a)

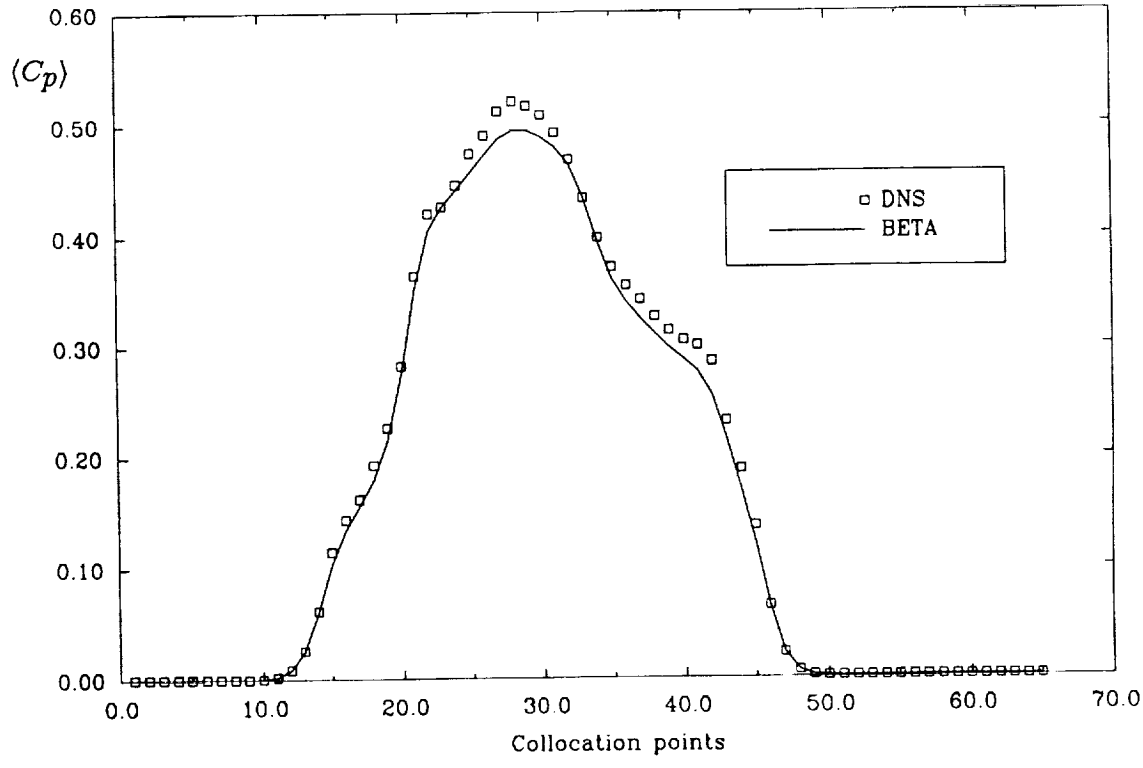

(b)

FIGURE 3 Cross stream variation of mean product concentration ($\langle C_p \rangle$) from the DNS and the model; (a) $x/\delta = 11$, (b) $x/\delta = 22$.

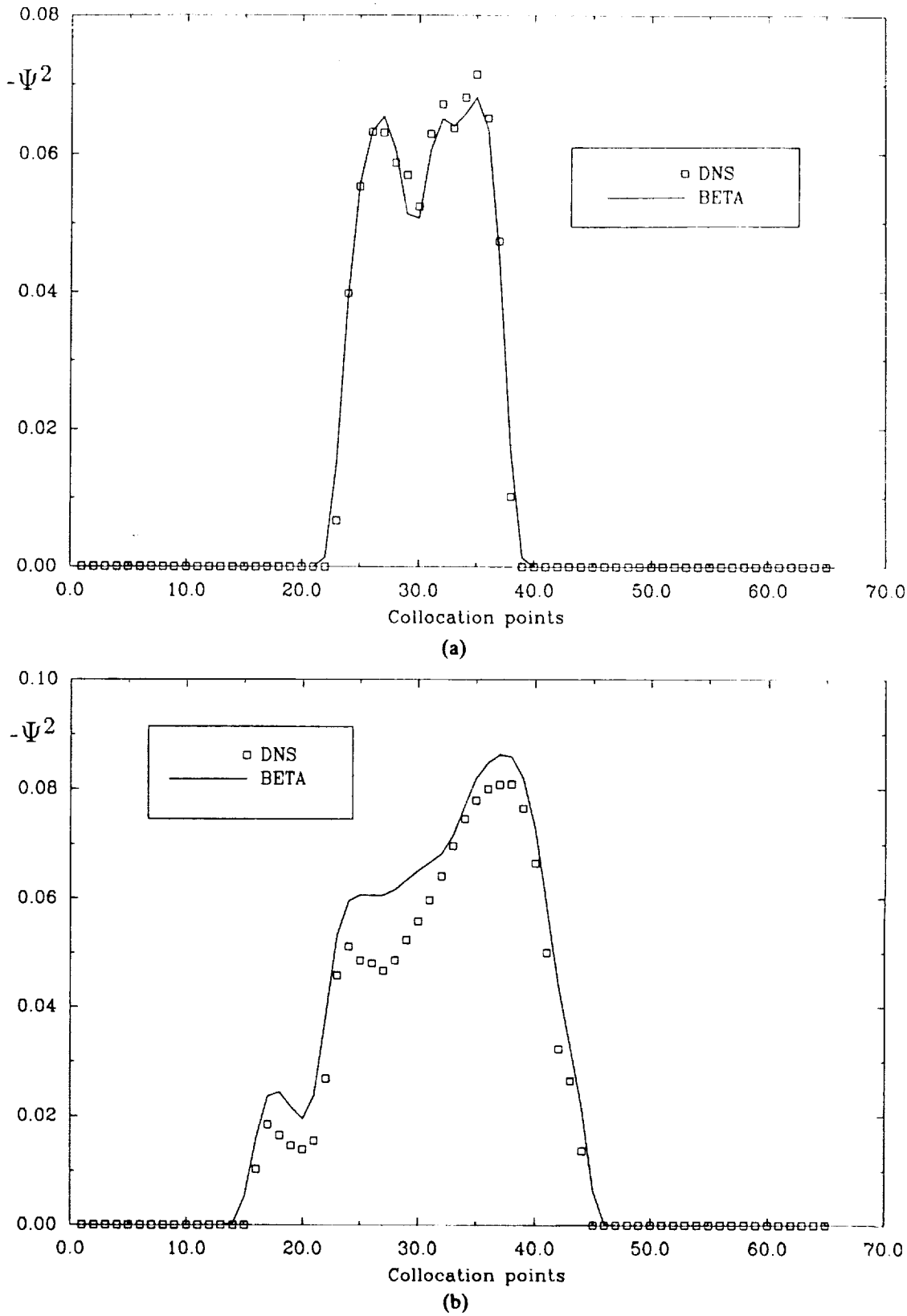

FIGURE 4 Cross stream variation of the negative of the unmixedness ($-\Psi^2$) from the DNS and the model; (a) $x/\delta = 11$, (b) $x/\delta = 22$.

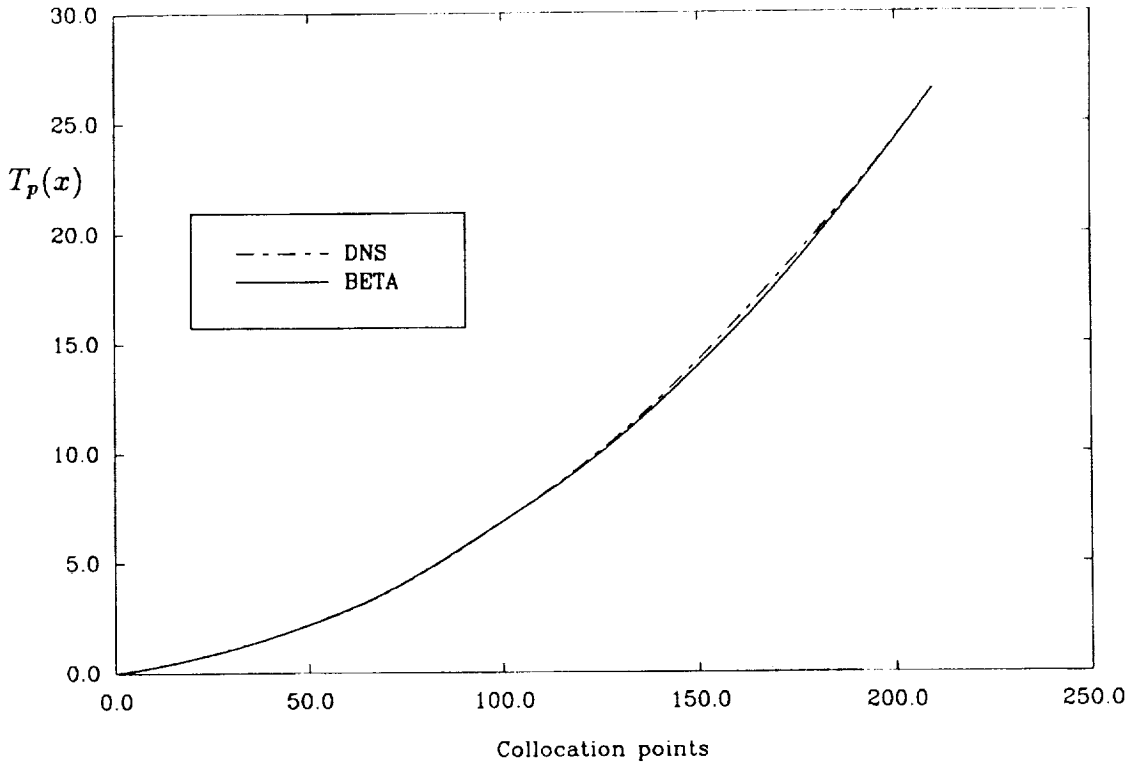

FIGURE 5 Streamwise variation of total product (T_p) from the DNS and the model.

DNS. These figures indicate that while the trend is somewhat similar in the two cases, the extent of agreement is not as good as those of lower level statistical quantities (Figures 2–5). This is primarily due to the mechanism of large scale entrainment in the shear flow, in that there are always unmixed fluids present within the core of the vortical structures. This results in a slight trimodal behavior in the probability distributions generated by DNS (Givi and Jou, 1988; Lowery and Reynolds, 1990) and observed experimentally (Koochesfahani, 1984, Dimotakis, 1989). This trimodal behavior cannot be captured by the Beta density which is at best suitable for producing bimodal distributions.

Recall that the specification of the Beta density is based on the knowledge of the first two moments of the conserved scalar. Here, these moments were supplied via DNS, but in an actual engineering application they must be provided by other means (*i.e.* an appropriate turbulence closure, or experimental data). However, specification of these parameters is substantially simpler than those of the reacting scalars, even with the assumption of an infinitely fast reaction. This is simply due to the fact that such data can be obtained in simpler, non-reacting flow experiments without any physical complications associated with the chemistry. With such data available, then Eqs. (1)–(4) are deemed very suitable, at least in the absence of better alternatives, for a reasonably accurate and inexpensive prediction of the limiting bounds of the reactant conversion rate. These equations are therefore recommended for this purpose in either homogeneous or non-homogeneous flows.

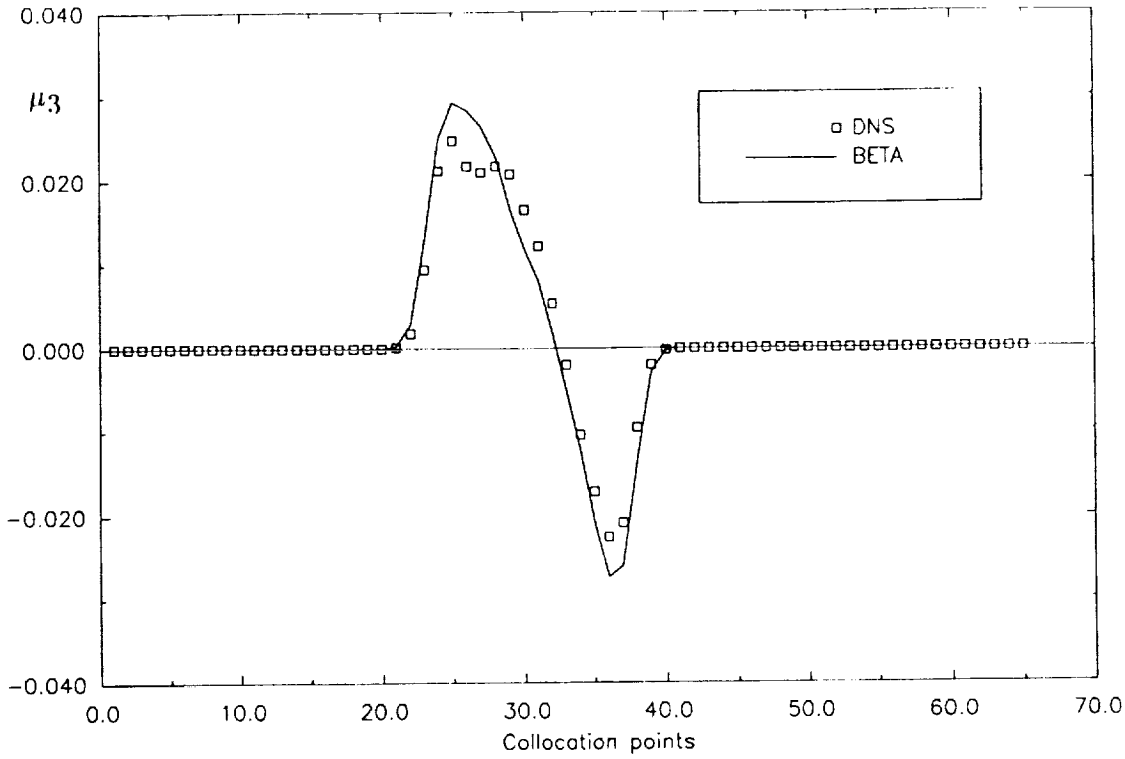

(a)

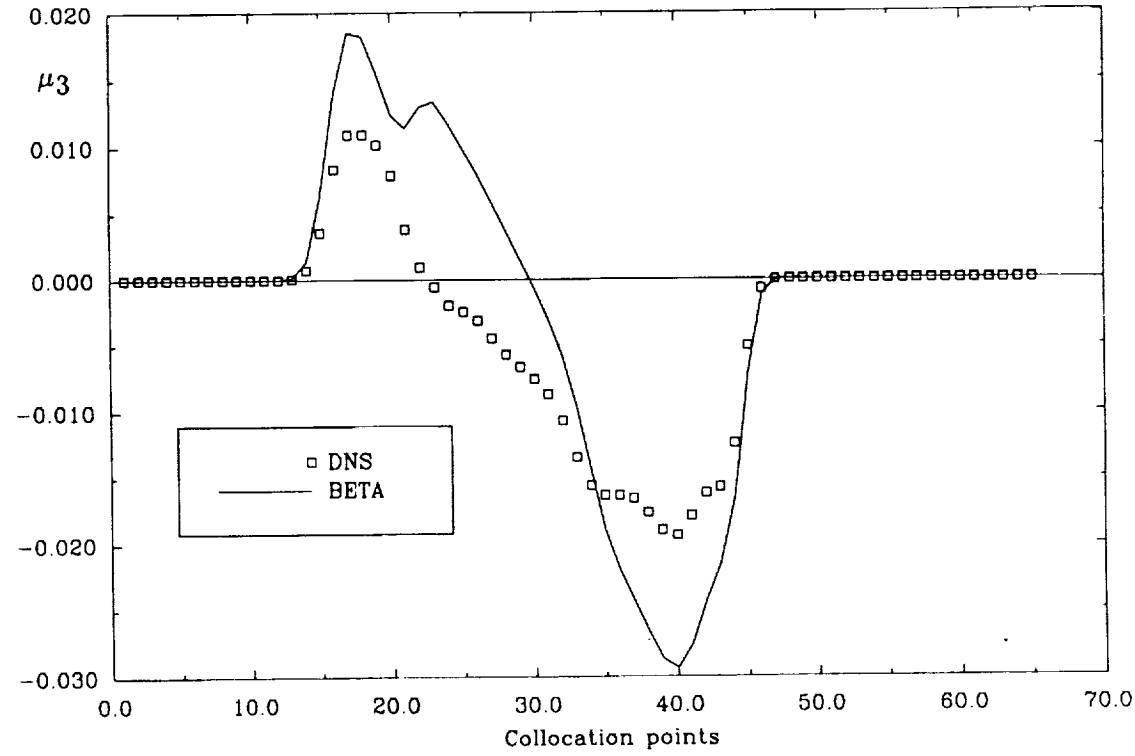

(b)

FIGURE 6 Cross stream variations of the third moment (μ_3) of the Shvab–Zeldovich variable from the DNS and the model; (a) $x/\delta = 11$, (b) $x/\delta = 22$.

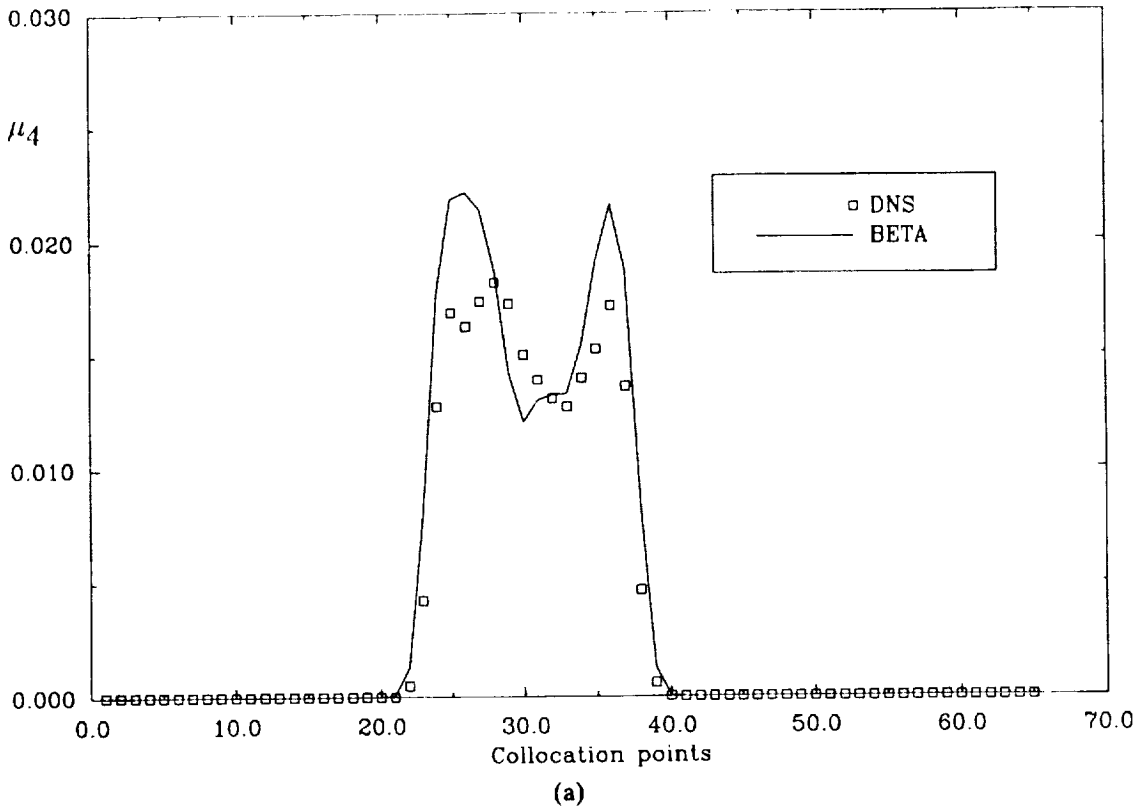

(a)

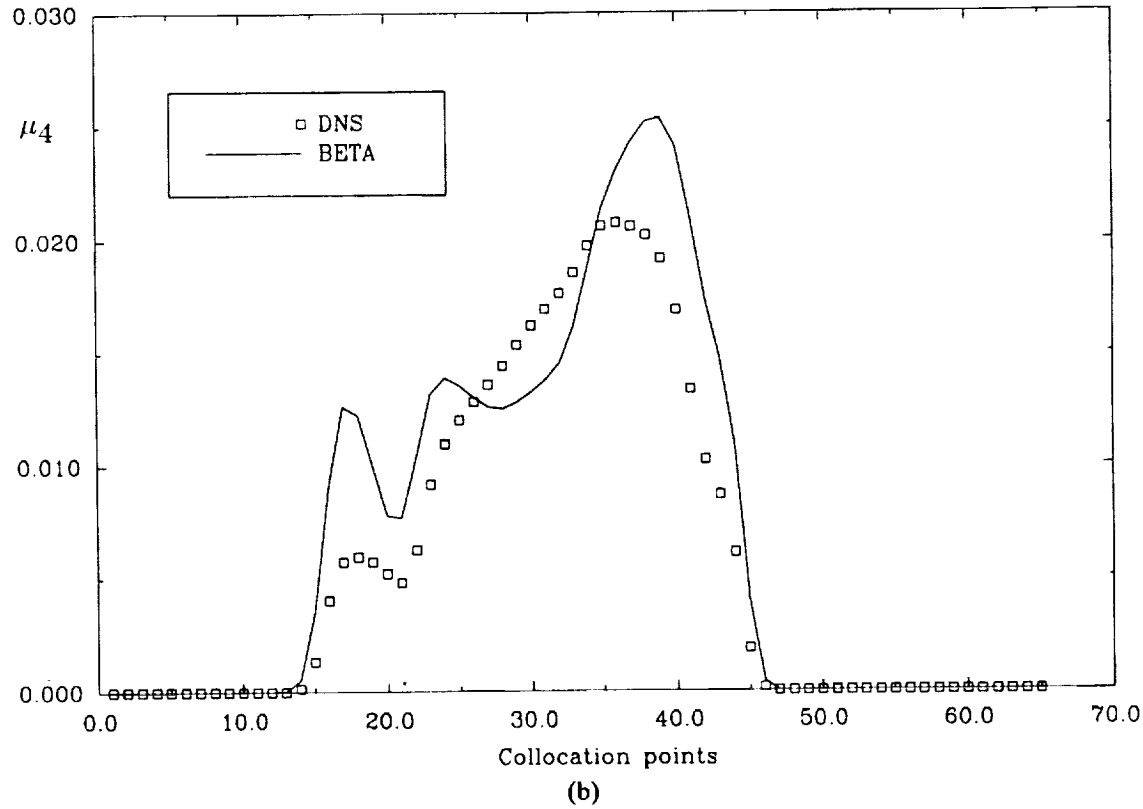

(b)

FIGURE 7 Cross stream variations of fourth moment (μ_4) of the Shvab–Zeldovich variable from the DNS and the model; (a) $x/\delta = 11$, (b) $x/\delta = 22$.

ACKNOWLEDGEMENTS

This work is supported by the National Science Foundation under Grant CTS-9012832 and by NASA Langley Research Center under Grant NAG-1-1122. Computational support is provided by NCSA at the University of Illinois and by NASA Langley Research Center.

NOMENCLATURE

A, B	Reactants.
C_p	Product Concentration.
$\mathcal{J}$	Shvab–Zeldovich variable.
Pe	The Peclet number.
Re	The Reynolds number.
$T_p(x)$	Total product = $\int_{-\infty}^{+\infty} dy \int_0^x dx \langle C_p \rangle (x, y)$.
x, y	The physical coordinates.
δ	Vorticity thickness at the inflow.
Ψ^2	The unmixedness.
μ_3	Third order moments of the Shvab–Zeldovich variable.
μ_4	Fourth order moments of the Shvab–Zeldovich variable.
$\langle\,\rangle$	Ensemble average.

REFERENCES

Dimotakis, P.E., Turbulent Free Shear Layer Mixing and Combustion, 9th ISABE, Athens, Greece, Sept. 3–9, (1989).

Frankel, S.H., Madnia, C.K., and Givi, P., Modeling of the Unmixedness in Homogeneous Reacting Turbulence, *Chem. Eng. Comm.*, **104,** 117, (1991).

Givi, P., and Jou, W.-H., Mixing and Chemical Reaction in a Spatially Developing Mixing Layer, *J. Nonequil. Thermodyn.*, **13**(4), 355, (1988).

Givi, P., and Jou, W.-H., Direct Numerical Simulations of a Two-Dimensional Reacting, Spatially Developing Mixing Layer by a Spectral Element Method, *Proceeedings of 22nd Symposium (Int.) on Combustion,* The Combustion Institute, Pittsburgh, PA, p. 635 (1989).

Givi, P., Model Free Simulations of Turbulent Reactive Flows, *Prog. Energy Comb. Science,* **15,** No. 1, 1 (1989).

Givi, P., and Riley, J.J., Current Issues in the Analysis of Reacting Shear Layers: Computational Challenges, chapter in *Major Research Topics in Combustion,* Editors: M.Y. Hussaini, A. Kumar and R.E. Voigt, Springer-Verlag, New York, p. 588 (1992).

Koochesfahani, M.M., Experiments on Turbulent Mixing and Chemical Reactions in a Liquid Mixing Layer, Ph.D. Thesis, California Institute of Technology, Pasadena, CA (1984).

Korczak, K.Z., and Hu, D., Turbulent Mixing Layers—Direct Spectral Element Simulation, AIAA Paper 87-0133 AIAA 25th Aerospace Sciences Meeting, Jan. 12–15 (1987).

Lowery, P.S., and Reynolds, W.C., Numerical Simulation of a Spatially Developing, Forced Plane Mixing Layer, Report No. TF-26, Department of Mechanical Engineering, Stanford University, Stanford, CA (1986).

Madnia, C.K., Frankel, S.H., and Givi, P., Direct Numerical Simulations of the Unmixedness in a Homogeneous Reacting Turbulent Flow, *Chem. Eng. Comm.*, **109,** 19 (1991a).

Madnia, C.K., Frankel, S.H., and Givi, P., Mathematical Modeling of Reactant Conversion Rate by Single-Point PDF Methods, Proceedings of the Eastern Section Meeting of the Combustion Institute, Ithaca, NY, October 14–16 (1991b).

McMurtry, P.A., and Givi, P., Direct Numerical Simulations of a Reacting Mixing Layer by a Pseudospectral–Spectral Element Method, Chapter 14 in *Finite Elements in Fluids*, Hemisphere Publishing Co., Washington, D.C., p. 361, in press (1991).

Michalke, A., On Spatially Growing Disturbances in an Inviscid Shear Layer, *J. Fluid Mech.*, **23**, 521 (1965).

Appendix VI

The Compositional Structure and the Effects of Exothermicity in a Nonpremixed Planar Jet Flame

C. J. STEINBERGER,* T. J. VIDONI, and P. GIVI
Department of Mechanical and Aerospace Engineering, State University of New York at Buffalo, Buffalo, NY 14260-4400

Results are presented of direct numerical simulation (DNS) of a randomly perturbed compressible, spatially developing two-dimensional planar jet under the influence of a finite rate chemical reaction of the type $F + O \rightarrow$ Product. The objectives of the simulations are to assess the compositional structure of the flame and to determine the influence of reaction exothermicity by means of statistical sampling of the DNS generated data. It is shown that even with this idealized kinetics model the simulated results exhibit features in accord with experimental data. These results indicate that the Damköhler number is an important parameter in determining the statistical composition of the reacting field and that the results are not very sensitive to the mechanism by which this parameter is varied. It is demonstrated that as the intensity of mixing is increased and the effect of finite rate chemistry is more pronounced, the magnitudes of the ensemble mean and variance of the product mass fraction decrease and those of the reactants' mass fraction increase. Also, at higher mixing rates the joint probability density functions of the reactants' mass fractions shift towards higher values within the composition domain, indicating a lower reactedness. These trends are consistent with those observed experimentally and are useful in portraying the statistical structure of nonequilibrium diffusion flames. The DNS-generated data are also utilized to examine the applicability of the "laminar diffusion flamelet model" in predicting the rate of the reactant conversion with finite rate chemistry. This examination indicates that the performance of the model is improved as the value of the Damköhler number is increased. Finally, the simulated results suggest that in the setting of a "turbulent" flame, the effect of the heat liberated by the chemical reaction is to increase the rate of reactant conversion. This finding is different from those of earlier DNS results and laboratory investigations that indicate a suppressed chemical reaction with increasing heat release.

INTRODUCTION

Recent advances in flow visualization and diagnostic techniques have made significant contributions to the understanding of turbulent combustion phenomena [1, 2]. With implementation of these advanced techniques it is now possible to make a detailed examination of the structure of turbulent flames and to establish a better understanding of the intricate physics of such flames. Among recent applications of these diagnostic techniques, Masri et al. [3, 4] have made noteworthy progress in describing the structure of nonpremixed turbulent jet flames under the influence of finite rate chemical reactions (see Refs. 5 and 6 for comprehensive reviews). In particular, they have reported results provided by statistical sampling of data obtained by Raman-Rayleigh scattering measurements of the species mass fractions and the temperature in a turbulent methane jet flame. These measurements are utilized primarily for constructing single-point statistics of the reacting field including the ensemble mean, the variance and probability density functions (pdfs) of the relevant thermochemical variables. The response of the flow under different mixing conditions is characterized by a comparison of the results obtained at various mixing rates. The sampling of the data in this way allows a systematic assessment of the compositional structure of the nonequilibrium flame. Such data are valuable in describing the phenomena of mixing and chemical reactions in nonpremixed turbulent combustion and in addressing some of the

* Corresponding author.

Published by Elsevier Science Publishing Co., Inc.

0010-2180/93/$6.00

existing problems in the modeling of such flames by means of statistical methods.

In order to provide a computational complement to laboratory investigations, there has been significant progress in the development and implementation of direct numerical simulation (DNS) of nonpremixed reacting flows [7–14] (see Refs. 15–19 for recent reviews). The extent of progress made by these contributions has been very encouraging, thus justifying further utilization of direct methods in the analysis of turbulent flames. In this work we intend to continue our investigation of nonpremixed reacting flows via DNS and to simulate such flows in a context relevant to laboratory investigations. Obviously, it is still impossible to perform DNS of a realistic "physical" flame [15]. Here, our intention is to make use of present computational capabilities to further address some of the fundamental and pertinent issues in regard to the dynamics of these flows.

In the next section the method of investigation is presented together with the underlying assumptions imposed in making the problem tractable for computational treatment. The ramifications associated with some of the assumptions are discussed, where appropriate, in the results. The focus is on assessing the compositional structure of the flame and on revealing the influences of reaction exothermicity. It is shown that some of the trends observed in laboratory experiments can be captured by DNS, and speculation is made regarding some of the other features not yet ascertained in laboratory investigations.

METHOD OF INVESTIGATION

The flow under investigation consists of a spatially developing, two-dimensional, planar jet flame. The schematic diagram of the jet is shown in Fig. 1a along with the specifications of physical dimensions. The fuel, F, discharges from the inner higher speed jet of width D with a velocity of U_F into a co-flowing lower velocity (U_O) oxidizer, O, stream. The hydrodynamic field is characterized by the velocity ratio $r = U_F/U_O$, the Reynolds number (Re) based on the velocity difference, $\Delta U = U_F - U_O$, across the layer ($\mathrm{Re} = \rho \Delta U D/\mu$), and the convective Mach number in each stream. The planar configuration considered here is different from that of a circular jet flame in Refs. 3 and 4, but allows the elucidation of some specific physical features that are believed to be invariant of the jet geometry [18]. The flow evolves spatially in the streamwise direction (x), and impermeable free slip boundary conditions are imposed in the cross-stream direction (y). The DNS computational procedure is the same as that employed in Refs. 14 and 20. The numerical discretization procedure is based on a *two–four* (second-order accurate in time and fourth-order truncation in space) compact parameter finite difference scheme. This scheme has been developed and made operational by Carpenter [21], and is utilized in the context of the SPARK computer code [22]. A generalized single-step chemistry model of the form $F + O \rightarrow$ Product is assumed. This model is simple enough to allow an efficient treatment via DNS and yet it is capable of capturing some of the important nonequilibrium effects associated with combustion. All the species involved in this reaction are assumed to be thermodynamically identical and the values of the physical transport parameters are assumed to be invariant with temperature.

The flowfield is initialized with a top hat mean streamwise velocity profile with a low amplitude random forcing at the inner jet entrance ($x = 0$). This forcing is imposed across the layer and is in terms of sinusoidal disturbances of specified frequency and phase shifts. The magnitudes of the frequency and the phase shifts between the different forcing modes are selected randomly from a seed with a uniform probability distribution and with specified values of the mean and variance. The random specification of the frequency and the phase shifts is intended to mimic the influence of turbulence in an otherwise deterministic simulation. The imposition of external perturbations expedites the formation of large scale structures; no attempt is made to investigate stability characteristics of the jet. The amplitudes of the perturbation are specified such that the maximum intensity of fluctuation at the inflow is no more than 7.5%. The inlet temperature (T) and pressure (P) are the same in both streams, and the reactants are com-

pletely segregated at the inlet. To initiate reaction, the temperature at the interface between the two reactants is increased at the inlet. An approximate Gaussian profile is adopted for the temperature distribution, and an error function profile is assumed for the mass fractions at the interfaces of the two reactants. With the assumption of a second-order chemistry model the rate of reactant conversion (ω) is expressed by $\omega = K_f C_F C_O$. Here, C and K_f

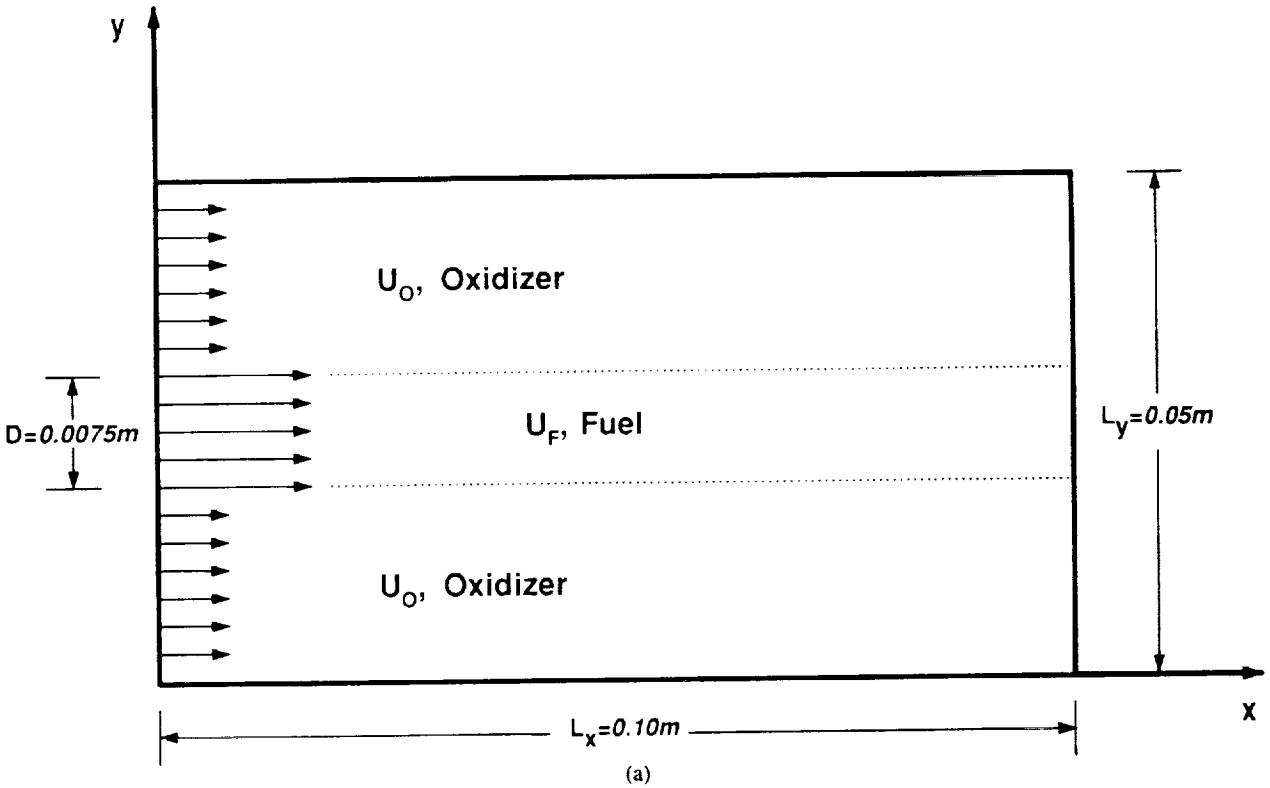

(a)

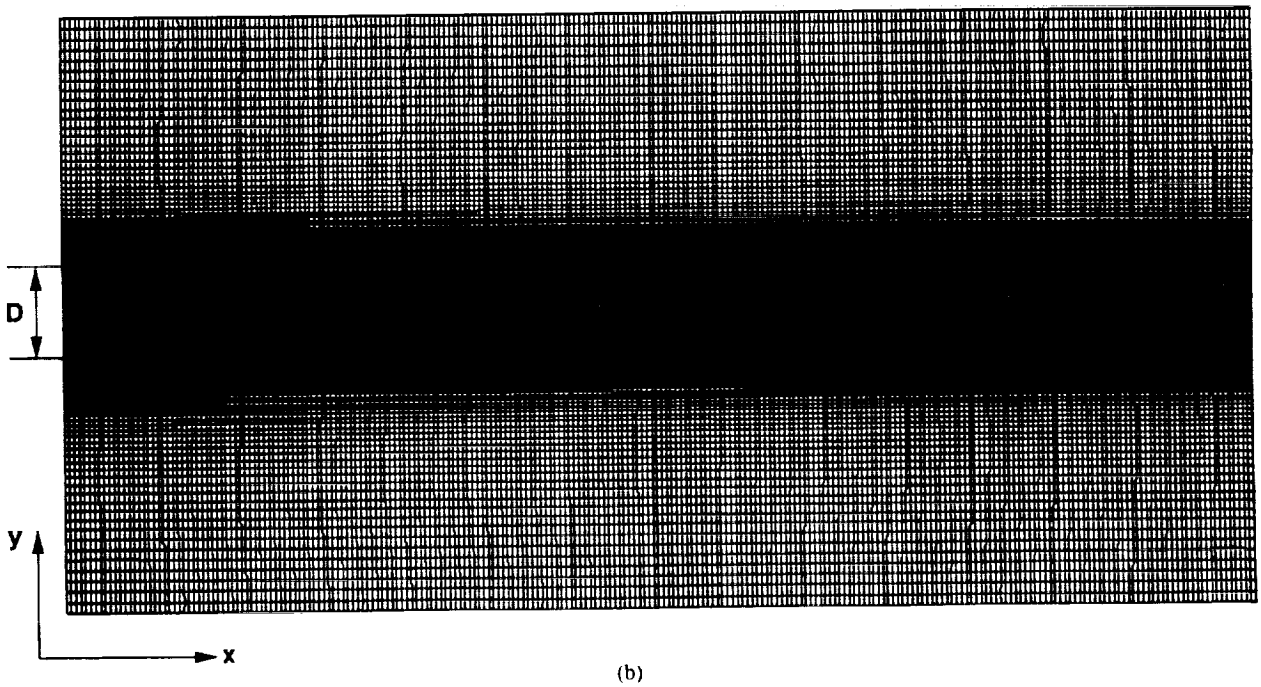

(b)

Fig. 1. (a) Schematic diagram of the planar jet configuration. (b) The grid.

denote the concentration and the reaction rate constant, respectively. Both constant rate kinetics and an Arrhenius chemistry model are considered. In the former K_f is constant, and in the latter $K_f = A_f \exp(-E/\mathscr{R}T)$. In this expression A_f denotes the preexponential factor, E is the activation energy, and $\mathscr{R}$ represents the universal gas constant. The nondimensional parameters influencing the rate of reactant conversion in this setting are the Damköhler number [$\mathrm{Da} = K_f C_{F_i}/(\Delta U/D)$], the Zeldovich number in the Arrhenius model ($\mathrm{Ze} = E/\mathscr{R}T_i$), the heat release parameter ($Q = -\Delta H^0/C_V T_{F_i}$), the Prandtl (Pr) number, and the Schmidt (Sc) number. In these expressions, the subscript i denotes the inlet, C_V is the specific heat at constant volume, and $-\Delta H^0$ indicates the enthalpy of combustion.

Several simulations are conducted. Table 1 provides a listing of the values of the physical parameters considered in each simulation. In these simulations, the influences of the Reynolds number, the velocity ratio, the Prandtl number, and the Schmidt number are not investigated. The values of the molecular Prandtl and the Schmidt numbers are set to unity ($\mathrm{Pr} = \mathrm{Sc} = 1$) to make the analysis associated with laminar diffusion flamelet modeling easier. The magnitude of the Zeldovich number is held constant in all the Arrhenius simulations but the values of the Damköhler numbers and the heat release parameter are altered to assess their influence on the dynamics of combustion. With the assumption noted above, the speed of sound (a) is uniform at the inflow. Therefore, the magnitude of the convective Mach number is the same in both streams at the inlet and is given by $M_c = (U_F - U_O)/a$ where the convective velocity, U_c is expressed as $U_c = (U_F + U_O)/2$. The full compressible form of the transport equations [23] are considered in the computational formulation. However, the magnitudes of the convective Mach numbers considered are not very large. Therefore, many of the physical issues associated with high-speed combustion [14, 18, 22] are not addressed. Also, the body forces are assumed negligible; therefore, the interesting physical problems associated with the buoyancy [24, 25] are not considered.

TABLE 1

Physical Parameters for Simulations

Flame	M_c	Da	Ze	Q
A	0.1	0.1	20	0.5
B	0.1	0.05	20	0.5
C	0.2	0.05	20	0.5
D	0.1	0.05	0	0.0
E	0.1	0.5	0	0.0
F	0.1	10.0	0	0.0
G	0.1	100.0	0	0.0
H	0.1	0.1	20	0.0
I	0.1	0.1	20	1.5
J	0.1	0.1	20	6.0

The compositional structure of the flame is assessed by means of examining the response of the flow to the Damköhler number in a manner similar to that in Ref. 3. This assessment is quantified by considering the statistical properties of the reacting field including the ensemble mean, the variance, and the pdfs of the mass fractions. The analysis has been made in a heat releasing reacting jet with an Arrhenius chemistry model. Flames A, B, and C (Table 1) are considered for this purpose. These flames are identified by the relative magnitude of the mixing intensity quantified by the value of the Damköhler number. In Flames B and C, the magnitudes of the Damköhler number are the same and are set equal to half of that in Flame A. However, the mechanism by which this is enacted is different. In Flame B, this is implemented by decreasing the magnitude of the chemical reaction frequency, and in Flame C by increasing the magnitude of the characteristic velocity of the jet. Both of these procedures result in the same reduction in the value of the Damköhler number. The magnitude of the convective Mach number is higher in Flame C than that in Flame A, but the value of this Mach number is not so large as to have a substantial influence on the spatial growth of the jet [14]. Also, the imposition of external forcing masks the effects of other possible mixing inhibition mechanisms (such as exothermicity, density stratification, etc.) [12, 14, 26–29].

To examine the performance of the diffusion flamelet model and to assess the effects of heat release, Flames D through J are considered (Table 1). In Flame D through G, a constant

rate non-heat-releasing chemical reaction is simulated. In Flames H through J, an Arrhenius reaction is considered with varying magnitude of heat release.

RESULTS

The simulations are performed on the mesh shown in Fig. 1b. The grid generation procedure involves a nonuniform mesh with a heavy concentration of grid points near the regions of maximum instantaneous shear [14, 20, 22]. With the computational resources available to us, routine numerical experiments with a resolution of 245 × 165 grid points are feasible. In some of the runs the independency of the results from the grid spacing was assessed by performing simulations with 405 × 255 grid points. This assessment was made for Flames A through C and the results indicate the convergence of the statistical results. Therefore, the simulated results presented here are based on a resolution consisting of 405 × 255 grids for Flames A through C, and of 245 × 165 grids for Flames D through J. These simulations are conducted with moderate values of the Reynolds, Peclet, Damköhler, and Zeldovich numbers within a domain $L_x = 13\frac{1}{3}D > x > 0$, $L_y = 6\frac{2}{3}D > y > 0$. With this resolution it was possible to perform simulations with $r = 2$ and $\mathrm{Re} = 1.0 \times 10^4$ free of spurious oscillations. The smallest grid spacing in the cross stream direction is near the center of the layer and is $\Delta y = 6 \times 10^{-5}$ m. This spacing is smaller than the diffusion length scale. However, at regions far from the center of the layer the spacing is relatively coarse. At these regions obviously the scales are not fully resolved, but the magnitudes of the gradients here are not that large to cause numerical oscillations. This is shown in the next section. The computational time increment varies at each time step and its value is the smallest of the characteristic time scales associated with hydrodynamics and chemistry. As shown in Table 1, the magnitudes of the Damköhler numbers are small enough to avoid the need for prohibitively small time increments. With the resolution adopted, a typical simulation requires about 35 h of CPU time on a Cray-2 supercomputer.

To visualize the global structures, contour plots of the instantaneous fuel mass fractions are shown in Fig. 2a. This figure shows how the growth of low-amplitude random perturbations manifest themselves in the formation of large scale coherent vortices downstream of the jet entrance. Due to the random nature of the forcing mechanism, the evolution of the large-scale structures is complex and, similar to laboratory shear flows, consists of random formation of vorticity rollups and subsequent pairing and coalescence of neighboring vortices. Also, due to the response of the layer to sinuous instabilities the layer is asymmetric with respect to the jet centerline. The formation of large-scale structures results in an enhancement of mixing. Large concentrations of vorticity on both sides of the jet centerline bring the fluid from the two streams into the core of the large scale structures. Within these structures the fluid elements are subject to further straining and the molecular diffusion between the two fluids results in final mixing at the molecular scale. The region of large gradients is confined to the inner jet zone where there is heavy concentration of grid points and there are no numerical oscillations in resolving these gradients. The enhanced mixing mechanism caused by large-scale vortices results in a general depletion of fuel. Near the entrance of the jet where the reactants are first brought into contact, the extent of chemical reaction is fairly uniform at the reactants' interface. Further downstream, as the magnitude of the instantaneous strain increases, the reaction rate approaches zero at the braids and the flame locally quenches at those locations. This mechanism of flame extinction is consistent with previous DNS results [9, 10], and is also corroborated by experimental observations [30, 31]. This behavior was observed in all Arrhenius simulations with moderate Damköhler numbers indicating the departure from chemical equilibrium.

Compositional Structure

To examine the effects of finite rate chemistry on the compositional structure, the results extracted by DNS are statistically analyzed. With the assumption of statistically stationary

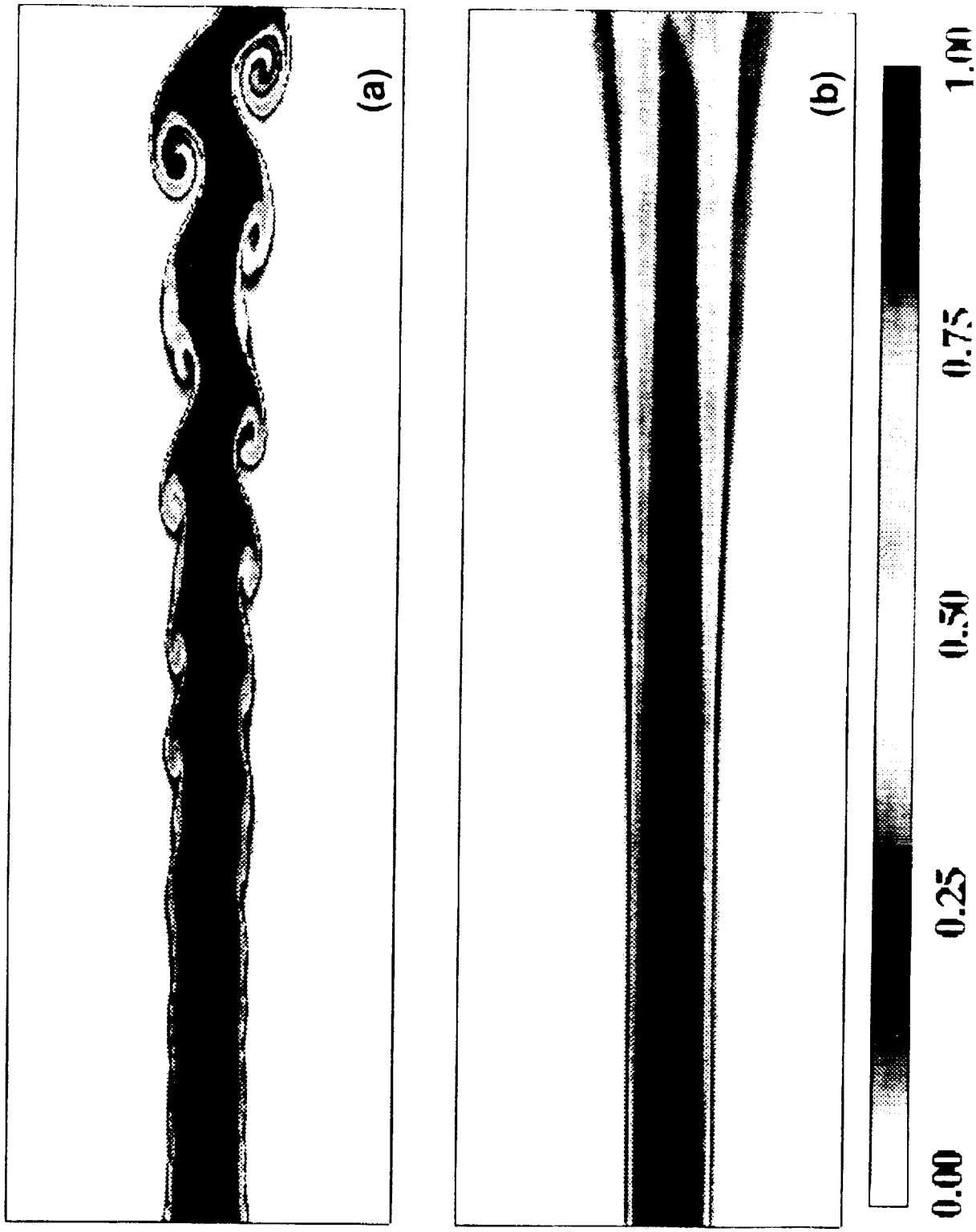

Fig. 2. (a) Plot of product mass fraction contours. (a) Instantaneous data. (b) Ensemble-averaged data.

flow, the instantaneous data can be used to construct ensemble-averages. Here, these averages are obtained by statistical analysis of 9000 samples gathered after the effects of initial transients are washed away at the outflow. The data sampling was performed within a period equivalent to 3 times the residence time of the flow. With this sampling, the maximum errors in evaluating the mean and the variance of the scalar quantities are estimated to be 4.3% and 8.7%, respectively. Typical results of such averaged quantities are presented in Fig. 2b in the form of a contour plot of ensemble-averaged fuel mass fraction.

To exhibit the effects of finite rate chemistry in a quantitative manner, comparisons are made between the statistical data in Flames A, B, and C. In Fig. 3 the cross stream variation of the ensemble-mean values (denoted by $\langle\ \rangle$) of the product mass fraction is shown at a streamwise location ($x = 10D$). Figure 3 shows that the magnitude of mean product mass fraction in Flame A is higher than those of Flames B and C. This suggests that as the flame approaches extinction, the mass fractions of the reactants in the reaction zone increase and the rate of product formation decreases. The same behavior is observed at all streamwise locations, as indicated by the spatial variation of the integrated product concentration T_{C_P}, shown in Fig. 4. Here $T_{C_P} = \int \langle C_P \rangle dy$. A similar behavior is observed in Fig. 5, which shows that the amplitude of the variance of the product mass fraction is higher in Flame A than those in Flames B and C. The trend observed in Figs. 3–5 is consistent with that in the laboratory measurements [3] and reveal the effects of the mixing intensity on compositional structure of the flame. These results also suggest that this behavior is somewhat insensitive of the procedure by which the Damköhler number is varied. In the experiments, the Damköhler number was altered only by means of increasing the hydrodynamic intensity (i.e., increasing the inner jet velocity). This was because a single fuel was used and, therefore,

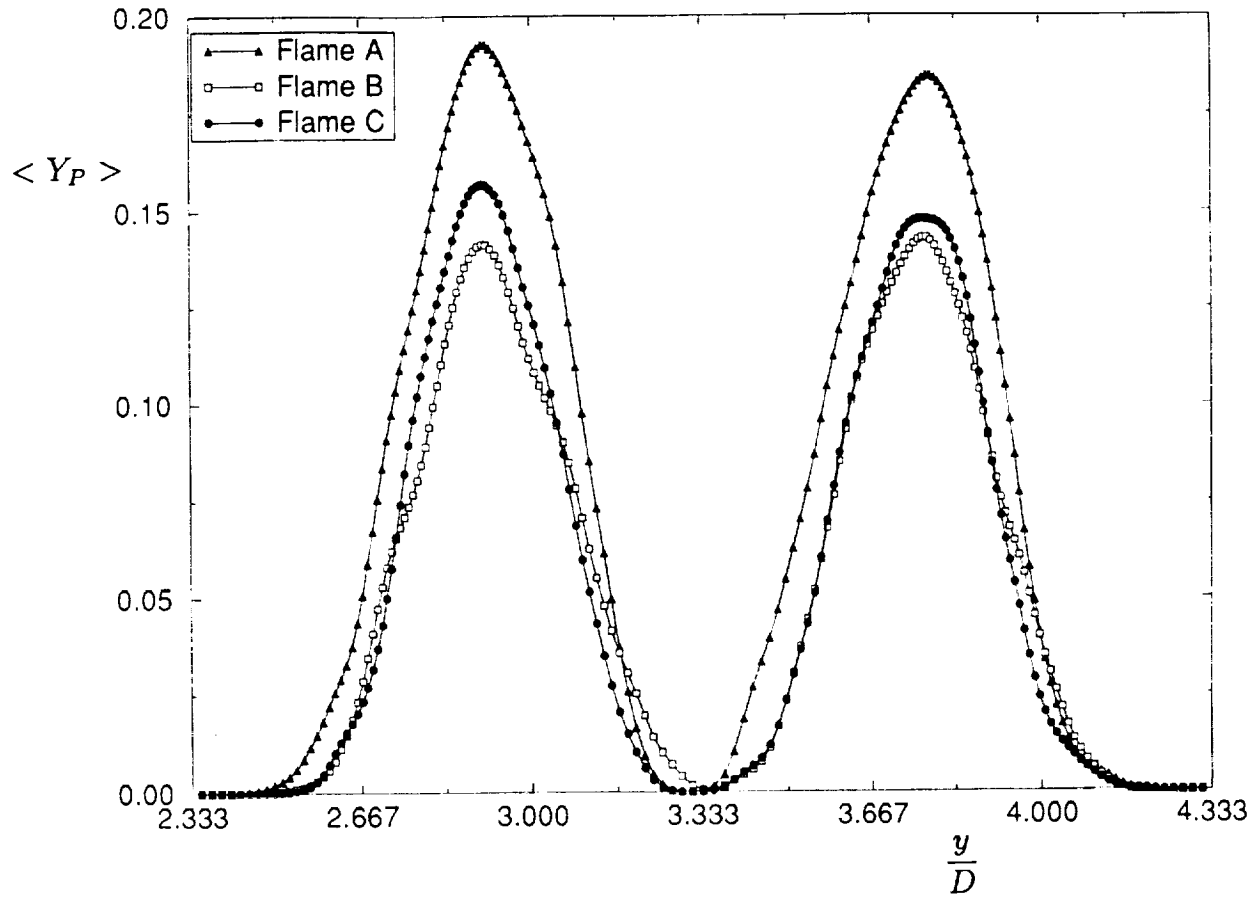

Fig. 3. Cross-stream variation of the ensemble-averaged product mass fraction at $x = 10D$.

the chemical frequency was constant in all the experiments. Our results indicate that this dependence is observed regardless of the procedure by which the change is made and Flames B and C portray approximately the same statistical conduct. The behavior observed in Figs. 3–5 demonstrates the dominant influence of the Damköhler number in quantitative analysis of nonequilibrium flames and also in the comparative assessment of the statistical results generated in our DNS with those obtained in laboratory experiments (See Ref. 32 for additional discussion concerning this issues).

The influence of finite rate chemistry on the compositional structure of the flame is further considered by examining the marginal and the joint pdfs of the reacting scalar variables. In Fig. 6, results are presented of typical single-point joint pdfs of the fuel and the oxidizer mass fractions, i.e., $\mathscr{P}(Y_F, Y_O)$ for Flames A and B. At a lower mixing rate, Flame A (Fig. 6a), there is a greater amount of product formed and the pdfs are higher at the mixed mass fraction values at the interior of the allowable region ($0 \leq Y_F, Y_O \leq 1$). At the higher mixing rate, Flame B (Fig. 6b), the mixture is composed of the two reactants with the joint pdfs concentrated closer to the line of $Y_F + Y_O = 1$. These results are consistent with those reported in Ref. 4 and indicate that at the higher levels of mixing intensity the results are closer to those obtained by cold mixing. The corresponding single-point marginal pdfs of the product mass fraction $\mathscr{P}(Y_P)$ are shown in Fig. 7 for Flames A, B, and C. In all of these flames the pdfs are concentrated near zero at free streams and become broader near the central region of the layer. As the mixing rate is decreased the pdfs are shifted toward higher values of mass fraction. Again, the pdfs for Flames B and C are very similar. The trend in Fig. 7 is consistent with the experimental data [4] and indicates lower reactedness at higher mixing rates. However, due to strong intermit-

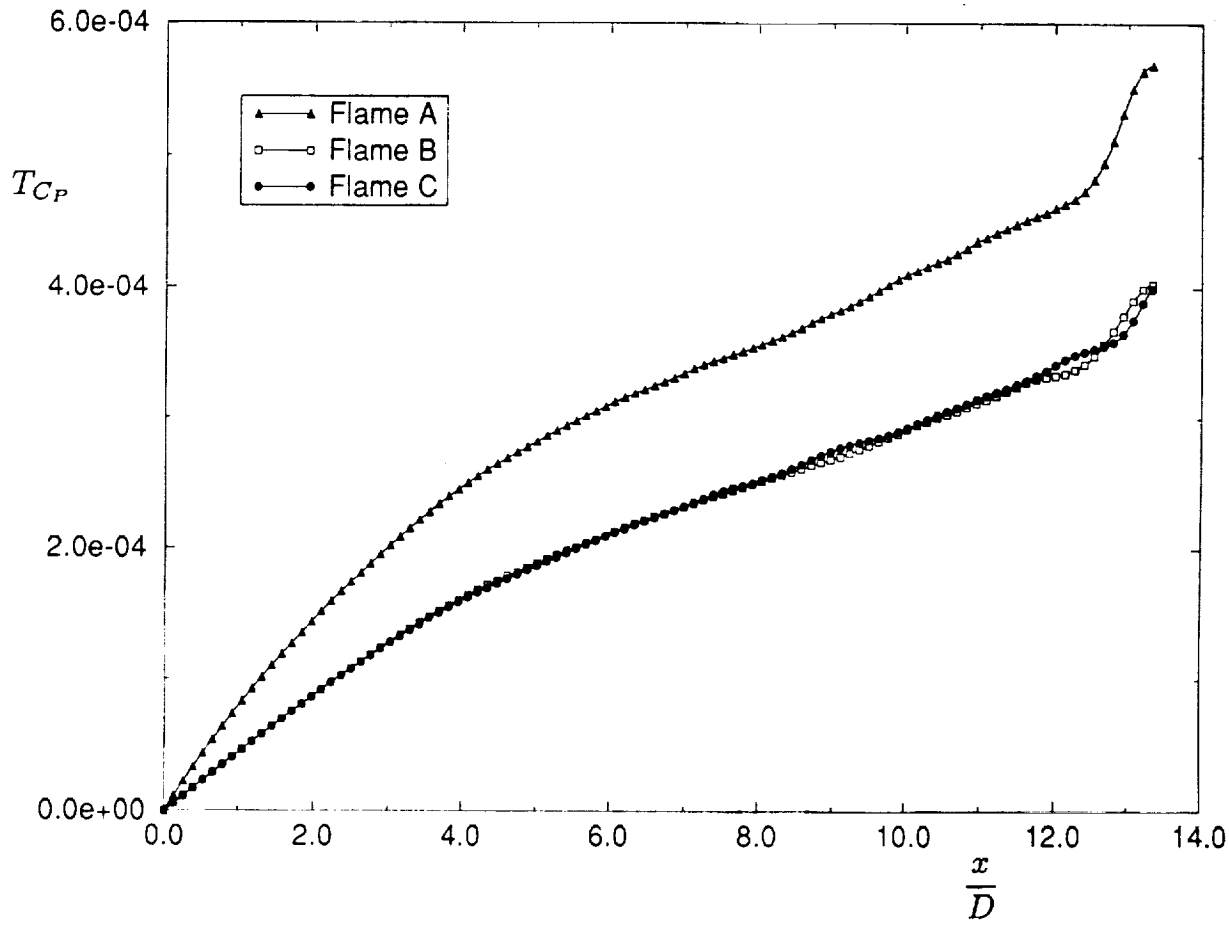

Fig. 4. Streamwise variation of the total product concentration.

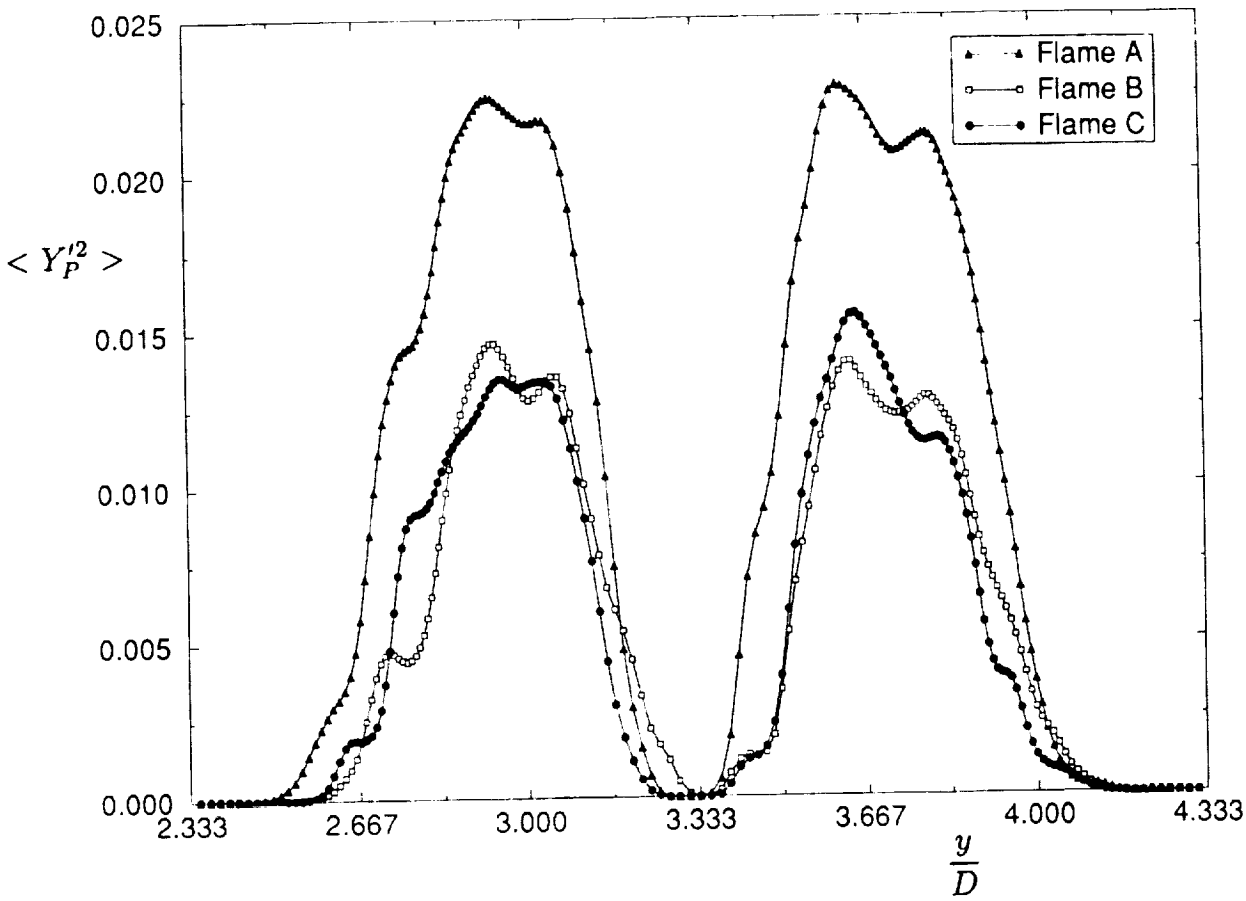

Fig. 5. Cross-stream variation of the variance of the product mass fraction at $x = 10D$.

tency of the flow in the two-dimensional simulations the pdfs do not adopt a Gaussian distribution, and are heavily populated near free stream values, that is, zero. Also, the tails of the pdfs become thinner as the mixing is intensified. This suggests a reduction in the variance of the product mass fraction as was reported in the experiments of Ref. 3 and also evident in Fig. 5.

Laminar Diffusion Flamelet Model

The data bank generated by DNS provides an effective means of assessing the performance of turbulence closures, at least in the setting of simple flows. In fact, within the past decade DNS-generated data have proven valuable in such assessments [15, 33]. One of the most recent closures for the analysis of nonequilibrium flames is the "laminar diffusion flamelet model" proposed in Refs. 31, 34, and 35. According to this model, a turbulent flame is viewed as an ensemble of thin laminar diffusion flamelets. With this view, effectively, the influences of hydrodynamics and chemical reactions are decoupled and the compositional structure of the flame is assumed to be the same as that in a laminar flame configuration with the same chemical characteristics. In the limit of an infinitely fast chemistry, or chemical equilibrium, this is obvious since the compositional structure depends on the magnitude of the mixture fraction. That is, the instantaneous values of a reacting scalar ψ is uniquely determined from the local values of the mixture fraction ξ, i.e., $\psi = \psi(\xi(\mathbf{x}, t))$ [23]. In finite chemistry, the laminar flamelet model implies that nonequilibrium effects manifest themselves through a dependence on a second parameter, namely, the dissipation rate of the mixture fraction, χ. That is, $\psi = \psi(\xi, \chi)$.

In order to examine the performance of the model in describing the compositional structure of the jet flame, simulations are performed of Flames D through G (Table 1). For ease of analysis in these simulations the reac-

tion rate (K_f) is assumed constant but is different in each flame, and the magnitude of heat release is set equal to zero. For the purpose of comparison with the flamelet model, a simple laminar system consisting of a steady one-dimensional opposed jet laminar flame configuration [36–38] is considered. In this setting, with the assumption of unity Lewis number the simulations based on the flamelet model involves the solution of the diffusion-reaction equation [38]:

$$\frac{d^2\psi}{d\xi^2} = \frac{-2\omega_\psi}{\rho\chi}. \tag{1}$$

Here, ω_ψ denotes the chemical source term corresponding to scalar ψ, and the variable χ is related to ξ through

$$\chi = \chi_{st} \exp\left[-2(\mathrm{erf}^{-1}(2\xi - 1))^2\right]. \tag{2}$$

where χ_{st} denotes the stoichiometric value of χ. In the laminar flame, this stoichiometric value is the same as the "stagnation value" of χ and is determined by the hydrodynamic intensity of the jet. However, for the unsteady jet flame considered in DNS, a single value cannot be adopted. Instead, only some representative values can be considered. With the instantaneous values of (ξ, χ) extracted from the DNS results, the flamelet library is constructed by means of Eqs. 1–2. With this construction the results are described in terms of $\psi(\xi, \chi_{st})$. In the laminar flame, these results are obviously single valued functions of the local Damköhler number, K_f/χ_{st}, as indicated by Eqs. 1–2. In the unsteady jet flame, the results are extracted directly by DNS and are parameterized in terms of the instantaneous values of K_f/χ_{st}. The comparison between the model and DNS results for one of these flames is shown in Fig. 8, which presents the "scatter plot" of product

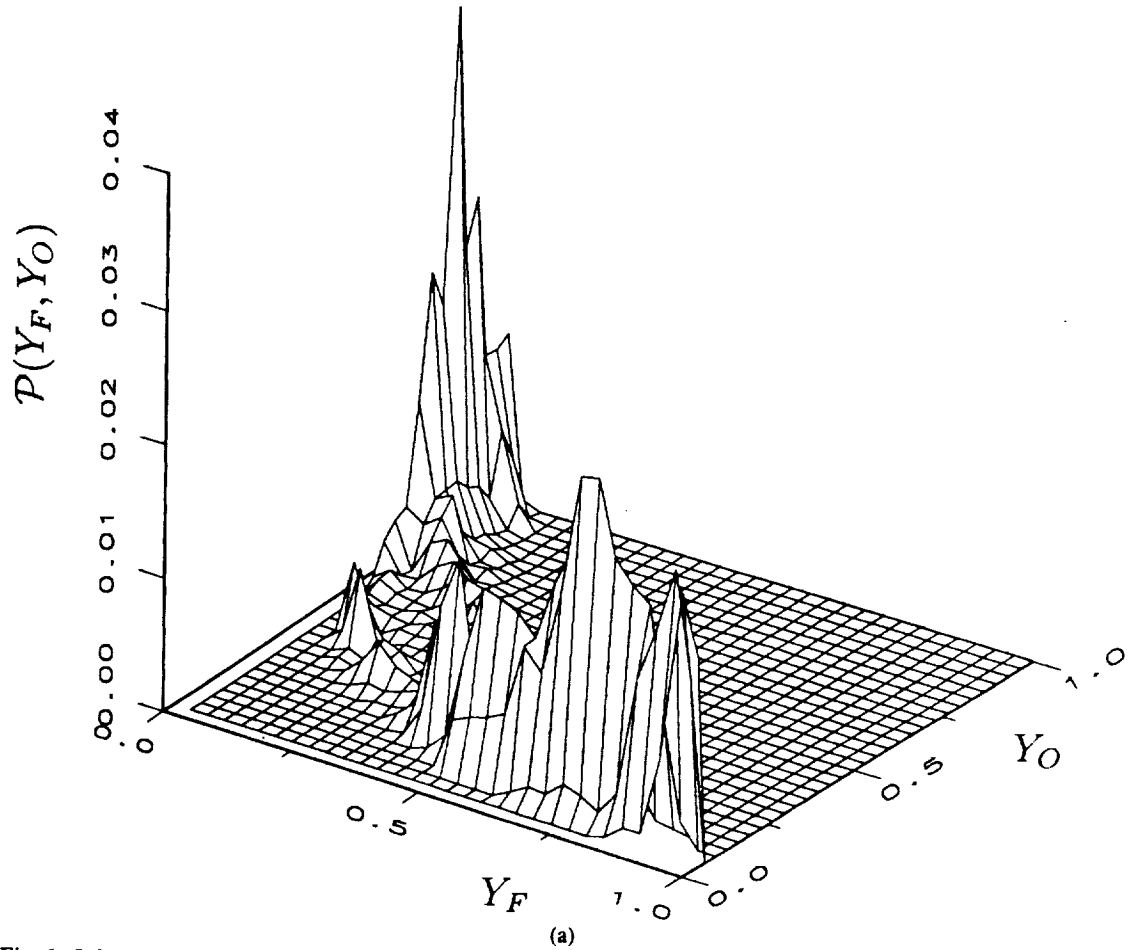

(a)

Fig. 6. Joint pdfs of the reactants mass fractions, $\mathcal{P}(Y_F, Y_O)$ at $x = 10D$, $y = 3.8D$. (a) Flame A. (b) Flame B.

C-3

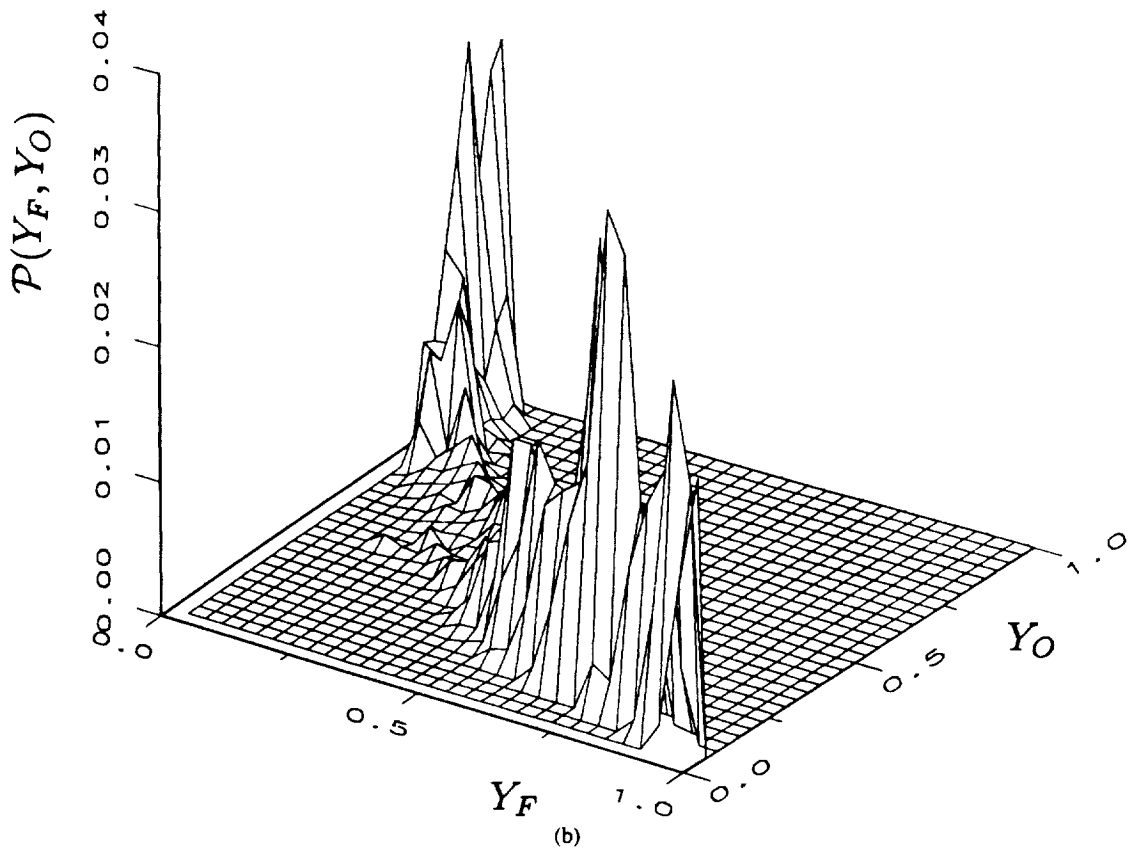

(b)

Fig. 6. Continued.

mass fractions versus the mixture fraction. For the laminar flame configuration, each of the curves with a constant value of K_f/χ_{st} represents a flamelet. For DNS, the compositional structure is constructed by parameterization of the data in terms of the instantaneous values of χ. If the laminar diffusion flamelet model is to be considered valid, then all the scatter data in the range $C_1 \leq K_f/\chi_{st} \leq C_2$ should fall between the laminar flamelet solution corresponding to $K_f/\chi_{st} = C_1$ and $K_f/\chi_{st} = C_2$. Figure 8 indicates that at low values of the local Damköhler number the model underpredicts the DNS data. The agreement becomes somewhat better at high values of this number. However, in all ranges of K_f/χ_{st}, there is a substantial portion of DNS data that fall outside the boundaries suggested by the flamelet model. The results are bounded in the upper limit as the value of the local Damköhler number approaches infinity. In this flame sheet limit both results obviously coincide and are single-valued functions of ξ. A more clear comparison is made in Fig. 9, which shows the scatter of product mass fractions versus the local Damköhler number, within the window of $0.45 \leq \xi \leq 0.55$, that is, $\xi \approx \xi_s = 0.5$. Figure 9 clearly shows that as the Damköhler number is increased, the data points shift towards the right and fall between the window of the two solutions predicted by the flamelet model. Based on these results, it is concluded that the laminar flamelet model predicts the compositional structure of the flame accurately at high Damköhler numbers, that is, near the limit of an infinitely thin flame. The use of the model in flames with strong departure from this limit cannot be guaranteed for general applications.

Exothermicity Effects

Despite the attractive features of our simulations in predicting the trends observed experimentally, it must be emphasized that in the context considered the factors influencing the stability characteristics of the jet are masked

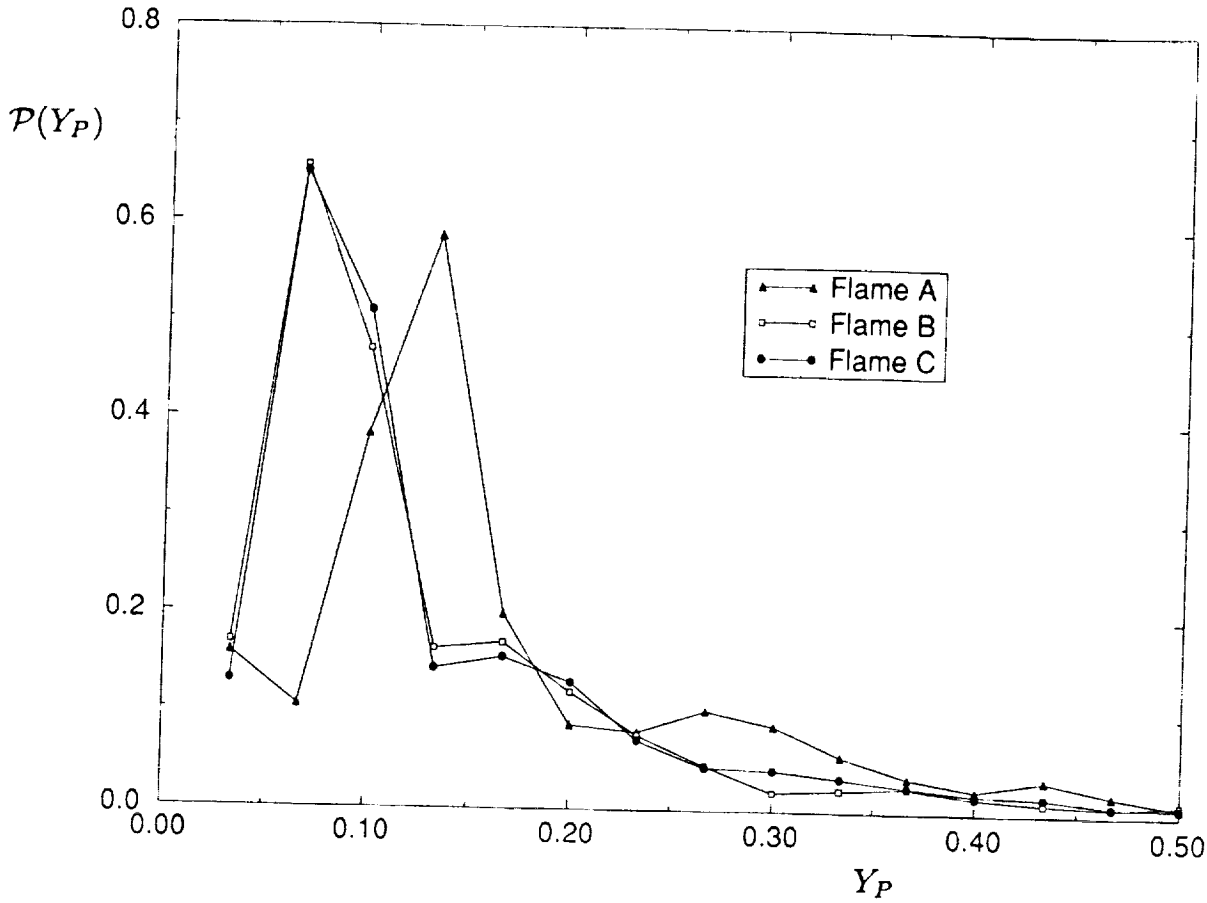

Fig. 7. Marginal pdfs of product mass fraction, $\mathcal{P}(Y_P)$ at $x = 10D$, $y = 3.8D$.

by addition of external forcing [28]. Note that these simulations are of a *transitional* flow, whereas the experimental data are obtained in a fully *turbulent* jet flame. The imposition of explicit forcing was therefore necessary to mimic a turbulent environment. This forcing, however, overcomes the mixing suppression caused by factors such as reaction exothermicity, compressibility, etc. [14, 26–29]. In order to make this point clear, simulations are performed of several heat releasing flames (Flames H through J in Table 1). In all these flames, the magnitudes of the velocities, the Damköhler number and the Zeldovich number are identical and are set equal to those in Flame A. However, the extent of exothermicity is varied. The total integrated product mass fraction $T_{Y_p}(x)$ generated by these flames is compared in Fig. 10, which reveals a higher rate of product formation as the magnitude of the heat release is increased. This observation is not consistent with any of the previous DNS [8, 14] or experimental [39] results. The reason for this discrepancy is due to the effects of the Arrhenius kinetics model in the present simulations and cannot be observed in constant rate kinetics simulations and/or experiments [8, 14, 39]. The increased level of heat release also delays the onset of extinction, since the heat transfer away from the flame is countered by the heat generated inside. This new observation, therefore, suggests that in the setting of a "turbulent" flame in which the transitional effects are not dominant, and where the chemical reaction is describable by an Arrhenius model, the heat release results in a higher reactant conversion, even though the rate of mixing may be somewhat less.

Based on our observation, we recommend that the effects of exothermicity be assessed by means of laboratory measurements. These measurements must involve a reacting system whereby the rate of reaction conversion is temperature dependent (unlike that employed in

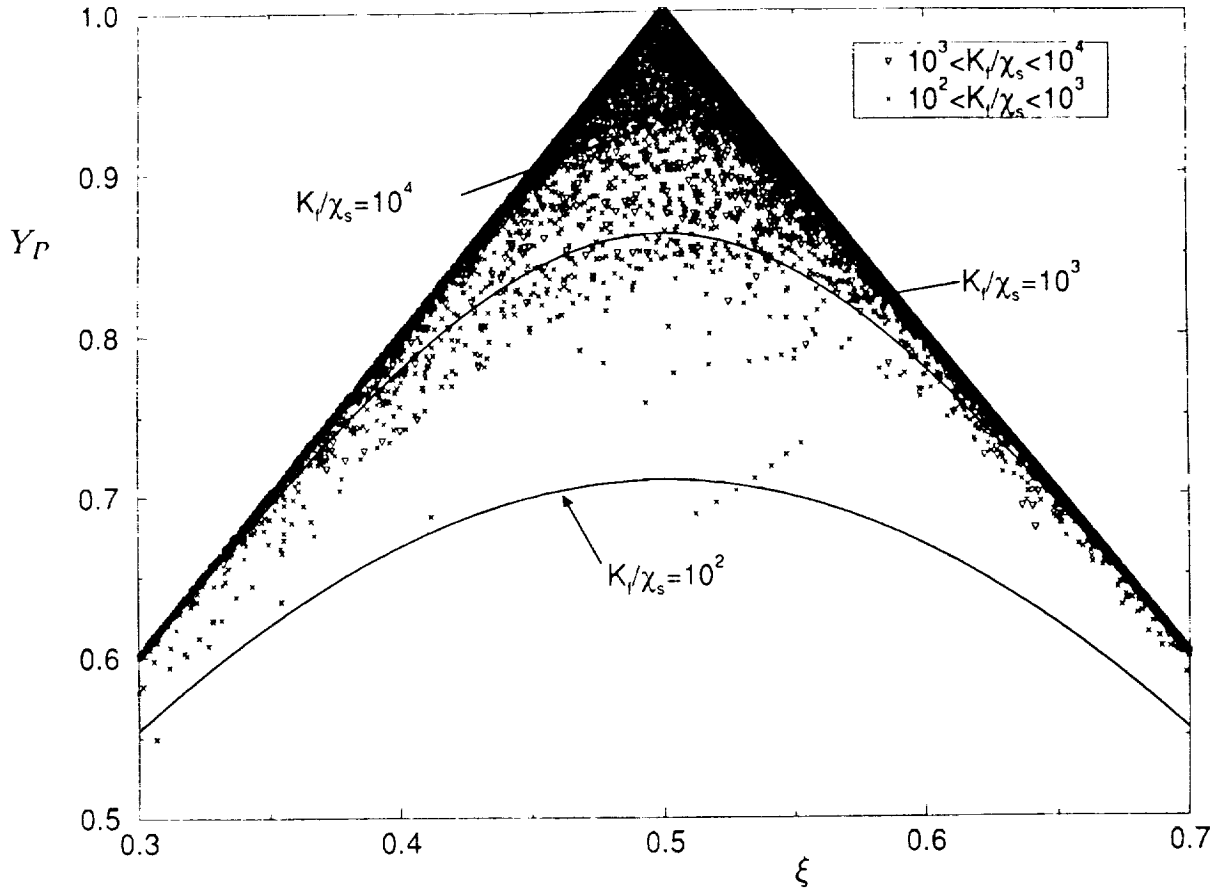

Fig. 8. Scatter plot of product mass fraction versus the mixture fractions for Flame E and its comparison with the laminar diffusion flamelet model. $x = 10D$.

Ref. 39, and in which the large-scale mixing intensity is not significantly affected by the heat release (see Refs. 11, 12, 17–19, 25 for discussions on the effects of heat release in low speed combustion, and Refs. 14 and 20 for discussions of such effects in high-speed combustion). It is important to note that the issue would not be resolved by a mere comparison of the mixing characteristics between a reacting and a nonreacting layer. An appropriate analysis requires the consideration of two flows with the same hydrodynamic characteristics but with different magnitudes of the enthalpy of combustion. The extent of validity of our conclusion under more complex chemistry models can be determined by these experiments.

CONCLUDING REMARKS

A two-four compact finite difference algorithm is employed for direct numerical simulations of a spatially developing planar jet flame under nonequilibrium chemical conditions. With the high numerical accuracy provided by this algorithm, it is possible to perform direct simulations under physically realistic conditions of variable density and exothermic reaction. Here, the kinetic mechanism is assumed to obey the idealized model of the type $F + O \rightarrow$ Products.

The data produced by DNS are statistically sampled to assess the compositional structure of the flame. The results of this analysis are shown to be consistent with those of laboratory measurements, even with the assumption of an idealized chemistry model. It is shown that as the intensity of mixing increases, the magnitudes of the ensemble mean and variance of the product mass fraction decrease, whereas those of the reactants increase. This conclusion is valid if the physical mechanisms by which the growth of instability waves is sup-

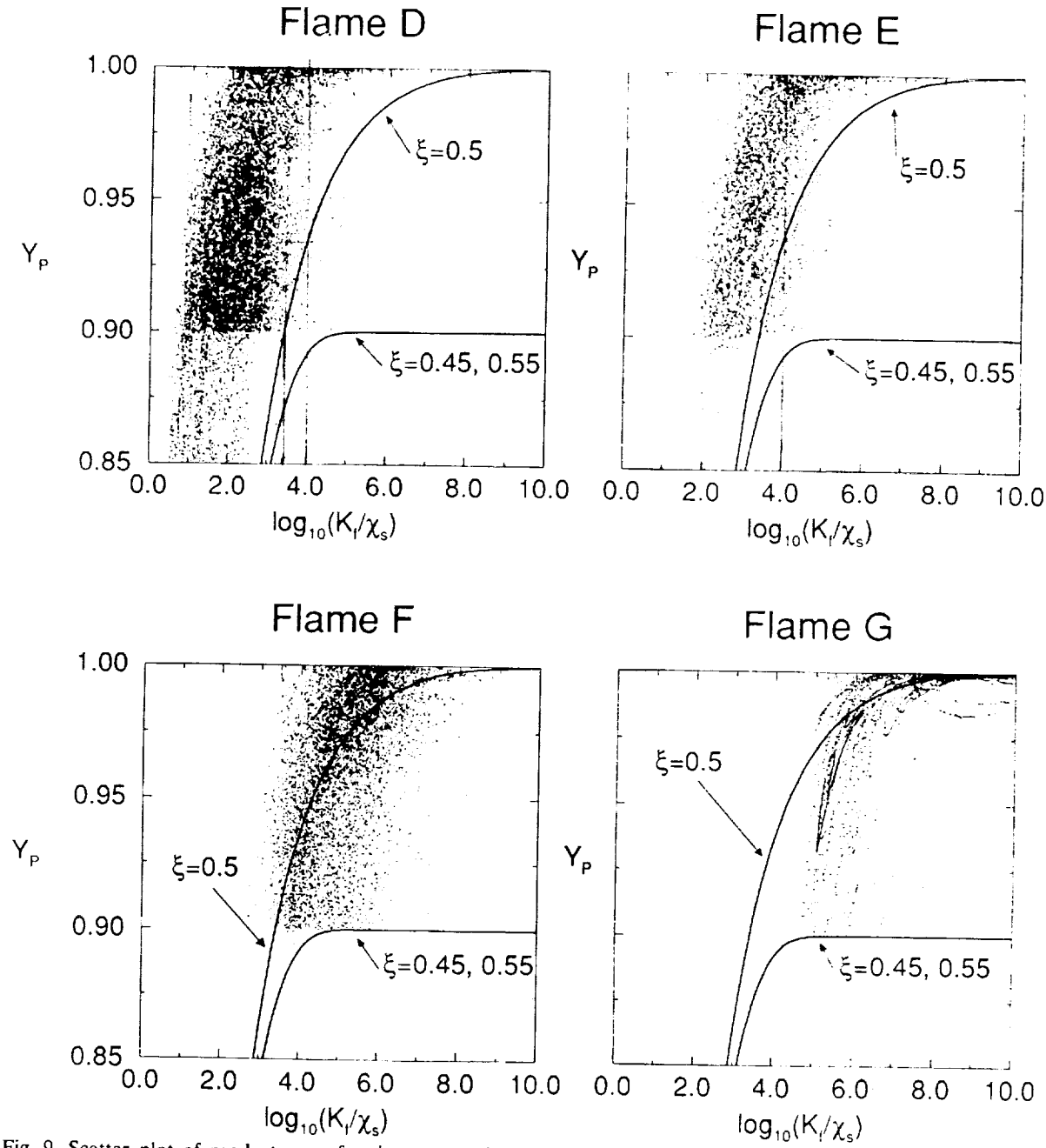

Fig. 9. Scatter plot of product mass fraction versus the reduced Damköhler number and its comparison with the laminar diffusion flamelet model. Mixture fraction in the range $0.45 \leq \xi \leq 0.55$, and $x = 10D$.

pressed are masked. This is implemented here by means of imposing a low amplitude random forcing at the entrance of the jet. The marginal and the joint pdfs of the reactants mass fractions, extracted from DNS data, show features in accord with laboratory data. That is, as the relative intensity of mixing is increased and the value of the Damköhler number is decreased, the pdfs show a lesser probability of product formation. The scatter plots of the instantaneous product formation indicate that the laminar diffusion flamelet model is capable of predicting the compositional structure of the flame when the magnitude of the Damköhler number is sufficiently large. Under this condition, the nonequilibrium effects are parameterized reasonably well by the instantaneous scalar dissipation rate in a simple laminar configuration with the same chemical characteristics. However, the flamelet library constructed in

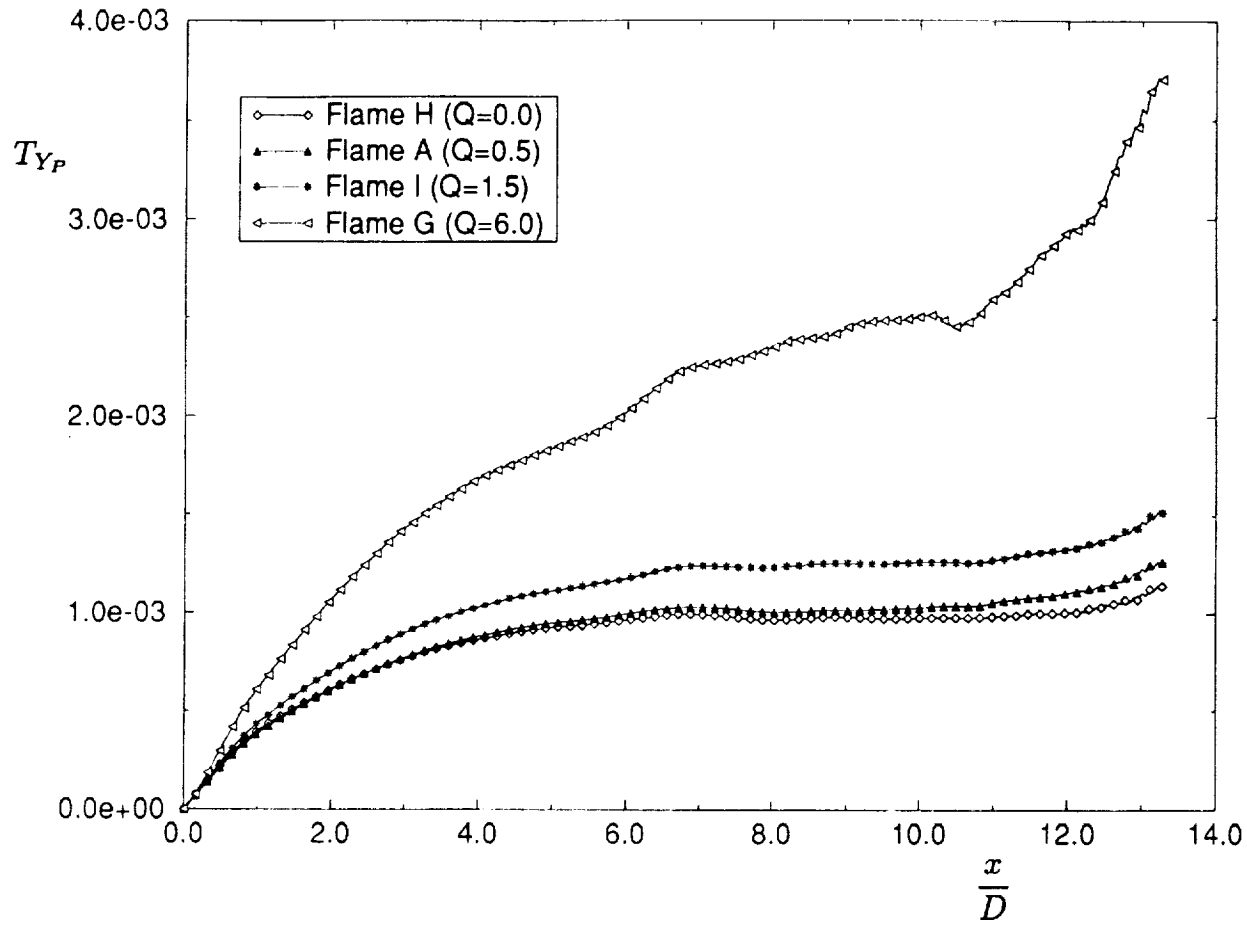

Fig. 10. Streamwise variation of the total product mass fraction.

this way does not yield satisfactory results at low Damköhler numbers. The results further indicate that in the setting of a "turbulent" flame, exothermicity results in an enhanced reactant conversion and an increased rate of product formation. This trend is not in accordance with previous DNS and laboratory results. The factors resulting in this discrepancy are (1) imposition of external forcing, and (2) the implementation of an Arrhenius kinetic model. Both of these factors are very important in diffusion flames in which the flow is fully turbulent and the chemical reaction rate can be assumed to obey the Arrhenius law. Therefore, we propose that in typical hydrocarbon turbulent diffusion flames, the effect of heat release is to increase the rate of product formation even though the rate of mixing may be somewhat reduced.

The work is sponsored by NASA Langley Research Center under Grant NAG-1-1122 and by the National Science Foundation under Grant CTS-9012832. Computational resources are provided by NASA LaRC and by NCSA at the University of Illinois.

REFERENCES

1. Yip, B., Lam, J. K., Winter, M., and Long, M., *Science* 235:1209–1211 (1987).
2. Long, M. B., Yip, B., Winter M., and Lam, K., in *Turbulent Reactive Flows* (R. Borghi and S. N. B. Murthy, Eds.), Lecture Notes in Engineering, Springer-Verlag, 1989, pp. 1–9.
3. Masri, A., Bilger, R. W., and Dibble, R. W., *Combust. Flame* 71:245–266 (1988).
4. Masri, A., Bilger, R. W., and Dibble, R. W., *Combust. Flame* 73:261–285 (1988).
5. Bilger, R. W., *Twenty-Second Symposium (International) on Combustion*, The Combustion Institute, Pittsburgh, 1988, pp. 475–488.
6. Bilger, R. W., *Ann. Rev. Fluid Mech.* 21:101–135 (1989).
7. Riley, J. J., Metcalfe, R. W., and Orszag, S. A., *Phys. Fluids* 29:406–422 (1986).

8. McMurtry, P. A., Jou, W.-H., Riley, J. J., and Metcalfe, R. W., *AIAA J.* 24:962–970 (1986).
9. Givi, P., Jou, W.-H., and Metcalfe, R. W., *Twenty-First Symposium (International) on Combustion*, The Combustion Institute, Pittsburgh, 1986, pp. 1251–1261.
10. Givi, P., and Jou, W.-H., *Twenty-Second Symposium (International) on Combustion*, The Combustion Institute, Pittsburgh, 1988, pp. 635–643.
11. McMurtry, P. A., Riley, J. J., and Metcalfe, R. W., *J. Fluid Mech.* 199:297–332 (1989).
12. Riley, J. J., and McMurtry, P. A., in *Turbulent Reactive Flows* (R. Borghi and S. N. B. Murthy, Eds.), *Lecture Notes in Engineering*, Springer-Verlag, 1989, pp. 486–514.
13. Mahalingham, S., Cantwell, B. J., and Ferziger, J. H., *Phys. Fluids A* 2:720–728 (1990).
14. Givi, P., Madnia, C. K., Steinberger, C. J., Carpenter, M. H., and Drummond, J. P., *Combust. Sci. Technol.* 78:33–68 (1991).
15. Givi, P., *Prog. Energy Combust. Sci.* 15:1–107 (1989).
16. Drummond, J. P., in *Numerical Approaches to Combustion Modeling* (E. S. Oran and J. P. Boris, Eds.), *Progress in Astronautics and Aeronautics*, vol. 135, AIAA, 1991, pp. 365–420.
17. McMurtry, P. A. and Givi, P., in *Numerical Approaches to Combustion Modeling* (E. S. Oran and J. P. Boris, Eds.), *Progress in Astronautics and Aeronautics*, vol. 135, AIAA, 1991, pp. 257–303.
18. Givi, P., and Riley, J. J., in *Major Research Topics in Combustion* (M. Y. Hussaini, A. Kumar, and R. G. Voigt, Eds.), Springer-Verlag, 1992, pp. 588–650.
19. Ghoniem, A., in *Numerical Approaches to Combustion Modeling* (E. S. Oran and J. P. Boris, Eds.), *Progress in Astonautics and Aeronautics*, vol. 135, AIAA, 1991, pp. 305–348.
20. Steinberger, C. J., AIAA Paper 92-0257, 1992.
21. Carpenter, M. H., in *Lecture Notes in Physics* vol. 371, (K. W. Morton, Ed.), Springer-Verlag, 1990, pp. 254–258.
22. Drummond, J. P., NASA TM 4055, NASA Langley Research Center, 1988.
23. Williams, F. A., *Combustion Theory*, 2nd ed. Benjamin/Cummings, Menlo Park, CA, 1985.
24. Davis, R., Moore, E., Roquemore, W., Chen, L.-D. Vilimpoc, V., and Goss, L., *Combust. Flame* 83:263–270 (1991).
25. Ellzey, J. L., and Oran, E. S., *Twenty-Third Symposium (International) on Combustion*, The Combustion Institute, Pittsburgh, 1990, pp. 1635–1640.
26. Jackson, T. L., and Grosch, C. E., in *Numerical Combustion* (A. Dervieux, and B. Larroutuiou, Eds.), Springer-Verlag, 1989, pp. 362–372.
27. Jackson, T. L., and Grosch, C. E., *J. Fluid Mech.*, 217:391–420 (1990).
28. Jackson, T. L., in *Major Research Topics in Combustion* (M. Y. Hussaini, A. Kumar, and R. G. Voigt, Eds.), Springer-Verlag, 1992, pp. 131–161.
29. Shin, D. S., and Ferziger, J. H., Report No. TF-53, Stanford University, Department of Mechanical Engineering, Thermosciences Division, Stanford, CA, 1992.
30. Tsuji, H., *Prog. Energy Combust. Sci.* 8:93 (1982).
31. Peters, N., *Prog. Energy Combust. Sci.* 10:319–339 (1984).
32. Magre, P., and Dibble, R. W., *Combust. Flame* 73:195–206 (1988).
33. Reynolds, W. C., in *Whither Turbulence? Turbulence at the Crossroads* (J. L. Lumley, Ed.), *Lecture Notes in Physics*, vol. 357, Springer-Verlag, 1990, pp. 313–343.
34. Williams, F. A., in *Turbulence in Mixing Operations* (R. S. Brodkey, Ed.), Academic, New York, 1975, pp. 189–209.
35. Peters, N., *Twenty-First Symposium (International) on Combustion*, The Combustion Institute, Pittsburgh, 1986, pp. 1231–1250.
36. Spalding, S. B., *J. Am. Rocket Soc.* 31:763–771 (1961).
37. Peters, N. *Combust. Sci. Technol.* 30:1–17 (1983).
38. Liñan, A., *Acta Astronaut.* 1:1007–1039 (1974).
39. Hermanson, J. C., Ph.D. thesis, California Institute of Technology, Pasadena, CA, 1985.

Received 24 July 1992; revised 23 February 1993

Appendix VII

Combust. Sci. and Tech., 1993, Vol. 91, pp. 21-52
Photocopying permitted by license only

Johnson-Edgeworth Translation for Probability Modeling of Binary Scalar Mixing in Turbulent Flows

R. S. MILLER, S. H. FRANKEL, C. K. MADNIA, and P. GIVI *Department of Mechanical and Aerospace Engineering, State University of New York, Buffalo, NY 14260*

(Received August 14, 1992; in final form November 2, 1992)

Abstract—A family of Probability Density Functions (PDF's) generated by *Johnson-Edgeworth* Translation (JET) is used for statistical modeling of the mixing of an initially binary scalar in isotropic turbulence. The frequencies obtained by this translation are shown to satisfy some of the characteristics of the PDF's generated by the *Amplitude Mapping* Closure (AMC) (Kraichnan, 1989; Chen *et al.*, 1989). In fact, the solution obtained by one of the members of this family is shown to be identical to that developed by the AMC (Pope, 1991). Due to this similarity and due to the demonstrated capabilities of the AMC, a justification is provided for the use of other members of JET frequencies for the modeling of the binary mixing problem. This similarity also furnishes the reasoning for the applicability of the *Pearson Family* (PF) of frequencies for modeling of the same phenomena. The mathematical requirements associated with the applications of JET in the modeling of the binary mixing problem are provided, and all the results are compared with data generated by Direct Numerical Simulations (DNS). These comparisons indicate that the *Logit-Normal* frequency portrays some subtle features of the mixing problem better than the other closures. However, none of the models considered (JET, AMC, and PF) are capable of predicting the evolution of the conditional expected dissipation and/or the conditional expected diffusion of the scalar field in accordance with DNS. It is demonstrated that this is due to the incapability of the models to account for the variations of the scalar bounds as the mixing proceeds. A remedy is suggested for overcoming this problem which can be useful in probability modeling of turbulent mixing, especially when accompanied by chemical reactions. While in the context of a single-point description the evolution of the scalar bounds cannot be predicted, the qualitative analytical-computational results portray a physically plausible behavior.

1 INTRODUCTION

The problem of binary mixing in turbulent flows has been the subject of widespread investigations over the past two decades (Dopazo, 1973; Pope, 1979; Pope, 1985; Pope, 1990; Givi, 1989; Kollmann, 1990). This problem has been particularly useful in assessing the extent of validity of the closures developed within this period for modeling of turbulent mixing by Probability Density Function (PDF) methods (Dopazo, 1973; Pope, 1976; Pope, 1979; Janicka *et al.*, 1979; Pope, 1982; Kosaly and Givi, 1987; Norris and Pope, 1991). Usually the problem is considered in the setting of a spatially homogeneous turbulent flow in which the temporal evolution of the PDF is considered. In this setting, development of a closure which can accurately predict the evolution of the PDF has been the main objective of these investigations (for recent reviews see Pope (1990); Kollmann (1990); Givi (1989)).

Computational experiments based on Direct Numerical Simulations (DNS) have proven very useful in evaluating the performance of new closures (Givi, 1989; Pope, 1990). The binary mixing problem is well-suited for DNS investigation, and current computational capabilities allow consideration of flows at sufficiently large Reynolds numbers in which the behavior of the models can be assessed (Eswaran and Pope, 1988; Givi and McMurtry, 1988; McMurtry and Givi, 1989; Madnia and Givi, 1992). The results of all the previous work on DNS of the binary mixing problem portray a clear picture of the PDF evolution, at least at the single-point level. A successful closure is one which can predict all the stages of mixing, as depicted by DNS, from an initially binary state (total segregated) to a final mixed condition.

Amongst the models developed in the literature, the recent Amplitude Mapping Closure (AMC) (Kraichnan, 1989; Chen *et al.*, 1989; Pope, 1991) has proven effective in producing a physically correct PDF evolution. In the application of this model to the problem of binary mixing it has been demonstrated that the closure is capable of approximating a reasonably correct evolution at all stages of mixing (Pope, 1991). Namely, the evolution from an initial double delta PDF to an asymptotic Gaussian distribution. This is a trend which has been observed in DNS (Eswaran and Pope, 1988; Givi and McMurtry, 1988; McMurtry and Givi, 1989; Madnia and Givi, 1992) and also corroborated by experimental investigations (Miyawaki *et al.*, 1974). However, it is shown by Gao (1991); O'Brien and Jiang (1991) that the PDF adopts an asymptotic Gaussian-like distribution only near the mean scalar value, and the conditional expected dissipation does not correspond to that of a Gaussian field everywhere within the composition domain.

Our first objective in this work is to present another means by which the AMC can be viewed. It is demonstrated that in the binary mixing problem, this closure can be considered as a member of the family of frequencies generated by the method of Johnson-Edgeworth Translation (JET). In fact, it is shown that the result produced by the AMC is identical to that generated by one of the members of this translation. With this observation, a justification for employing other simpler "assumed" frequencies is provided. Our second objective is to make a detailed examination of the conditional expected dissipation and the conditional expected diffusion of the scalar variable as predicted by the closures. This examination provides an effective means of demonstrating the deficiencies of these models in reproducing the correct physical behavior as depicted by DNS results. With the development of analytical relations for some of these closures, a remedy is suggested for overcoming the model deficiencies.

1.1 Outline

In the next section, the problem of binary mixing and its solution via the AMC is briefly reviewed. In Section 3, the Johnson-Edgeworth Translation is introduced with a highlight on the mathematical constraints associated with its application for the modeling of the mixing problem. Due to the previously established similarity of the JET frequencies with those based on the Pearson Family (PF), the Beta density of the first kind is also presented in this section. The PDF's generated by these three models (AMC, JET and PF) are compared against each other and also with data generated by Direct Numerical Simulations (DNS) in Section 4. The results for the conditional expected scalar dissipation, and the conditional expected scalar diffusion for all the closures are discussed, respectively, in Section 5 and in Section 6. In Section 7, some theoretical remarks pertaining to the evolution of the scalar in an isotropic field are presented. With this presentation, the problems associated with all three closures become more clear. In Sections 2-7, the discussions are limited to those associated with the transport of a passive scalar from an initially symmetric binary state in isotopic turbulence. Therefore, in Section 8 some discussions are presented of the applications of the models for treating more general problems. This paper is drawn to a conclusion in Section 9.

2 BINARY MIXING PROBLEM

We consider the mixing of a scalar variable $\phi = \phi(\mathbf{x}, t)$ ($\mathbf{x}$ is the position vector, and t denotes time) from an initially symmetric binary state within the bounds $\phi_\ell \leq \phi \leq \phi_u$. In this section, we assume that the lower and the upper bounds of the scalar range remain fixed (*i.e.* ϕ_u, ϕ_ℓ are constant). Within this domain, the single-point PDF of the variable ϕ at initial time is given by

$$P_1(\phi, t = 0) = \frac{1}{2}[\delta(\phi - \phi_\ell) + \delta(\phi - \phi_u)], \tag{1}$$

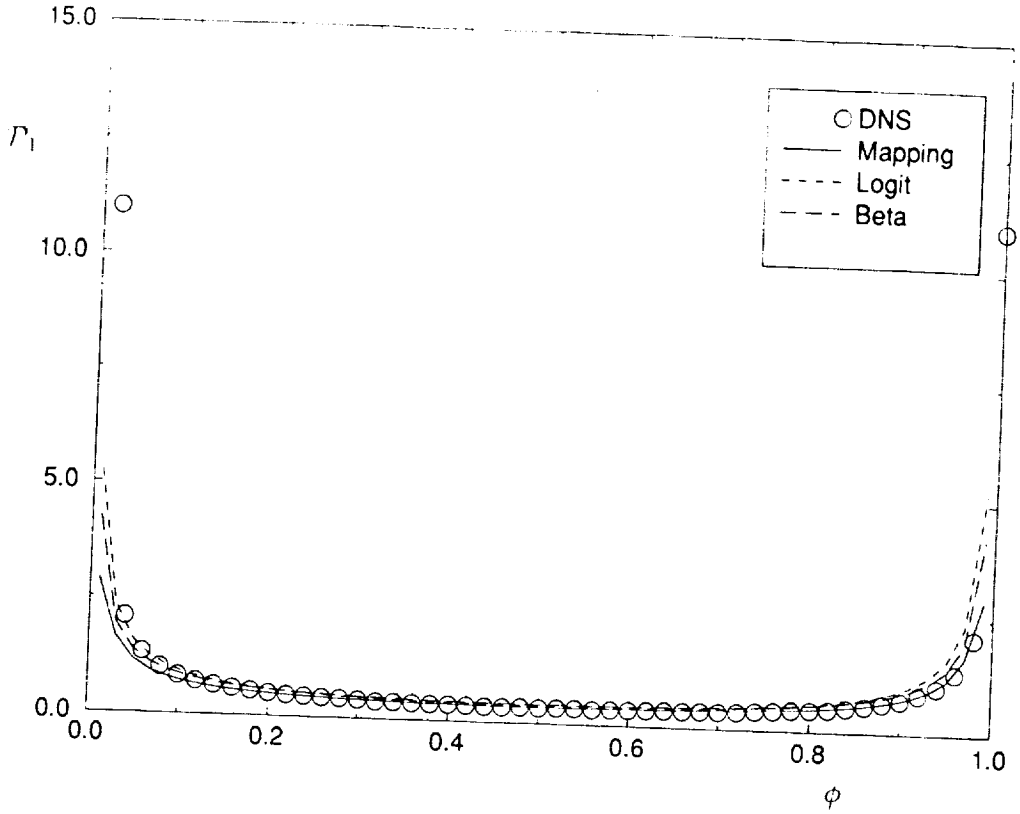

FIGURE 1a The comparison of the PDF's as predicted by the models with DNS data. (a) $\sigma^2 = 0.173$.

which obviously infers the following relations for the mean and the variance

$$< \phi >= (\phi_u + \phi_\ell)/2, < \phi'^2 >= \sigma^2 = \frac{1}{4}(\phi_u - \phi_\ell)^2. \tag{2}$$

Here, <> indicates the probability mean, σ^2 denotes the variance, and the prime represents the instantaneous deviation from the mean. In isotropic incompressible turbulence, the evolution of the PDF is governed by the transport equation

$$\frac{\partial P_1}{\partial t} + \frac{\partial^2(\varepsilon P_1)}{\partial \phi^2} = 0, \qquad \phi_\ell \le \phi \le \phi_u \tag{3}$$

where ε represents the expected value of the scalar dissipation with diffusion coefficient Γ, $\xi(= \Gamma \nabla\phi \cdot \nabla\phi)$, conditioned on the value of the scalar $\phi(\mathbf{x}, t)$,

$$\varepsilon = \varepsilon(\phi, t) =< \xi | \phi(\mathbf{x}, t) > . \tag{4}$$

Equation (3) can alternatively be expressed by

$$\frac{\partial P_1}{\partial t} + \frac{\partial(DP_1)}{\partial \phi} = 0, \qquad \phi_\ell \le \phi \le \phi_u, \tag{5}$$

where D denotes the conditional expected value of the scalar diffusion

$$D = D(\phi, t) =< \Gamma \nabla^2 \phi | \phi(\mathbf{x}, t) > . \tag{6}$$

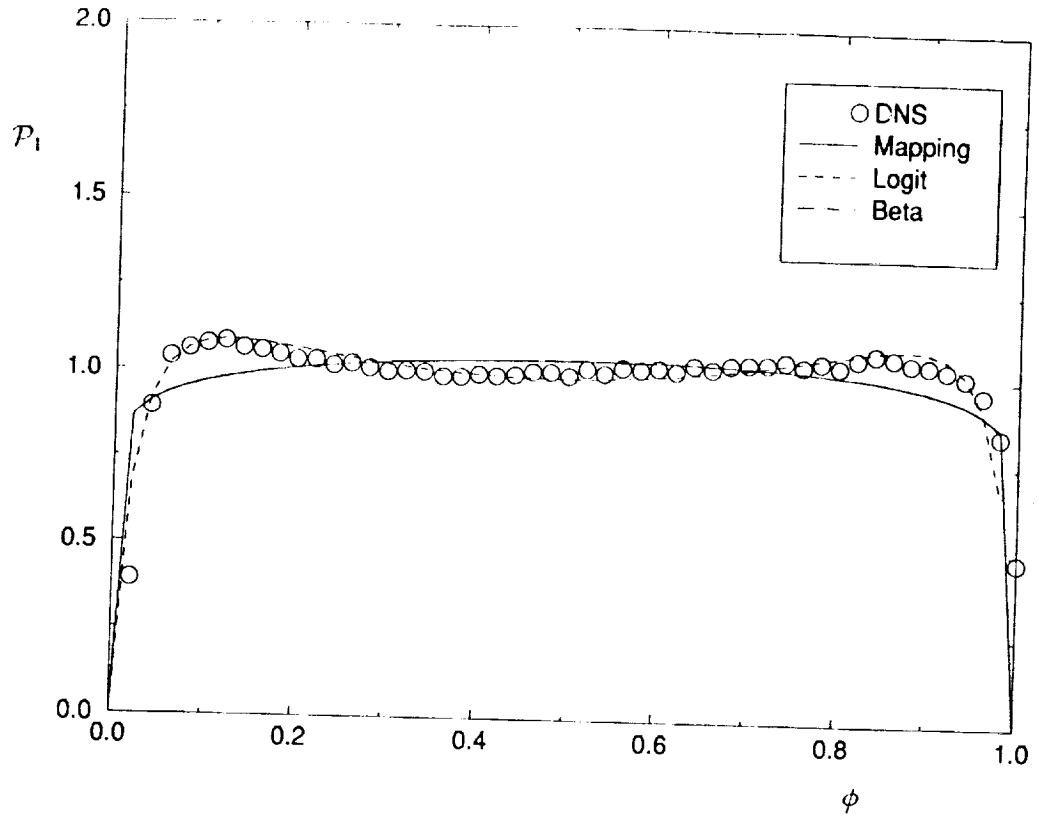

FIGURE 1b The comparison of the PDF's as predicted by the models with DNS data. (b) $\sigma^2 = 0.079$.

The closure problem in determining the PDF, P_1, is associated with the unknown conditional expected dissipation, ε, and/or the conditional expected diffusion, D. These two are related through Eqs. (1)-(6),

$$D(\phi, t) = \frac{1}{P_1(\phi, t)} \frac{\partial(\varepsilon P_1)}{\partial \phi}. \tag{7}$$

At the single-point level neither the conditional mean dissipation nor the conditional mean diffusion are known (neither are their unconditional mean values). Their specifications require external information.

With the application of the AMC, this external information is obtained in an implicit manner. As explained in detail by Pope (1991), the AMC involves a *mapping* of the random field of interest ϕ to a stationary Gaussian reference field ϕ_0, via a transformation $\phi = \chi(\phi_0, t)$. Once this relation is established, the PDF of the random variable ϕ, $P_1(\phi)$, is related to that of a Gaussian distribution. In a domain with fixed upper and lower bounds, *i.e.* fixed ϕ_ℓ, ϕ_u, the corresponding form of the mapping function is obtained by Pope (1991). The solution for a symmetric field with zero mean, $< \phi >= 0, \phi_u = -\phi_\ell$, is represented in terms of an unknown time τ

$$\chi(\phi_0, \tau) = \phi_u \quad \text{erf}\left(\frac{\phi_0}{\sqrt{2}G}\right), G(\tau) = \sqrt{\exp(2\tau) - 1}. \tag{8}$$

With this transformation, the PDF is determined from the physical requirement

$$P_1(\chi(\phi_0, \tau), \tau) d\chi = P_G(\phi_0) d\phi_0, \tag{9}$$

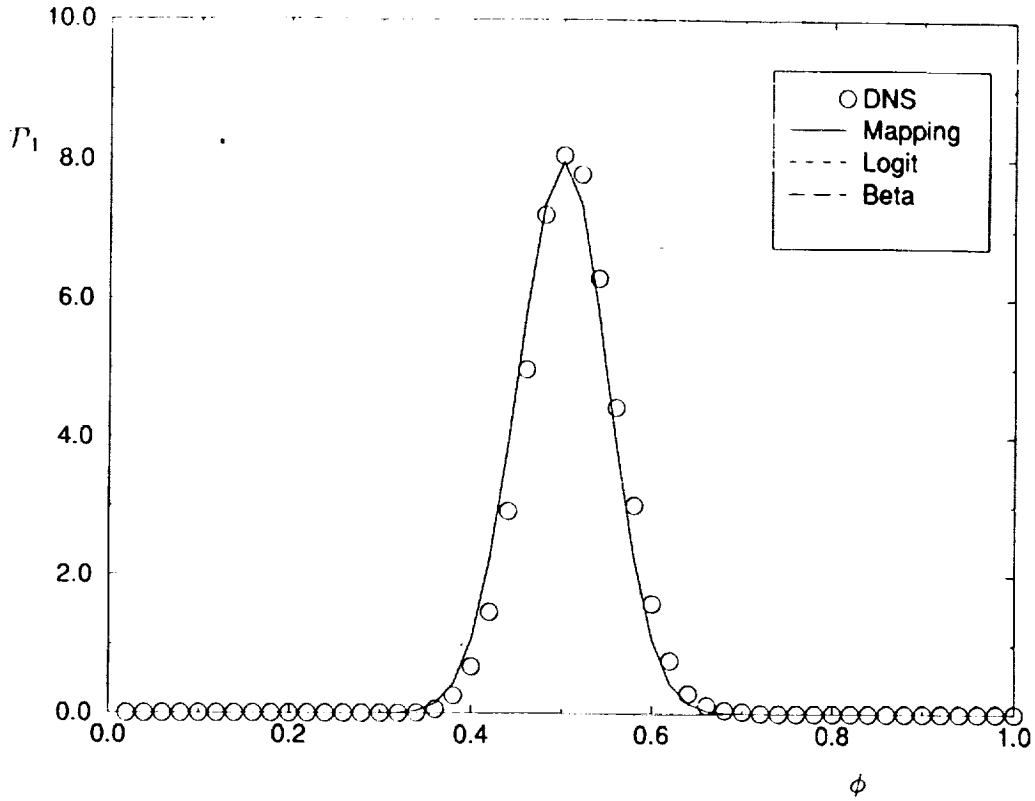

FIGURE 1c The comparison of the PDF's as predicted by the models with DNS data. (c) $\sigma^2 = 0.00247$.

where P_G denotes the PDF of a standardized Gaussian distribution, *i.e.* $P_G(\phi_0) = \frac{1}{\sqrt{2\pi}} \exp(-\phi_0^2/2)$. A combination of Eq. (8) and Eq. (9) yields

$$P_1(\phi, \tau) = \frac{G}{2\phi_u} \exp\left\{-(G^2 - 1)\left[\text{erf}^{-1}(\frac{\phi}{\phi_u})\right]^2\right\}. \tag{10}$$

In these equations, the relation between τ and the physical time t is unknown in the context of a single-point description. This relation can be obtained only through knowledge of the higher order statistical properties of the scalar field. For example, it is shown by Madnia *et al.* (1992); Frankel *et al.* (1992a) that the mapping closure yields the algebraic relation for the normalized variance,

$$\frac{<\sigma^2>(\tau)}{<\sigma^2>(0)} = \frac{2}{\pi} \arctan\left(\frac{1}{G\sqrt{G^2+2}}\right), \tag{11}$$

in which the variance is related to the unknown mean dissipation $\epsilon(t)$ by integrating Eq. (3),

$$\sigma \frac{d\sigma}{dt} = -\epsilon(t), \tag{12}$$

where,

$$\epsilon(t) = \int_{\phi_l}^{\phi_u} P_1(\phi, t)\epsilon(\phi, t)d\phi = -\int_{\phi_l}^{\phi_u} \phi P_1(\phi, t)D(\phi, t)d\phi. \tag{13}$$

3 JOHNSON-EDGEWORTH TRANSLATION

The AMC captures some of the basic features of the binary mixing problem as described by Pope (1991). Namely, the inverse diffusion of the PDF in the composition domain from a double delta distribution to an asymptotic Gaussian distribution centered around $< \phi >$, as $\sigma^2 \to 0$ (or $G \to \infty$). This asymptotic Gaussian distribution near the mean scalar value cannot be realized in any of the previous mixing models based on the so called Coalescence/Dispersion (C/D) closures (Curl, 1963; Janicka *et al.*, 1979; Pope, 1982; Kosaly and Givi, 1987). And those modified C/D models which do yield such an asymptotic state, *e.g.* Pope (1982), do not predict the initial stages of mixing correctly (Kosaly, 1986). This deficiency of the C/D models in yielding asymptotic Gaussianity has been a motivating factor for recent investigations resulting in the development of the AMC (Pope, 1991).

In the spirit of "mapping" to a specified reference field, it is speculated that there are perhaps other means of "driving" the PDF toward Gaussianity in a physically acceptable manner. In fact, this subject has been of major interest to statisticians and biometricians within the last century since the early work of Edgeworth (1907). The scheme was referred to by Edgeworth as the Method of Translation, and was later detailed by Johnson (1949a). In today's literature of statistics and biometrics, the scheme is known as Johnson-Edgeworth frequency generation, and has many applications in statistical analysis.

The essential element of Johnson-Edgeworth Translation (JET) is similar to that of the AMC. Namely, it involves the transformation of the random physical field, here, ϕ, to a fixed standard Gaussian reference field by means of a translation (or mapping) of the form

$$\phi = Z\left[\frac{\phi_0}{\gamma(t)}\right],$$

$$\gamma(t=0) = 0 \leq \gamma(t) \leq \gamma(t \to \infty) \to \infty. \tag{14}$$

In this equation, the function $\gamma(t)$ plays a role similar to that of G in the AMC. With an appropriate form for the function Z, the scalar PDF is determined from Eq. (9). For application in the problem of mixing from an initially symmetric binary state of zero mean within a fixed domain $\phi_\ell = -\phi_u \leq \phi \leq \phi_u$, the appropriate JET must satisfy the following physical constraints:

$$(i)\mathrm{Lim}_{(\gamma \to 0)} Z\left(\frac{\phi_0}{\gamma}\right) \approx H(\phi_0)$$

$$(ii)\mathrm{Lim}_{(\gamma \to \infty)} Z\left(\frac{\phi_0}{\gamma}\right) \approx C\phi_0 + O(\phi_0^3) + \ldots$$

(iii) $Z\left(\frac{\phi_0}{\gamma}\right)$ is an odd function with respect to the scalar mean for any value of σ^2.

(iv) $Z\left(\frac{\phi_0}{\gamma}\right)$ is bounded and is a non-decreasing function of ϕ_0, and $-\phi_u \leq Z \leq \phi_u$ at all times.

(15)

In these relations, H denotes the Heaviside function, and C is constant. Constraint (i) implies an initially symmetric and segregated binary state. The second constraint ensures an asymptotic Gaussian distribution for $P_1(\phi)$ near the mean scalar value. Condition (iii) preserves the symmetry of the PDF around the mean value at all times, and constraint (iv) implies the boundedness of the scalar field, *i.e.* $-\phi_u \leq \phi \leq \phi_u$. A function Z

which satisfies all the above constraints, is therefore expected to provide an acceptable means of approximating the PDF. An example is the *Logit*-Normal (or $\tanh^{-1}$-Normal) distribution, as originally proposed by Johnson (1949a). For the symmetric problem within a fixed domain, this distribution is produced by a mapping of the form[1]

$$Z = \phi_u \tanh\left(\frac{\phi_0}{\gamma}\right). \tag{16}$$

With this mapping, together with Eq. (9), the PDF of the scalar adopts the form,

$$P_1(\phi, t) = \frac{\gamma}{\sqrt{2\pi}\left(1 - (\frac{\phi}{\phi_u})^2\right)} \exp\left\{-\frac{\gamma^2}{2}\left[\tanh^{-1}(\frac{\phi}{\phi_u})\right]^2\right\}. \tag{17}$$

It is easily verified that this frequency satisfies the physical constraints of the symmetric binary mixing problem (Eq. (15)). At $t = 0$, the PDF is approximately composed of two delta functions at $\phi = \pm\phi_u$, and as $t \to \infty$ the PDF adopts an approximate Gaussian-like distribution centered around the zero mean. These features are similar to those portrayed by the PDF generated by the AMC (Eq. (10)).

This example demonstrates that with the satisfaction of the above indicated constraints, several other frequencies can be generated for effective modeling of the binary mixing problem. In fact, it is easy to show that the solution generated by the AMC can also be viewed as a member of the JET family. This is demonstrated by considering a translation of the form

$$Z = \phi_u \operatorname{erf}\left(\frac{\phi_0}{\gamma}\right), \tag{18}$$

From Eq. (9), this translation yields the PDF

$$P_1(\phi, t) = \frac{\gamma}{2\sqrt{2}\phi_u} \exp\left\{-(\frac{\gamma^2}{2} - 1)\left[\operatorname{erf}^{-1}\left(\frac{\phi}{\phi_u}\right)\right]^2\right\}. \tag{19}$$

This frequency can be termed the erf^{-1}-Normal distribution and is identical to the form presented by Eq. (10). The difference is due to the terms containing G and γ. But this is unimportant since in the context of single-point statistics neither of the two parameters can be determined by the PDF. Therefore, with $G \equiv \frac{\gamma}{\sqrt{2}}$, both expressions are equivalent. With this equivalence, the closed form relation for the variance of the erf^{-1}-Normal distribution has the same algebraic form given by Eq. (11). It is easy to show that many other distributions can be generated to display similar characteristics. In the discussions to follow, we only consider the Logit-Normal and the erf^{-1}-Normal distributions, the latter being identical to the distribution generated by AMC.

Pearson Family

The similarity of the AMC and JET in generating equivalent PDF's is also useful in explaining the applicability of the frequencies generated by the Pearson family (Pearson, 1895). For a "bimodal" distribution, a physically acceptable frequency is the Pearson

[1] In recent literature, the Logit-Normal is usually expressed by the mapping $Z = \phi_u \left\{2[1 + \exp(\phi_0/\gamma)]^{-1} - 1\right\}$.

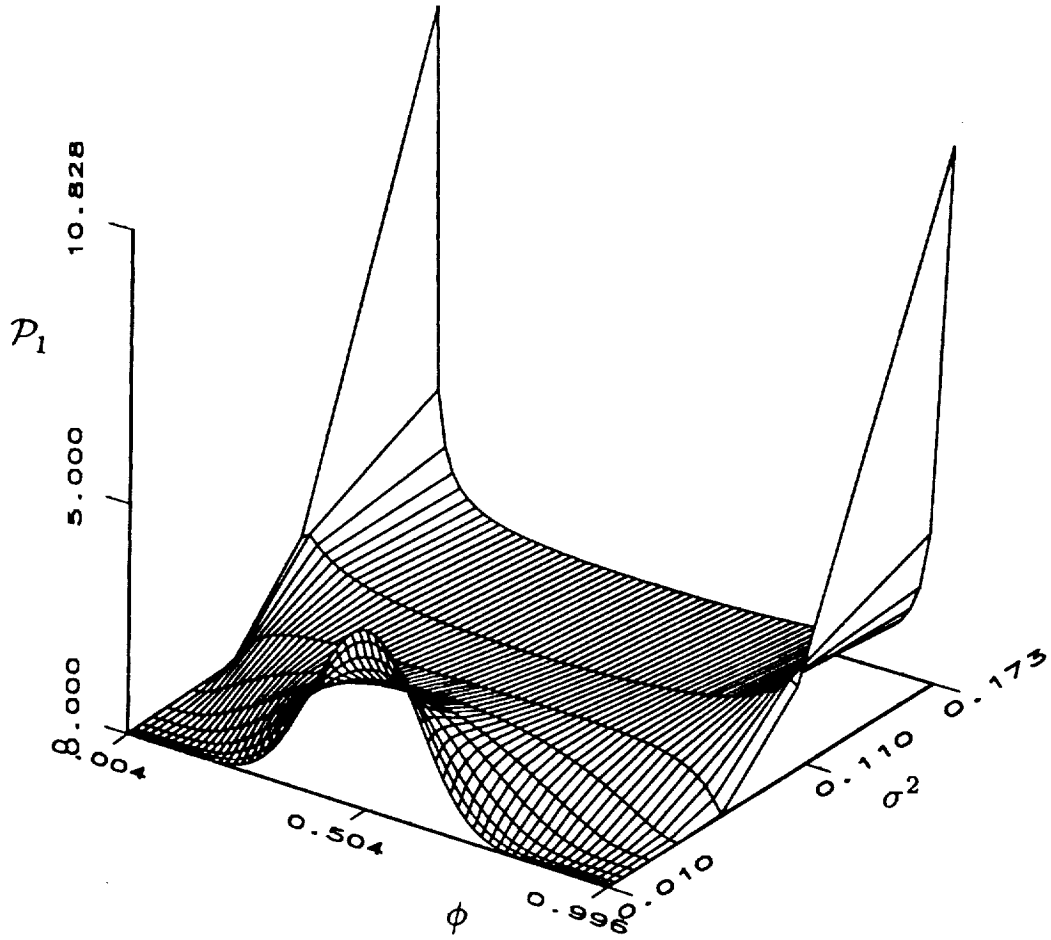

FIGURE 2 Temporal evolution of the Logit-Normal PDF.

Type I, known as the general form of the "Beta density of the first kind". This density is typically expressed in a fixed domain within the range $0 \leq \phi \leq 1$,

$$P_1(\phi) = \frac{1}{B(\beta_1, \beta_2)} \phi^{\beta_1 - 1}(1 - \phi)^{\beta_2 - 1}, 0 \leq \phi \leq 1. \tag{20}$$

Here B denotes the Beta function, and the parameters β_1 and β_2 are determined from the knowledge of the mean and the variance of the random variable. In a symmetric field within [0,1], $< \phi >= \frac{1}{2}$, $\beta_1 = \beta_2 = \beta$, and thus the PDF is characterized by the variance alone.

The similarity of the Pearson distributions and the JET frequencies is well recognized in the statistics literature (see Johnson (1949a)). Therefore, with the equivalence of the AMC and the JET as demonstrated above, it is not surprising that the Beta density and the AMC are also similar. This similarity, without a mathematical proof, has been recognized in previous works (Madnia *et al.*, 1991; Madnia and Givi, 1992).

4 COMPARATIVE ASSESSMENTS

The probability distributions obtained from the three frequency generation methods described above are all capable of providing a reasonable stochastic approximation of

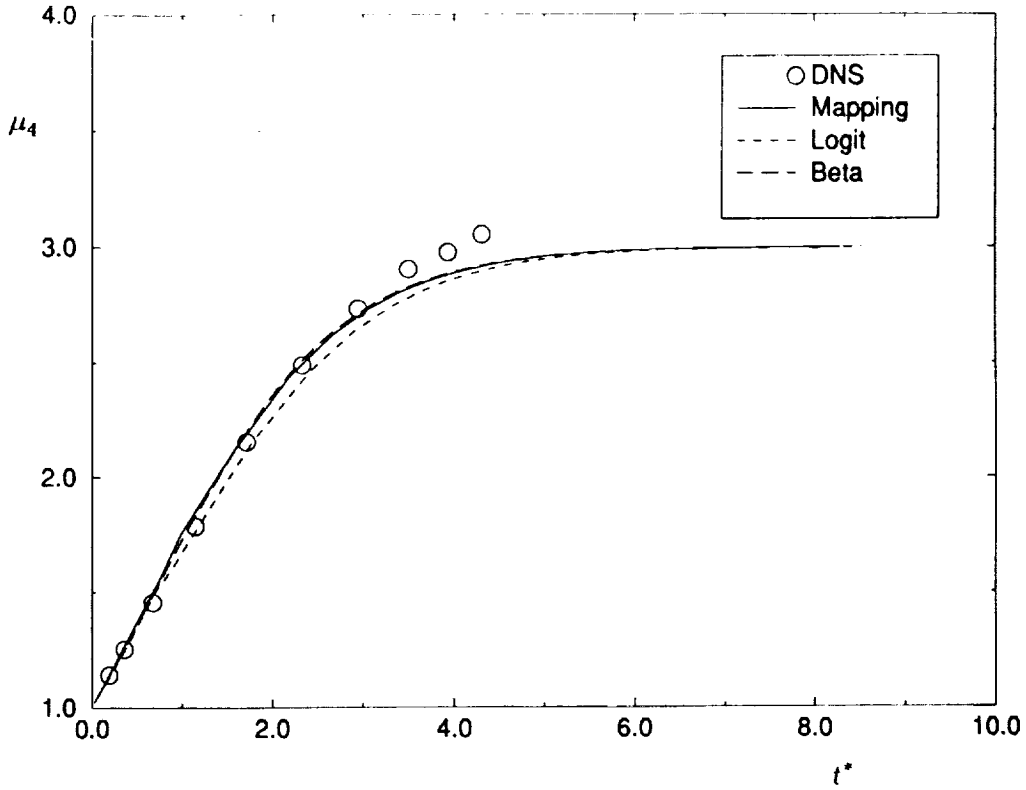

FIGURE 3a Temporal evolution of the centralized moments of the scalar variable as predicted by the models and the comparison with DNS data. (a) μ_4 vs. t*.

the mixing problem from an initially binary state. Namely, an approximate double delta distribution at $t = 0$, and an approximate Gaussian-like distribution as $t \to \infty$. The former can be realized in the limit of unity normalized variance $\sigma^2(t)/\sigma^2(0) = 1$. In a fixed composition domain, this corresponds to $G = 0$ for AMC ($\gamma = 0$ in JET), and to $\beta = 0$ for the Beta density. The latter is realized in the limit $G, \gamma, \beta \to \infty$. The limiting Gaussian distribution for the AMC has been asserted by Pope (1991). For the JET, the criterion (ii) in Eq. (15) guarantees this condition. For the Beta density, the assertion of an asymptotic Gaussian distribution in the limit of zero variance is established in elementary texts on statistics (*e.g.* Casella and Berger (1990)). At the intermediate stages, however, the PDF's are not identical. It is easily verified by Eqs. (10), (20) that the AMC and the Beta distributions become constant ($P_1(\phi) = \text{constant} = \frac{1}{2}\phi_u$) for $G = \beta = 1$. However, the Logit-Normal PDF does not yield a uniform distribution at any stage of its evolution. Also, as indicated by Johnson (1949a) it is not possible to provide a closed form algebraic expression similar to Eq. (11) for the variance of the Logit-Normal distribution.

In order to make comparative assessments of the models, the frequencies generated by the three methods (AMC, JET, and PF) are compared with each other, and also with PDF's generated by Direct Numerical Simulations (DNS). The DNS procedure is similar to that of previous simulations of this type. Since these simulations are not the major focus of this paper, only a brief outline of the procedure is described; for a detailed discussion we refer the reader to Madnia and Givi (1992). The subject of the DNS is a three-dimensional periodic homogeneous box flow carrying a passive scalar variable. The initial scalar field is composed of square waves with maximum and minimum values of 1 and 0, respectively. These limiting values are arbitrary, and can be translated to

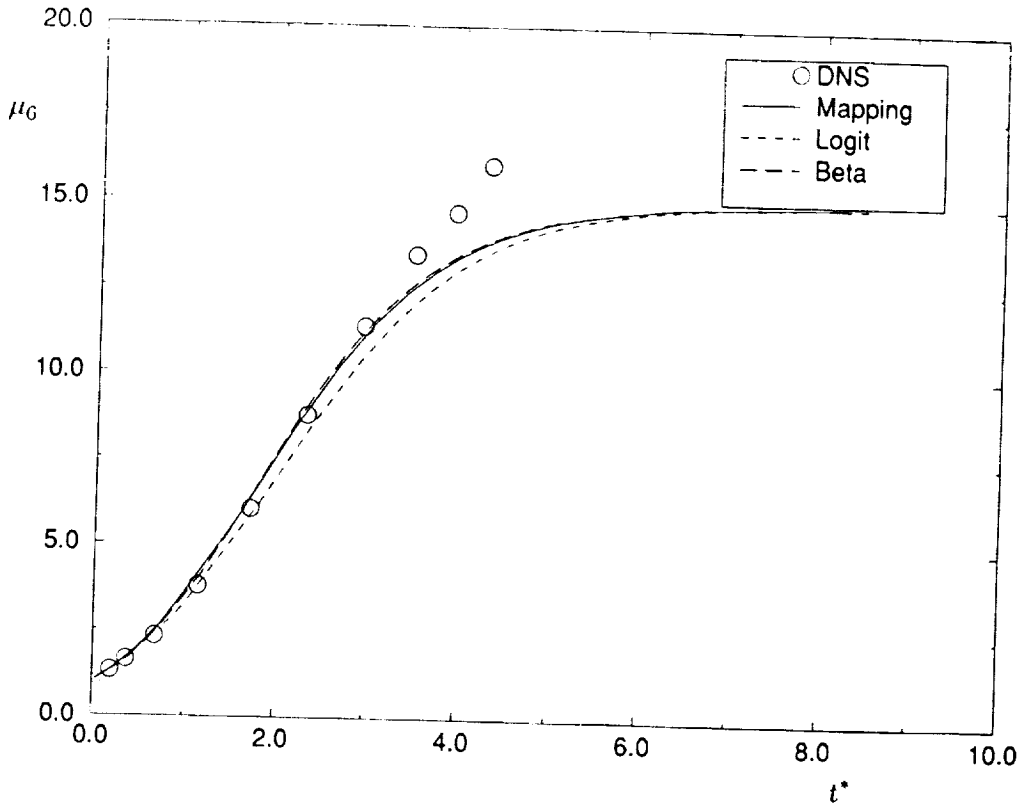

FIGURE 3b Temporal evolution of the centralized moments of the scalar variable as predicted by the models and the comparison with DNS data. (b) μ_6 vs. t*.

appropriate ϕ_u, ϕ_ℓ for comparison to each of the models. At time zero, in most regions of the flow, the scalar adopts these limiting values (with equal probability), and the spatial regions between the initial maxima and minima are smoothed by a polynomial fit. The degree of this smoothing is minimized, but limited by the computational resolution, to ensure an approximate initial double delta distribution. The computational scheme is based on a spectral-collocation procedure using Fourier basis functions developed by Erlebacher *et al.* (1990a); Erlebacher *et al.* (1987); Erlebacher *et al.* (1990b). The hydrodynamic field is assumed isotropic and is initialized in a similar manner to that by Erlebacher *et al.* (1990a); Passot and Pouquet (1987). The code is capable of simulating flows with different levels of compressibility (Hussaini *et al.*, 1990). Here, only the results obtained for a low compressible case are discussed. The resolution consists of 96 collocation points in each direction. Therefore, at each time step 96^3 is the sample size for statistical analysis. With this resolution, simulations with a Reynolds number (based on the Taylor microscale) of $Re_\lambda \approx 41$ are attainable. The value of the molecular Schmidt number is set equal to unity.

As indicated in Section 1, in order to compare the model predictions with DNS results a matching is required of the higher order statistics of the field as generated by each method. Here, this matching is done through the variance of the conserved scalar. These results are presented in Fig. 1. This figure indicates that at initial times, $\frac{\sigma^2(t)}{\sigma^2(0)} \approx 1$, all the PDF's are approximately composed of two delta functions at $\phi = 0,1$ indicating the initial binary state. At longer times, the PDF's evolve through an inverse-like diffusion in the composition space. The heights of the delta functions decrease and the PDF's are redistributed at other ϕ values within the range [0,1]. At very long times, the PDF's

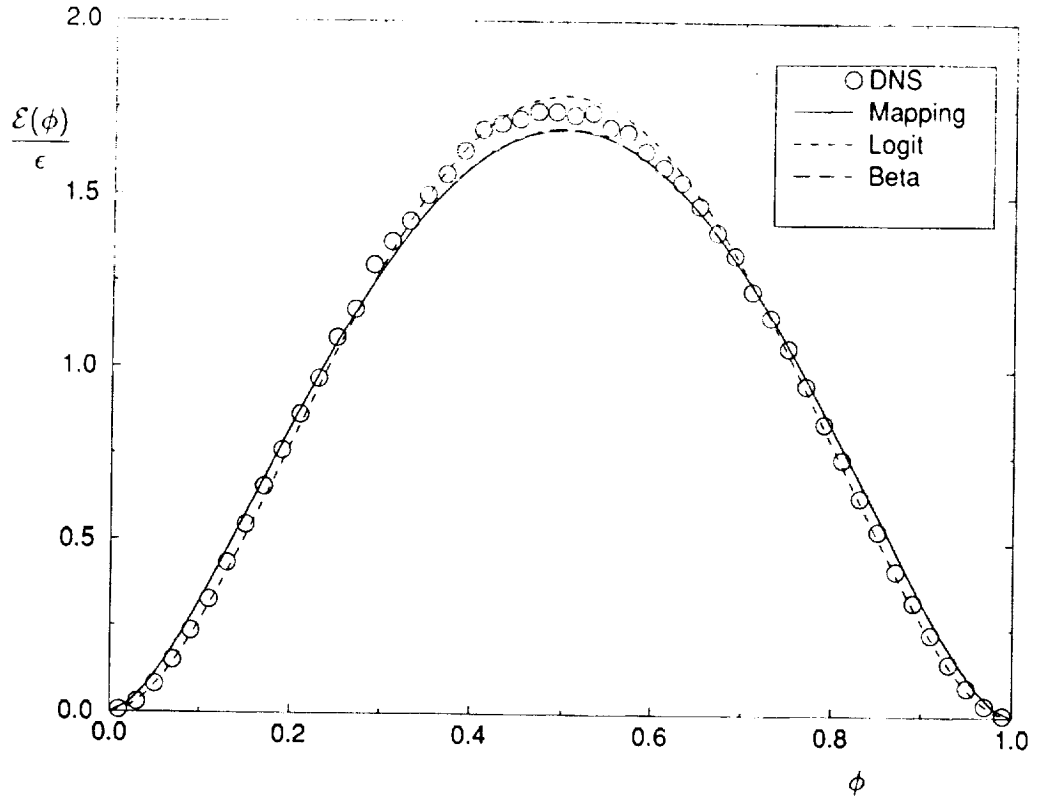

FIGURE 4a Comparisons of the normalized conditional dissipation as predicted by the three models with the DNS data. (a) $\sigma^2 = 0.079$.

become asymptotically concentrated around the mean value in a manner that can be approximated by a Gaussian distribution.

An interesting feature captured in Fig. 1(b), is the capability of the Logit-Normal distribution in depicting a subtle behavior in the frequency distribution. This feature is the double "hump" characteristic of the DNS data at intermediate times and cannot be realized by the AMC or the PF generated frequencies. All the previous DNS results including those of Eswaran and Pope (1988); Givi and McMurtry (1988); Pope (1991) portray this feature. The PDF's generated by the AMC, and the Beta distributions adopt a constant value (of 1/2) when $\sigma^2 = \frac{1}{12}$ (for $0 \leq \phi \leq 1$). This corresponds to $G = 1, \gamma = \sqrt{2}, \beta = 1$. This uniform distribution is not exactly realized in any previous or present DNS results. Therefore, it can be speculated that in the absence of a better alternative, the Logit-Normal distribution may provide the simplest means of providing an *assumed* distribution for the statistical modeling of the symmetric binary mixing problem. The complete evolution of the Logit-Normal PDF is shown in Fig. 2.

Further quantification of the agreements noted above are made by comparing the higher moments of the scalar field. This comparison is made in Fig. 3. In this figure, results are presented for the temporal variations of the kurtosis (μ_4) and the superskewness (μ_6) of the scalar variable ϕ. For the Beta density, the higher order moments are obtained analytically based on the knowledge of the variance. For the AMC, the analytical-numerical results by Jiang *et al.* (1992) are used, while for the Logit-Normal PDF the moments are calculated strictly by numerical means. This figure shows that initially, all these moments are close to unity, and monotonically increase as mixing proceeds. For all the models, the magnitude of the moments asymptotically approach the limiting values of 3 and 15, respectively, corresponding to those of a Gaussian distribution. The DNS

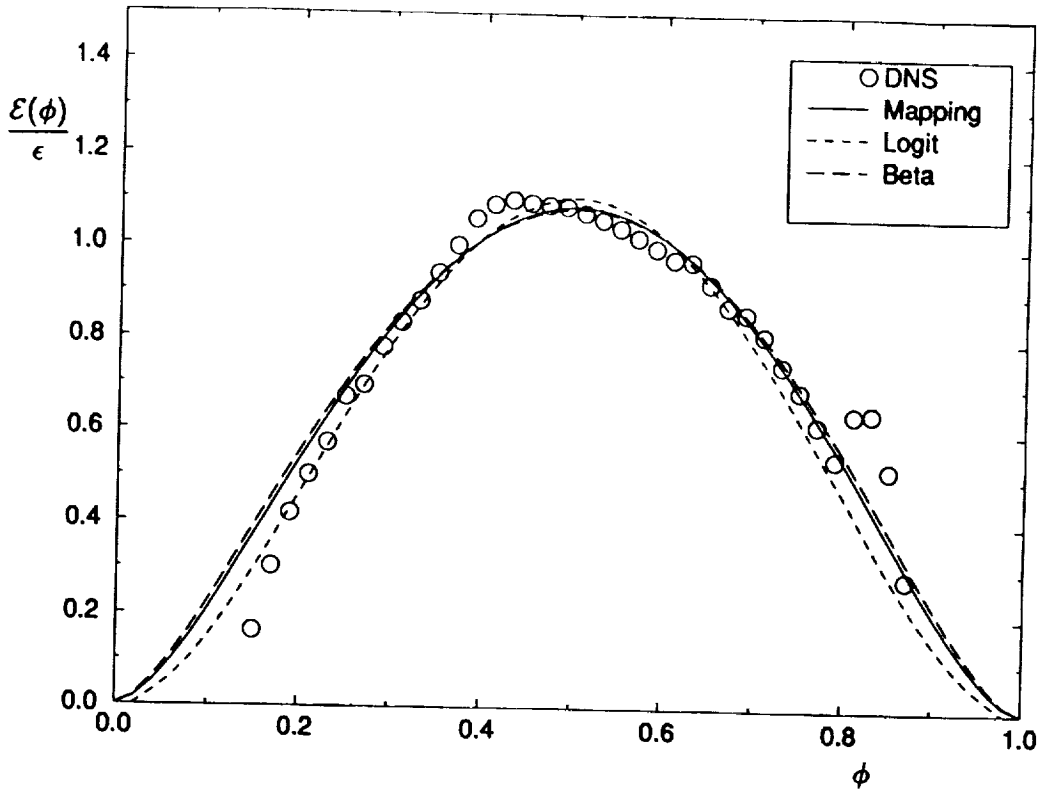

FIGURE 4b Comparisons of the normalized conditional dissipation as predicted by the three models with the DNS data. (b) $\sigma^2 = 0.013$.

results are in good agreement with the model predictions at all times. However, due to obvious numerical difficulties, the simulations could not be continued until the variance approaches zero identically.

5 SCALAR DISSIPATION

The results presented above indicate a good agreement between the model predicted single-point statistics (PDF's and high-order moments) and the DNS data at all the stages of mixing. These results also suggest an approximate asymptotic Gaussian state for all the closure PDF's and those of the DNS. Here, it will be demonstrated that the agreement between the DNS and the model predictions is very good at the initial and the intermediate stages of mixing. However, the agreement worsens at the final stages. Also it will be shown that none of the closures yield "exact" Gaussian distributions at the final stages of mixing. In doing so, it is useful to note that a Gaussian PDF is defined, and is only valid, for an unbounded domain. The frequencies generated here, are all defined within a *fixed and finite* domain. For AMC, it has been established (Gao, 1991; O'Brien and Jiang, 1991) that the finite boundary size at the initial time "maintains" its influence at *all* the subsequent stages of mixing. In other words, the PDF adopts a Gaussian distribution in the limit of zero variance only near the mean value of the scalar. In order to show the departure from Gaussianity at scalar values away from the mean, the conditional expected dissipation of the scalar field is considered.

Given the PDF, as is the case here, Eq. (3) can be used to determine the expected conditional dissipation. It has been shown by Girimaji (1992) (and will be discussed in

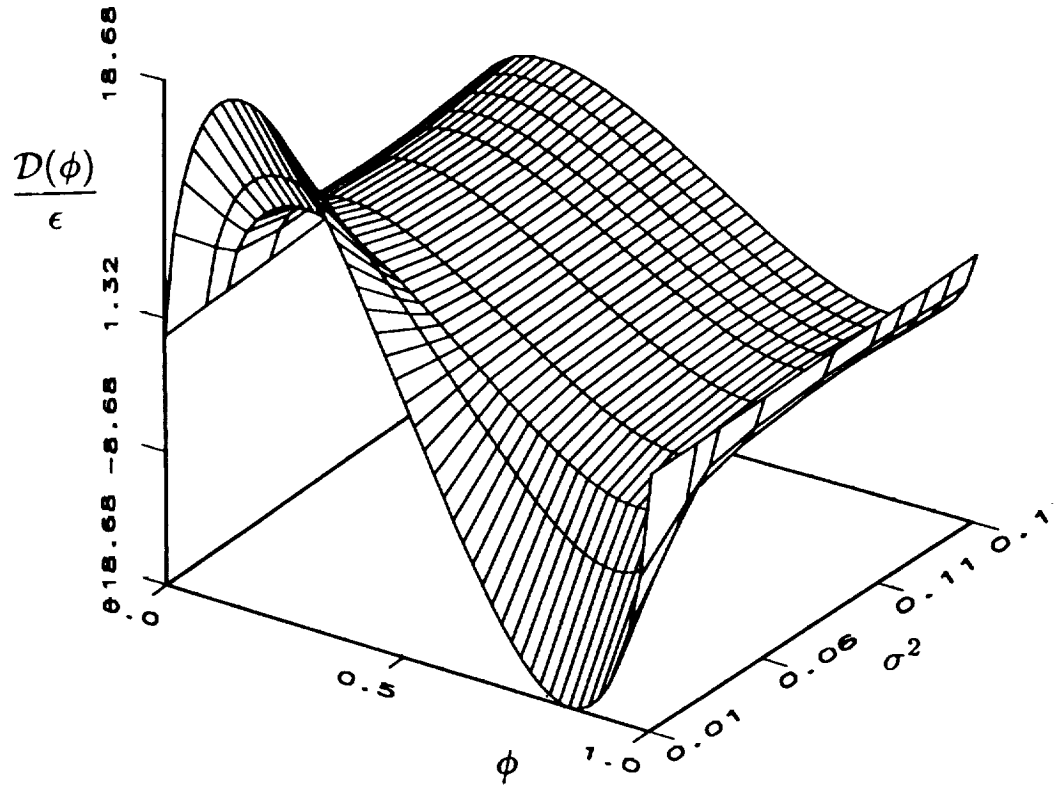

FIGURE 5a Temporal evolution of the conditional expected diffusion normalized with the total dissipation. (a) erf^{-1}-Normal.

detail in Section 7) that for a valid PDF within a defined range, $-\phi_u \leq \phi \leq \phi_u$, the expected conditional scalar dissipation is given by

$$\varepsilon(\phi,t) = -\frac{1}{P_1(\phi,t)}\frac{\partial}{\partial t}\left(\int_{-\phi_u}^{\phi} F(\psi,t)d\psi\right), \tag{21}$$

where F denotes the cumulative distribution function (CDF)

$$F(\phi,t) = \int_{-\phi u}^{\phi} P_1(\psi,t)d\psi. \tag{22}$$

With Eq. (21), the expected conditional dissipation can be evaluated for a given PDF. For example, for a Gaussian distribution of zero mean, $P_G(\phi,\sigma^2) = \frac{1}{\sqrt{2\pi}\sigma}\exp(-\frac{\phi^2}{2\sigma^2})$, $-\infty = -\phi_u \leq \phi \leq \phi_u = \infty$, with a non-stationary variance, $\sigma^2 = \sigma^2(t)$, it is easily shown that,

$$\varepsilon(\phi,t) = \left[\frac{1}{P_G(\phi,\sigma^2)}\right]\frac{\partial}{\partial t}\left(\frac{\phi}{2} + \frac{\phi}{2}\text{erf}(\frac{\phi}{\sqrt{2}\sigma}) + \frac{\sigma}{\sqrt{2\pi}}\exp(-\frac{\phi^2}{2\sigma^2})\right), -\infty \leq \phi \leq \infty \tag{23}$$

Noting that ϕ is an independent variable (of t), and evaluating the derivatives on the RHS of Eq. (23) yields, after some simple manipulations,

$$\varepsilon(\phi,t) = \text{constant} = -\sigma\frac{d\sigma}{dt}, \tag{24}$$

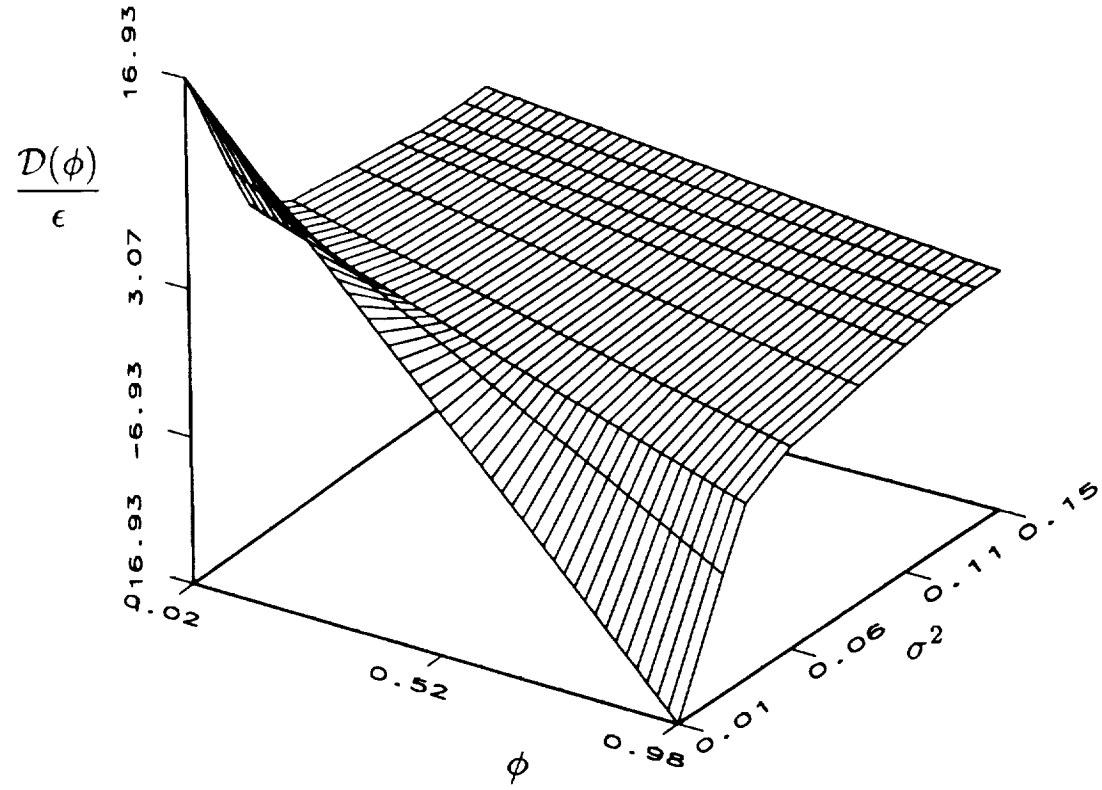

FIGURE 5b Temporal evolution of the conditional expected diffusion normalized with the total dissipation. (b) LMSE.

with the implications (derived from Eqs. (12)-(13)),

$$\frac{\varepsilon(\phi, t)}{\epsilon(t)} = \text{constant} = 1, \tag{25}$$

at all times for *all* ϕ values in the range $-\infty$ to $+\infty$. Equations (24-25) indicate the independence of the conditional scalar dissipation and the composition domain for a Gaussian field. These results have also been obtained by Gao (1991); O'Brien and Jiang (1991) by following a different mathematical procedure.

The conditional expected dissipation predicted by the models can be obtained by following a similar course. For the AMC and the PF distribution, the conditional dissipation fields have been obtained by Gao (1991); O'Brien and Jiang (1991) and by Girimaji (1992), respectively. For the purpose of the discussions to follow, these results are presented here in a different form for all three closures. For the erf^{-1}-Normal distribution, the instantaneous CDF is given by

$$F(\phi, t) = \frac{1}{2}\left(1 + \text{erf}\left[\frac{\gamma}{\sqrt{2}}\text{erf}^{-1}\left(\frac{\phi}{\phi_u}\right)\right]\right). \tag{26}$$

Therefore, with Eq. (21), the conditional dissipation can be expressed in terms of the corresponding PDF,

$$\varepsilon(\phi, t) = -\frac{1}{P_1(\phi, t)}\frac{\partial}{\partial t}\left\{\frac{1}{2}\int_{-\phi_u}^{\phi} \text{erf}\left[\frac{\gamma}{\sqrt{2}}\text{erf}^{-1}\left(\frac{\phi}{\phi_u}\right)\right] d\phi + \frac{1}{2}(\phi + \phi_u)\right\}. \tag{27}$$

Again, with an independence of ϕ and t this equation reduces to,

$$\varepsilon(\phi, t) = -\frac{1}{P_1(\phi, t)} \frac{\partial H}{\partial t}, \tag{28}$$

where,

$$H = \frac{\phi_u}{\sqrt{\pi}} \int_{-\phi_u}^{\mathrm{erf}^{-1}(\frac{\phi}{\phi_u})} \mathrm{erf}(\frac{\gamma}{\sqrt{2}} z) \exp(-z^2) dz. \tag{29}$$

For a PDF within a fixed domain, the integration procedure becomes simplified by evaluating the time derivatives inside the integral. In this way, the results can be expressed analytically. After some manipulations,

$$\frac{dH}{dt} = \frac{-\sqrt{2}\phi_u \frac{d\gamma}{dt}}{\pi(2+\gamma^2)} \exp\left\{-(1+\frac{\gamma^2}{2})\left[\mathrm{erf}^{-1}(\frac{\phi}{\phi_u})\right]^2\right\}, \tag{30}$$

and, therefore

$$\varepsilon(\phi, t) = \frac{4\phi_u^2 \frac{d\gamma}{dt}}{\pi\gamma(2+\gamma^2)} \exp\left\{-2\left[\mathrm{erf}^{-1}(\frac{\phi}{\phi_u})\right]^2\right\}. \tag{31}$$

From this equation, the total dissipation is obtained by direct integration of the conditional mean dissipation field. The results, after significant algebraic manipulations yield

$$\epsilon(t) = \frac{4\phi_u^2 \frac{d\gamma}{dt}}{\pi(2+\gamma^2)\sqrt{4+\gamma^2}}, \tag{32}$$

$$\frac{\varepsilon(\phi, t)}{\epsilon(t)} = \left(\sqrt{\frac{1+\sin\left[\frac{\pi\sigma^2(t)}{2\sigma^2(0)}\right]}{1-\sin\left[\frac{\pi\sigma^2(t)}{2\sigma^2(0)}\right]}}\right) \exp\left\{-2\left[\mathrm{erf}^{-1}(\frac{\phi}{\phi_u})\right]^2\right\}. \tag{33}$$

In the form presented above, Eqs. (31)-(33) portray several insightful features of the solution. First, Eq. (33) indicates that the conditional dissipation is always dependent on the magnitude of the scalar, and it maintains the same self-similar functional form of dependence $\exp\left\{-2\left[\mathrm{erf}^{-1}(\frac{\phi}{\phi_u})\right]^2\right\}$. This has been previously indicated by Gao (1991); O'Brien and Jiang (1991). Here, the amplitude $\varepsilon(\phi = 0, t)$ can be conveniently expressed in terms of the variance decay, which is very useful for further manipulations. Second, it is interesting to note the similarity of Eqs. (31) and (33) with the results obtained for the instantaneous dissipation of Fickian mixing of a conserved scalar in laminar non-homogeneous flows (such as the typical shear flows (Spalding, 1961; Liñan, 1974; Peters, 1984)). This similarity further asserts the "permanent" influence of the boundaries since in non-homogeneous mixing, the scalar bounds are "fixed" due to the physical constraints. Finally, Eq. (32) suggests an infinitely large dissipation at time zero, *i.e.* when $\sigma^2(t)/\sigma^2(0) = 1$, and the asymptotic behavior

$$\mathrm{Lim}_{(\sigma^2 \to 0)} \frac{\varepsilon(\phi)}{\epsilon}|_{\phi=0} = 1. \tag{34}$$

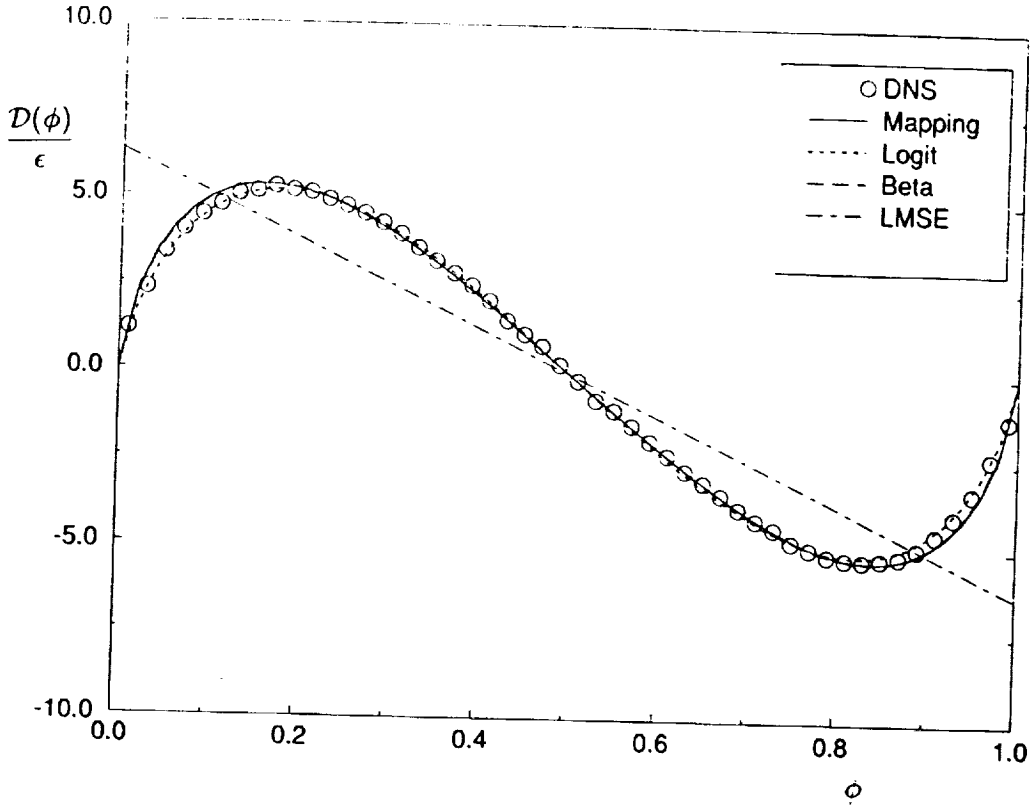

FIGURE 6a Comparisons of the normalized conditional diffusion as predicted by the three models and the LMSE closure, with the DNS data. (a) $\sigma^2 = 0.079$.

This limiting behavior near zero indicates the Gaussianity of the PDF only at the mean value of the scalar.

Following a similar procedure, the conditional expected dissipation can be obtained for the other closures. For the Beta density in the range $0 \leq \phi \leq 1$, the final results can be expressed as

$$\varepsilon(\phi,t) = -\frac{1}{P_1(\phi,t)}\frac{\partial}{\partial t}\left(\int_0^{\phi} I_{\phi}(\beta,\beta)d\phi\right), \tag{35}$$

where, I denotes the Incomplete Beta Function (Abramowitz and Stegun, 1972). For the Logit-Normal distribution, the corresponding form is

$$\varepsilon(\phi,t) = -\frac{1}{P_1(\phi,t)}\frac{\partial}{\partial t}\left\{\frac{1}{2}\int_{-\phi_u}^{\phi} \mathrm{erf}\left[\frac{\gamma}{\sqrt{2}}\ln\left(\frac{1+\frac{\phi}{\phi_u}}{1-\frac{\phi}{\phi_u}}\right)\right]d\phi\right\}. \tag{36}$$

Neither of the equations (35-36) can be simplified further. Therefore, in order to evaluate the conditional expected dissipation (and the total dissipation), these equations must be evaluated numerically.

In Fig. 4, the evolution of the conditional expected dissipation (normalized by the total dissipation) is presented for the models and the DNS data. This figure shows the similarity of the conditional expected dissipation for all of the models. The bell shape distribution is evident in all the figures with a maximum amplitude near the mean value. Also, as the variance decreases and the PDF becomes concentrated near the mean, the

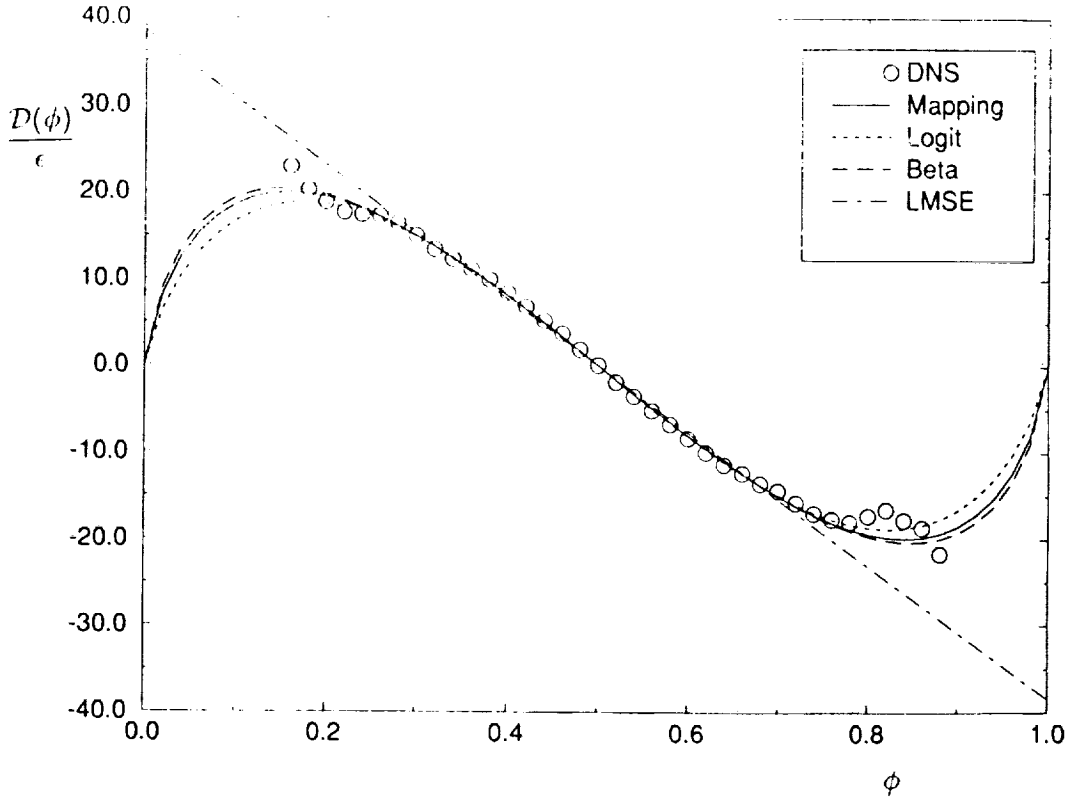

FIGURE 6b Comparisons of the normalized conditional diffusion as predicted by the three models and the LMSE closure, with the DNS data. (b) $\sigma^2 = 0.013$.

amplitude tends to unity. This shape is typical of that observed in previous DNS results of Eswaran and Pope (1988); Nomura and Elgobashi (1992).

The results in Fig. 4 show the ϕ dependency of the results at *all* the stages of mixing. That is, the PDF asymptotically adopts an apparent Gaussian-like distribution only near the mean value of the scalar, and the conditional dissipation does not become independent of the scalar everywhere. For the AMC, this has been discussed by Gao (1991); O'Brien and Jiang (1991). Considering the similarity of the three models, it is therefore concluded that all three models yield the same characteristics. These results also suggest a poor agreement between the model predicted conditional expected dissipations and the DNS data. Note that at the initial stages of mixing, the predicted results compare well with DNS data. However, with mixing progression, at smaller variance values, the agreement is only good near the mean scalar value and worsens near the bounds of the composition domain. This, as described above, is due to the permanent influence of the scalar boundaries at all the stages of mixing.

6 SCALAR DIFFUSION

Albeit directly related to the conditional expected dissipation (Eq. 7), it is useful to examine the behavior of the conditional expected diffusion in light of the discussions above. Given the PDF, again within the fixed range $-\phi_u \leq \phi \leq \phi_u$, the conditional expected diffusion can be determined from

$$D(\phi, t) = -\frac{1}{P_1(\phi, t)} \frac{\partial F}{\partial t}. \tag{37}$$

This equation is very useful in illustrating the properties of the PDF. For example, for a Gaussian distribution within an infinite domain

$$\frac{\partial F}{\partial t} = -\frac{\phi}{\sqrt{2\pi\sigma^2}} \frac{d\sigma^2}{dt} \exp(-\frac{\phi^2}{2\sigma^2}), \tag{38}$$

and consequently

$$\frac{D(\phi,t)}{\epsilon(t)} = \frac{-\phi}{\sigma^2(t)}. \tag{39}$$

It is noted that Eq. (39) is in accord with the Linear Mean Square Estimation (LMSE) closure (O'Brien, 1980).

The mean conditional diffusion can be determined for the three models considered. For the erf^{-1}-Normal PDF with zero mean

$$\frac{\partial F}{\partial t} = \frac{1}{\sqrt{2\pi}} \frac{d\gamma}{dt} \exp\left\{-\frac{\gamma^2}{2}\left[\mathrm{erf}^{-1}(\frac{\phi}{\phi_u})\right]^2\right\} \mathrm{erf}^{-1}(\frac{\phi}{\phi_u}) \tag{40}$$

Again with explicit equations for the total dissipation and the variance, it is possible to obtain an algebraic expression for the conditional expected diffusion. The results after substantial algebraic manipulations yield

$$\frac{D(\phi,t)}{\epsilon(t)} = \left(\frac{-\sqrt{\pi}}{\sin\left[\frac{\pi\sigma^2(t)}{2\sigma^2(0)}\right]} \sqrt{\frac{1+\sin\left[\frac{\pi\sigma^2(t)}{2\sigma^2(0)}\right]}{1-\sin\left[\frac{\pi\sigma^2(t)}{2\sigma^2(0)}\right]}}\right) \exp\left\{-\left[\mathrm{erf}^{-1}(\frac{\phi}{\phi_u})\right]^2\right\} \mathrm{erf}^{-1}(\frac{\phi}{\phi_u}). \tag{41}$$

In this form Eq. (41) is very pleasing since it does reveal the (t,ϕ) separability, and thus the self-similarity, of the diffusion field. The terms inside the parenthesis on the RHS are time dependent, whereas the remaining terms depend explicitly on ϕ only. As indicated by O'Brien and Jiang (1991), this separability cannot be easily deduced from Eq. (5), but is possible with the analytical procedure followed above. The temporal evolution of the conditional expected diffusion for the erf^{-1}-Normal distribution, and its comparison with that of the LMSE closure is presented in Fig. 5.

By following the procedure above, analogous expressions are obtained for the other two closures. Namely,

$$\frac{D(\phi,t)}{\epsilon(t)} = \frac{2\phi_u}{\gamma} \frac{d\gamma}{d\sigma^2} \left[1-\left(\frac{\phi}{\phi_u}\right)^2\right] \tanh^{-1}(\frac{\phi}{\phi_u}), \tag{42}$$

for the Logit-Normal distribution of zero mean, and

$$\frac{D(\phi,t)}{\epsilon(t)} = \frac{2}{P_1(\phi,t)} \frac{\partial I_\phi(\beta,\beta)}{\partial\sigma^2} \tag{43}$$

for the symmetric Beta density within [0,1]. Equations (42)-(43) cannot be simplified further due to the lack of an explicit analytical relation for the variance of the Logit-Normal distribution (Johnson, 1949a), and the unknown analytical form of the derivatives of the Incomplete Beta Function.

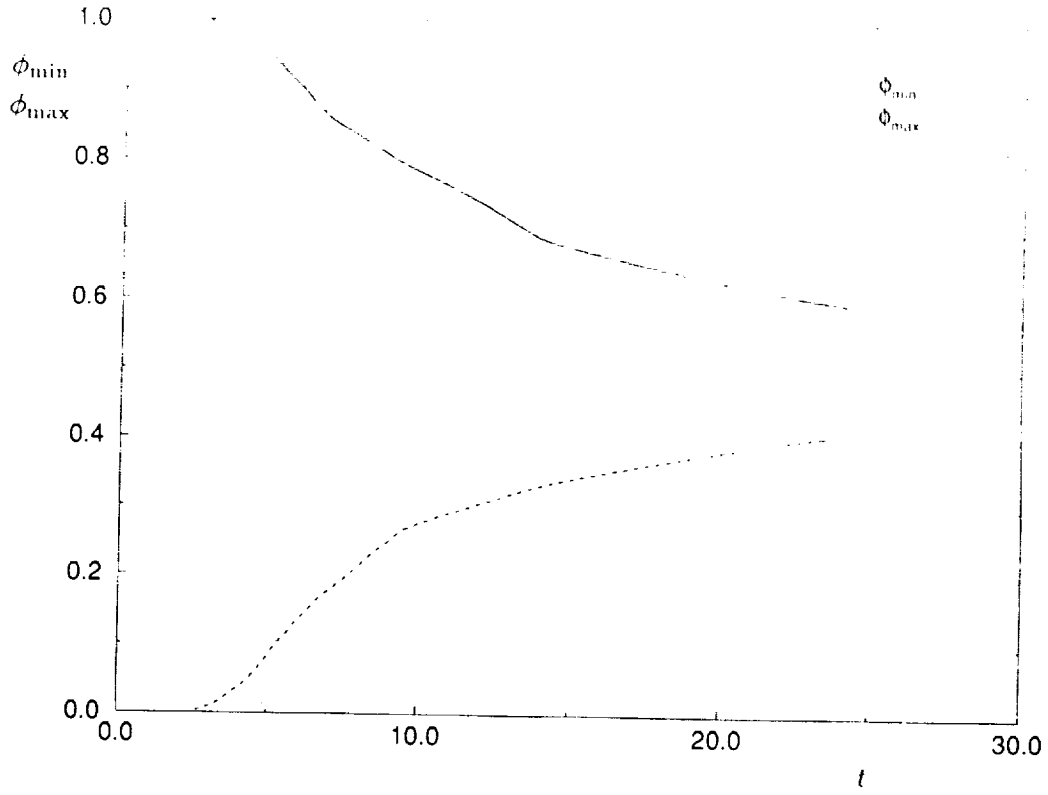

FIGURE 7 The temporal variations of ϕ_{max} and ϕ_{min} generated by DNS.

In Fig. 6, results are presented of the conditional expected diffusion as predicted by the three models, and also that of the LMSE closure. In these figures, the DNS data are also provided at several variance values. The similarity of the modelled results are once again revealed in these figures, which is expected in view of the PDF similarities. At all times, the conditional diffusion field has an odd distribution near the mean scalar value. On the right half of the composition domain, all three closures yield a monotonic decrease of D to an instantaneous minimum, and then a monotonic increase to zero at the upper bound of the scalar. The location and the magnitude of the instantaneous maxima and minima is not the same for the three closures. Also, as Eqs. (41)-(43) indicate, the zeroes of D can only be realized at $\phi = 0, \pm\phi_u$. At the initial times, *i.e.* large variances, all three closures agree reasonably well with the DNS data. This agreement is better for the three models than for the LMSE closure. However, as the variance becomes smaller, the agreement between the model predictions and the DNS data worsens. It is noted that as the variance becomes small, all the closures yield a Gaussian-like PDF near the mean value of the scalar. This is shown in the figures near $\phi =< \phi >$ ($= \frac{1}{2}$ for DNS), where the predicted results are in accord with the LMSE closure, *i.e.* linear profiles of similar slopes. In this region, the results are also in accord with DNS data for all the closures including the LMSE. However, again, the predicted results deviate from the DNS data away from the mean value. It is clearly noted that the DNS generated D values do not go to zero at the scalar bounds.

7 EVOLUTION OF THE SCALAR FIELD

The problems described at the conclusion of the previous two sections stem from a lack of capability of all of the models in accounting for the variations of the scalar

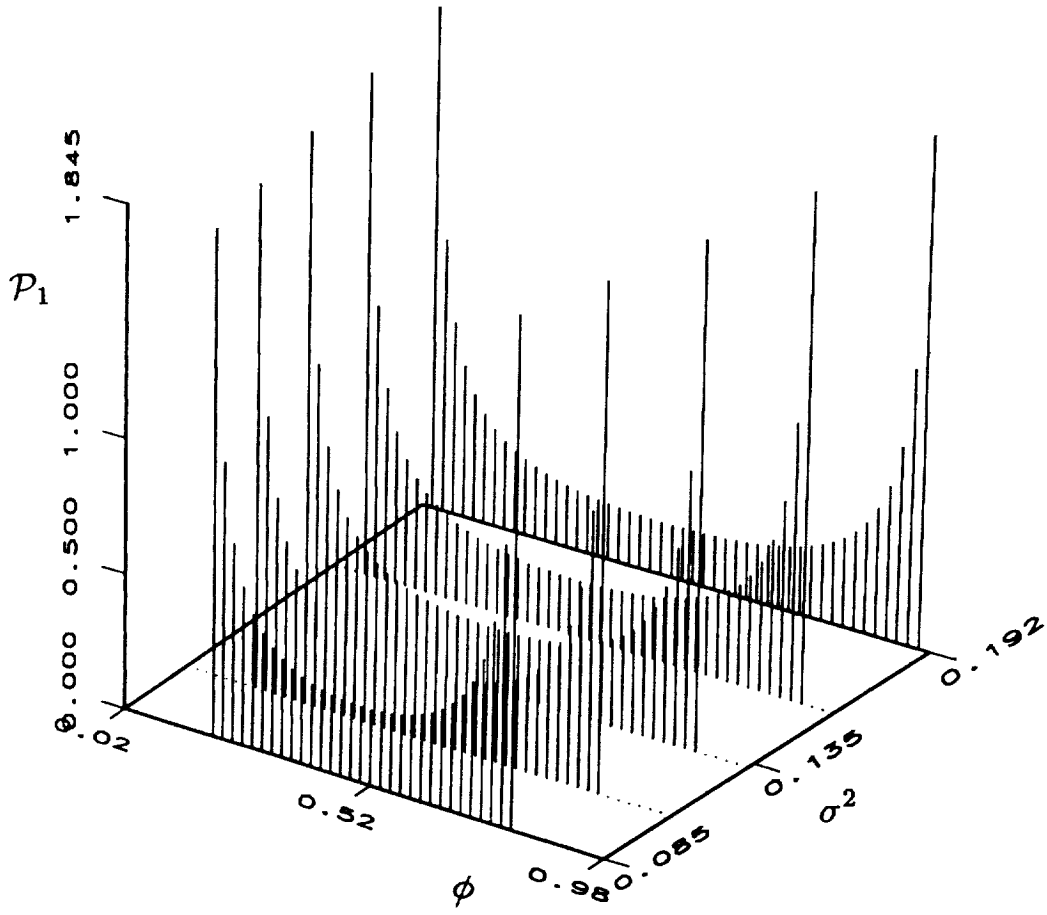

FIGURE 8 The Beta density (Pearson Type II) for a domain with moving boundaries, and $\beta = 0.1$.

bounds as the mixing proceeds. For all three models, the PDF is always *defined* within a fixed range through its course of evolution. It is easy to show that both the conditional expected dissipation and the conditional expected diffusion are correctly predicted by all the models near the mean scalar value. For the erf^{-1}-Normal distribution, this is evident from Eqs. (33) and (41) and can be also shown by analyzing the behavior of Eq. (31) near the region $\phi \approx 0$, as the variance becomes small. Noting that

$$\text{Lim}_{(\phi \approx 0)} \quad \text{erf}\left(\frac{\phi}{\phi_u}\right) \approx \frac{\sqrt{\pi}}{2}\frac{\phi}{\phi_u} \tag{44}$$

and, from Eq. (11)

$$\text{Lim}_{(\sigma^2 \to 0)} \quad \frac{d\gamma}{dt} = \frac{-2\phi_u}{\sqrt{\pi}\sigma^2}\frac{d\sigma}{dt}, \tag{45}$$

it is easily concluded that

$$\text{Lim}_{(t \to \infty)} \quad \varepsilon(\phi \approx 0, t) = -\sigma\frac{d\sigma}{dt}. \tag{46}$$

Following the same procedure, it is derived

$$\mathrm{Lim}_{(t\to\infty)} \quad D(\phi \approx 0, t) = -\frac{\epsilon}{\sigma^2}\phi. \tag{47}$$

Due to the similarity of the three closures, it is reasonable to expect similar behaviors for the other models as well. Equations (46)-(47) indicate a Gaussian-like distribution near the mean $\phi \approx 0$ (Eqs. (24,39)). This is in accord with the DNS data. However, at distances away from the mean value the predicted results do not correspond to that of a Gaussian field. Neither do these results agree well with DNS data. The deficiency of the models in predicting the DNS results is made clear by considering the bounds of the scalar field as the mixing proceeds. This is demonstrated in Fig. 7, showing the temporal decay/growth of the scalar maxima/minima obtained by DNS. This trend is consistent with physical intuition, but is not incorporated into any of the three models. In the AMC and the JET generated frequencies, due to the nature of the translation $Z(\phi_0, t)$ and the constraints imposed by Eq. (15), the scalar is always bounded within the same range. This problem is also encountered in the PF, in that Type I and II distribution families are always defined within the same fixed domain regardless of the magnitude of the variance.

With the examination of the PDF transport equation, it is shown that the physics of the problem requires the migration of the scalar bounds toward the mean value as the mixing proceeds. That is, the instantaneous values of the scalar minima and maxima change with mixing progression. To demonstrate this, again consider a symmetric field with a PDF, $P_1(\phi, t)$, defined within the *time-dependent* domain of zero mean, $\phi\epsilon[\phi_{\min}(t) = -\phi_{\max}(t), \phi_{\max}(t)]$. At all the stages of the evolution, the PDF must satisfy the physical requirements

$$\begin{aligned}
&\int_{\phi_{\min}(t)}^{\phi_{\max}(t)} P_1(\phi, t)d\phi = 1,\\
&<\phi>= \int_{\phi_{\min}(t)}^{\phi_{\max}(t)} \phi P_1(\phi, t)d\phi = 0,\\
&\sigma^2(t) = \int_{\phi_{\min}(t)}^{\phi_{\max}(t)} \phi^2 P_1(\phi, t)d\phi,\\
&\vdots
\end{aligned} \tag{48}$$

The first of Eq. (48) requires

$$\frac{d}{dt}\int_{\phi_{\min}(t)}^{\phi_{\max}(t)} P_1(\phi, t)d\phi = 0 \tag{49}$$

Evaluating this integral via Leibnitz's rule, and making use of Eqs. (3)-(7), it is shown that

$$P_1(\phi_{\max}(t), t)\frac{d\phi_{\max}}{dt} = -P_1(\phi_{\min}(t), t)\frac{d\phi_{\min}}{dt} = \left\{\frac{\partial}{\partial\phi}[\epsilon(\phi, t)P_1(\phi, t)]\right\}_{\phi=\phi_u}$$

$$P_1(\phi_{\max}(t), t)\left[\frac{d\phi_{\max}}{dt} - D(\phi_{\max}(t), t)\right] = P_1(\phi_{\min}(t), t)\left[\frac{d\phi_{\min}}{dt} - D(\phi_{\min}(t), t)\right] = 0,$$

$$\phi_{\max}(0) = \phi_u, \quad \phi_{\min}(0) = \phi_\ell = -\phi_u. \tag{50}$$

Following the same procedure for the second of Eq. (48), yields the obvious requirement

$$\int_{\phi_{\min}(t)}^{\phi_{\max}(t)} D(\phi, t) P_1(\phi, t) d\phi = 0. \tag{51}$$

The third part of Eq. (48) yields Eq. (12), and

$$P_1(\phi_{\max}(t), t)\varepsilon(\phi_{\max}(t), t) = P_1(\phi_{\min}(t), t)\varepsilon(\phi_{\min}(t), t) = 0,$$

$$P_1(\phi_{\max}(t), t)\left[\frac{d\phi_{\max}}{dt} - D(\phi_{\max}(t), t)\right] =$$

$$-P_1(\phi_{\min}(t), t)\left[\frac{d\phi_{\min}}{dt} - D(\phi_{\min}(t), t)\right] = 0. \tag{52}$$

The remaining parts of Eq. (48) yield higher order statistical information pertaining to the inner integrated evolution of the conditional expected dissipation and diffusion, and their relation with the higher central moments. With an additional assumption of a nonzero PDF within the region of its definition, that is by defining $\phi_{\max}(t)$ and $\phi_{\min}(t)$ as the extreme locations with nonzero PDF, a combination of Eqs. (50) and (52) yields

$$\varepsilon(\phi_{\max}(t), t) = \varepsilon(\phi_{\min}(t), t) = 0,$$

$$\frac{d\phi_{\max}}{dt} = \frac{\partial \varepsilon}{\partial \phi}|\phi_{\max} = D(\phi_{\max}(t), t),$$

$$\frac{d\phi_{\min}}{dt} = \frac{\partial \varepsilon}{\partial \phi}|\phi_{\min} = D(\phi_{\min}(t), t),$$

$$\phi_{\max}(0) = \phi_u, \phi_{\min}(0) = \phi_\ell. \tag{53}$$

Equation (53) indicates that with fixed boundaries, the conditional dissipation would adopt a zero slope at the boundaries and the conditional diffusion would also be zero there. However, Fig. 7 indicates that in a physical situation the boundaries are not fixed and move inwards as the mixing proceeds. It is interesting to note that this problem is not observed in the numerical results obtained by the C/D type closures. That is, while the C/D closures are not capable of predicting the PDF evolution in accord with DNS data, they do have the mechanism for shrinking the bounds of the composition space. Obviously, in the context of single-point description without the knowledge of the dissipation field, it is not possible to determine *a priori* the temporal bounds of the scalar field. Therefore, the closures can be modified only by making further assumptions in describing this transport. For a general case, the JET frequencies can be generated by the original form proposed by Johnson (1949a)

$$\phi(\phi_0, t) = \lambda(t) z\left(\frac{\phi_0}{\gamma(t)}\right) + \varrho(t), \tag{54}$$

where the additional parameters $\lambda(t)$ and $\varrho(t)$ provide the extra degrees of freedom in order to account for the variations of the instantaneous boundaries of the composition domain. For the PF, the problem can be overcome, for example, by considering a "four-parameter Beta distribution"

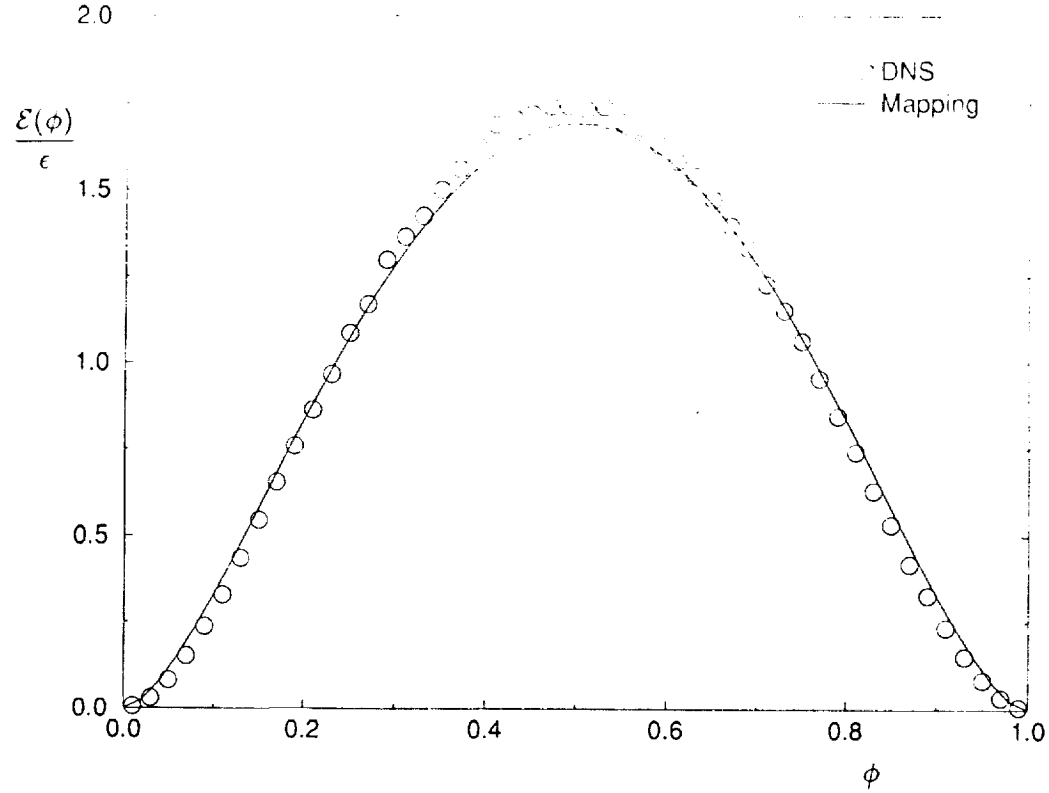

FIGURE 9a The comparison of the conditional expected scalar dissipation normalized with the total dissipation with DNS data as predicted by the AMC with the scalar bounds determined from the DNS results. (a) $\sigma^2 = 0.079$.

$$P_1(\phi,t) = \frac{1}{[\phi_{\max}(t) - \phi_{\min}(t)]B(\beta_1,\beta_2)} \left(\frac{\phi - \phi_{\min}(t)}{\phi_{\max}(t) - \phi_{\min}(t)}\right)^{\beta_1 - 1} \left(1 - \frac{\phi - \phi_{\min}(t)}{\phi_{\max}(t) - \phi_{\min}(t)}\right)^{\beta_2 - 1}, \quad \phi_{\min}(t) \le \phi \le \phi_{\max}(t), \tag{55}$$

with the extra two parameters being $\phi_{\min}(t)$ and $\phi_{\max}(t)$. For a symmetric PDF in the range $[0,1] \equiv [\phi_{\min}(t=0) = \phi_\ell, \phi_{\max}(t=0) = \phi_u]$; therefore, the variance decay can be influenced by increasing β, and/or by decreasing the scalar range $\Delta\phi(t) = \phi_{\max}(t) - \phi_{\min}(t)$. The former recovers the well-known two-parameter Beta distribution (Pearson Type II), while the latter is approximately equivalent to the LMSE closure (O'Brien, 1980). This latter case is presented in Fig. 8 showing a symmetric Beta density with $\beta(t) =$ fixed $= 0.1$. Note that as the mixing proceeds, the variance decays but the PDF preserves its initial approximate double delta shape. In a physical problem, the situation is somewhere between these two limiting cases. The exact situation depends on the characteristics of a particular mixing problem.

The discussions above suggest that in order to predict the final stage of mixing correctly, the effects of mixing on the shrinkage of the domain must be taken into account. To demonstrate this point, the results shown in Fig. 7 can be incorporated into the mixing models to determine the evolution of the conditional expected dissipation and diffusion. This is done here only for the erf^{-1}-Normal, and the results of the conditional expected dissipation are shown in Fig. 9. In the calculations resulting in this figure, analytical

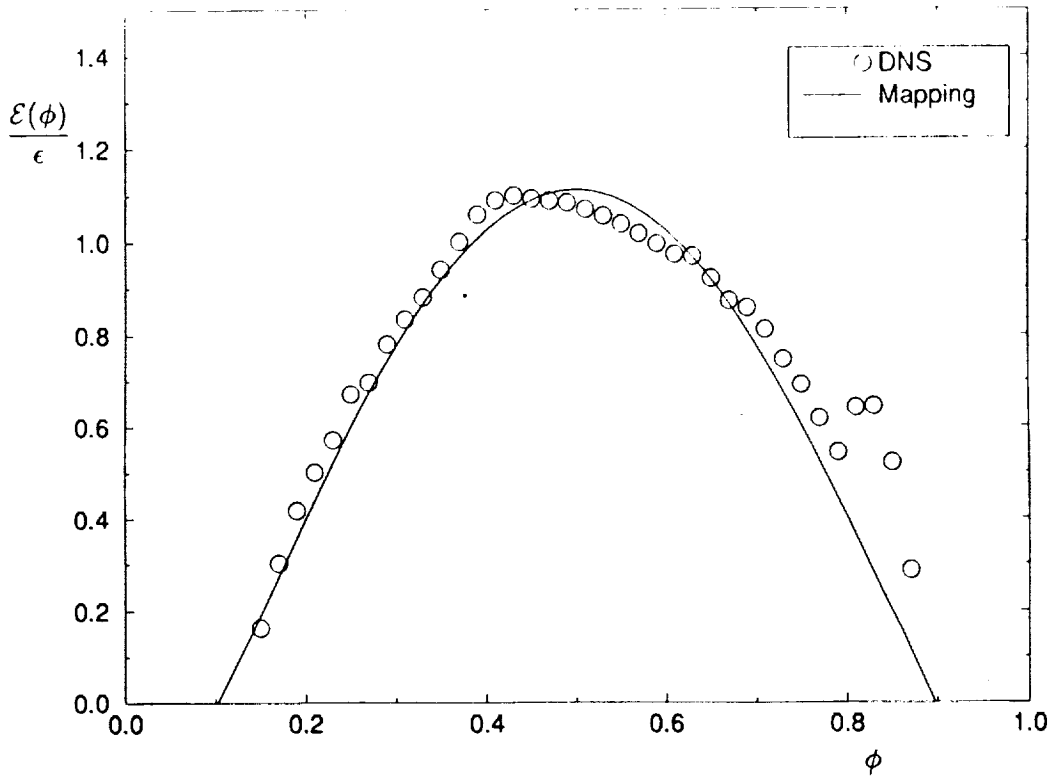

FIGURE 9b The comparison of the conditional expected scalar dissipation normalized with the total dissipation with DNS data as predicted by the AMC with the scalar bounds determined from the DNS results. (b) $\sigma^2 = 0.013$.

solutions are not possible for the moving boundary case. This is demonstrated by the equivalent form of Eq. (29)

$$H(t) = \frac{-\phi_{\max}(t)\gamma}{\sqrt{2}\pi} \int_0^1 \frac{\exp\left\{-\left[\mathrm{erf}^{-1}\left(\frac{\phi}{\phi_{\max}(t)}\right)\right]^2 \left(1+\frac{z^2\gamma^2}{2}\right)\right\}}{1+\frac{z^2\gamma^2}{2}} dz + \frac{1}{2}(\phi+\phi_{\max}(t)). \quad (56)$$

With this equation, therefore, the effect of the temporal variation of the PDF on the conditional dissipation is through the $\partial H/\partial t$ term in Eq. (28). This term has the form

$$\frac{dH}{dt} = \frac{-\sqrt{2}\phi_{\max}(t)\frac{d\gamma}{dt}}{\pi(2+\gamma^2)} \exp\left\{-(1+\frac{\gamma^2}{2})\left[\mathrm{erf}^{-1}\left(\frac{\phi}{\phi_{\max}(t)}\right)\right]^2\right\} + \frac{1}{2}\frac{d\phi_{\max}}{dt}$$

$$\left(1 - \frac{\phi}{\phi_{\max}(t)} \exp\left\{\left[\mathrm{erf}^{-1}\left(\frac{\phi}{\phi_{\max}(t)}\right)\right]^2\right\} + \right.$$

$$\left. \frac{2}{\sqrt{\pi}} \int_{-\infty}^{\mathrm{erf}^{-1}\left(\frac{\phi}{\phi_{\max}(t)}\right)} \mathrm{erf}\left(\frac{\gamma z}{\sqrt{2}}\right) \exp(-z^2) dz \right). \quad (57)$$

The first term on RHS of Eq. (57) is the same as that in Eq. (30), and the effects of moving boundaries manifest themselves through the second term. This term cannot be evaluated

analytically. However, Eqs. (56)-(57) show that due to the direct dependence on $\frac{d\phi_{max}}{dt}$, the conditional dissipation does not retain its original functional dependence, suggested by Eq. (33). Also, Fig. 9 shows that the effect of the moving boundaries is to force the conditional expected dissipation to zero at the current scalar maxima/minima. Therefore, the predicted results compare much better with DNS data than those presented in Fig. 4. Due to the similarity of the PDF's, it is expected that the other two closures would also behave in the similar fashion.

The influence of boundary encroachment is also sensed in the conditional expected diffusion field. For the erf^{-1}-Normal scalar PDF, the equivalent form of Eq. (41) is

$$D(\phi,t) = -\frac{2\phi_{max}(t)}{\gamma\sqrt{\pi}}\frac{d\gamma}{dt}\exp\left\{-\left[\text{erf}^{-1}(\frac{\phi}{\phi_{max}(t)})\right]^2\right\}$$

$$\text{erf}^{-1}\left(\frac{\phi}{\phi_{max}(t)}\right) + \left(\frac{\phi}{\phi_{max}(t)}\right)\frac{d\phi_{max}}{dt}, \tag{58}$$

with an average dissipation of

$$\epsilon(t) = \frac{4\phi_{max}^2(t)}{\pi(\gamma^2+2)\sqrt{\gamma^2+4}}\frac{d\gamma}{dt} - \frac{2\phi_{max}(t)}{\pi}\arctan\left(\frac{2}{\gamma\sqrt{\gamma^2+4}}\right)\frac{d\phi_{max}}{dt}. \tag{59}$$

Equations (58)-(59) show the influence of the boundary movement through the last term on the RHS of both these equations. With these additional terms, the normalized form similar to Eq. (41) is not very useful, and Eqs. (58)-(59) are evaluated numerically.

The equivalent of Eq. (58) for the Logit-Normal and the Beta density are, respectively,

$$D(\phi,t) = \frac{(\phi_{max}^2-\phi^2)}{\phi_{max}\gamma}\frac{d\gamma}{dt}\tanh^{-1}\left(\frac{\phi}{\phi_{max}(t)}\right) + \left(\frac{\phi}{\phi_{max}(t)}\right)\frac{d\phi_{max}}{dt}, \tag{60}$$

$$D(\phi,t) = -\frac{1}{P_1(\phi,t)}\frac{\partial}{\partial t}\left(I_{\left\{\frac{\phi-\phi_{min}}{\phi_{max}-\phi_{min}}\right\}}(\beta,\beta)\right) \tag{61}$$

An interesting characteristic displayed by Eqs. (58) and (60) is the influence of the terms containing the temporal derivative of $\phi_{max}(t)$. Note that at the boundaries, *i.e.* $\phi = \phi_{max}(t)$, the first term on the RHS of these equations vanishes, but the last term prohibits the conditional expected diffusion from going to zero. This is in accordance with the DNS data as shown in Fig. 6. In order to demonstrate this more clearly, results are presented in Fig. 10 of the conditional expected diffusion predicted by the erf^{-1}-Normal, with the input of the variance and the scalar bounds from DNS. A comparison between this figure and Fig. 6 show the influence of the boundary movement, and a better agreement between the model predictions and the DNS data. This agreement is more pronounced at scalar values away from the mean. Near the mean value, the influence of the boundary migration is slight, as also indicated by Eqs. (58) and (59).

8 DISCUSSIONS AND APPLICATIONS

In previous sections, a rather detailed discussion was presented of the problem of scalar mixing from an initially symmetric binary state. These discussions were primarily intended to provide a means of assessing the differences between the currently available tools in probability modeling of the scalar mixing problem. This problem is of significant interest,

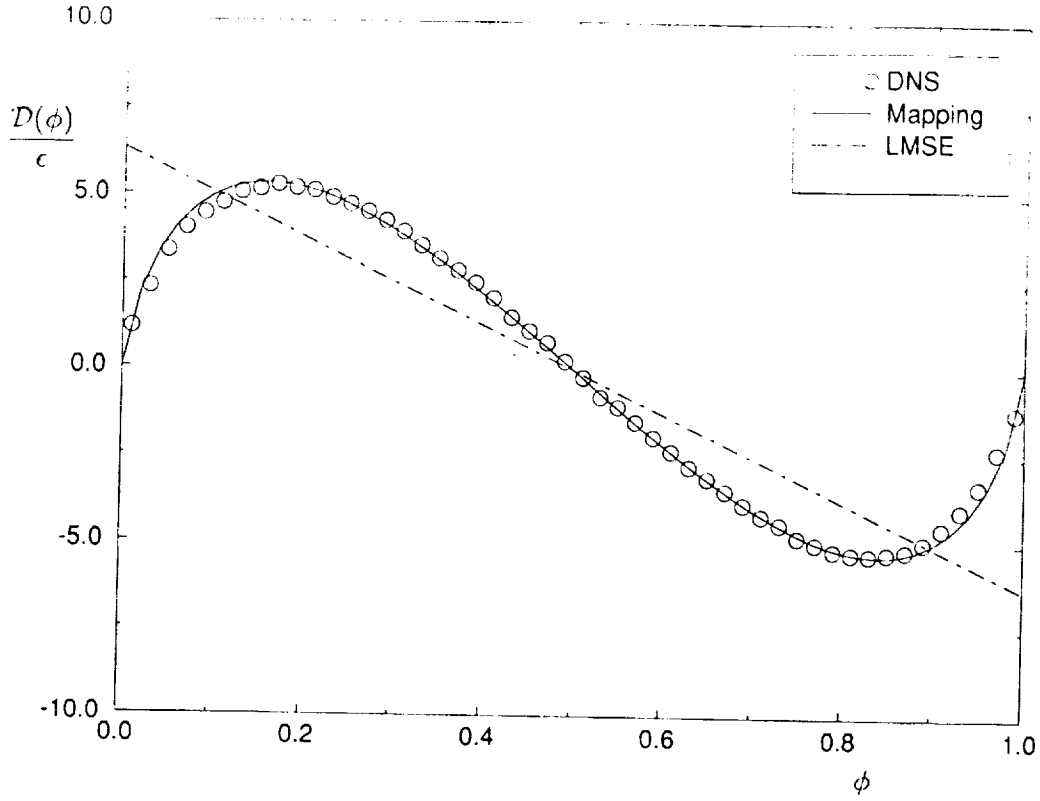

FIGURE 10a The comparison of the conditional expected scalar diffusion normalized with the total dissipation with DNS data as predicted by the AMC and the LMSE closures with the scalar bounds determined from the DNS results. (a) $\sigma^2 = 0.079$.

considering the extent of previous works focused on its analysis (Pope, 1976; Pope, 1979; Pope, 1982; O'Brien, 1980; Dopazo, 1973; Kosaly and Givi, 1987; Pope, 1991; Gao, 1991; O'Brien and Jiang, 1991; Nomura and Elgobashi, 1992). The results obtained here are particularly useful in highlighting some of the deficiencies of these closures, and in suggesting future research towards overcoming these drawbacks. There are, however, many other physical problems that are not subject to the restricting conditions imposed in these analyses. In this section, therefore, some discussions are presented as to the practical implications of these models, together with some speculations on their extensions for future applications.

Perhaps one of the most important practical applications of the closures considered here is the treatment of reactive flow phenomena. In fact, the most important advantage of scalar PDF methods is due to their applicability in the modeling of turbulent combustion (Pope, 1979; Pope, 1985; Pope, 1990; Kollmann, 1990; O'Brien, 1980). The results generated here can be used directly in the modeling of *mixing controlled* homogeneous chemically reacting systems. Namely, in examining the compositional structure of a reacting system under chemical equilibrium, or in determining the limiting rate of reactant conversion in a simple chemistry of the prototype Fuel + Air $\rightarrow$ Products. The determination of this rate has been the subject of extensive investigations over the past forty years (see Hawthorne *et al.* (1949); Toor (1962); Williams (1985)). It is now well-established that in a mixing controlled binary irreversible reaction of this type, the statistics of the reacting fields can be related to those of an appropriately defined conserved scalar (such as ϕ) (Bilger, 1980; Toor, 1975; Williams, 1985). Therefore, the frequencies generated herein can be utilized for estimating the statistics of the reacting

field with an infinitely fast chemistry model in a homogeneous flow with initially segregated reactants under stoichiometric conditions. Albeit very restricting, this problem is of great practical importance for modeling and design of batch mixers and plug flow reactors in which these conditions prevail (Toor, 1975; Brodkey, 1981; Dutta and Tarbell, 1989). Madnia *et al.* (1991); Madnia *et al.* (1992) have shown that with the erf^{-1}-Normal (AMC) and the Beta density models, this rate can be predicted by simple analytical means. For the Logit-Normal density, a complete analytical solution cannot be obtained and determination of the statistics requires numerical integration of the PDF. The results generated by these closures agree with DNS data better than those obtained by means of the C/D closures (McMurtry and Givi, 1989), or other models previously available in the chemical engineering literature (Dutta and Tarbell, 1989) (see Givi (1989) for a review). Also, the results provided by the AMC (Frankel *et al.*, 1992a) are shown to compare well with experimental data on plug flow reactors if the additional information pertaining to the evolution of the scalar length scale is accurately provided.

The most obvious issues in regard to the applications of these models are associated with their extension for the treatment of (1) non-symmetric binary scalar mixing, (2) non-binary scalar mixing, (3) multiple scalar mixing, and (4) non-homogeneous mixing. The first problem constitutes a more general form of the binary mixing problem and is also important for the analysis of non-stoichiometric reacting systems. The second problem is appropriate for the analysis of other mixing systems in which the initial conditions are not of a two-feed configuration. The third problem is of interest in reacting systems in which the transport of a passive scalar (like ϕ) is not sufficient for a complete analysis. For example, any reacting system under non-equilibrium conditions. Finally, the importance of the fourth problem is obvious in view of the fact that the flow within most practical mixing devices cannot be assumed homogeneous.

In regard to the first issue, all of the three closures considered here can be used for the probability modeling of scalar mixing within a *fixed* scalar domain. The use of the AMC is straightforward, but the mathematical procedure is somewhat complex (Madnia *et al.*, 1992). The Pearson frequencies can be generated easily for non-symmetric problems. In this case, the Pearson Type I provides a reasonably accurate representation of the scalar field regardless of the degree of asymmetry of the PDF (Frankel *et al.*, 1992b; Madnia *et al.*, 1992). The use of the JET in this regard is most difficult, since closed form analytical expressions are not available for the variance of the scalar by which the PDF can be characterized (Johnson, 1949a). In treating these problems, therefore, the first two models can be more readily employed and subsequently used for the treatment of mixing controlled reacting systems under non-stoichiometric conditions. In fact, as demonstrated by Madnia *et al.* (1992) the solution of the non-symmetric form of the AMC and the Beta density provide a very good means of predicting the limiting rate of reactant conversion in homogeneous reacting flows. However, it should be indicated that with both models the problem associated with the scalar bounds still exists and must be dealt with as discussed in Section 7.

In addressing the second issue, it is obvious that the AMC is more appropriate than the other closures for simulating the mixing problem from an initially "arbitrary" state. The extension of JET and PF for treating multi- (higher than bi-) modal distributions have been reported in statistics literature. However, as the degree of modality of the PDF increases the procedure becomes more complex and not suitable for practical applications. Fortunately, in most mixing problems in simple flows, *i.e.* homogeneous turbulence and turbulent shear flows, the PDF exhibits strong bimodal features (Madnia *et al.*, 1992; Frankel *et al.*, 1992b). In those cases, the use of the Beta density can be justified. In fact, in non-homogeneous flows it is easier to use this density, at least until further development of the AMC for practical applications (see Frankel *et al.* (1992b); Gaffney *et al.* (1992)).

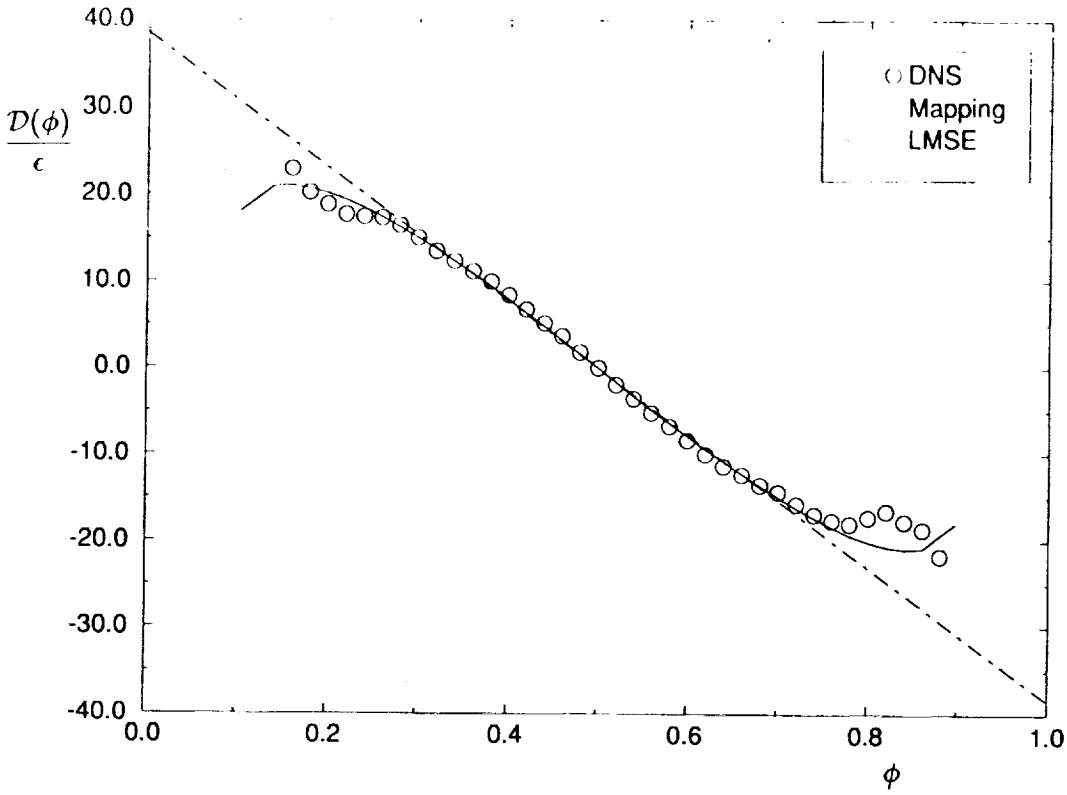

FIGURE 10b The comparison of the conditional expected scalar diffusion normalized with the total dissipation with DNS data as predicted by the AMC and the LMSE closures with the scalar bounds determined from the DNS results. (b) $\sigma^2 = 0.013$.

The extension of all of the three models in describing multi-scalar mixing is possible. The problem naturally falls within the realm of the *multivariate* statistical analyses. In these analyses, the implementation of the AMC is relatively straightforward since it provides a transport equation for the joint PDF's of the scalar variable in a multivariable sense (Pope, 1991). However, it is not presently clear how to devise an efficient computational procedure, typically based on Monte Carlo methods (Pope, 1981), for the numerical treatment of these equations. Some work in this regard is currently under way (Valiño and Gao, 1991). The extension of assumed distributions based on the Beta density for treating multi-scalars is more straightforward but less trivial to justify. The most obvious means is to implement the multivariate form of the PF. The direct analog of the Beta density is the *Dirichlet* frequency (Johnson, 1987; Narumi, 1923; Johnson and Kotz, 1972). The application of this density in modeling of multiple species reactions has been discussed by Girimaji (1991a); Girimaji (1991b); Gaffney *et al.* (1992). However, the use of the Dirichlet frequency cannot be justified for modeling of reacting flows in a general sense (Frankel, 1992). Finally the extension of the JET in generating multivariate frequencies has been reported in statistics literature since the subsequent work of Johnson (1949b). As one may suspect, the procedure is more complex, and the same reservations as those associated with the Dirichlet distributions apply.

All of the models considered here can be extended for the analysis of non-homogeneous mixing (and reacting) systems. Obviously, in most cases, the problem requires numerical integration of the appropriate conservation equations. For instance, the AMC can be invoked in the *mixing* step of a fractional stepping procedure, similar to that of typical Monte Carlo procedures (Pope, 1981). The PF densities (*e.g.* Beta or Dirichlet) and JET

generated frequencies require modelled transport equations for the first two moments and cross moments of the scalar field. These equations, "hopefully", include the essential information pertaining to the spatial inhomogeneity of the flow. Naturally, the PDF is not generally symmetric, and must be determined from the knowledge of the parameters $\beta_1, \beta_2, \gamma, \lambda, \varrho$, and the local $\phi_{\max}(t), \phi_{\min}(t)$ values. With this information, all the higher order statistics of the scalar field can be determined. In regard to this last issue, it must be indicated that the Beta density has been extensively used for the modeling of non-homogeneous reacting systems (*e.g.* Rhodes (1975); Jones and Priddin (1978); Lockwood and Moneib (1980); Janicka and Peters (1982); Peters (1984); Frankel *et al.* (1992b); Gaffney *et al.* (1992); for recent reviews, see Givi (1989); Priddin (1991)). Due to their special mathematical properties, the Beta and/or the Dirichlet frequencies yield relatively simple analytical solutions for the higher order statistics of the reacting fields. From this point of view, the use of the PF is more practical than the AMC since the solution procedure does not require the numerical treatment of the PDF transport equation. This point has been discussed in detail by Girimaji (1991b). However, as indicated above, the use of the Dirichlet frequency cannot be justified for modeling of unpremixed reacting flow in a general sense. Also, there is no way of implementing this density directly for modeling of non-equilibrium flames, involving strong correlation of the temperature and the species mass fractions. Even with the assumption of statistical independence of the reacting species and the temperature, the question of the local scalar range imposes a severe restriction on the validity of this approximation. For example, it is demonstrated by Gaffney *et al.* (1992) that in the modeling of a reacting turbulent shear flow, depending on the *a priori* choice of the magnitudes of the local scalar bounds the predicted results can be altered significantly. Obviously, this problem is not eliminated with the usage of JET frequencies in either a univariate or multivariate sense.

9 CONCLUDING REMARKS

It is shown that the family of frequencies generated by the Johnson-Edgeworth Translation (JET) provides a reasonable means for statistical modeling of binary symmetric scalar mixing in homogeneous turbulence. It is also shown that the results predicted by one of the members of this family is identical to the solution generated by the Amplitude Mapping Closure (AMC) of Kraichnan. This similarity is useful in two regards: (1) establishing a mathematical reasoning for the similarity of the probability frequency of the Pearson Family (PF) and that of the AMC for the description of the problem, and (2) suggesting the possible use of other members of the JET frequencies in approaches in which the Probability Density Function (PDF) is assumed *a priori*. The PDF's generated by all these models are shown to compare well with each other and also with the results obtained by Direct Numerical Simulations (DNS). However, none of the models are capable of accurately predicting the conditional expected dissipation and the conditional expected diffusion of the scalar field. This problem is associated with the incapability of the models to account for the migration of the scalar bounds as mixing proceeds.

ACKNOWLEDGEMENTS

We are indebted to Dr. Gordon Erlebacher for the use of his computer codes. We also appreciate the efforts of Ms. Debbie Young for assisting us with the literature search. This work is sponsored by the Office of Naval Research under Grant N00014-90-J-1403, by NASA Langley Research Center under Grant NAG-1-1122, and by the National Science Foundation under Grant CTS-9253488. The computational resources are provided by NSF through NCSA at the University of Illinois, and by the NAS program at NASA Ames Research Center.

REFERENCES

Abramowitz, M. and Stegun, I. A. (1972). *Handbook of Mathematical Functions and Formulas, Graphs, and Mathematical Tables.* Government Printing Office, Washington, D.C.

Bilger, R. W. (1980). Turbulent flows with nonpremixed reactants. In Libby, P. A. and Williams, F. A., editors, *Turbulent Reacting Flows,* chapter 3, pages 65-113. Springer-Verlag, Heidelberg.

Brodkey, R. S. (1981). Fundamental of turbulent motion. *Chem. Eng. Comm.* **8,** 1-23.

Casella, G. and Berger, R. L. (1990). *Statistical Inference.* Brooks/Cole Publishing Company, Belmont, CA.

Chen, H., Chen, S., and Kraichnan, R. H. (1989). Probability distribution of a stochastically advected scalar field. *Phys. Rev. Lett.* **63,** 2657-2660.

Curl, R. L. (1963). Dispersed phase mixing: I. Theory and effects in simple reactors. *AIChE J.* **9,** 175-181.

Dopazo, C. (1973), *Non-Isothermal Turbulent Reactive Flows: Stochastic Approaches.* Ph.D. Thesis, Department of Mechanical Engineering, State University of New York at Stony Brook, Stony Brook, NY.

Dutta, A. and Tarbell, J. M. (1989). Closure models for turbulent reacting flows. *AIChE J.* **35,** 2013-2027.

Edgeworth, F. Y. (1907). On the representation of statistical frequency by a series. *Journal of the Royal Statistical Society, Series A.* **70,** 102-106.

Erlebacher, G., Hussaini, M. Y., Speziale, C. G., and Zang, T. A. (1987). Toward the large eddy simulation of compressible turbulent flows. ICASE Report 87-20, NASA Langley Research Center, Hampton, VA. Also available as *NASA CR 178273.*

Erlebacher, G., Hussaini, M. Y., Speziale, C. G., and Zang, T. A. (1990a). Toward the large eddy simulation of compressible turbulent flows. ICASE Report 90-76, NASA Langley Research Center, Hampton, VA. Also available as *NASA CR 187460.*

Erlebacher, G., Hussaini, M.Y., Kreiss, H. O., and Sarkar, S. (1990b). The analysis and simulation of compressible turbulence. *Theoret. Comput. Fluid Dynamics* **2,** 73-95.

Eswaran, V. and Pope, S. B. (1988). Direct numerical simulations of the turbulent mixing of a passive scalar. *Phys. Fluids* **31,** 506-520.

Frankel, S. H., Jiang, T.-L., and Givi, P. (1992a). Modeling of isotropic reacting turbulence by a hybrid mapping-EDQNM closure. *AIChE J.* **38,** 535-543.

Frankel, S. H., Madnia, C. K., and Givi, P. (1992b). Modeling of the reactant conversion rate in a turbulent shear flow. *Chem. Eng. Comm.* **113,** 197-209.

Frankel, S. H. (1992). Ph.D. Thesis, Department of Mechanical and Aerospace Engineering, State University of New York at Buffalo, Buffalo, NY. in preparation.

Gaffney, R. L., White, J. A., Girimaji, S. S., and Drummond, J. P. (1992). Modeling of turbulent/chemistry interactions using assumed pdf methods. AIAA paper AIAA-92-3638.

Gao, F. (1991). Mapping closure and non-Gaussianity of the scalar probability density functions in isotropic turbulence. *Phys. Fluids A* **3,** 2438-2444.

Girimaji, S. S. (1991a). Assumed β-pdf model for turbulent mixing: Validation and extension to multiple scalar mixing. *Combust. Sci. and Tech.* **78,** 177-196.

Girimaji, S. S. (1991b). A simple recipe for modeling reaction-rates in flows with turbulent-combustion. AIAA paper AIAA-91-1792.

Girimaji, S. S. (1992). Towards understanding turbulent scalar mixing. NASA CR 4446.

Givi, P. and McMurtry, P. A. (1988). Non-premixed reaction in homogeneous turbulence: Direct numerical simulations. *AIChE J.* **34,** 1039-1042.

Givi, P. (1989). Model free simulations of turbulent reactive flows. *Prog. Energy Combust. Sci.* **15,** 1-107.

Hawthorne, W. R., Wedell, D. S., and Hottel, H. C. (1949). Mixing and combustion in turbulent gas jets. In *3rd Symp. on Combustion, Flames and Explosion Phenomena,* pages 266-288. The Combustion Institute, Pittsburgh, PA.

Hussaini, M. Y., Speziale, C. G., and Zang, T. A. (1990). The potential and limitations of direct and large eddy simulations. In Lumley, J. L., editor, *Whither Turbulence? Turbulence at the Crossroads,* volume 357 of *Lecture Notes in Physics,* pages 354-368. Springer.

Janicka, J. and Peters, N. (1982). Prediction of turbulent jet diffusion flame lift-off using a pdf transport equation. In *Proceedings of 19th Symp. (Int.) on Combustion* pages 367-374. The Combustion Institute, Pittsburgh, PA.

Janicka, J., Kolbe, W., and Kollmann, W. (1979). Closure of the transport equation for the probability density function of turbulent scalar field. *J. Nonequil. Thermodyn.* **4,** 47-66.

Jiang, T.-L., Givi, P., and Gao, F. (1992). Binary and trinary scalar mixing by Fickian diffusion-some mapping closure results. *Phys. Fluids A* **4,** 1028-1035.

Johnson, N. L. and Kotz, S. (1972). *Distributions in Statistics: Continuous Multivariate Distributions.* John Wiley and Sons, New York, NY.

Johnson, N. L. (1949a). Systems of frequency curves generated by methods of translation. *Biometrika* **36,** 149-176.

Johnson, N. L. (1949b). Bivariate distributions based on simple translation systems. *Biometrika* **36,** 297-304.

Johnson, M. E. (1987). *Multivariate Statistical Simulation.* John Wiley and Sons, New York, NY.

Jones, W. P. and Priddin, C. H. (1978). Predictions of the flowfield and local gas composition in gas turbine combustors. In *17th Symp. (Int.) on Combustion*, pages 399-409. The Combustion Institute, Pittsburgh, PA.

Kollmann, W. (1990). The pdf approach to turbulent flow. *Theoret. Comput. Fluid Dynamics* **1**, 249-285.

Kosaly, G. and Givi, P. (1987). Modeling of turbulent molecular mixing. *Combust. Flame* **70**, 101-118.

Kosaly, G. (1986). Theoretical remarks on a phenomenological model of turbulent mixing. *Combust. Sci. and Tech.* **49**, 227-234.

Kraichnan, R. H. (1989). Closures for probability distributions. *Bull. Amer. Phys. Soc.* **34**, 2298.

Liñan, A. (1974). The asymptotic structure of counterflow diffusion flames for large activation energies. *Acta Astronautica* **1**, 1007-1039.

Lockwood, F. C. and Moneib, H. A. (1980). Fluctuating temperature measurement in a heated round free jet. *Combust. Sci. and Tech.* **22**, 63-81.

Madnia, C. K. and Givi, P. (1992). On DNS and LES of homogeneous reacting turbulence. In Galperin, B. and Orszag, S. A., editors, *Large Eddy Simulations of Complex Engineering and Geophysical Flows*. Cambridge University Press, Cambridge, U.K. in press.

Madnia, C. K., Frankel, S. H., and Givi, P. (1991). Mathematical modeling of the reactant conversion rate by single-point pdf methods. In *Proc. Fall Technical Meeting of the Combustion Institute, Eastern Section*, Ithaca, NY.

Madnia, C. K., Frankel, S. H., and Givi, P. (1992). Reactant conversion in homogeneous turbulence: Mathematical modeling, computational validations and practical applications. *Theoret. Comput. Fluid Dynamics*, **4**, 79-93.

McMurtry, P. A. and Givi, P. (1989). Direct numerical simulations of mixing and reaction in a nonpremixed homogeneous turbulent flow. *Combust. Flame* **77**, 171-185.

Miyawaki, O., Tsujikawa, H., and Uraguchi, Y. (1974). Turbulent mixing in multi-nozzle injector tubular mixers. *J. Chem. Eng. Japan* **7**, 52-74.

Narumi, S. (1923). On the general form of bivariate frequency distributions which are mathematically possible when regression and variation are subjected to limiting conditions, I. *Biometrika* **15**, 77-88.

Nomura, K. K. and Elgobashi, S. E. (1992). Mixing characteristics of an inhomogeneous scalar in isotropic and homogeneous sheared turbulence. *Phys. Fluids A* **4**, 606-625.

Norris, A. T. and Pope, S. B. (1991). Turbulent mixing model based on ordered pairing. *Combust. Flame* **83**, 27.

O'Brien, E. E. and Jiang, T.-L. (1991). The conditional dissipation rate of an initially binary scalar in homogeneous turbulence. *Phys. Fluids A* **3**, 3121-3123.

O'Brien, E. E. (1980). The probability density function (PDF) approach to reacting turbulent flows. In Libby, P. A. and Williams, F. A., editors, *Turbulent Reacting Flows*, chapter 5, pages 185-218. Springer-Verlag, Heidelberg.

Passot, T. and Pouquet, A. (1987). Numerical simulation of compressible homogeneous flows in the turbulent regime. *J. Fluid Mech.* **181**, 441-466.

Pearson, K. (1895). Contributions to the mathematical theory of evolution: II. skew variations in homogeneous material. *Philos. Trans. of the Royal Soc. of London, Series A.* **186**, 343-414.

Peters, N. (1984). Laminar diffusion flamelet models in non-premixed turbulent combustion. *Prog. Energy Combust. Sci.* **10**, 319-339.

Pope, S. B. (1976). The probability approach to modelling of turbulent reacting flows. *Combust. Flame* **27**, 299-312.

Pope, S. B. (1979). The statistical theory of turbulent flames. *Phil. Trans. Royal Soc. London* **291**, 529-568.

Pope, S. B. (1981). A Monte Carlo method for the pdf equations of turbulent reactive flow. *Combust. Sci. and Tech.* **25**, 159-174.

Pope, S. B. (1982). An improved turbulent mixing model. *Combust. Sci. and Tech.* **28**, 131-145.

Pope, S. B. (1985). PDF methods for turbulent reacting flows. *Prog. Energy Combust. Sci.* **11**, 119-192.

Pope, S. B. (1990). Computations of turbulent combustion: Progress and challenges. In *Proceedings of 23rd Symp. (Int.) on Combustion*, pages 591-612. The Combustion Institute, Pittsburgh, PA.

Pope, S. B. (1991). Mapping closures for turbulent mixing and reaction. *Theoret. Comput. Fluid Dynamics* **2**, 255-270.

Priddin, C. H. (1991). Turbulent combustion modelling-A review. In Johansson, A. V. and Alfredsson, P. H., editors, *Advances in Turbulence 3*, pages 279-299. Springer-Verlag, Berlin.

Rhodes, P. R. (1975). A probability distribution function for turbulent flows. In Murthy, S. N. B., editor, *Turbulent Mixing in Non-Reactive and Reactive Mixing*, pages 235-241. Plenum Press, New York, NY.

Spalding, S. B. (1961). Theory of mixing and chemical reaction in the opposed-jet diffusion flame. *Journal of the American Rocket Society* **31**, 763-771.

Toor, H. L. (1962). Mass transfer in dilute turbulent and nonturbulent systems with rapid irreversible reactions and equal diffusivities. *AIChE J.* **8**, 70-78.

Toor, H. L. (1975). The non-premixed reaction: $A + B \rightarrow Products$. In Brodkey, R. S., editor, *Turbulence in Mixing Operations*, pages 123-166. Academic Press, New York, NY.

Valiño, L. and Gao, F. (1991). Monte Carlo implementation of the mapping closure for turbulent reacting flows. In *Fluid Dynamics Division Meeting of the American Physical Society*, Phoenix, Arizona.
Williams, F. A. (1985). *Combustion Theory*. The Benjamin/Cummings Publishing Company, Menlo Park, CA, 2nd edition.